City Research Online

City, University of London Institutional Repository

REMOTE CATIONIC CURING

KENNETH SHAUN TRANTER

THESIS SUBMITTED FOR THE DEGREE OF

DOCTOR OF PHILOSOPHY

CITY UNIVERSITY

LONDON, U.K.

CHEMISTRY DEPARTMENT

FEBRUARY 2000

Pour être digne de ce nom, l'expérimentateur doit être à la fois théoricien et praticien. S'il doit posséder d'une maniere complète l'art d'instituer les faits de l'expérience, qui sont les matériaux de la science, il doit aussi se rendre compte clairement des principes scientifiques qui dirige notre raisonnement au milieu de l'étude expérimental si variée des phénomènes de la nature. Il serait impossible de séparer ces deux choses: la tête et la main. Une main habile sans la tête qui la dirige est un instrument aveugle; la tête sans la main qui réalise reste impuissante.

Claude Bernard

Introduction à l'étude de la médecine expérimental

1865, publ.1947

(I) TABLE OF CONTENTS

(II) TABLE OF FIGURES

13

14

17

(III)   TABLE OF TABLES

21

(IV) TABLE OF SCHEMES

23

(V) ACKNOWLEDGEMENTS

I GRANT POWERS OF DISCRETION TO THE UNIVERSITY LIBRARIAN TO ALLOW THIS THESIS TO BE COPIED IN WHOLE OR IN PART WITHOUT FURTHER REFERENCE TO ME. THIS PERMISSION COVERS ONLY SINGLE COPIES MADE FOR STUDY PURPOSES, SUBJECT TO NORMAL CONDITIONS OF ACKNOWLEDGEMENT.

KENNETH SHAUN TRANTER

FEBRUARY 2000

27

(VII) ABSTRACT

A procedure is described for the polymerisation of cationically polymeriseable resins, using solid- state onium and organometallic salt photoinitiators bearing complex anions of group V elements.

The initiator is irradiated in the solid state by UV light and the gas(es) produced are allowed to diffuse into the resin film which is adjacent to but not in contact with the initiator, within a closed cell. Epoxide and vinyl ether monomers were successfully cured in this manner. The progress of polymerisation is followed by FTIR spectroscopy. The reaction is thought to be initiated via a Lewis Acid catalyst, but propagated via Brønsted species following interaction of the former with trace water in the film.

The effects of water on the polymerisation of epoxides were studied. Atmospheric moisture (humidity) was found to have a detrimental effect on the polymerisation while bulk water was tolerated at levels up to 5% w/w. These results are discussed in detail in the context of industry findings.

The presence of HF (hydrogen fluoride) in the gaseous photodecomposition products was determined by gas phase FTIR. and confirmed by ion chromatography. The rate of evolution of gaseous products upon irradiation of the initiator(s) is quantified in real time by dissolution in water and conductometric measurement using a fluoride ion specific electrode. A large proportion of the detected fluoride ion yield is attributed to the presence in the gaseous photo-products of XF_5, the pentafluoride of the group V element. This is subsequently hydrolysed to yield multi-molar equivalents of fluoride ion per initiator molecule irradiated.

Hybrid systems are described which permit the selective and step-wise polymerisation of acrylate resins (by the conventional process) and epoxide resins by the above method.

(VIII)   ABBREVIATIONS

ATR	attenuated total reflectance
BA	BrØnsted acid
BS	borosilicate
DPI	diphenyliodonium
DPIHFAs	diphenyliodonium hexafluoroarsenate
DPIHFP	diphenyliodonium hexafluorophosphate
DPIHFSb	diphenyliodonium hexafluoroantimonate
DR	diffuse reflectance
DSC	differential scanning calorimetry
DVE	divinyl ether
Dz	diazonium
EB	electron beam
ER	external reflection
FR	free radical
FSE	fluoride specific electrode
FTIR	fourier transform infrared
GCMS	gas chromatography - mass spectrometry
GPC	gel permeation chromatography
HDDA	Hexanediol diacrylate
HFAs	hexafluoroarsenate
HFP	hexafluorophosphate

HFSb	hexafluoroantimonate
IEC	ion exchange chromatography
IR	infrared
Irg.184/Irgacure 184	™Ciba Geigy, 1-benzoylcyclohexan-1-ol
Irg.261/Irgacure 261	™Ciba Geigy, (η^5-2,4-Cyclopentadiene-1-yl) [(1,2,3,4,5,6-η)-(1-methyl ethyl)benzene]-iron(+)- hexafluorphosphate(-1)
Irg.651/Irgacure 651	™Ciba Geigy, 2,2-dimethoxy-2-phenyl acetophenone
Irg.907/Irgacure 907	™Ciba Geigy, 2-methyl-1-[4-(methylthio)phenyl]-2- morpholino propanone -1
ISC	inter-system crossing
IST	interfacial surface tension
KI185	™Degussa,(bis[4-(diphenylsulphonio)- phenyl]sulphide-bis-hexafluorophosphate)
LA	Lewis acid
MR	mixed reflectance
MS	mass spectrometry
NMR	nuclear magnetic resonance
PI	photoinitiator
PPE	polypropylene
PTFE	polytetrafluoroethylene
PVA	Polyvinyl acetate
PVC	Polyvinyl chloride
RA	Reflection-absorption

REDOX	reduction-oxidation
RH	relative humidity
SCO	spin orbit coupling
SR	specular reflectance
SSC	spin-spin coupling
ST	surface tension
TGA	thermo-gravimetric analysis
THF	tetrahydrofuran
TPS	triphenylsulphonium
TPSHFAs	triphenylsulphonium hexafluoroarsenate
TPSHFP	triphenylsulphonium hexafluorophosphate
TPSHFSb	triphenylsulphonium hexafluoroantimonate
TS	transition state
UV	ultraviolet
UVR6110	Cyracure UVR6110, ™Union Carbide, 3,4-Epoxycyclohexylmethyl-3',4'-epoxycyclohexane carboxylate
VCHDO	vinylcyclohexene dioxide
VIS	visible
VOC	volatile organic contaminant

Synopsis

This project demonstrates a novel approach for photo-polymerisation of cationically polymeriseable resins with widely studied photoinitiators of the onium salt class. This approach, which may be termed 'Remote Cationic Polymerisation', involves the irradiation of the photoinitiator in the solid state to generate gases capable of polymerising thin films of suitable monomers. The monomer film is adjacent to but not in contact with the solid-state initiator. Remote Cationic Polymerisation is explored here with regard to clear surface coatings but may also have application for surface coatings of other types.

The purpose of this work is to explore the phenomenon of Remote Cationic Polymerisation at a fundamental level. Particular interest is focused on (a) verifying and characterising the evolution of gases obtained following U.V. irradiation of photoinitiators in the solid state and (b) verifying and characterising the use of such gases for cationic polymerisation.

This information is of specific interest to those who may wish to adapt the process for practical purposes. The study also has more general chemical implications with regard to the mechanism of photodecomposition of onium salts, particularly with regard to the role and function of the anion in cationic polymerisation. Proposals are made here which amount to clear divergence from the preceding thinking in this area.

Thesis Organization

In most respects, this thesis respects the conventional format, consisting of an introduction and two experimental chapters followed by a summary/conclusion.

The introduction provides a general description of the coatings industry. This is intended to assist newcomers to the industry who will be assailed by confusing and contradictory definitions and terminology, and who may wish to locate the chemistry with which they will become involved in a useful context. More importantly, the introduction contains a review of the literature concerning cationic polymerisation with particular focus on onium salt photodecompositon. This review is comprehensive but selective, attempting to distinguish only those contributions that have withstood subsequent discussion in the literature.

The experimental work is divided into two chapters. The first such chapter describes and discusses experiments which concern the evolution of gases from the solid state decomposition process. The second such chapter describes and discusses experiments in which the aforesaid gases were used to achieve polymerisation of cationically polymeriseable resins. The summary and conclusion combines these findings and highlights their significance with regard to the objectives of this work.

Each experimental chapter contains an 'experimental' section and a 'results and discussion' section. With regard to the 'experimental' section the reader may note a divergence from accepted thesis format; in addition to containing the usual details, the 'experimental' section also contains some element of discussion of the experimental methodology that other writers frequently divide between the introduction section and the results and discussion section.

In the present case, an effort has been made to preserve the clarity and intactness of the experimental work having primary scientific value (photodecomposition and photo-polymerisation), by separating aspects of secondary interest (explanation of techniques, methodology, precautionary experiments etc.). These are combined in a separate location.

In this manner, the reader may be assured, prior to addressing the main body of the work, that the experimentation has been properly considered, that the techniques used are valid and that the results are reliable. A reader who seeks to reproduce the work or use the techniques for other purposes may also appreciate this approach. Such a reader will therefore find all the methodological information and appropriate considerations collected in one place and presented on consecutive pages.

Efforts have been made to enable each of the four main chapters to be read independently as complete entities. Consequently each experimental chapter begins with an introductory statement of which the main points are reiterated at the beginning of the summary/conclusion. Also, in the results and discussion sections, certain comparisons with supporting literature may reappear in different contexts. The reader who reads the entire work may encounter some repetition, which is intended to be helpful rather than irksome.

Since, this work was undertaken, a small number of related articles from other workers have appeared in the literature addressing related questions. Since these articles were not available at the outset, they have been excluded from the introductory literature review and are, if appropriate, dealt with in the relevant discussion section.

With further regard to the use of literature, a distinction has been made between those areas of interest that are now fully understood, and those that remain open for discussion. The former, such as the photodecomposition of the cation, are addressed in the introduction. The latter, such as the stability of the anion and the effect of water on cationic polymerisation, are addressed in the relevant results/discussion section where a new contribution is being made. Review of such open questions, with the exception of the one central to the thesis, is excluded from the introduction.

1 INTRODUCTION

1.1 THE COATINGS INDUSTRY - AN OVERVIEW

1.1.1 Surface Coatings – Description And Terms

1.1.1.1 What Are Surface Coatings And How Are They Used?

For most purposes a coating may be defined [1] as a pigmented or non-pigmented organic film of less than 50 microns in thickness which is applied to a substrate as a liquid, levelled by forces of surface tension, and hardened by physical or chemical modification to form a solid film. As such, a coating may be a clear film, ink, paint, enamel, lacquer or varnish.

Surface coatings find application in numerous commercial processes including multi-stage automotive paint finishes, finishing of wood products, food packaging, weather protected materials and graphic art products - to name only a few. This variety of uses arises from the diversity of properties that can be imparted with the wide range of possible processes and formulation permutations.

Sometimes the coating application may be one of the primary manufacturing steps - as in the case of printed circuit boards or printing plates. More often the coating step may be the last in a series of treatments leading to a finished product, the purpose of which is either functional - to modify, protect or render permanent a primary coating or treated surface - or decorative, being applied for aesthetic effect or visual impact.

1.1.1.2 What Does A Coating Consist Of?

In general any formulation will consist of 4 elements (or 5 elements if the coating is to be coloured):

- resins   (also known as binders, vehicles)
- solvents   (also known as diluents, reducers)
- additives   (also known as modifiers)
- colourants   (including pigments and dyes)
- hardeners   (also known as driers, catalysts, initiators)

Powder coatings are exceptions to this principle, as they require no solvent.

The nature of any of these materials and the ratio of them in a given formulation will depend upon the properties required for the coating process and final product.

1.1.1.3 Which Properties Are Important?

The properties that must be developed for a coating fall into 2 categories:

- Processing - aspects of manufacture, storage, handling, application
    - stability - chemical and physical stability of pre-applied coatings
    - rheology - viscosity, tack, thixotropy
    - drying - rate of cure, residual contaminants
    - regulatory - toxicology, handling, shipment
- Performance - attributes required for the end product
    - chemical resistance - solvents, oils, detergents, acids, bases
    - environmental stability - light fastness, photodecomposition, oxidation
    - permeability - to electric current, to liquids, gases and other chemicals
    - appearance - colour, gloss, clarity, texture
    - mechanical - hardness, elasticity, tensile strength, adhesion, lubricity, abrasiveness

The wide range of properties required for various markets has given rise to a large number of approaches to formulation in terms of chemistry and application methodology.

1.1.1.4 How Are The Technologies Of Surface Coatings Described And Related?

The industry is replete with jargon and a range of terms is in use in different sectors to distinguish one technology from another - coatings can be subdivided into a number of overlapping categories.

Coating technologies may be grouped (Table 1.1-1) according to the nature of the materials, or the mode of application, or the mode of drying, or the properties obtained, or the market reached.

An ink for magazine printing, for example, is a coating which may be referred to as a 'conventional' pigmented coating based on a 'natural resin' vehicle and 'mineral' solvents delivered through a 'roller' applicator with 'heat set' drying, producing a film with properties of 'colour', and 'low cost' and which is sold in the 'graphic arts' market

classified by	example categories
pigmentation	clear coats, paints, inks, enamels
vehicle type	natural materials (vegetable oils, mineral oils, rosins) synthetic resins (polyesters, polyolefins, polyurethanes, polyureas, polyacrylics, polyethers) chemically modified natural materials (epoxidised/acrylated vegetable oils)
solvent system	'conventional' (non-reactive) 'non conventional' (reactive)
solvent type	'mineral' (paraffins) 'solvent' (organic, other than paraffins) 'water borne' (aqueous)
application process	powder, spray, dip, roller, brush, curtain
drying process	'heat setting' (thermoplasticity and/or evaporation of solvent) 'cold setting' (oxidative cross linking and/or substrate absorption of solvent) polymerisation (thermally, chemically or radiation induced)
property	chemical resistant, fire retardant, stain resistant, heat resistant, fibre optic, high gloss, barrier etc.
market /application	automotive, flooring, graphic arts, specialty, wood finishing, electronics

Table 1.1-1   Categorization of surface coatings

The demand for novel properties, the development of new chemistries and the effects of regulation continually favour the emergence of new coating technologies.

38

1.1.2 The Alternatives To 'Conventional' Technologies?

In the last 3 decades the coatings industry has been strongly affected by environmental regulation from governments in many parts of the world. This has provided an impetus for the acceptance of technologies, which have fewer ecological drawbacks. In particular, the industry has come under pressure to reduce levels of volatile organic contaminants (VOC's) emitted from industrial processes.

'Solvent' based coating systems make use of large percentages of organic solvents as viscosity reducers which must be removed after application to the substrate, in order that the film may be solidified. These organic wastes must be reduced to permitted levels for emission and annual quotas for them respected. The process of emissions control is costly to the industry and these quotas effectively restrict line capacity. New and expanding producers will be attracted to processes that circumvent this regulation. Two alternatives to the 'conventional' solvent technology have emerged which are not subject to this restriction;

- Water-borne chemistries - make use of water as the resin carrier. Water can be more safely and more cheaply emitted without risk of regulatory breach. The volatiles from such processes are much less hazardous.
- Radiation curable chemistries - make use of non-volatile functional solvents (reactive diluents). Radiation curable products are cured to form a film which incorporates the solvent and of which the final composition is approximately 100% of the original wet coat weight. No volatiles are produced.

These 'non-conventional' approaches have attracted selected markets within the coatings industry.

1.1.3 Radiation Curable Coatings

1.1.3.1 General

'Radiation Curing' is the term that has been coined to encompass the established technology of Ultra Violet Curing and the newer technology of Electron Beam Curing. UV curing and EB curing are based on very similar chemistries but rely on different energy sources and initial reaction processes.

Radiation curable coatings may be described then, as formulations consisting of synthetic resins bearing acrylate, epoxide or vinyl ether functional groups which are capable of undergoing polymerisation induced by high energy ultra violet light or by electron beam radiation. The final product is typically a highly cross-linked, hard, glossy film.

Radiation curable coatings may be pigmented as in the case of inks, or clear as in the case of over print varnishes and wood coatings. Their purpose may be aesthetic, or functional. The advantages and disadvantages of radiation curable coatings are compared in Table 1.1-2.

	Advantages	Disadvantages
Technical	• very fast curing • high cross linking density produces a hard strong film	• curing process difficult to study • poor adhesion to plastic and metal substrates (free radical) • high shrinkage • high viscosity diluents produce rheological limitations • limited film thickness with pigmented formulations (UV) • poor exterior durability due to photodecomposition • discoloration of clear films over time due to residual photoinitiator fragments (UV)
Commercial	• low capital cost (UV) • low unit cost of coated product • low energy costs • special properties obtained - high gloss, good chemical resistance • less space required • no emission costs	• high capital cost (EB) • high unit cost of materials • factory processing only • 'line of sight' curing - difficulty with 3D objects • re-working difficult
Regulatory	• no emission quotas - no VOC's • plant planning permits more easily granted	• safety issues in handling and shipment of materials • restricted list of materials approved for use

Table 1.1-2   Advantages and disadvantages of radiation curing technologies

41

1.1.3.2 The Radiation Curing Market In The 1990's

In 1990 the world market for radiation curable materials was estimated [2] at 70,000 metric tonnes of which 62% was accounted for by Western Europe and North America in equal proportions. In the previous 5 years growth had been estimated at 2-3000 metric tonnes per annum.

The principal driving force behind the expansion of the radiation curing industry is evidenced by the markets [2], , in which radiation curable products have found application: graphic arts and food packaging, wood coating and off-line varnishing, see Table 1.1-3.

Sector	consumption of radiation curable materials
Graphic Arts	40%
Wood Finishing	20%
Off line varnishing	30%

Table 1.1-3   **Principal uses for radiation curable materials**

The market has been created by the customers' interest in the high gloss finishes and superior chemical resistance offered by radiation curable products.

At the same time, capacity has been made increasingly available because producers have seen the market potential and the economic advantage offered by radiation curing technology over more established coating technologies. Radiation curing is a very fast and relatively low cost process. Higher line speeds, reduced energy costs and space savings have combined to reduce the unit cost of a coated product despite the higher costs associated with base materials.

Nevertheless, the tendency of many radiation curable systems to shrink on curing and the poor adhesion of these materials to plastic and metal, have accounted for the limitation of this technology to paper and wood coating products (and in Japan, electronics). Radiation curing, although a rapidly expanding sector, remains a niche that, in North America for example, accounted for only about 3% of the industry volume in 1996 [3].

While suppliers of radiation curable products have made great play to the coatings industry of the 'green' aspects of the technology, industry studies have shown that these advantages - although clearly recognised - have not motivated the growth in the sector[4]. The predominant issue has been economics.

However, analysts of radiation curing predict that new and upgrading producers, experiencing an increasing impact of regulatory issues on the economics of technology selection, will be opting more and more in the future for 'non-conventional' approaches. This shift will benefit the radiation curing industry and sustain market expansion [5]. One forecast [3] anticipates a doubling of the market size in Europe for acrylic resins within 10 years of 1995.

Areas in which the largest growth potential have been identified [4] are in medical devices and electronics packaging, which have been expected to grow annually at rates of 45% and 35% respectively between 1995 and 1999.

1.2 CATIONIC POLYMERISATION – POLYMERISATION INDUCED BY ACIDIC SPECIES

Cationic polymerisation has been defined as "chain growth reactions promoted by active species possessing electrophilic character" [6].

Chemically induced polymerisations of this type involve the formation of unitarily charged carbo-cations, or similar species as the fundamental intermediate. They proceed via two-electron transpositions i.e. heterolytic bond cleavage and formation. They therefore involve fairly stable intermediates and propagation through step-wise addition, with transfer of the active centre. The reaction proceeds in a highly specific or 'controlled' manner, involving only functional groups capable of sustaining formal charge.

By contrast, see Table 1.2-1, free-radical polymerisations involve highly reactive unpaired electrons. The polymerisation is thus mediated by addition of activated functional groups and by random homolysis and recombination throughout the medium.

Cationic	Free Radical
• paired electrons	unpaired electrons
• heterolytic cleavages	homolytic cleavages
• charged intermediates	uncharged intermediates
• long(er) lifetimes	short lifetimes
• less reactive	highly reactive

Table 1.2-1   **Comparison of basic chemical processes in free radical and cationic chemistries**

Two classes of substrate have been exploited for cationic polymerisations, namely cyclic ethers (particularly epoxides) and vinyls (particularly vinyl ethers).

The carbo-cation or carbonium ion is generated via attack of a protic acid, or other electrophile, on an electron-rich centre. The species so formed is termed an 'activated complex'.

44

1.2.1 Polymerisation With Protic/Brønsted Acids

1.2.1.1 Basic Processes

With protic acids the cationation step proceeds as follows, Scheme 1.2-1, [1,7,8,9]:
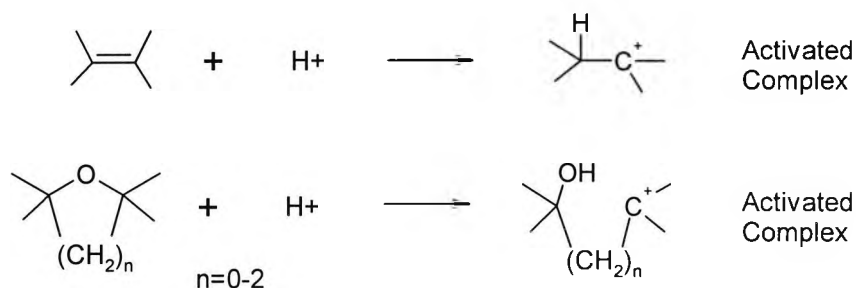
Scheme 1.2-1   **Formation of carbo-cation activated complex**

Propagation (Scheme 1.2-2) may then be envisaged as a sequential addition reaction with chain elongation and regeneration of the cation:
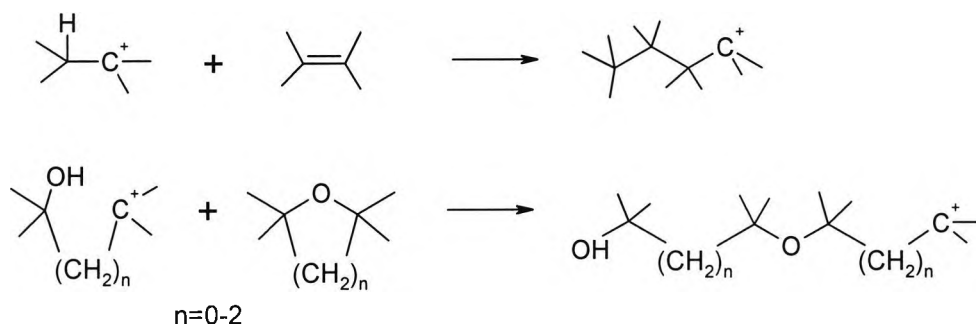
Scheme 1.2-2   **Propagation through a carbo-cation intermediate**

The reaction can thus be viewed [1,6,10,11] as an S_N1 type process in which the nucleophile, is an electron-rich site on the incoming monomer (Π-bond electrons in vinyls, lone pair electrons in epoxides), and the electrophilic centre is the activated complex carbocation at the α-end of the activated complex. The electrophilicity of the activated complex is thus achieved by loss of valence electrons, effectively to the proton.

Although the carbocation is a relatively stable intermediate, the S_N1 mechanism has limited application to epoxides, and is known for only a few simple examples. Epoxides are more commonly thought to proceed through a tertiary oxonium ion intermediate in an S_N2 process [1,6,12].

The electrophilicity of the activated complex is likewise achieved by loss of valence electrons to the incoming proton, but in this case by over-coordination of the oxygen, Scheme 1.2-3.

$$\triangleright O \ + \ H^+ \ \longrightarrow \ \triangleright \overset{+}{O}-H \qquad \text{Tertiary Oxonium Ion}$$

Scheme 1.2-3   **Formation of oxonium ion activated complex**

Propagation then proceeds via nucleophilic attack by the incoming monomer, Scheme 1.2-4:

$$H-\overset{+}{O}\triangleleft_{d^+} \ :O\triangleleft \ \longrightarrow \ \overset{OH}{\underset{O\triangleleft}{\vert}}$$
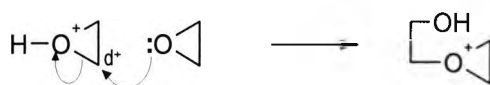
Scheme 1.2-4   **Propagation through an oxonium ion intermediate**

The α-carbon of the activated complex is electron deficient and is therefore susceptible to nucleophilic attack. Carbon-oxygen bond formation occurs with cleavage between the oxonium oxygen and the α-carbon. The oxonium ion is thus transferred.

Regardless of whether the intermediate is a carbo-cation or an oxonium ion, the thermodynamic driving force behind this process is the same - in cyclic ethers the release of ring strain. Larger rings are also susceptible [13], notably oxetanes and hydro-furans (THF), Figure 1.2-1.

Epoxide   Oxetane   Tetrahydro-furan
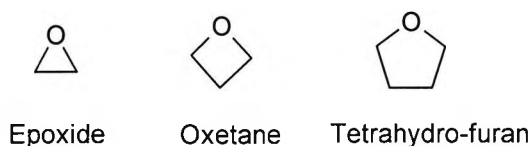
Figure 1.2-1   **Cationically polymerisable monomers**

1.2.1.2 Counterion Stabilisation

In practice the carbocation or oxonium ion requires stabilisation by the presence of a counterion, which in the case of protic acids, is the complex anion obtained from dissociation of the latter. Propagation therefore proceeds by maintaining oxonium/carbocation-anion interaction and translation of the anion with chain elongation, Scheme 1.2-5.

$$HX \rightleftharpoons H^+ + X^-$$

$$H^+ + X^- + \triangle\!\!O \longrightarrow \underset{\triangle}{\overset{H}{\underset{|}{\overset{|}{O}}}}{}^+ \cdots X \xrightarrow{\triangle\!O} \overset{OH}{\underset{\triangle}{\underset{O}{|}}}{}^+ \cdots X$$
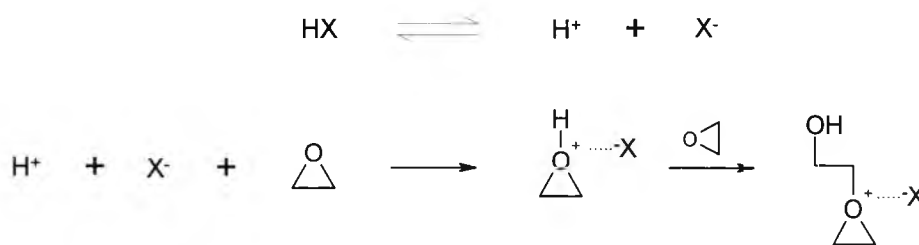
Scheme 1.2-5   Role of counterion in cationic polymerisation

The nature of the anion has been shown [13-18] to have a very significant impact on the rate and extent of polymerisation and the molecular weight and yield of polymer obtained.

For polymerisation to proceed effectively, the anion should have limited nucleophilicity maintaining a charge separation sufficient to stabilise the oxonium or carbo-cation but enabling preferential nucleophilic attack by the monomer. A counterion more nucleophilic than the monomer will promote ring opening and anion addition without chain extension [19B], by displacement of the oxygen from the α carbon, deactivating the complex and restoring the binary valence of oxygen, Scheme 1.2-6.

$$Cl^- \underset{\triangle}{\overset{H}{\underset{|}{\overset{|}{O}}}}{}^+ \longrightarrow \overset{OH}{\diagup}\overset{Cl}{\diagdown}$$
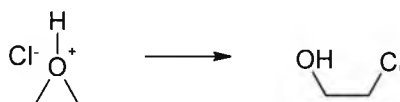
Scheme 1.2-6   Epoxide ring opening and addition (deactivation) with nucleophilic counterion

Studies have shown that efficiency of polymerisation follows the reverse order of nucleophilicity of the anion [13-18], Figure 1.2-1.

i.e.

Cl^-	NO_3^-	BF_4^-	PF_6^-	
high				low

nucleophilicity

low				high

polymerising efficiency
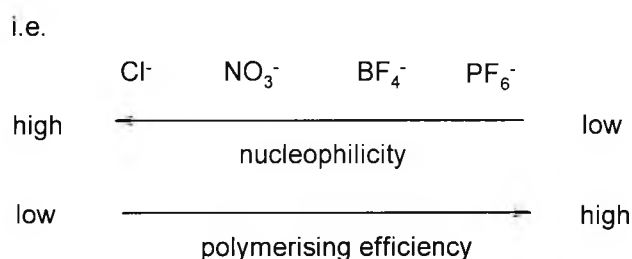
Figure 1.2-2   Relationship between counterion nucleophilicity and polymerising efficiency

1.2.1.3 Some Thermodynamic Considerations

The transition state of the activated complex can be described by 3 resonance hybrids and an examination of these hybrids will provide information as to the outcome of the

47

reaction with the incoming epoxide, Scheme 1.2-7.
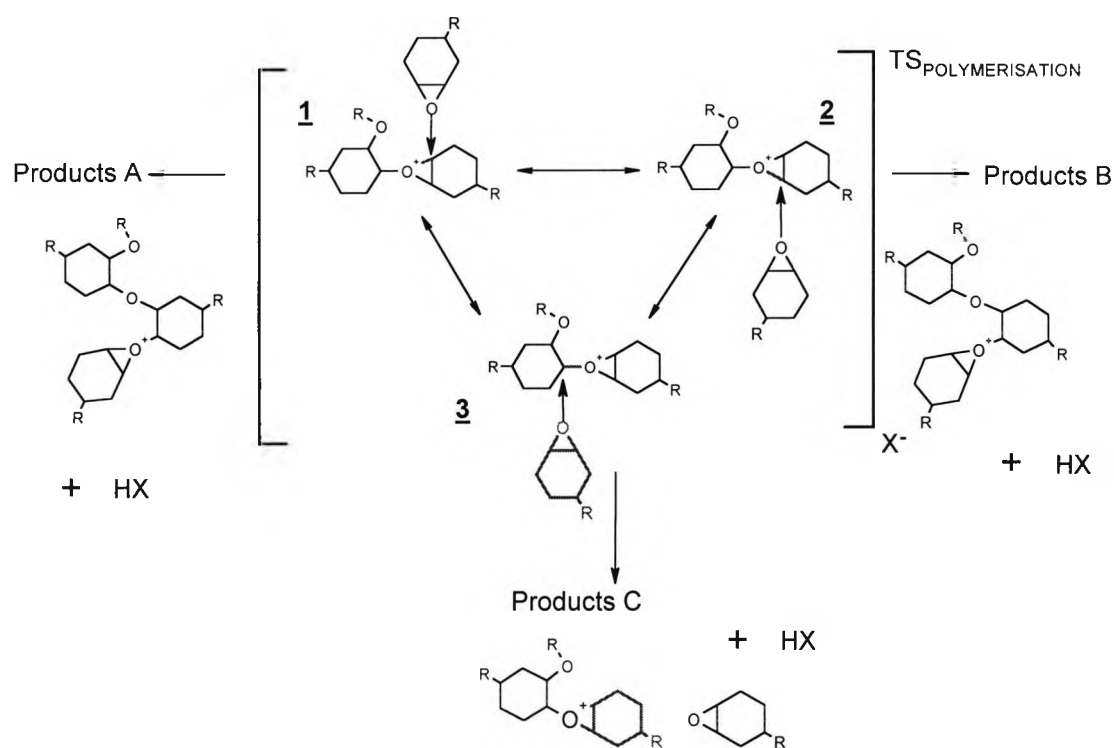
Scheme 1.2-7   **Resonance stabilisation of the oxonium ion transition complex**

Products A and B are essentially identical and the thermodynamic driving force behind the process will be the release of ring strain from the activated epoxide resulting in a negative ΔH for the reaction. These products are thermodynamically favoured, Figure 1.2-3.

It is clear that the energy barrier associated with this transition state, TS, will be largely affected by steric factors as the incoming epoxide monomer is bulky and must compete for space in a volume also occupied by complex anion, X^-, which is required for stabilisation.
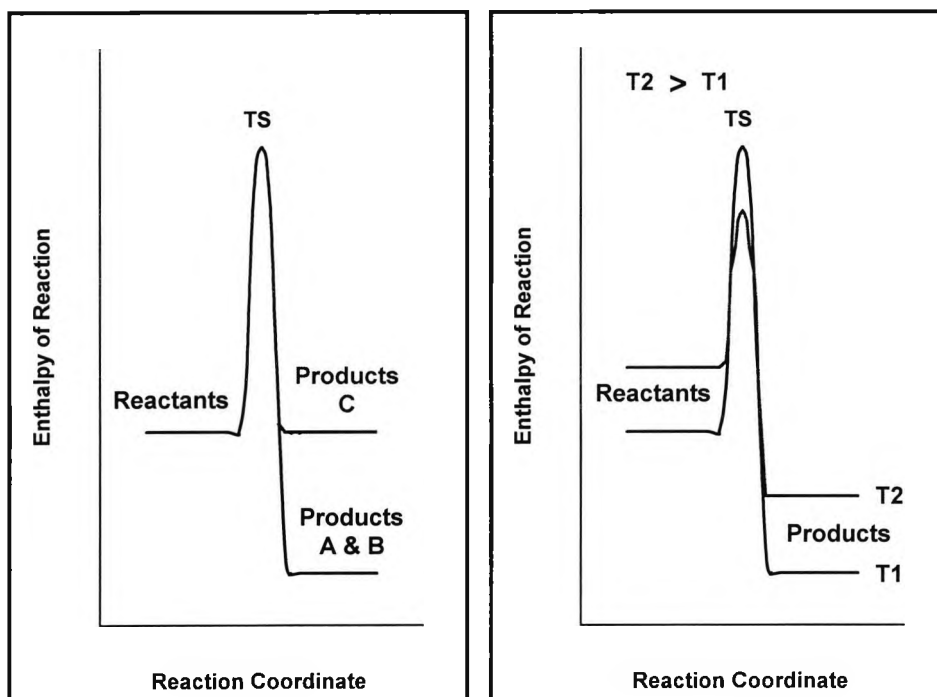
Figure 1.2-3   **(left) Comparison of schematic thermodynamic profiles for routes A/B (release of ring strain) and route C (no ring strain release)**

Figure 1.2-4   **(right) Effect of increased temperature on schematic thermodynamic profile for routes A/B (release of ring strain)**

This energy barrier will be strongly reduced by factors which increase the mobility of monomer (viscosity) or which permit an increased separation of charges (dielectric permittivity). Both of these factors are substantially dependent on temperature. Increasing the temperature will reduce the viscosity of the medium, increase the dielectric permittivity, permitting increased charge separation and increased mobility. Both of these factors will reduce the steric interaction, lowering the energy of the transition complex and accelerating the former reaction, Figure 1.2-4.

Consistent with this description, various studies have shown that polymerisation (a) is attended by a substantial exotherm [19,20,21] and (b) the reaction proceeds more rapidly at higher temperatures [20,22,23].

1.2.2 Polymerisation With Lewis Acids

Initiators comprising or generating Lewis acids have also been successfully employed to achieve polymerisation of cationically polymeriseable monomers[16]. Much work has been done to elucidate the mechanism with such species, and several reviews have attempted to organise these findings coherently [7,24,25].

Nevertheless the field remains unclear and authors readily admit that theories rely upon considerable speculation.

However, consensus exists concerning a crucial point:

Lewis acid initiators require a protogen, water or alcohol, to provide the de facto initiating entity. Such materials are said to be adventitious contaminants in most commercially supplied resins.

This finding arises principally from the work of Plesch [26] who showed that systems having reduced water (*sic rigorously dried*) do not polymerise readily with Lewis acid catalysts. Subsequent addition of water or other protogen accelerates the process immediately.

Furthermore, Kennedy [7] has also pointed out that the necessary concentration of water required for polymerisation is in fact below the limit of analytical detection. Consequently polymerisation with Lewis acids in the absence of water has never been verifiably achieved.

The mechanism is thus presumed [10,11,19A,27] to be of the type, Scheme 1.2-8:
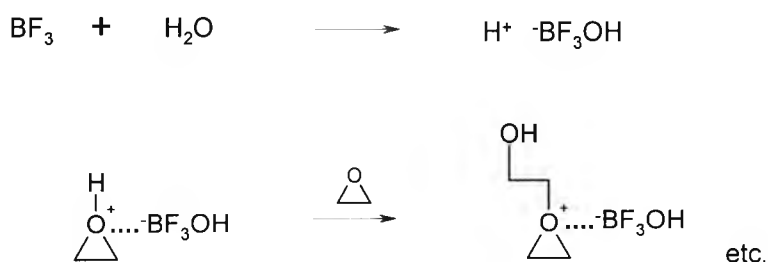
Scheme 1.2-8   **Activation and propagation with Lewis acid in the presence of water**

1.3 CATIONIC PHOTOINITIATION – PHOTOINDUCED ACID GENERATION

Numerous sources exist which describe fully the theory of elementary photochemistry. The interaction of light with absorbing matter, the nature of chemically excited states arising from internal electronic transitions following irradiation by light of the appropriate energy, and the means by which species in the excited state may return to the ground state, are all obtainable in the preliminary pages of these standard texts[28-30].

Nevertheless, it is germane to state that photochemical processes usually occur in two stages:

(a) **The primary photochemical reaction**, which is the absorption of a photon or quantum to generate electronically excited states.

(b) **The secondary photochemical reactions**, which are the generation of chemically active species from deactivation of the excited states, and subsequent reactions of these species. These reactions are also referred to as dark reactions.

In the context of cationic polymerisation, a photoinitiator may be described as a chemical entity which is capable of absorption of UV/Visible light to reach an excited state (**primary photochemical reaction**), and which is subsequently deactivated by heterolytic and/or homolytic processes to produce either a Lewis or Brønsted acid (**secondary photochemical reactions**).

These acids, as described in previous sections, are capable of bringing about cationic polymerisation in the presence of suitable monomers. Cationic photoinitiators may thus be regarded as photo-activated "acid generators".

1.3.1 Chemical Types Of Photointiators

Several categories of cationic photoinitiators are known

1.3.1.1 Aryl Diazonium Salts - Lewis Acid Generators

The use of diazonium salts for the curing of epoxides was first demonstrated photochemically by Crepeau [31] and explored more fully by Schlesinger [32]. These salts decompose according to the Schiemann reaction [33] to release a Lewis acid, nitrogen and the aryl fluoride, Scheme 1.3-1.
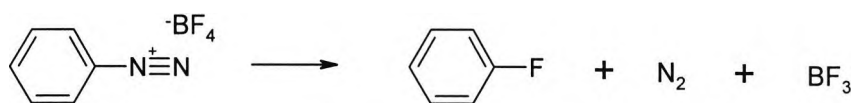
Scheme 1.3-1   **Schiemann reaction for the photodecomposition of diazonium salts**

Diazonium salts did not find widespread use in the coatings industry for at least two reasons:

- production of nitrogen limits film thickness

- poor shelf life of formulations - thermal polymerisation is reported in the literature which contributes to light-independent polymerisation

1.3.1.2 Di-Aryl Iodonium Salts And Tri-Aryl Sulphonium Salts - Brønsted Acid Generators

Diaryliodonium salts (1) were first used as curatives of epoxides by Crivello and Lam [14], and these were quickly followed [22] by the successful development of Triarylsulphonium salts (2), See Figure 1.3-1. Both have strong absorptions in the 230-260nm range.

$X^- = PF_6^-, AsF_6^-, SbF_6^-$
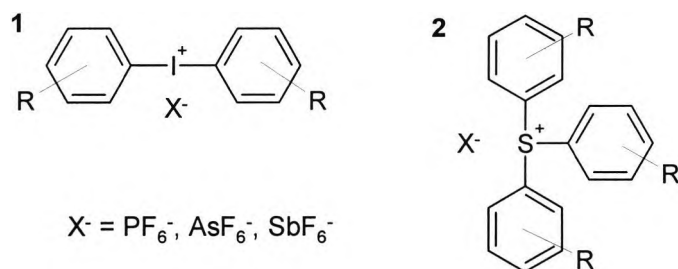
Figure 1.3-1   **Diaryliodonium (1) & Triarylsulphonium (2) salts**

Both types are presumed to generate the Brønsted acid HX. The direct photolysis and decomposition of the cation has been the subject of many investigations, which are discussed later. Both types have the advantage over diazonium salts that they do not produce nitrogen and are thermally stable.

Diphenyl iodonium salts are known to produce benzene, Iodobenzene and 4-iodobiphenyl, Scheme 1.3-2 [34-36].
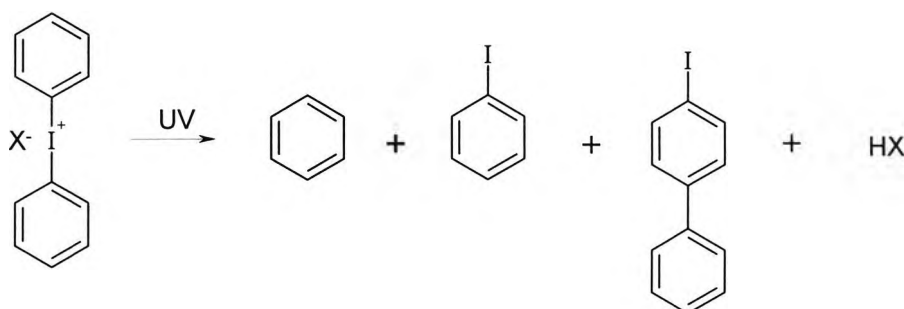
Scheme 1.3-2   **Principal photo-decomposition products of diphenyliodonium salts**

Triphenyl sulphonium salts are known [37] to produce benzene, diphenyl sulphide, and phenyl substituted diphenylsulphides, Scheme 1.3-3.
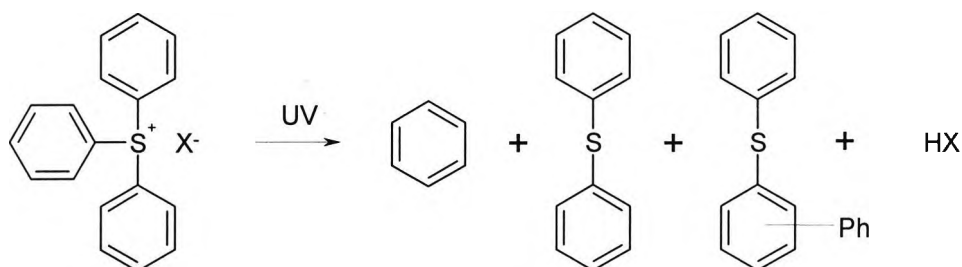
Scheme 1.3-3   **Principal photo-decomposition products of triphenysulphonium salts**

Various counterions have been studied and the most successful polymerisations were obtained [13,15] with hexa-fluoro group V elements:

i.e. $X^- =$ PF_6^-, AsF_6^-, SbF_6^-

The success of these complex ions in cationic poymerisation is attributed [11,13] to their low nucleophilicity and high stability to decomposition.

1.3.1.3 Organometallic Iron Arene Complexes – Lewis Acid Generators

The most recently introduced class of commercially available photoinitiators are the iron arene (ferrocenium) type complexes bearing complex anions, Figure 1.3-2.

$X^- = PF_6^-$, AsF_6^-, SbF_6^- Irgacure 261
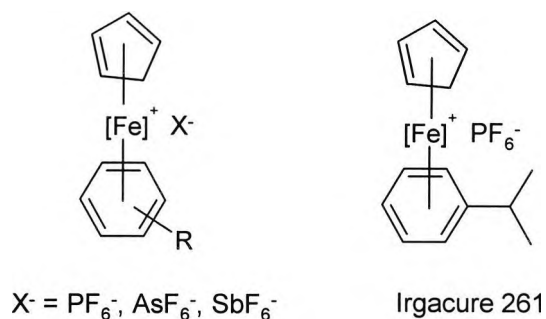
Figure 1.3-2   Iron-arene salt photoinitiators

Irradiation of these complexes results in decomposition and, in the presence of suitable monomer, to polymerisation. It is interesting that this class of photoinitiators is effective only with epoxides. The mechanism, which does not provide for the development of protic acid, was first proposed by Meier and Zweiffel [38] and is generally accepted [39], Scheme 1.3-4.
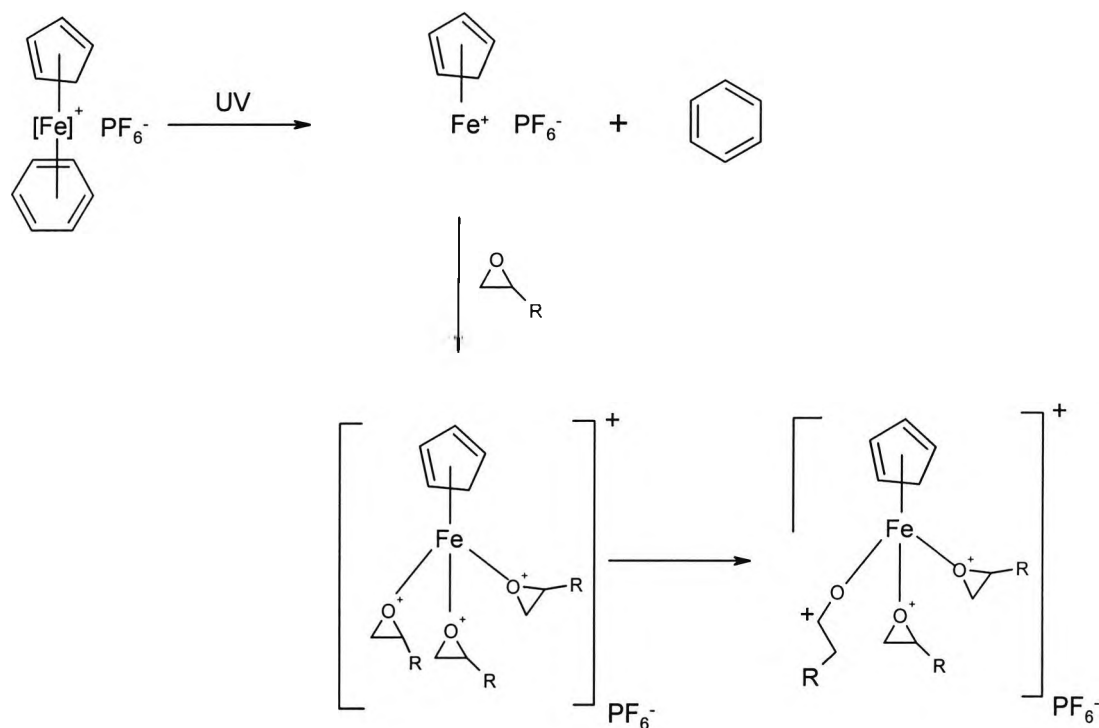
Scheme 1.3-4   Proposed reaction scheme for photo-decomposition of iron-arene salts, and polymerisation of epoxides

54

Photolysis results in the ejection of the aromatic ligand and simultaneously generates a coordinatively unsaturated iron complex. This complex has considerable Lewis acid character and co-ordinates to 3 molecules of the epoxide monomer.

Ring opening of the epoxide follows with the generation of a cationic species (not specified), which initiates a cationic chain reaction leading to the formation of a polymer.

This mechanism, however, requires clarification with the regard to the role of the counterion, the number of polymer chains which can be initiated from a single ligand shell, and the oxidation state of the iron as the polymerisation(s) get underway.

These initiators are not suitable for clear coats as they are highly coloured. They have not found widespread industry application due to the lower cure speed obtained, compared to the onium salts.

1.3.2 Onium Salt Photodecomposition – Determining The Source Of Acid

1.3.2.1 The Experimental Findings

In 1936, Fletcher and Hinchelwood [40] carried out photolysis experiments with aqueous alkali solutions of diphenyl iodonium hydroxide and determined some of the photo-products.

In 1960, Irving and Reid [41] determined some of the photo-products for diphenyliodonium iodide in CCl_4.

In 1965, Banks [42] confirmed the ionic nature of the iodonium class of compounds, reporting the decomposition of diphenyl iodonium chloride in the solid state and the instability of organic solutions of some iodonium salts in the presence of ultra violet light.

For diphenyliodonium salts, Crivello proposed a dual photolysis mechanism [13] to account for the products obtained, and a polymerisation mechanism, Scheme 1.3-5, which became widely accepted, [43-45].
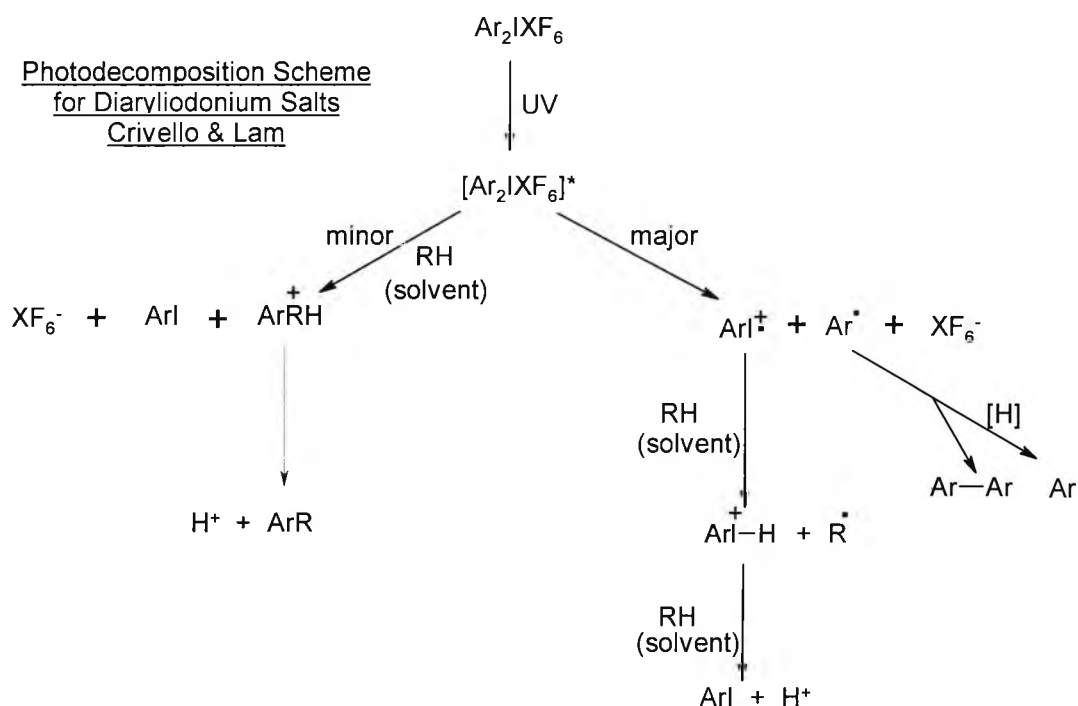
Scheme 1.3-5   **Photodecomposition scheme for diaryliodonium salts: Crivello and Lam, 1977**

Nevertheless, by the late 1980's a lack of consensus was becoming apparent in the literature as a substantial body of sometimes-contradictory work accumulated, supporting alternatives or modifications to the Crivello mechanism [27,34,46,47].

It is perhaps worth summarizing, in an empirical manner, the main evidential findings arising from work in this field.

The salt is essentially ionic in nature [42]

UV irradiation of salt solutions results in decomposition of the cation.

- Crivello [13] demonstrated the disappearance of the cation by 1H NMR of ring-substituted diaryl iodonium salts.
- Hacker [34] followed the disappearance of the cation photometrically by complexation of the cation with cobalt thiocyanate.

The main decomposition products are benzene, iodobenzene and acid (H+)

- Knapczyk [36,48] irradiated Diphenyliodonium chloride, nitrate, and tetrafluoroborate in ethanol and determined the products by GC.

$$\text{Eg.} \quad PhINO_3 \longrightarrow \quad PhI \, [96\%] \quad + Ph \, [89\%] \quad + HNO_3 \, [92\%]$$
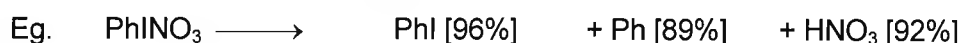
- Crivello [13], obtained similar results showing that PhI is the main product and normally disappearance of salt and appearance of PhI are concomitant.
- Hacker[34], obtained similar results by GC.

The decomposition process involves some free radical processes

- Knapczyk [36] reported large reductions in the chemical yields of benzene and acid in the presence of oxygen. Yields of iodobenzene were slightly reduced. Knapczyk interpreted the reductions in the yield of acid, benzene and iodobenzene as strong evidence that the decomposition process proceeded via a free radical pathway.
- Crivello [13] reported that the yield of iodobenzene was unaffected by the presence of oxygen. Crivello asserted that the major decomposition pathway was mediated largely by free radical species, and explained the lack of interference by radical traps on iodobenzene formation, and the lack of oxygen inhibition on iodobenzene formation, as indicating a free radical route involving very few steps.
- Ketley and Tsao [19A] reported that acrylates are polymerised when irradiated in the presence of onium salts. Since the ionic polymerisation of acrylates is unknown, the polymerisation of acrylates in the presence of onium salts would indicate that onium salt photodecomposition occurs with the appearance of some free radical species, in addition to the acid, HX.
- Pappas [46] reported the identification of the phenyl iodide radical cation, $PhI^{\bullet+}$. Homolytic fragmentation of the salt to generate the phenyl radical and the phenyl iodide radical cation is implied as a major step in the process.

57

The decomposition process involves some ionic processes

- Crivello [13] showed that the yield of PhI was unaffected by the presence of a radical trap (and inferred a very short FR pathway, similar results were obtained with sulphonium salts [16]). Crivello also proposed a minor (ionic) pathway via heterolytic fission of the cation, which could produce iodobenzene involving a solvent molecule. This process would not be affected by oxygen but does not imply the aryl cation.

- Knapczyk [36] reported the isolation of small quantities of chlorobenzene and phenoxy-ethane from a photolysed ethanol solution of diphenyl iodonium chloride. This would suggest the formation of the aryl cation.(Knapczyk considered the yield of chlorobenzene (1.1-1.6%) and phenoxyethane (0.43%) too low to suppose the formation of an aryl cation or to indicate an ionic route.)

- Davidson and Goodin [47] obtained significant yields (17%) of fluorobenzene from a photolysed methanol solution of diphenyl iodonium tetrafluoroborate. This would require the formation of the aryl cation in the presence of the BF_4^- ion, Scheme 1.3-6.

$$Ph+ \quad + \quad BF_4^- \text{--------}\rightarrow PhF \quad + \quad BF_3$$

Scheme 1.3-6   **Fluorobenzene formation from photo-decomposition of phenyldiazonium tetrafluoroborate: Davidson and Goodin**

- Hacker [34] found that following photolysis in the presence of the chloride anion in aqueous acetonitrile, PhCl accounted for 13% of escape products.

Decomposition products arise from long-lived 'cage escape' intermediates

- Crivello [13] showed that when mixed solutions of differently substituted diaryl iodonium salts are photolysed, 'crossover' recombination products are obtained containing fragments originating from a combination of source salts, Scheme 1.3-7. 'Photolysis of diaryl iodonium salts produces intermediates which are sufficiently long-lived to diffuse outside the solvation shell' or 'cage' and form 'cage escape' recombination products. Crivello accounted for all products by 'cage escape' processes'.
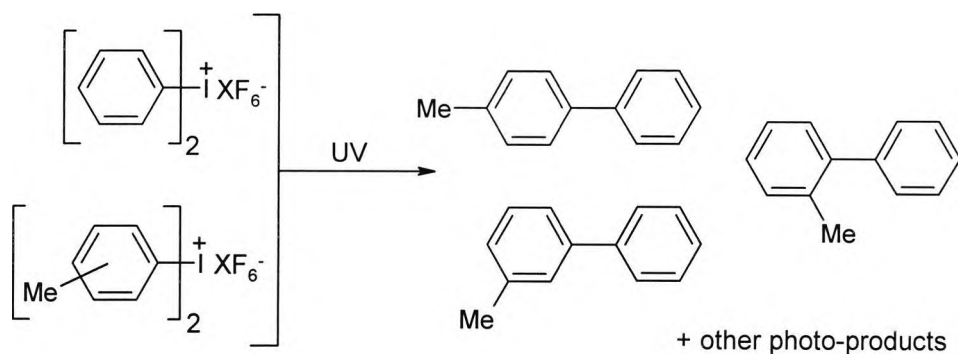
Scheme 1.3-7   Formation of 'cross-over' escape products from photodecomposition of mixed aryliodonium salts: Crivello

The pre-irradiated salt is only partly dissociated in most solvents and in pre-polymer formulations higher aggregates probably predominate [49]

Decomposition products arise from 'in cage' recombination/rearrangement processes

- Pappas [11,27,46,50,51] detected iodobiphenyls among the photolysis products from low concentration salt solutions. Due to the low concentration of the salt solutions irradiated (0.03M), the probability of iodobiphenyl being formed by 'cage escape' fragments was thought to be low. Each iodobiphenyl was considered to have arisen from the immediate recombination, within a solvent shell or 'cage', of the primary intermediates formed from the parent diphenyl iodonium salt, Scheme 1.3-8. The recombination step allows for the formation of a stoichiometric quantity of iodine containing products (not necessarily iodobenzene), and is consistent with the observation that the quantum yield of iodobenzene is less than the quantum yield of acid.
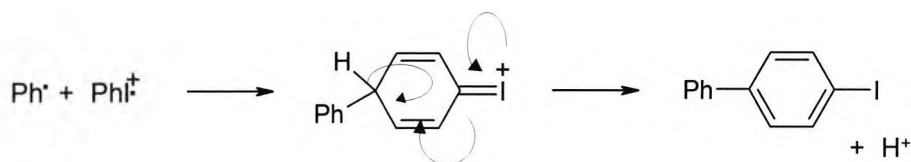
Scheme 1.3-8   Formation of iodobiphenyl from 'in-cage' recombination processes in the photodecomposition of diphenyliodonium salts

59

Anion does not participate in the photodecomposition of the salt and anion selection has no impact on the photosensitivity or UV\VIS absorbance of the salt

- Crivello [13-15] showed that the quantum yield of photodecomposition (PhI yield) is unaffected (0.20-0.22) by the choice of anion in the photolysis of di-tertbutylphenyliodonium salts of PF_6^-, AsF_6^- and SbF_6^-. The same is true for triphenylsulphonium salts.

- Photoproducts are the same regardless of the choice of anion.

- Irving, Turner and Reid [52] showed that UV/VIS absorbance of iodonium cations is insensitive to the selection of the anion. The anion itself is UV inactive.

Anion selection has strong impact on rate and extent of polymerisation

The effect of anion variation on the polymerisation has been studied in several ways:

- Gravimetric and GPC measurements; polymerisation of epoxybutane and epoxy propane using diazonium salts of BF_4^-, PF_6^- and SbF_6^- [16].

- Gravimetric and GPC measurements; polymerisation of THF in chloroform using DPI salts [13,14].

- Gravimetric and GPC measurements; polymerisation of styrene oxide and cyclohexene oxide using TPS salts of BF_4^-, PF_6^-, AsF_6^-, SbF_6^- [15].

- Determination of maximum attainable line speed; polymerisation of divinyl ethers using TPS salts with the counterions PF_6^- and ClO_4^- [17].

- DSC; polymerisation of divinyl ethers using TPS salts of PF_6^- and SbF_6^- [18].

The consistent picture emerging from these studies is that anion choice has a significant impact on rate of polymerisation, degree of conversion and molecular weight of polymers obtained. These aspects always follow the trend:

$$ClO_4^- < BF_4^- < PF_6^- < AsF_6^- \ll SbF_6^-$$
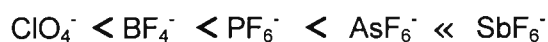
This is generally attributed [11] to (1) the order of anion nucleophilicity being in the reverse of the above order and (2) the stability of the anions being also in the reverse order. There will be corresponding participation in the following termination reaction.

i.e. Participation $SbF_6^- > ClO_4^-$

Anion survives irradiation intact

Crivello [13-15] found no evidence to support, as in the case of aryl diazonium salts, the formation of Lewis acids i.e. a fluorinated aryl compound. Thus lacking any trace of fluorinated photolysis products he presumed the cation to remain intact. Crivello [13] also claimed to have recovered HXF_6 in photo-products.

Initiating species is long-lived and polymerisation reaction is photo-independent

- Pappas and Jilek [43,53] found that the pre-irradiated solution of photoinitiator could polymerise monomer (cyclohexene oxide) in the dark.

Initiating species could be HXF_6

- Pappas and Jilek [43,53] showed that addition of hexafluoroantimonic acid to monomer samples results in rapid polymerisation.
- Crivello [15] stated that since counterions remain intact (sic) they must be the ultimate initiators of polymerisation.

1.3.2.2 The Hacker Mechanism [24,35,37,54-58]

Hacker and co-workers have put forward a comprehensive theory to explain their own experimental contributions and the plethora of observations made by previous workers:

1.3.2.2.1 Iodonium Salts – Cage Escape Processes

Excitation of the diarylhalonium salt results in a singlet excited state which may fragment homolytically or heterolytically. Heterolytic fragmentation, Scheme 1.3-9, is in the manner of the Crivello and Lam minor route [13], to yield the aryl iodide, the aryl cation and the counterion. The cage escape products from these intermediates are aryl Iodide, solvent

recombination products and the Brønsted acid, HX. The proton thus originates from the solvent.

$$Ar_2IX \xrightarrow{UV} [Ar_2IX]^* \longrightarrow [Ar_2IX]^1$$

Heterolytic Photodecomposition
Route for
Diaryliodonium salts
Hacker & Co-workers

$$\downarrow 1$$

$$ArI \quad Ar^+ \quad X^-$$

$$\downarrow$$

$$ArI + Ar^+ + X^-$$

$$Ar^+ + RH \longrightarrow ArR\text{-}H \longrightarrow \begin{array}{c} ArR \\ + \\ H^+ \end{array} \Bigg] \Rightarrow \begin{array}{c} Cage \\ Escape \end{array} \Big| RH\,(solvent)$$

solvent

$$\downarrow$$

$$ArI + ArR + HX$$
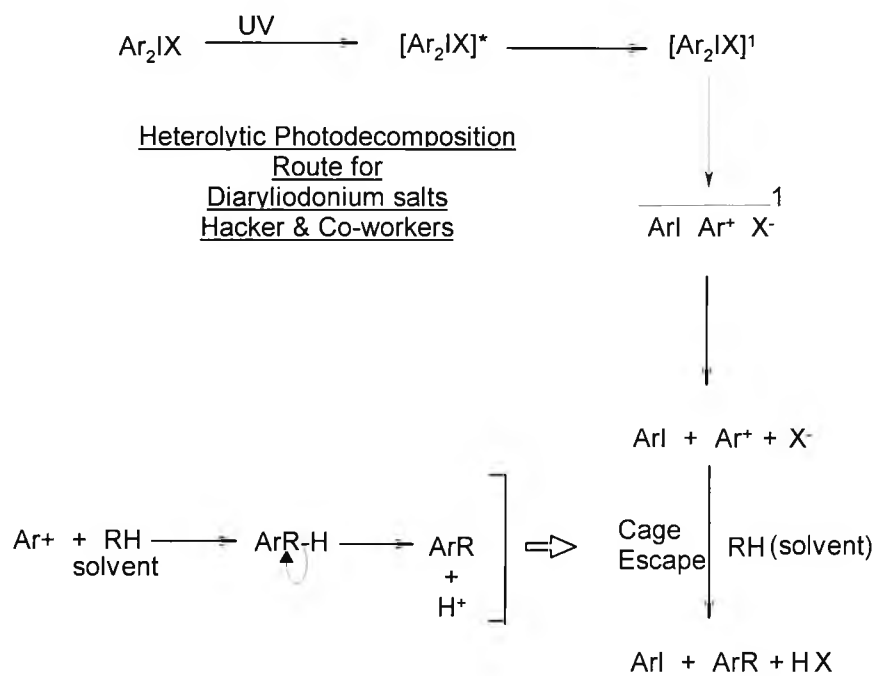
Scheme 1.3-9   Heterolytic photodecomposition route: Hacker

Electron transfer between the initial singlet intermediates may also occur to yield the aryl iodide radical cation, the aryl radical and the counterion, Scheme 1.3-10.

$$\overline{ArI \quad Ar^+ \quad X^-}^1 \quad \xrightarrow[\text{transfer}]{\text{electron}} \quad \overline{ArI^{\ddagger} \quad Ar^{\bullet} \quad X^-}^1$$

Scheme 1.3-10   Electron transfer within the singlet excited state: Hacker

The cage escape products from these intermediates are essentially those of the Crivello and Lam major route [13], which is a homolytic pathway, Scheme 1.3-11; namely benzene (or aryl substituted analogue) aryl iodide, solvent recombination products and the acid HX. The proton likewise originates from the solvent.

$$Ar_2IX \xrightarrow{UV} [Ar_2IX]^* \longrightarrow [Ar_2IX]^1$$

Homolytic Photodecomposition
Route for
Diaryliodonium salts
Hacker & Co-workers

$$\overline{ArI^{\ddagger} \quad Ar^{\bullet} \quad X^-}^1$$

$$ArI^{\ddagger} \nearrow H{-}R$$
$$\downarrow$$
$$ArI^+{-}H + R^{\bullet}$$
$$\downarrow$$
$$ArI + R^{\bullet} + H^+$$

$$\Rrightarrow$$

$$\Big| \quad RH \text{ (solvent)}$$

$$ArI + Ar^{\bullet} + R^{\bullet} + HX$$

$$Ar^{\bullet} + RH$$
$$\downarrow$$
$$ArH + R^{\bullet}$$

$$\Rrightarrow \quad \text{Cage Escape} \quad \Big| RH \text{ (solvent)}$$

$$ArI + ArH + ArR + HX$$
$$+ RR + ArAr$$
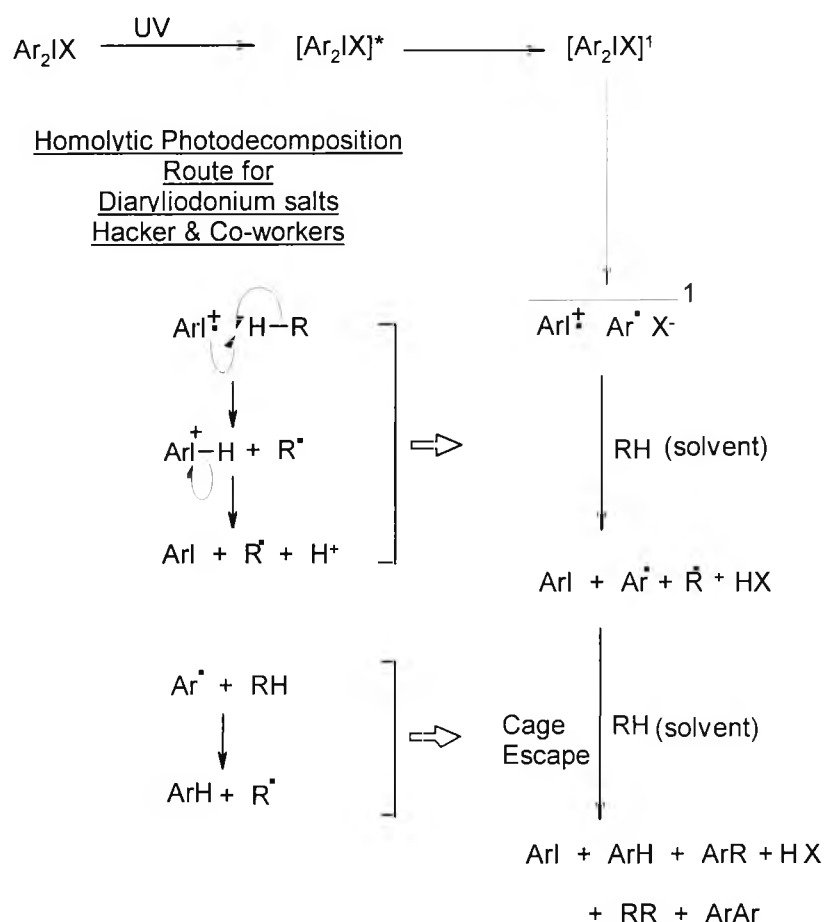
Scheme 1.3-11   Homolytic photodecomposition route: Hacker

The role of a second molecule of solvent accounts for the reduction of the aryl radical to benzene (or analogue), and accounts for the various aryl-aryl, aryl-solvent and solvent-solvent recombination products that have been obtained.

63

The cage escape products, both homolytically and heterolytically derived, will predominate in dilute solutions. Polar solutions will favour the heterolytic route and non-polar solutions the homolytic route. In the presence of an unstable anion such as the tetrafluoroborate, (i.e. $X=BF_4^-$), the detection of aryl fluoride in polar media is accounted for by Davidson & co-workers [47].

1.3.2.2.2   Iodonium Salts – In Cage Recombination Processes

Cage recombination products are also possible from the initial singlet intermediates by heterolytic transpositions, and from the intermediates obtained following electron transfer, by homolytic transpositions. These are, essentially, the processes proposed by Pappas and co-workers, Scheme 1.3-12 [11,27,46,50,51].

Heterolytic Transpositions

Heterolytic & Homolytic Recombination Products
in the Photodecomposition of Diaryliodonium Salts
Hacker and Co-Workers

+ H$^+$

Homolytic Transpositions
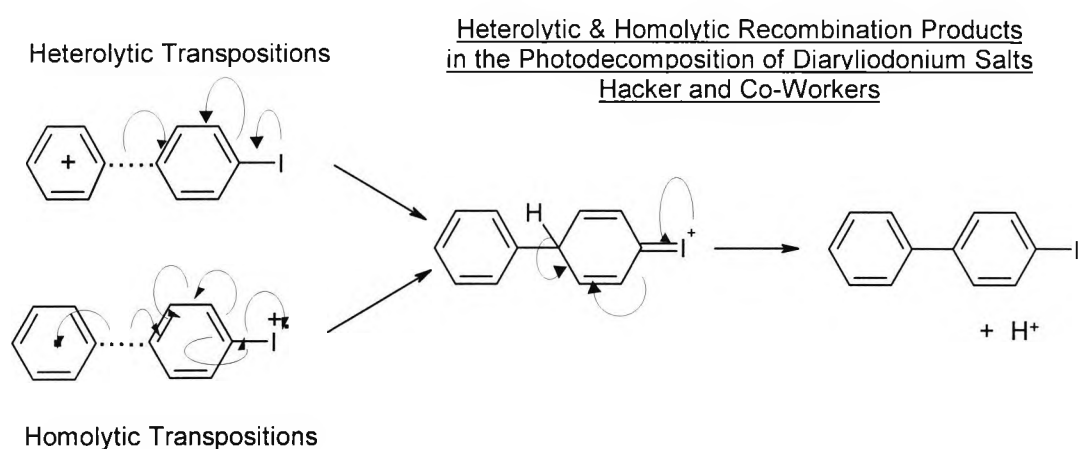
Scheme 1.3-12   Recombination pathways leading to the formation of iodobiphenyl following the photodecomposition of iodonium salts: Hacker

It is interesting to point out that these recombination processes account for the production of acid, H$^+$, without the need for solvent involvement.

These cage recombination processes will predominate in viscous media such as incured and curing pre-polymer films, and following photodecomposition in the solid state. Hacker has shown [55] that cage/escape ratio of products is strongly influenced by viscosity. Furthermore he suggests that in the solid state and in most pre-polymer films, such processes may account for the totality of acid production.

1.3.2.2.3   Iodonium Salts – Processes From The Triplet State

The triplet excited state may also be reached either by inter-system crossing (ISC) or by external sensitisation, Scheme 1.3-13. Photodecomposition from the triplet excited state proceeds exclusively via the homolytic pathways as the electron transfer process does not

occur in the reverse direction. As the triplet intermediates are long-lived, triplet activated photodecomposition produces predominantly escape products.

Interconversions Between
Singlet and Triplet Excited States
Hacker and Co-Workers

$[Ar_2IX]^1$ $\xleftarrow{\text{ISC}}$ $[Ar_2IX]^3$

$\underline{\hspace{3cm}}$ 1 $\xrightarrow{\text{SSC}}$ $\underline{\hspace{3cm}}$ 3
ArI^{+} $Ar^{•}$ $X-$ ArI^{+} $Ar^{•}$ $X-$

Escape & Recombination
Products

Escape
Products
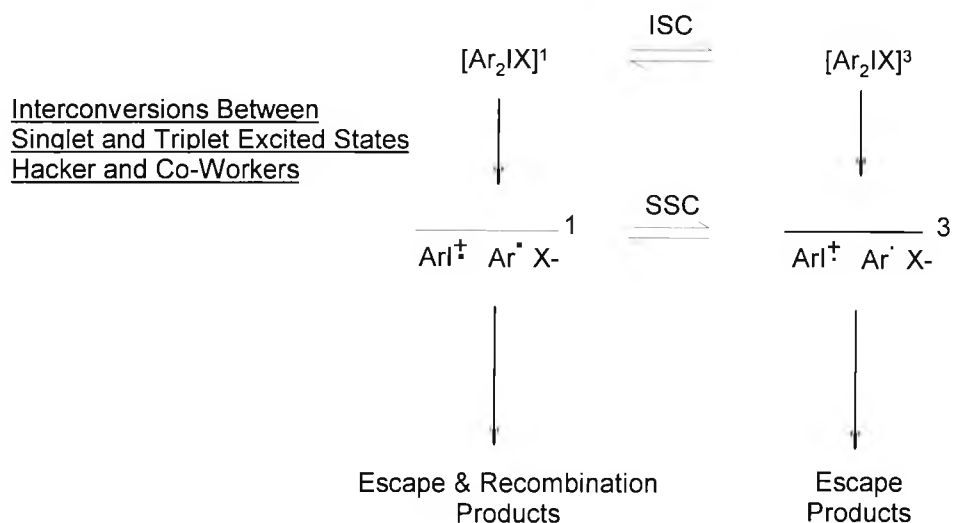
Scheme 1.3-13   Interconversions between singlet and triplet excited states: Hacker

Nevertheless by reversion to the singlet excited state of the salt by ISC, or by reversion to singlet state intermediates via spin-spin coupling, recombination products are also possible.

1.3.2.2.4 Sulphonium Salts

Similar processes account for the products obtained following photodecomposition of onium salts. Sulphonium salts, however, are not able to undergo spin-spin coupling and so triplet sensitization results exclusively in the formation of escape products. Neither do the singlet state intermediates obtained from direct excitation or ISC undergo the electron transfer reaction. Thus homolytically derived products are obtained directly from cleavage of the singlet excited state and triplet derived intermediates favour the formation of escape products.

65

1.3.2.3 Summary

Ar_2IX

UV

The Photodecomposition of
Diaryliodonium salts
Hacker & Co-workers

$[Ar_2IX]^*$

ISC

$[Ar_2IX]^1$ ⟶ $[Ar_2IX]^3$

$\overline{ArI \quad Ar^+ \quad X^-}^1$ electron transfer $\overline{ArI^{\ddagger} \quad Ar^{\cdot} \quad X^-}^1$ SSC $\overline{ArI^{\ddagger} \quad Ar^{\cdot} \quad X^-}^3$

Cage Escape Products

In-Cage Recombination Products

Cage Escape Products
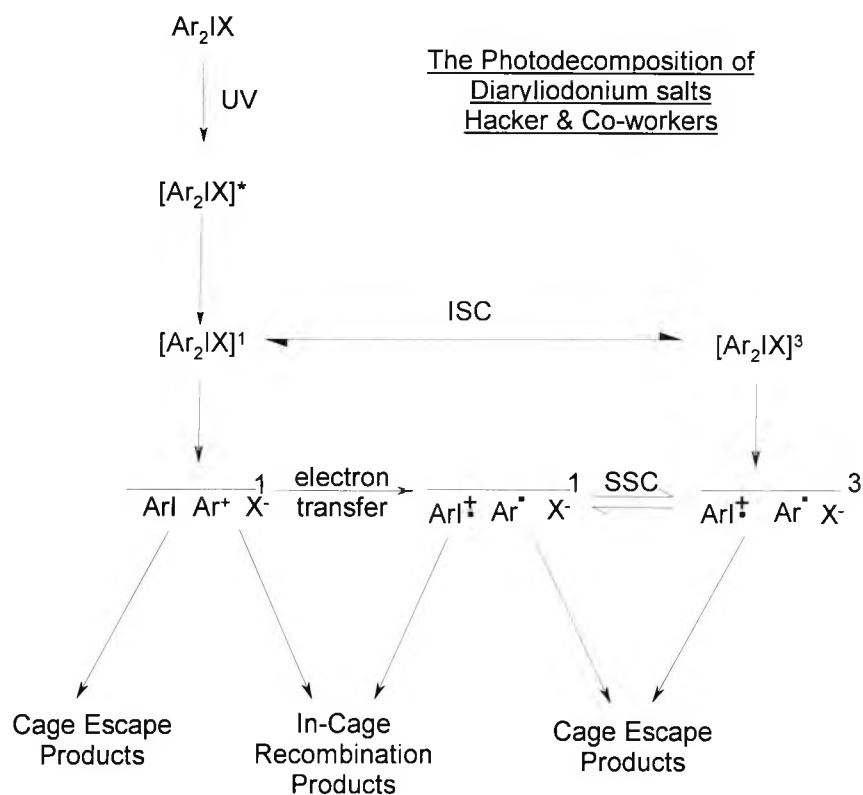
Scheme 1.3-14   **Summary of main processes in the photodecomposition of diaryliodonium salts**

1.3.3 Fate Of The Counterion - Nature Of The Acidic Species In Cationic Polymerisation

1.3.3.1 Early Work - The Intact Counterion & Brønsted Mediation

The photodecomposition of diphenyliodonium salts and of triphenylsulphonium salts have been the subject of many investigations [13-15,27,36,37,43,56]. An early and undisputed observation [36] was the production of large quantities of acid, H^+, and subsequent efforts have generally focused on the means by which the acid is produced and the fate of the cation. This mechanism has now been authoritatively determined and the organic photoproducts established [37,56].

By contrast, the fate of the anion has received comparatively little attention and the XF_6^- counterion is presumed to survive irradiation intact [11,13,15,56].

The most frequently quoted polymerisation mechanism [9-11,15,59] supposes a crucial role for the complex acid, HXF_6. In the presence of epoxides, an activated complex is obtained when the proton attacks the electron-rich oxygen of the epoxide, resulting in the formation of an oxonium ion - the 'priming' or initiation step. The positive charge thus developed on the oxygen is stabilised by the anion XF_6^- that migrates intact with the active centre, as the polymer chain is extended - propagation.

Nevertheless, very little experimental data exists to verify the fate of the counterion or to determine unambiguously the exact nature of the acidic species, which initiates and propagates polymerisation with diphenyliodonium and triphenylsulphonium salts.

Crivello [14,15], comparing photoproducts from diazonium salts with those of diphenyliodonium and triphenylsulphonium salts, contends that the absence of fluorinated photoproducts following irradiation of diphenyliodonium and triphenylsulphonium salts implies the intact anion and Brønsted mediation of polymerisation.

By contrast, the detection of fluorobenzene [60] following photolysis of diazonium salts, is seen as solid evidence, in this case, of anion decomposition and mediation – at least initially - by Lewis acid species such as XF_3/XF_5. Fluorinated photoproducts should also be obtained from iodonium and sulphonium salts (sic) if the anion, XF_6^-, were to decompose to produce the Lewis acid, XF_5 in an analogous manner. Following this reasoning, the anion remains intact and the acid species involved in polymerisation is not the Lewis acid, XF_5, but the Brønsted acid, H^+/XF_6^-.

Pappas and Jilek [43,53] also provide corroborative experimental results for the Brønsted acid, to the extent that they show that hexafluoroantimonic acid is capable of polymerising epoxide monomers when added separately in the dark. Here also, the actual active species has not been identified directly.

Secondary support for the theory of Brønsted acid mediation may be derived from the (previously discussed) work of Plesch [26] and Kennedy [7] whose combined contributions suggest that mediation by pure Lewis acid species is unlikely, and that even in cases where Lewis acids are generated initially, the ultimate polymerising species is likely to be the Brønsted acid, $HOXF_5^-/H^+$. Alternatively, but to similar effect, ^{31}P NMR evidence [61,62] has been produced which points to a reorganisation of the Lewis acid/monomer conjugate to form propagating centres with formal (positive) charges and stabilised by the Brønsted counterion, XF_6^-.

The body of experimental evidence, although limited, tends towards a universal view of cationic polymerisation mediated by Brønsted species. These may be derived directly with an intact counterion (diphenyliodonium and triphenylsulphonium salts), or indirectly with a decomposing and/or reorganizing counterion (diazonium salts).

1.3.3.2 The Fate Of The Anion Revisited - The Decomposing Counterion & Alternative Acidic Species

Nevertheless, in the case of diphenyliodonium and triphenylsulphonium salts, the theory of the intact counterion has recently been challenged by Davidson and Wilkinson [63] who have noted a disappearance of IR bands in EB-irradiated films associated with the intact counterion. Sundell [64] has also noted disappearance of the counterions in γ-irradiated solutions with the concomitant development of acid H+ equivalents exceeding 1.0 per mole of initiator irradiated.

Further experiments involving irradiation of onium salt crystals in the solid state were carried out by Wilkinson [63]. Indirect IR evidence was found for the development of HF gas (1 equivalent) and PF_5 gas. Additional HF gas (2 equivalents) is also theorized to arise from subsequent hydrolysis of PF_5.

Consistent with this explanation, the antimonate salt was also irradiated producing less significant quantities of the HF derived species. The latter result was explained in terms of the liquid and polymeric nature of SbF_5 and in terms of the stability of the latter to hydrolysis. Consequently all HF produced arises directly from the initial reorganization of the salt - 1 equivalent.

68

These findings are highly relevant to the mechanism of epoxide polymerisation in bulk media. Ledwith [49] points out that in viscous media, higher aggregates predominate. Solid-state photodecomposition is therefore likely to produce more realistic and informative data than irradiation in dilute organic media.

Wilkinson also found that epoxide films exposed to the gases produced from UV irradiation of the crystalline initiator, were polymerisable. Epoxide ring opening was measured by FTIR following the band at $792cm^{-1}$. This '3-phase' or 'remote' polymerisation was examined with a number of triphenylsulphonium salts. Interestingly the PF_6^- salt was found to achieve almost complete consumption of the epoxide with 120 mins of exposure. The SbF_6^- salt, which according to Wilkinson, produces only HF (no SbF_5), demonstrates only very limited consumption (around 7%) with the same exposure time.

Based on her evidence, Wilkinson suggests that the polymerising species may, in fact, be HF.

It is worth pointing out, however, that the published IR evidence refers only to ring opening of the epoxide, rather than polymerisation. Information on the appearance in the IR of the ether linkage band at $\sim1040cm^{-1}$ would be particularly informative in the case of the SbF_6^- salt, where the only gaseous species produced is HF. This band is associated with polymerisation.

Furthermore, ring opening with the SbF_6^- salt is very limited, and not consistent, when compared with the value obtained with the PF_6^- salt, with the theoretical quantity of HF available from photolysis, Table 1.3-1.

Salt	theoretical quantity of HF produced from photolysis	epoxide ring opening after 120 mins exposure
TPSPF$_6$	3	93%
TPSSbF$_6$	1	7%

Table 1.3-1   **Comparison of IR data for epoxide ring opening with triphenylsulphonium hexafluoro-group 5 salts after UV irradiation in the solid state: Wilkinson**

It seems likely that Wilkinson is correct to point out that the anion does in fact decompose to yield the pentahalide and hydrogen fluoride, and that the former may decompose under certain experimental conditions to yield 2 additional equivalents of HF. However it seems

more likely that polymerisation is mediated by the unhydrolysed pentahalide. Wilkinson's data with the antimonate salt could be more reasonably explained in terms of either ring opening and fluorohydrin formation and/or limited (short chain-length) polymerisation occurring at a rate secondary to the main process which is mediated by the pentahalide when available. The feasibility of HF mediated polymerisation therefore remains unproven.

In 1968, Shahak and co-workers [19B] used HF to open the epoxide ring of certain monomers with fluorohydrin production. Certain epoxides, were found to undergo polymerisation – no mechanism proposed – giving gravimetric yields as high as 60%.

However, these reactions were conducted at 0°C in anhydrous conditions in the presence of THF, which is also a cationically polymerisable monomer, as a co-solvent. Neither the chemical identity of the polymer nor the polymer molecular weights were determined.

Nevertheless, polymerisation did occur in some cases and was shown to depend on certain factors. Cyclohexene oxide was found to polymerise while 4-t-butyl-1,2-epoxycyclohexane produced only fluorohydrin. The lack of polymerisation in the latter case was attributed to the steric immobility of the t-butyl group imposing rigidity on the ring. Ring flexibility is supposed, in an unspecified manner, to be essential in preferring the epoxide for polymerisation rather than fluorohydrin formation.

If the Shahak explanation is indeed valid, the cycloaliphatic epoxide used in the Wilkinson study, would, for the same reason, resist polymerisation with HF and undergo fluorohydrin formation preferentially. In a coating, where the medium is essentially 100% monomer, ring flexibility will presumably be further restricted.

2 SOLID-STATE PHOTODECOMPOSITION

2.1 CHAPTER OVERVIEW

Mechanistic studies concerning the photodecomposition of onium salts have generally focused on the fate of the cation, and the anion is usually presumed to remain intact during photolysis and polymerisation. A trend has been established with respect to polymerising efficiency, which is usually explained in terms of anion nucleophilicity.

This chapter study addresses the fate of the anion following irradiation of the initiator in the solid state, and seeks to examine qualitatively and quantitatively the process of decomposition.

In this study, the gases evolved during the photodecomposition were subjected to gas phase FTIR spectroscopy, and following dissolution in water, to ion exchange chromatography. Information gained from these methods was then applied to the selection of an ion specific electrode, which enabled the evolution of these gases to be followed quantitatively under certain conditions of interest.

Some inferences as to the identity of the photodecomposition products have been possible. The results described in this chapter are both consistent and explanatory with regard to certain aspects of earlier studies. Nevertheless, the decomposition of the anion under UV irradiation anion is clearly demonstrated. This is a significant departure from earlier thinking which leads to the proposal that the trends in polymerisation efficiency described earlier may also be described in terms of anion stability.

2.2 <u>EXPERIMENTAL</u>

Study of the UV solid-state photodecomposition of initiators required the development of new experimental methods and equipment. These experimental methods and PTFE photodecomposition equipment are described in this section.

This section also contains details of precautionary experiments that were conducted with the PTFE photodecomposition equipment to verify that results are free of artefacts. Efforts were made (a) to determine the temperature range operative during photodecomposition experiments and verify the thermal stability of initiators in this experimental temperature range, and (b) to verify the UV opacity of the PTFE window of the cell in the region of the spectral output of the lamp. The chemical stability of PTFE to UV irradiation is considered.

2.2.1 Apparatus And Methodology

2.2.1.1 Chemicals

The following materials were obtained from Ciba Geigy, and used as supplied:

Diphenyliodonium hexafluorophosphate

Diphenyliodonium hexafluoroarsenate

Diphenyliodonium hexafluoroantimonate

Triphenylsulphonium hexafluorophosphate

Triphenylsulphonium hexafluoroantimonate

Irgacure 261,   (η^5-2,4-Cyclopentadiene-1-yl) [(1,2,3,4,5,6-η)-(1-methyl ethyl)benzene]-iron(+)-hexafluorphosphate(-1)

Irgacure 651,   2,2-dimethoxy-2-phenyl acetophenone

Irgacure 184,   1-benzoylcyclohexan-1-ol

Acetone (HPLC grade) and Dichloromethane (HPLC grade) were supplied by the Aldrich Chemical Company

2.2.1.2 Photodecomposition

Photodecomposition experiments were carried out in a custom designed PTFE cell – see Figure 2.2-1 and Figure 2.2-2.

At the centre of a solid PTFE block (15.0 cm x 13.0 cm x 6.25 cm, l x w x h) has been cut a cylindrical chamber of diameter 8.0 cm and depth 1.5 cm (volume 75.0 cm^3). The chamber is equipped with inlet and outlet lines stopped on the outside with pressure sealed PTFE fittings. The upper boundary surface of the cell consists of a PTFE membrane of diameter 10.0 cm and thickness 0.012cm to form a window. A pressure tight seal is achieved by clamping the PTFE membrane between a groove cut in the block and a rubber 'O' ring by means of a brass plate (thickness 0.4 cm) and a hexagonal arrangement of thumb screws around the cell chamber.
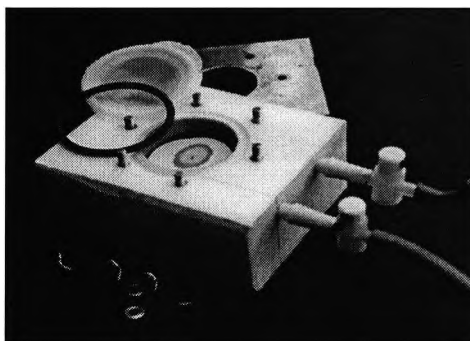
Figure 2.2-1   **PTFE solid-state photodecomposition cell - open – with initiator displayed**
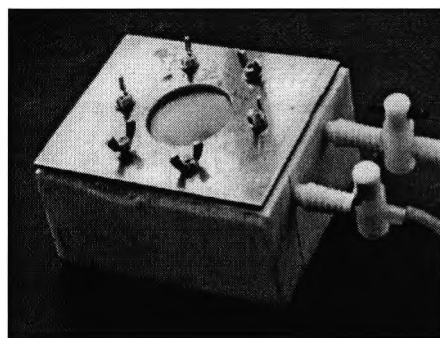
Figure 2.2-2   **PTFE solid-state photodecomposition cell – closed – during UV irradiation**

The photodecomposition cell was modified to accept a flexible wire thermocouple via a narrow channel. The channel was plugged with a commercial Araldite™ formulation that was allowed to cure to hardness.

Photoinitiator (0.1-0.2g) is dissolved in acetone (1 ml, HPLC grade) and applied drop wise to a filter disk (cellulose, PTFE or borosilicate glass fibre). The solution is evaporated to dryness above an IR lamp for about 20 minutes at 65°C surface temperature. The crystallised initiator is then stored in a drying oven at 50°C for 4-24 hours.

The initiator sample is placed in the chamber of the photodecomposition cell and the vessel sealed. After purging with dried air the chamber is isolated with a slight positive internal gas pressure. After priming the UV lamp, the photodecomposition cell is placed in the exposure compartment of the UV unit and the shutter opened. The cell is exposed for a period of 30-1200 minutes.

Continuous Irradiation was achieved using a 1500W 'D bulb' which is a medium pressure mercury halide discharge tube doped with iron iodide, (Amba Lamps AM677X). The lamp was mounted in a custom housing (Figure 2.2-3) with manual shutter (shown below with front panel detached). Output (Figure 2.2-4) was focused by an aluminium reflector. Separation of source and sample was approximately 15 cm.
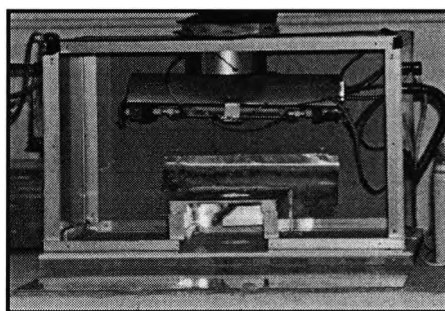
Figure 2.2-3   **UV Lamp and housing for solid-state photodecomposition experiments – front cover removed**
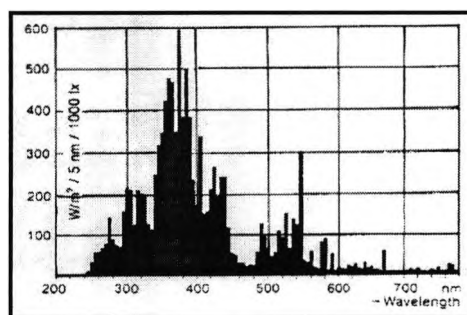
Figure 2.2-4   **'D bulb' UV spectral output for solid-state photodecomposition experiments**

The gaseous photoproducts are directed to the FTIR cell or in a continuous stream to a flask of distilled water where the resulting solution is subjected to ion exchange chromatography or conductometric analysis with fluoride ion specific electrode.

76

2.2.1.3 FTIR Analysis Of Photo-products

Infra red spectra were obtained with a Digilab FTS60 FTIR spectrometer. The scanning resolution was 8.0cm^{-1}, the aperture was OPEN and the scan speed 5 KHz. Spectra were acquired with 16 scans using a Spectra-Tech 10 cm cell with KBr windows of 0.30 cm thickness. The cell was baked at 140°C for 24 hours prior to each experiment.

The pre-baked gas cell is installed in the spectrometer and flushed with dry air. The cell is evacuated to a pressure of approximately 10 mm Hg and isolated by closing the stop cock.

The PTFE photodecomposition cell is irradiated for 30 mins and on completion is connected via a PTFE tube (60 cm) to the inlet of the IR gas cell. The spectrometer is executed to begin acquiring a 16 scan spectrum and, simultaneous with the 3rd scan, the inlet stop cock of the IR cell and the outlet stop cock of the photodecomposition cell are opened. Pressure equalisation causes a flow of the gaseous contents of the photodecomposition cell (positive pressure) into the IR cell (partial vacuum) when the 2 cells are connected. The remainder of the spectrum is acquired with the gaseous photodecomposition products in the beam path.

2.2.1.4 Ion Exchange Chromatography Of Photo-product Ions

Ion Exchange Chromatography was carried out on a Dionex 2010i chromatograph equipped with a HPICAS4A column and conductometric detector. The eluant (aqueous $NaHCO_3$, 0.00075M, and Na_2CO_3, 0.0022M) was pumped at a rate of 1.2 mlmin^{-1}. An ionic suppression solvent (H_2SO_4, 0.025M) was supplied at 2.5 mlmin^{-1} through an AG4A guard column.

The photodecomposition cell outlet is connected via a PTFE tube to a PTFE flask containing distilled water (0.4l) with dried air flowing continuously through the cell and bubbling into the water at a rate of 100 mlmin^{-1} (bubble flow meter). The cell is exposed for a period of 75 minutes.

An aliquot (1.0 ml) of the aqueous solution of photodecomposition products is diluted in a known quantity of distilled water and subjected to ion exchange chromatography against reference standards including the fluoride ion. Replicate injections are made in each case.

2.2.1.5 Conductometric Measurements With Fluoride Ion Specific Electrode, FSE

Conductometric measurement of aqueous fluoride concentration was achieved by means of a Fluoride Specific Electrode, FSE (Philip Harris,1991-cat.no.P42-8501) and Calomel Reference Electrode (Philip Harris,1991cat.no.P42-858) in conjunction with a standard pH meter (EIL 7055) and analogue continuous feed XY paper plotter.

The fluoride electrode has a response time specification of 4 seconds. The guaranteed detection limit is 1.0 x 10^{-6}M, the lower limit of linear detection being 5.0 x 10^{-6}M. The linearity is guaranteed between the pH values of 4.0 and 9.0.

The electrode and meter are calibrated as per manufacturer's instructions with NaF solutions of concentration 10^{-4},10^{-5},10^{-6}M.

The photodecomposition cell outlet is connected via a PTFE tube to a PE flask containing distilled water (0.50l) and the fluoride selective electrode, with dried air flowing continuously through the cell and bubbling into the water at a rate of 30 mlmin^{-1} (bubble flow meter). The cell is exposed for a period up to 1200 minutes. The molarity of the fluoride ion is plotted against time and values from the chart used to calculate the quantity of fluoride ion evolved.
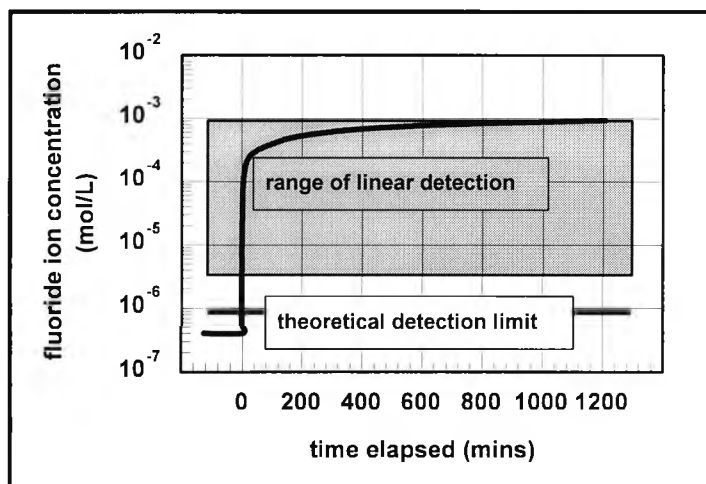
Figure 2.2-5 **Typical XY output – fluoride ion detection (FSE) with UV irradiation of solid-state photoinitiator**

In a typical experiment – see Figure 2.2-5 - the baseline reading prior to irradiation is about 0.4×10^{-6}M. Having an electrode response time of 4 seconds, the trace departs sharply from this reading after a lag of about 60 seconds (Figure 2.2-6), passing the guaranteed detection limit (1.0×10^{-6}M) after about 70 seconds and reaching the lower limit of the range of linear detection (5.0×10^{-6}M) after about 90 seconds.
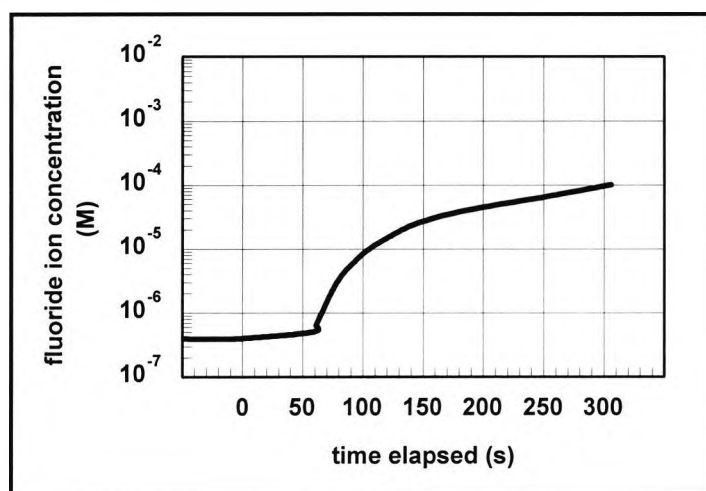
Figure 2.2-6 **Onset of fluoride ion detection (FSE) with UV irradiation of solid-state photoinitiator**

Within the range of linear detection the concentration then doubles (10.0×10^{-6}M) in the next 25 seconds, and doubles again (20.0×10^{-6}M) in the next 50 seconds.

The measured concentration continues to increase throughout the experiment reaching a level around 10^{-3}M - and still rising - as measurement is terminated after 20 hours of irradiation. The linearity of the electrode is guaranteed within the range of pH 9.0-3.0 which corresponds to a range of H ion concentration of 10^{-9}-10^{-3}M. The upper limit is

79

therefore reached after several hours of exposure, assuming that a proton is generated for each fluoride ion.

The correct quantity of fluoride ions evolved can be obtained by adjusting for the solution volume (500 cm^3) and dividing the molarity by a factor of 2. The data can be conveniently exhibited in log-log format (Figure 2.2-7)
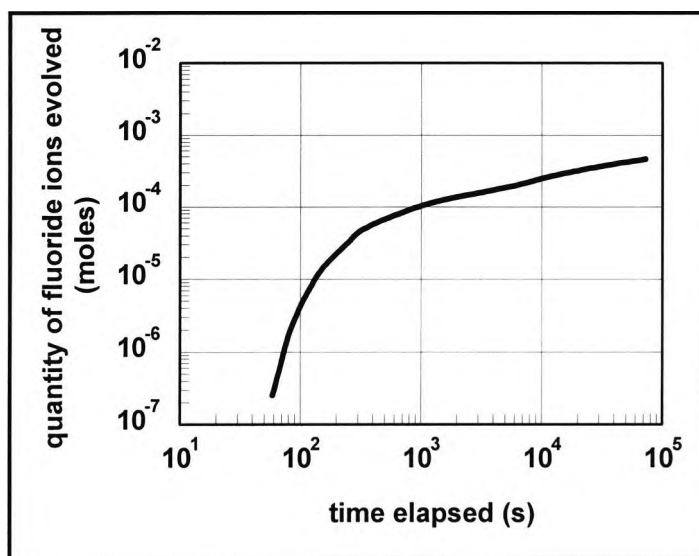
Figure 2.2-7   **Log-Log display of fluoride ion yield as a function of time with UV irradiation of solid-state photoinitiator**

2.2.2 <u>Analysis Of Experimental Conditions For Photodecomposition Experiments</u>

2.2.2.1 Purpose And Objectives

The data obtained from the FTIR, IEC and FSE experiments are described and discussed fully in the Results and Discussion Section (2.3). This data indicates that the photoinitiator (diphenyliodonium hexafluorophosphate) undergoes decomposition during the UV irradiation, yielding at least one chemical species, which can be identified and quantified.

It is a matter of some importance to show that in the described experiments: (1) the PTFE decomposition cell is transparent to UV light, (2) the decomposition cannot be accounted for by other means, particularly thermal and (3) that the products identified do not arise from any degradation - whether thermal or radiation induced - of the apparatus itself.

2.2.2.2 Examination Of Experimental Conditions

2.2.2.2.1 <u>UV Transparency Of PTFE Window</u>

The transparency to UV light of PTFE of various thicknesses was determined in an effort to select a window for the decomposition cell, which would permit the transmission of UV light at the required wavelength and provide sufficient physical strength to be functional.

A radiometer and UV curing unit was used for determining the transparency of thin PTFE films, to UV light in different regions. A belt driven UV curing unit (RPC Industries) with 2 x 120 Wcm^{-1} (3600W) medium pressure mercury vapour lamps and maximum belt speed of 70 $mmin^{-1}$ was used. Determination of UV dosage was made using a EIT radiometer (model number PP2000) from which output data can be obtained for 4 spectral regions:

- UV-A (355nm +/- 35nm)
- UV-B (300nm +/- 20nm)
- UV-C (255nm +/- 5nm)
- UV-V (420nm +/- 25nm).

After warming up the lamps, the radiometer was passed through the machine and the lamp output recorded in units of Jcm^{-2} for all wavelength bands: 255,300,345 and 420nm. A total of 3 experiments were carried out and means ($\alpha_{255,300,345,420}$) obtained from the 3 values at each of the 4 wavelength centres.

The radiometer detector was covered with a PTFE sample of a given thickness and 3

The radiometer detector was covered with a PTFE sample of a given thickness and 3 runs made producing averaged transmission values at the 4 wavelengths ($\beta_{255,300,345,420}$). A per cent transmission value can be calculated for the PTFE sample at each wavelength (eg α_{255}/β_{255} x100)

The process was repeated for PTFE samples at 4 thicknesses, between 0.050mm and 0.225mm
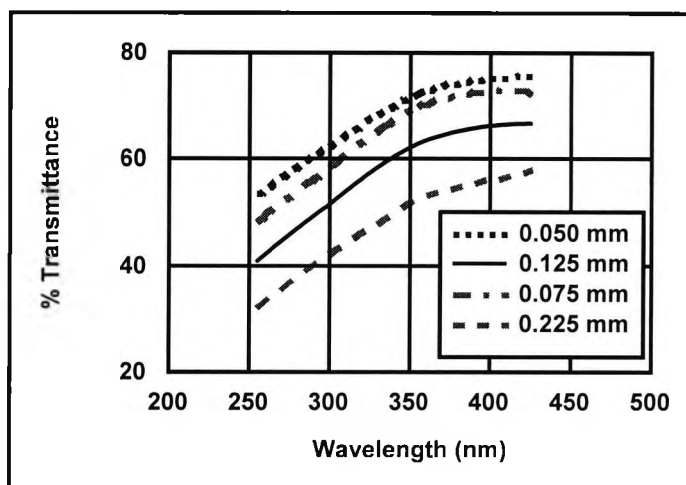
Figure 2.2-8   **UV transmission of PTFE as a function of wavelength with variation in thickness**

The data (Figure 2.2-8) shows that PTFE of 0.125mm thickness - which was found to be the minimum thickness required for physical strength - will transmit around 40% of UV-C light and around 50% of UV-B light. The radiant intensity of the lamp used for this determination is similar to that used in photodecomposition experiments

2.2.2.2.2 Irradiation And Temperature Rise Within Cell

The photodecomposition cell was sealed (empty) and exposed in the UV unit. The temperature change was recorded at intervals from a digital thermometer output over a 5-hour period.
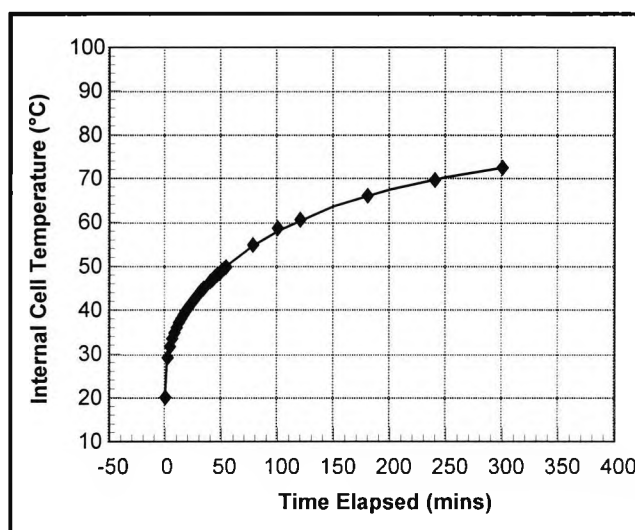
Figure 2.2-9 Temperature rise within PTFE photodecomposition cell as a function of UV irradiation time

The data shows (Figure 2.2-9) that during the course of the decomposition experiment the internal temperature of the cell remains below 80°C - even after 5 hours of irradiation.

The photodecomposition experiments using the fluoride specific electrode involved an open system in which the cell was continuously infiltrated with a stream of gas (at room temperature). This cooling effect of such a gas stream would have mitigated the temperature in the cell and the above result can be considered a worst-case outcome for most experiments.

2.2.2.2.3   Thermal Stability Of Photoinitiators

Thermal stability of DPIHFP and Irgacure 261 photoinitiators was determined on a TGA2950 thermogravimetric analyser. TGA was carried out on samples of size 11-14 mg. Weight loss was recorded with a heating profile consisting of a temperature increase at a rate of 5°C/min^{-1} from room temperature to 300°C.
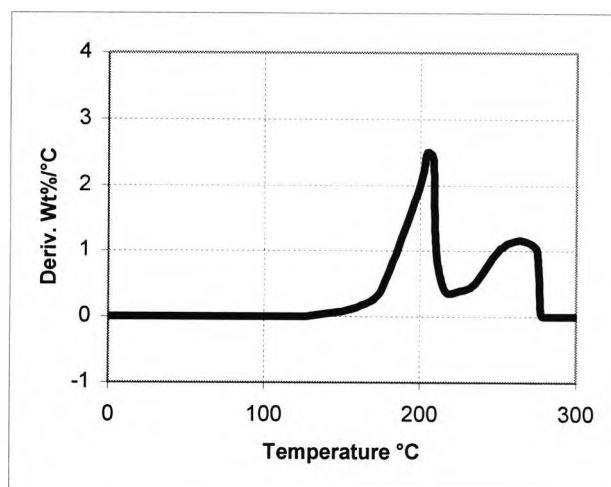
Figure 2.2-10 1st derivative TGA profile for DPIHFP
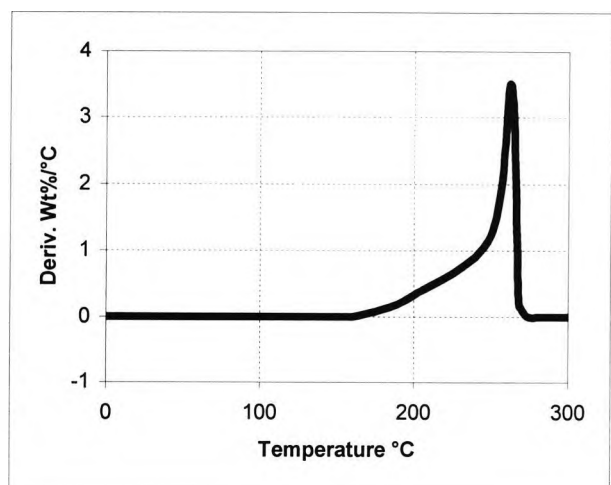
Figure 2.2-11 1st derivative TGA profile for Irgacure 261

Thermo-gravimetric analyses indicates that thermal decomposition of DPIHFP (Figure 2.2-10) does not begin until a temperature of 150°C is reached and has a maximum rate of about 2.5 wt%°C^{-1} at around 200°C. The lack of significant weight reduction below 150°C is clear evidence for the thermal stability of DPIHFP under experimental conditions. In fact, in a separate stability scan, DPIHFP was sustained at a temperature of 90°C for 2 hours with an overall weight loss of less than 2.0%, which can be attributed to loss of moisture.

Likewise, Irgacure 261 (Figure 2.2-11) is also stable to 150°C and at 90°C undergoes negligible weight loss over a 2-hour period. The lack of significant weight reduction below 150°C is clear evidence for the thermal stability of Irgacure261 under experimental conditions.

84

2.2.2.2.4 Stability Of PTFE To Photodegradation

Some deterioration of the PTFE membrane was noted experimentally in this study, which necessitated frequent cleaning and occasional replacement of the membrane. The membrane would become discoloured (brownish deposit) - on the inside only - and would eventually tear after continued use. No deterioration was noted on the outside of the membrane subjected to extremes of light, heat, moist air and the presence of ozone. This would suggest that the degradation of membrane was not induced by UV light.

Nevertheless, some experiments were carried out with an empty cell to verify this. These experiments produced gas(es), which yielded fluoride ions when exhausted through water. However the quantity was very low necessitating a reduction in the volume of the water solution by half so that the detection limit for the fluoride ion could be reached.

In general the rate of output of fluoride ions in this case did not exceed $5 \times 10^{-10} s^{-1}$. This value is 4 orders of magnitude less than experimental rates (rate $x 10^{-6} s^{-1}$). - and yields from this source could not at anytime account for more than 5% of the total fluoride yield obtained from experiments involving photoinitiators.

These latter experiments were completed towards the end of the study, after exposure of the cell to hundreds of hours of irradiation and photodecomposition products. It is possible that even after rigorous cleaning, residual fluorine containing photo-contaminates could explain the yield of fluoride ions from the empty cell.

These observations suggest that although it is possible that the vessel is contributing as much as 5% of the fluoride yield, whether by photo-degradation of the cell/window or by effects of accumulated contaminants, the bulk of the yields obtained must originate from the photoinitiator decomposition.

Consistent with these findings, the absence in the literature of reports concerning photo-degradation above 250nm, suggests, given the widespread use of this material, that it is probably not a significant factor in this case. Indeed, PTFE is recognised [65] as a material with good resistance to the effects of heat, chemicals and solvents. Nevertheless, PTFE is known to be extremely susceptible to degradation with certain kinds of radiation. However remarks in the literature concern only ionising radiation such as electron beam, X-ray and γ-radiation and are restricted to the impact on mechanical and morphological properties. Gaseous production, where indicated, usually refers to CF_4 or CO_2 or CO [66].

2.2.2.3 Summary Of Experimental Conditions For Photodecomposition Experiments

The spectrum of the lamp used in photodecomposition experiments (see Figure 2.2-4) extends below 300nm with output as low as 240nm. The data indicates a substantial transmission of UV light through the PTFE membrane in the range of the lamp output. The UV sensitivity of the initiator salts to photodecomposition is long established [42] and they are known to absorb within this spectral region.

The temperature profile data of the PTFE cell and thermal stability of the initiator salts together confirm that the decomposition of the initiator salts is not mediated thermally under experimental conditions.

PTFE was selected as a design material for the decomposition cell due to its non - reactivity with most chemicals and solvents - particularly potential fluorine containing decomposition products. The effects of cell photo-degradation are shown to be minor. It is unlikely that this material contributes to the decomposition gases in the experiments.

2.3 RESULTS AND DISCUSSION

2.3.1 Photodecomposition Of DPIHFP, IR Analysis Of Gaseous Photoproducts

The UV irradiation for 30 minutes of the DPIHFP photoinitiator (0.2g on cellulose substrate) in the solid state has a very clear effect on its physical appearance (Figure 2.3-1). Beginning as an off-white solid, diphenyliodonium hexafluorophosphate undergoes an obvious decomposition to yield a brownish-yellow solid.
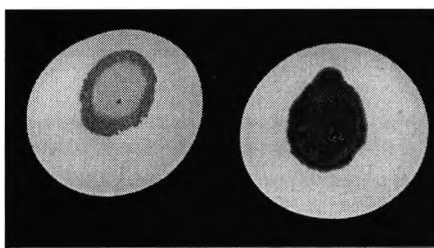
Figure 2.3-1   **Appearance of solid-state photoinitiator sample before (left) and after (right) UV irradiation (30 mins.)**

The infrared spectrum of the decomposition gases (Figure 2.3-2) indicates the presence of hydrogen fluoride, acetone and at least 1 unknown material.
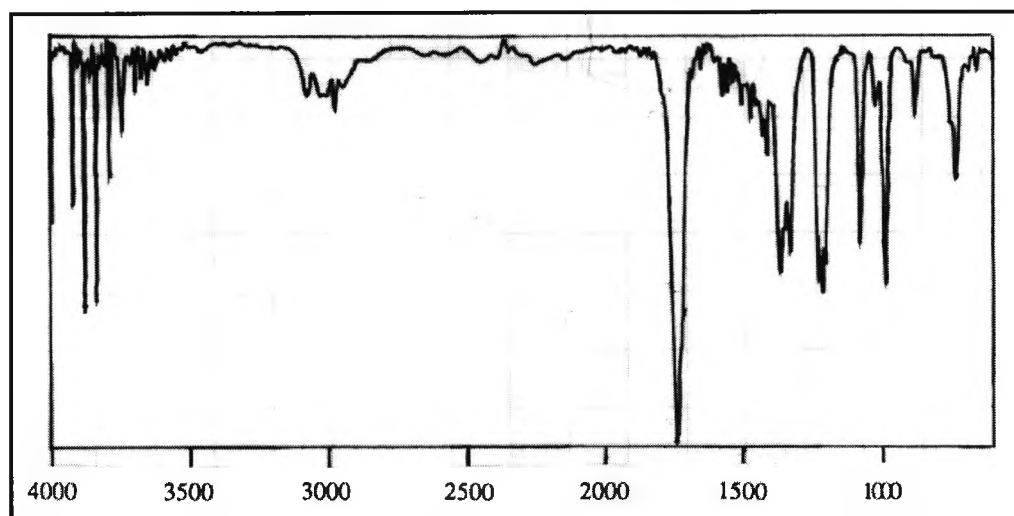
Figure 2.3-2   **IR spectrum of gaseous photodecomposition products obtained after UV irradiation of DPIHFP in the solid state**

The bands at 2880-3080, 1440, 1369, 1355, 1228, 1218,1206 and 880 cm^{-1} can all be attributed to the C-H deformations of acetone. This identification is supported by the strong C=O stretching band at 1740 cm^{-1} and confirmed by library data [67].

The presence of acetone can be explained, as it was the solvent used for the deposition of the photoinitiator onto the substrate. Residual solvent will be retained even after extensive drying of the photoinitiator sample, and, having a low boiling point (56ºC) and a relatively high vapour pressure under experimental conditions (80KPa at 50ºC), the presence of residual acetone in the photodecomposition gases is to be expected.

The presence of hydrogen fluoride in the gas mixture is supported by the appearance in the spectrum of 7 sharp bands between 3690 and 4000 cm^{-1} (Figure 2.3-3), which compare very favourably to those reported by other workers [68].
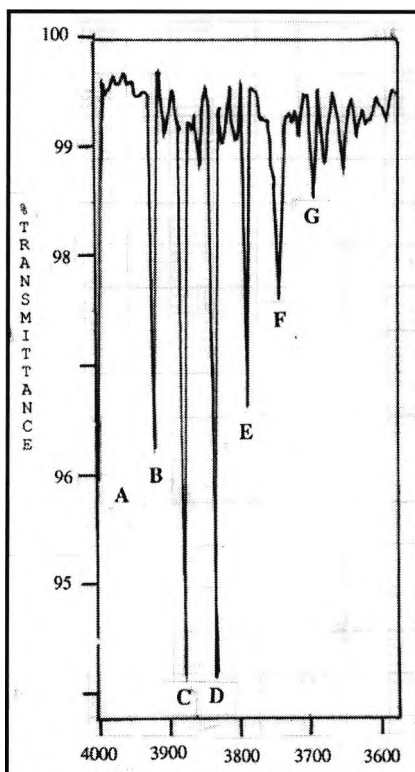
Figure 2.3-3   **4000-3600cm^{-1} portion of IR spectrum of gaseous photodecomposition products obtained from UV irradiation of DPIHFP in the solid state**

The bands labelled 'B'-'G' in Figure 2.3-3 correspond very closely to the first 6 bands $(P_{(1)}...P_{(6)})$ from the 'P' branch of the first fundamental transition for hydrogen fluoride. The 'P' series contains a total of 11 bands.

The band labelled 'A' in Figure 2.3-3 corresponds to the highest energy band $(R_{(0)})$ in the 'R' branch of the first fundamental. The 'R' series contains 12 bands (4001 - 4322cm^{-1}) of which all but the highest energy band lie outside the limits of data acquisition in this case.

Label	Assignment	Experimental (cm^{-1})	Literature [68] (cm^{-1})	Difference (cm^{-1})
A	R(0)	4000	4001	-1
B	P(1)	3919	3920	-1
C	P(2)	3877	3878	-1
D	P(3)	3834	3834	0
E	P(4)	3788	3788	0
F	P(5)	3742	3742	0
G	P(6)	3692	3694	-2

Table 2.3-1   **Comparison of experimental IR spectral bands with published values for HF - identification of HF in gaseous products obtained from UV irradiation of DPIHFP in the solid state**

Given the resolution of the spectrum (8.0cm^{-1}), the correlation of the literature and experimental data (Table 2.3-1) for the 7 bands to a precision of +/- 1cm^{-1} (in 6 out of 7 cases) represents strong evidence for the identification of hydrogen fluoride gas.

Unassigned bands are located at 1415, 1340, 1100, 1025, 980 and 710cm^{-1}.

Previous workers have taken many precautions in their effort to obtain HF spectra due to the extreme reactivity of this molecule and its tendency to react with vessels and etch glass. Subsequent efforts to reproduce the above spectrum at higher resolution and over the entire spectral range (3400-4400cm^{-1}) were not successful.

The spectrum of the photodecomposition gases is interesting for the clear identification of the presence of hydrogen fluoride.

Solid-state photoinitiator residues were triturated in acetone, filtered and sent to an external laboratory for GCMS analysis (see Appendix B, Sec.5.1). The diphenyliodonium hexafluorophosphate salt residues produced various fractions. Mass ions for 2 of these fractions were located at M/e 280, which probably corresponds to iodobiphenyl, and at M/e 204, which corresponds (by comparison to an authentic sample) to iodobenzene. Similar results were obtained for the hexafluorarsenate salt.

However, the IR spectrum is notable for the absence in the gaseous mixture of iodobenzene, iodobiphenyl, and indeed benzene. In early work [36], which focused on the photodecomposition of the cation following irradiation of diphenyliodonium

hexafluorophosphate in organic solvents, benzene and iodobenzene were identified as the primary photodecomposition products. Subsequent work [11,27,46,50,51] also identified iodobiphenyl(s) as products, arising from recombination processes.

Benzene [69], would produce strong bands at 1470, 1030 and 670cm^{-1}. These are not present. Iodobenzene [70] would produce strong bands at 1575, 1470, 1440, 1015, 1000, 730 and 680cm^{-1}. Similar bands would be expected from iodobiphenyl. These bands are not present.

The absence of evidence in the spectrum for these photodecomposition products can be explained in terms of volatility (Table 2.3-2) and is not at odds with the previous work.

[71,72]	Vapour Pressure at 50°C (KPa)	Boiling Point (°C)
Acetone	80	56
Benzene	35	80
Fluorobenzene	30	85
Iodobenzene	0.7	188
Iodobiphenyl		183

Table 2.3-2   **Volatility of some materials relevant to the UV induced photodecomposition of DPIHFP in the solid state**

In particular, iodobenzene, which has a high boiling point and low vapour pressure under experimental conditions, would not be expected among gaseous products at atmospheric pressure. Benzene, boiling at 80°C and having a vapour pressure less then half that of acetone, is perhaps not detected for the same reason. Iodobiphenyl, which is a known solid-state photodecomposition product, is certain to be a solid (m.pt. 113-114, [72]) under experimental conditions.

It not impossible also, that benzene, if generated, could be subject to chemical attack under experimental conditions (gas phase/strong acid/UV light). However, it is perhaps worth pointing out that fluorobenzene, cannot be confirmed in the spectrum either. Fluorobenzene is also a possible product from anion decomposition. Fluorobenzene [73] would produce strong bands at 1587,1493,1190,and 750cm^{-1}. These are not present. This may also be explainable in terms of low volatility.

The spectra of phosphorus trifluoride [74] and pentafluoride [75] are available in the literature.

The trifluoride produces strong bands at 892 and 860cm^{-1}. In the obtained spectrum only one band is observed in this region (880cm^{-1}). On this basis the presence of PF$_3$ cannot be confirmed.

The pentafluoride produces its strongest bands at 1029, 1026, 956, 948 and 935cm^{-1} (Table 2.3-3). The spectrum above (Figure 2.3-2) contains a band at 1025cm^{-1} and a much stronger band at 980cm^{-1}, which is otherwise unidentified. On this basis the presence of PF$_5$, cannot be confirmed.

Literature [75]		Experimental	
Band (cm^{-1})	Intensity (rel.)	Band (cm^{-1})	Intensity (rel.)
935	43		
948	80	980	100
956	61		
1026	97	1025	17
1029	100		

Table 2.3-3   **Comparison of IR absorption spectrum of PF$_5$ and some experimental values**

2.3.2 Confirmation Of The Presence Of Fluorine - Ion Exchange Chromatography

Ion exchange chromatography was carried out after the gases obtained following 75 mins of irradiation of diphenyliodonium hexafluorophosphate (0.4g on cellulose substrate) were exhausted through water.

The chromatogram of the solution obtained from the photodecomposition gases (Figure 2.3-4) clearly supports the presence of fluorides in the solution. The retention at 1.90 minutes was identified by the reference sample (Figure 2.3-5) as being consistent with the fluoride ion (1.88 mins).
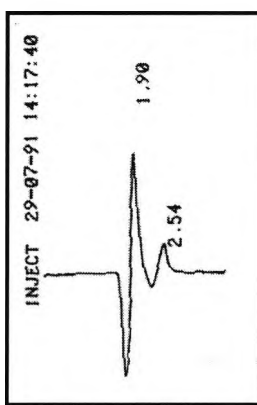
Figure 2.3-4   **I.E.C. chromatogram - sample injection of aqueous solution of gaseous products obtained from UV irradiation of solid-state DPIHFP**
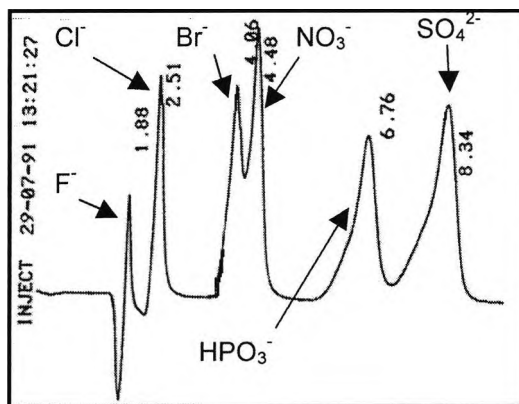
Figure 2.3-5   **I.E.C. chromatogram - reference standards**

The fluoride can be quantified (in ppm) by multiplying the response factor obtained from the reference standard for the fluoride ion by the area count obtained from the sample injection at the appropriate retention time.

<u>Reference standard:</u>

Response factor, Rf_{F^-} = $conc_{F^-}$ / area $count_{F^-}$ = 0.30ppm/2,865,000=1.05×10^{-5}

<u>Sample solution:</u>

$conc_{F^-}$ = area $count_{F^-}$ x RF_{F^-} = 4,039,000 x 1.05×10^{-5} = 0.42ppm

From the double injections of standards and samples a value of 0.42 ppm is obtained for the fluoride ion. Taking into account the dilution (1:100) this figure becomes 42 ppm and, in view of the original volume of solution (400 ml) represents a fluoride yield of 0.000880 moles. Since the quantity of photoinitiator irradiated in the solid state was 0.000940 moles, the yield of fluoride ion was therefore 0.94 equivalents with respect to the initiator quantity irradiated – i.e. almost 1 mole of fluoride ion was produced for every mole of initiator irradiated.

Fluoride Equivalents = $\dfrac{\text{Fluoride ions obtained (moles)}}{\text{Quantity of photoinitiator irradiated (moles)}}$

$$= \quad \frac{0.00088}{0.00094} \quad = \quad 0.94$$

The elution of a fraction at retention time 2.54 minutes is identified, by comparison with the reference standards, as the chloride anion. The quantity detected is about 0.15 ppm. Such a level can be accounted for in terms of incomplete de-ionisation of the supply - tap water contains chloride at levels of 100-200 ppm and residual chloride level of 0.1-0.2 ppm after de-ionisation is typical.

The data obtained from the I.E.C. analysis with diphenyliodonium hexafluorophosphate, is interesting for several reasons:

- These experiments show that the DPIHFP decomposes under UV light in the solid state.

- This decomposition gives rise to one or more gaseous materials which when dissolved in water produce fluoride ions in significant quantities.

- Through the IEC measurements it became clear that the quantity of fluoride producing materials was at measurable levels. This observation led to the evaluation of the fluoride selective electrode as a measurement device.

In interpreting this data, the answer to at least one important question is critical to all further discussion: What are the identities of the fluoride producing gas(es)?

The infrared spectrum of the gaseous photoproducts clearly indicates the presence of hydrogen fluoride gas. The link between this gas and fluoride ions is not hard to make, as it will dissolve readily in water to yield hydrofluoric acid with complete dissociation, Scheme 2.3-1.

$$HF \longrightarrow H^+_{(aq.)} + F^-_{(aq.)}$$

Scheme 2.3-1   **Dissolution of HF gas**
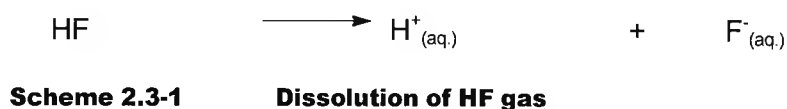
This is consistent with the findings of Wilkinson [63] who showed:

(1) That under electron beam conditions the anion certainly does not remain intact; decomposition of the anion certainly occurs.

(2) That under UV irradiation, the solid-state DPIHFP salt decomposes to yield gaseous materials with the subsequent accumulation of fluorine-containing end products.

Wilkinson postulated that the initial gaseous decomposition products of the counter ion may be HF and PF_5, Scheme 2.3-2.

viz. $\qquad YH^+ \ ^-PF_6 \longrightarrow Y^+ + HF + PF_5$

Scheme 2.3-2   **Counterion decomposition products: Wilkinson**

Wilkinson did not identify directly the existence of HF. The production of HF was deduced from the appearance of an infrared band at $1024cm^{-1}$ which was attributed to the appearance of SiF_4 following reaction of the short lived HF with the walls of the quartz vessel (SiO_2), Scheme 2.3-3.

viz. $\quad SiO_2 + 4HF \longrightarrow SiF_4 + 4H_2O$

Scheme 2.3-3   **Consumption of HF by reaction with silicon dioxide (quartz): Wilkinson**
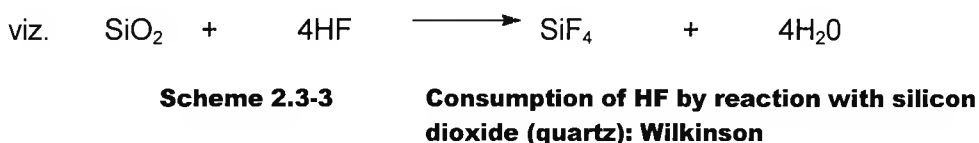
SiF_4 is a gas at room temperature and would mix with the photoproducts to appear in the spectrum.

Wilkinson was also unable to find direct evidence for PF_5 but inferred this also from the appearance of a band at $1415cm^{-1}$, which was attributed to POF_3 arising from hydrolysis of PF_5 in the presence of residual water, Scheme 2.3-4 in the apparatus and the water arising from Scheme 2.3-3.

viz. PF_5 + H_2O $\longrightarrow$ POF_3 +   2HF

Scheme 2.3-4   **Consumption of PF_5 by reaction with water:**
Wilkinson

In the present work, IR absorption bands were also noticed (and otherwise unidentified) at $1025cm^{-1}$ and $1415cm^{-1}$ and could be attributable to the same species. It is perhaps for the same reason that PF_5 was not identified in the IR spectrum.

2.3.3 <u>Evolution Of Fluoride Ions From Photodecomposition Of Diphenyliodonium Hexafluorophosphate</u>

The photoinitiator was dissolved in solvent and the solution deposited on an absorbent substrate. The solvent was removed by evaporation. The solid-state initiator was UV irradiated in a constant stream of air. The air stream is exhausted to a volume of water where a solution of the gaseous products was formed. The progress of the decomposition was followed conductometrically by means of a fluoride ion selective electrode.

Irradiation of the photoinitiator (2.3×10^{-4} moles) is accompanied by a rapid rise in the concentration of fluoride ions detected (Figure 2.3-6).

The yield after 20 hours of hours of irradiation is 4.6×10^{-4} moles of fluoride ions. This corresponds to almost 2 equivalents of fluoride ion generated for every mole of photoinitiator irradiated.
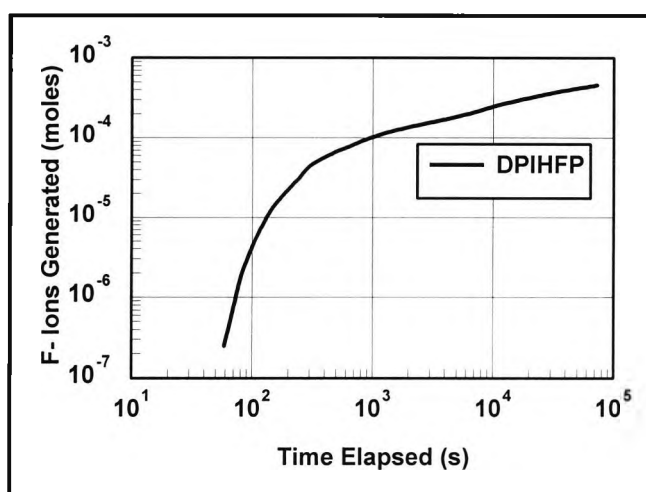
Figure 2.3-6   **Fluoride ion evolution following UV irradiation of DPIHFP in the solid state**

The rate of fluoride evolution can be calculated and plotted as a function of quantity of fluoride evolved (Figure 2.3-7) to reveal several important features of the decomposition.
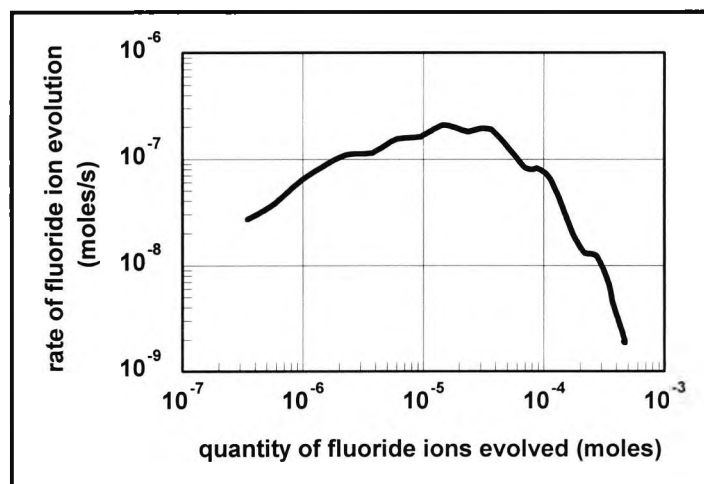
Figure 2.3-7   **Rate of fluoride ion evolution as a function of quantity of fluoride ion evolved, UV irradiation of solid-state DPIHFP**

The rate increases to a maximum which can be determined accurately using the numerical treatment described in appendix A (Sec.4). The maximum rate is 2.6×10^{-7} mols^{-1} with the evolution of about 4×10^{-5} moles, after 185s. The rate decreases sharply (as a function of quantity evolved) to the order of 10^{-9} mols^{-1}.

The quantity of evolution at the point of maximum rate corresponds to about 1/8th of the final yield, representing about 0.25 equivalents of the initiator laid down for irradiation. This point is achieved within 4 minutes of irradiation.

This indicates the importance of the early stages of the experiment in terms of analysis and discussion.

2.3.4 Evolution Of Fluoride Ion From Other Group 5 Hexafluorophosphate Initiators

Like the hexafluorophosphate salt, the hexafluoroarsenate and hexafluoroantimonate salts are gaseous sources of fluorine when irradiated with UV light in the solid state and have behaviour, which is essentially similar. The arsenate would appear to decompose faster than the phosphate while the antimonate is slower (Figure 2.3-8).
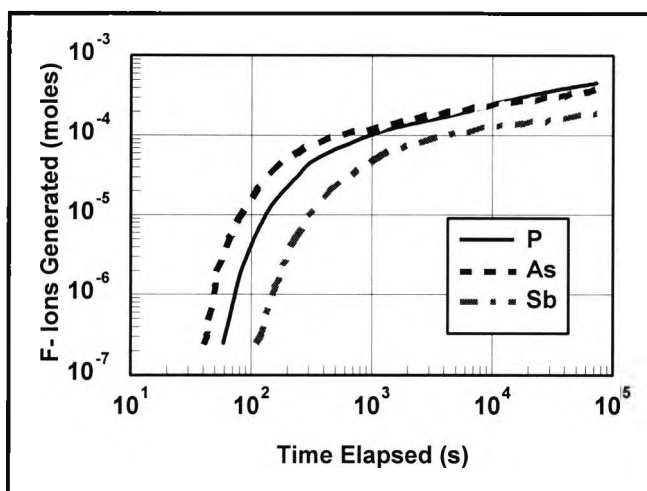
Figure 2.3-8 **Fluoride evolution following UV irradiation of solid-state DPI hexafluoro-(group 5) salts**

The rate of evolution of fluoride ions as a function of the quantity of fluoride evolved is shown in Figure 2.3-9 for the three salts. In each case the rate of evolution increases to a maximum with the evolution of about $1\text{-}3 \times 10^{-5}$ moles, decreasing sharply (as a function of quantity evolved) to the order of 10^{-9} mols^{-1} as the quantity evolved increases.
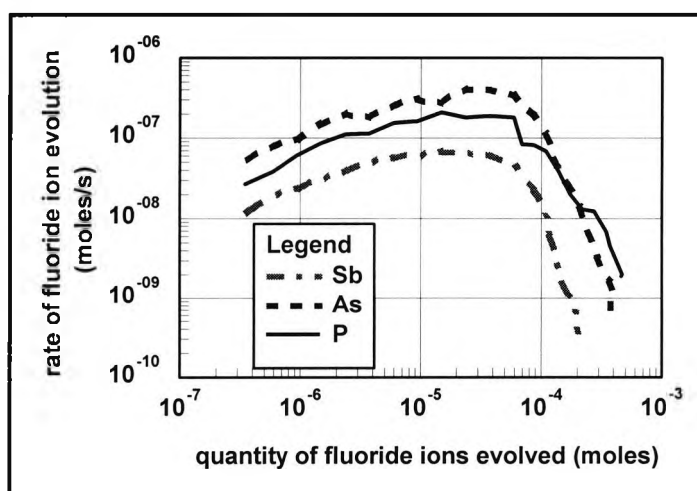
Figure 2.3-9 **Rate of fluoride evolution as a function of quantity of fluoride ions evolved, UV irradiation of solid-state DPI hexafluoro-(group5) salts**

98

The maximum rates, see Table 2.3-4, can be more accurately determined via the numerical treatments described in appendix A (Sec.4). The arsenate salt reaches a maximum faster than the phosphate and at the maximum point the arsenate evolves fluoride ions at a rate almost twice as fast as the phosphate. The rate in each case decreases after about 0.1 fluoride equivalents are produced.

After 20 hours of irradiation the phosphate accounts for 4.6×10^{-4} moles of fluoride evolved versus the 3.8×10^{-4} moles for the arsenate. For the phosphate this translates to a figure of 2.0 equivalents of initiator irradiated versus 1.7 for the arsenate.

	P	As	Sb
rate_{max} (10^{-7} mols^{-1})	2.3	4.2	0.9
$\text{time}_{to\,max\,rate}$ (s)	180	120	330
$\text{yield}_{max\,rate}$(10^{-5} moles)	2.1	2.6	1.3
$\text{Equiv}_{max\,rate}$	0.09	0.11	0.06
$\text{rate}_{1000\,mins}$(10^{-9} mols^{-1})	2.2	1.1	2.7
$\text{yield}_{1200\,mins}$($10^{-4}$ moles)	4.6	3.8	2.0
$\text{Equiv}_{1200mins}$	2.0	1.7	0.8

Table 2.3-4   **Parameters for fluoride ion evolution following UV irradiation of solid-state DPI hexafluoro-(group 5) salts**

The decomposition of the antimonate salt would appear to be much slower. The time required to reach a maximal rate is about double that of the other salts and the maximum rate is about one fifth of the arsenate and one third of the phosphate. The rate begins to decrease when the yield is about half that of the other salts.

After 20 hours of irradiation the antimonate yields only 2.0×10^{-4} moles of fluoride, which corresponds to less than 1 equivalent (0.8).

The decomposition of the phosphate and the arsenate to produce 1.95 and 1.65 equivalents of fluoride can be explained in terms of the formation of both HF and PF_5 from the salts. The trifluorides may also be formed, but this cannot be verified. The tri- and pentafluorides of phosphorus and arsenic are known to be gases at room temperature (Table 2.3-5). If evolved, they would certainly produce multiple fluoride equivalents as they are known to undergo very rapid hydrolysis in water.

[71,72]	Trifluorides		Pentafluorides	
	Boiling Pt.(°C)	Hydrolysis	Boiling Pt.(°C)	Hydrolysis
Phosphorus	-101.8	Fast	-84.6	Fast
Arsenic	63	Fast	-53.2	Fast
Antimony	376 (dimer)	slow/limited	149.5 (dimer)	Slow/limited

**Table 2.3-5   Physical data – trihalides and pentahalides
of group 5 elements**

However, it is not clear how many equivalents of fluoride would arise from the hydrolysis of a pentafluoride. Mazeika and Neumann [76] studied the hydrolysis of the hexafluoroantimonate salt and showed that the process has an indefinite completion time, occurring in a stepwise manner to yield 3 fluoride equivalents within practical time limits. The rate constants for each of the 3 hydrolysis steps are different.

The first step, Scheme 2.3-5, occurs very rapidly - within the time frame of dissolution;

viz SbF_6^- + H_2O $\longrightarrow$ $SbF_5(OH)^-$ + H^+ + F^-

**Scheme 2.3-5   1st hydrolysis step for the
hexafluoroantimonate anion**

However, the second and third steps, Scheme 2.3-6, have half lives in the order of hours and days respectively in acid solutions such as was the case in the present study.

viz $SbF_5(OH)^-$ + H_2O $\longrightarrow$ $SbF_4(OH)_2^-$ + H^+ + F^-

viz $SbF_4(OH)_2^-$ + H_2O $\longrightarrow$ $SbF_3(OH)_3^-$ + H^+ + F^-
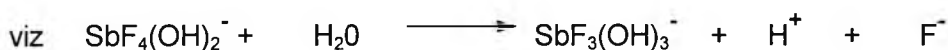
**Scheme 2.3-6   2nd & 3rd hydrolysis steps for the
hexafluoroantimonate anion**

Comparable data is not available for the hexafluorophosphate or the hexafluoroarsenate, or for any pentafluoride but a similar outcome seems likely in these cases.

Such a scenario would explain why the evolution of fluoride ion continued over such a long time frame (20 hours) and why the rate was so slow ($10^{-9}s^{-1}$) at that time.

Such hydrolysis steps, which can be considered as secondary to the main photochemical process, could occur 'in-situ' within the photodecomposition vessel or upon contact with the volume of water in the fluoride measurement flask.

Sundell [64] reported multiple equivalents of acid (and presumably fluoride) on hydrolysis

of group 5 salts, and Gatechair [77] also observed the hydrolysis of arsenate salts yielding multiple acid equivalents. In the present work, Figure 2.3-10, the antimonate was noted for its low yield of fluoride (0.83) and this is explainable also in terms of the boiling point of the antimony pentafluoride. The latter is a viscous polymeric liquid in bulk. Under experimental conditions a strong tendency to associate may also be predicted which will exclude the antimony pentafluoride from the volatile products of a solid-state photodecomposition. Consequently, any fluoride anions detected in this experiment arise solely from the dissolution of the hydrogen fluoride gas or from 'in-situ' hydrolysis of polyfluorides in the decomposition vessel.
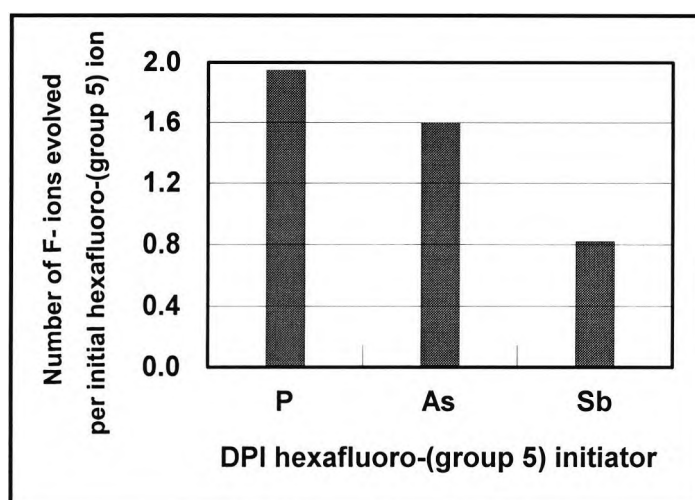
Figure 2.3-10   Relative yield of fluoride ions after UV
                       irradiation of solid-state DPI hexafluoro-
                       (group 5) salts

Wilkinson [63] made a parallel observation in her study. When the antimonate salt was irradiated in place of the phosphate salt the strength of the band at 1025cm^{-1} corresponding to the formation of SiF_4 from HF was much smaller. This was explained in terms of the lack of a participating pentafluoride due to the higher boiling point of the antimony pentafluoride.

	Maximum Rate (mols^{-1})
PF_6^-	2.3×10^{-7}
AsF_6^-	4.2×10^{-7}
SbF_6^-	0.9×10^{-7}

Table 2.3-6   maximal rate of fluoride ion evolution
                     following UV irradiation of solid-state DPI
                     hexafluoro-(group 5) salts

It is clear from Table 2.3-6 that the arsenate anion decomposes more rapidly than the

phosphate anion by a factor of 1.6:1 which suggests that the arsenate anion is less stable than the phosphate anion.

Several studies exist [13,15-18] which show that in the cationic polymerisation of epoxides and vinyl ethers by triarylsulphonium salts, diaryliodonium salts and aryl diazonium salts bearing various anions, the reactivities of the initiators follow a common sequence according to the anion.

The rates of reaction, yields of polymer, and polymer molecular weights are always in the same order:

$$SbF_6^- > AsF_6^- > PF_6^- > ClO_4^- > BF_4^-$$

These observations have provoked a great deal of speculation in the literature concerning their significance with regard to the mechanism of polymerisation in such cases. Nevertheless, little or no hard experimental data yet exists to identity unambiguously the exact nature of the acidic species within the matrix of polymerisation.

Authors have generally assumed a Brønsted pathway, referring to the "crucial role played by the counterion" [16,78] and noting that the reactivity follows the same order as anion size (and therefore nucleophilicity) [15]. Further to this point, Crivello [15] cites Pepper [79] in suggesting that the degree of separation between the propagating cation and the stabilising anion is crucial to its effectiveness in permitting polymerisation. A higher degree of separation (larger, less nucleophilic anion) would lead to an energetically more feasible propagation step. There is support for this in DSC data by Jonsson and Sundell [18].

Pappas [11] and Bal [16] have suggested that the larger anions, in addition to being less nucleophilic, are more stable and less likely to participate in chain termination reactions which might yield the polymer fluoride and the Lewis acid pentafluoride, Scheme 2.3-7:
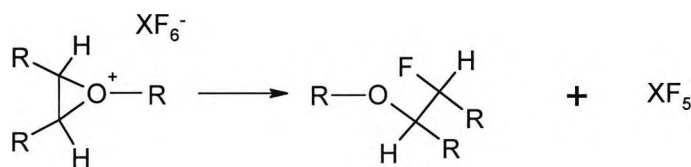
Scheme 2.3-7   Anion fragmentation and chain termination

In view of the experimental data contained in the present study concerning the anion stability following irradiation in the solid state, it seems that an alternative theory is

required to account for the experimental findings of previous workers and those of the present work.

The anion is intrinsically unstable and rarely survives polymerisation intact. The more likely case is that the anion decomposes fairly rapidly to yield the hydrogen fluoride and the Lewis acid pentafluoride.

The stability of the anion follows the order discussed by Pappas [11] but it is in fact the Lewis acid, XF_5, and not the intact Brønsted acid, HXF_6, which is the principal driving force behind polymerisation. This suggestion is consistent with the increased reactivity of the arsenate over the phosphate described by many workers, and the finding here of the increased fluoride generating power (and hence instability) of the arsenate over the phosphate.

The hydrogen fluoride will bring about a modest degree of polymerisation resulting in short chains quickly terminated by a fluoride termination. Preliminary experiments in our laboratories have shown that aqueous hydrofluoric acid brings about a rapid and exothermic polymerisation when added drop-wise to an epoxide monomer.

Following formation of the pentafluoride, the polymerisation may proceed, as in the case of diazonium salt chemistry, via an essentially Lewis acid route of which many variations are described in the literature [1,8,9,11], Scheme 2.3-8. More likely, the reaction proceeds via a regenerated Brønsted acid in the presence of unavoidable moisture and/or impurities.

viz   ROH   + XF_5 $\longrightarrow$ $ROXF_5^-{}^+H$
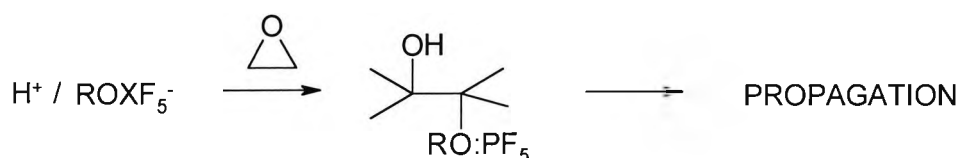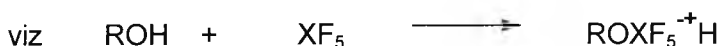
Scheme 2.3-8   **Aquation of the Lewis acid and formation of propagating species: Pappas**

Such a scenario is consistent with all experimental findings. Moreover, such a process would tolerate, if not be accelerated by, atmospheric or bulk water. This observation has been reported by several workers [11,80] and has also been noted in the present work (Sec. 3.3.7). The tolerance of water has puzzled authors who have assumed an intact anion because it is supposed to bring about early termination and chain transfer reactions - which in fact do not appear to be a significant problem.

anion because it is supposed to bring about early termination and chain transfer reactions - which in fact do not appear to be a significant problem.

The instability of the anion has also been described by Sundell [64] who noted the disappearance of the anion via infrared spectroscopy soon after the onset of irradiation.

2.3.5 Effect Of Cation Selection On Fluoride Ion Evolution

The hexafluorophosphate salts bearing the diphenyliodonium and diphenylsulphonium cations were investigated (on an equi-molar basis) to examine the effects of cation selection on the rate of fluoride evolution and the yield of fluoride obtained (Figure 2.3-11).

The data clearly indicates that the initiators decompose at different rates. Such variation would appear to arise from the choice of cation.
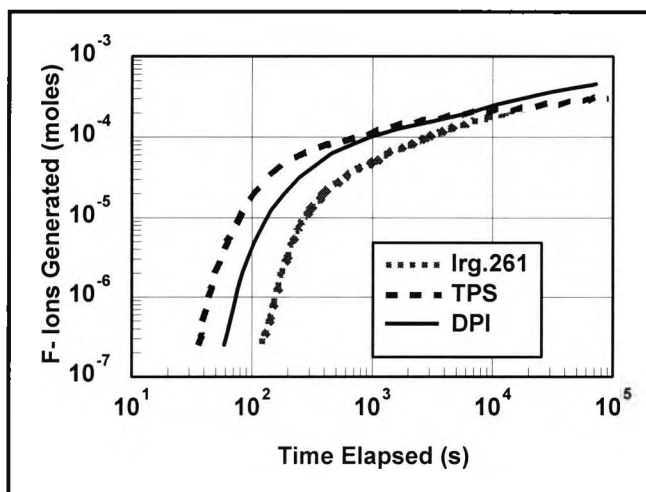
Figure 2.3-11   **fluoride ion evolution following irradiation of various solid-state initiators bearing the HFP anion - effect of cation variation**

The rate and yield data obtained for these experiments are contained in Table 2.3-7.

The triphenylsulphonium salt provides a maximum decomposition rate that is 1.7 times faster than the diphenyliodonium salt, while Irgacure 261 is considerably slower than either of the former salts.

However after 16 hours of irradiation the yield for the diphenyliodonium salt (1.9 equivalents) exceeds that for the triphenylsulphonium salt (1.2 equivalents) as the rate of decomposition of the former exceeds the latter after 4 minutes of irradiation.

Irgacure 261 produced a yield after 16hours of irradiation (1.3 fluoride equivalents), which was also substantially less than obtained from diphenyliodonium hexafluorophosphate (1.9 fluoride equivalents).

	DPIHFP	TPSHFP	Irg.261
$rate_{max}$ $(10^{-7}$ mols$^{-1})$	2.3	3.9	0.9
$time_{to\ max\ rate}$ (s)	180	110	360
$yield_{max\ rate}(10^{-5}$ moles)	2.1	2.2	1.6
$Equiv_{max\ rate}$	0.09	0.09	0.07
$rate_{1000\ mins}(10^{-9}$ mols$^{-1})$	2.2	0.7	0.7
$yield_{1000\ mins}(10^{-4}$ moles)	4.4	2.9	3.1
$Equiv_{1000mins}$	1.9	1.2	1.3

Table 2.3-7   **Parameters for fluoride ion evolution following irradiation of various solid-state initiators having the HFP anion**

Compared to the experiments involving variation of anion, the experiments involving variation of cation are simpler in an important respect. Since the anion is in every case the hexafluorophosphate, the yield of fluoride ions at any stage is affected equally, although to an unknown degree, by the rate of evolution and extent of hydrolysis of the pentafluoride gas. Consequently the fluoride yield at any point can be directly interpreted as an index of the photochemical reactivity of the initiator.

The data show that the diphenyliodonium salt decomposes faster than the triphenylsulphonium salt, producing a higher quantity of fluoride ions after 16 hours of irradiation.

This is consistent with the findings of Crivello who studied the photolysis of bis(4-methylphenyl)iodonium hexafluoroarsenate [13,14] and tris(4-methylphenyl)sulphonium hexafluoroarsenate [15] in solution (acetone).

Crivello tracked the decomposition of the cations with the appearance by GC of 4-methylphenyliodide and bis(4-methylphenyl)sulphide respectively. By comparing the data from the respective articles (obtained under identical experimental conditions), it becomes apparent that, in solution also, the sulphonium salt decomposes more slowly than the iodonium salt.

In Crivello's experiments the sulphonium salt had undergone about 30% conversion after 20 minutes of irradiation and the iodonium salt about 65% conversion after the same period.

This cation effect has thus been noted in both the solid and dispersed phases, and in terms of cation fragmentation and anion decomposition. Furthermore Pappas [11,43] noted a parallel effect on epoxide polymerisation rates for sensitised initiators.

However the cation effect is hard to explain as similarly substituted iodonium salts and sulphonium salts have very similar UV maxima and extinction coefficients [13-15], quantum yields at 254nm [27] and similar excitation energies [43] for the singlet and triplet states. Differences in crystalline structure probably affect the light absorption properties of the respective salts and account for this effect.

The sulphonium salt does have a second maximum - not shared by the iodonium salt - in the U.V Spectrum at 278nm, with an extinction coefficient 4900. Nevertheless the quantum yield at 313nm [27] for the sulphonium salt is a fraction of that of the iodonium salt. It is perhaps low level absorptions at longer wavelength that account for the efficiency of the iodonium salt.

It is interesting to note in the present work the faster maximum rate (3.9×10^{-7} mols^{-1}) obtained initially for the sulphonium salt versus the iodonium salt (2.3×10^{-7} mols^{-1}). This may be attributable to the choice of solvent. As in all previous cases acetone was used for the iodonium salt. However methanol was used for the sulphonium salt as the latter has limited solubility in acetone.

Pappas [46] showed that the rate of reaction of PhI$^+$ (primary decomposition product of diphenyliodonium hexafluorophosphate) with a range of nucleophilic solvents varies substantially. In particular methanol reacts about 5 times faster than acetone. Thus solvents of high nucleophilicity will make the decomposition of the salt more energetically feasible compared to solvents of low nucleophilicity. This will make an initiator salt in a nucleophilic solvent more reactive.

However, the present case involves the diphenylsulphonium salt for which Pappas is unable to provide data with acetone due to the insolubility of the salt in this solvent. Nevertheless Pappas' data indicates a similar phenomenon with other solvents and it seems reasonable to assume that the data for methanol and acetone with diphenyliodonium salts would be paralleled with diphenylsulphonium salts in the solid state with residual solvents.

The iron arene complex, Irgacure 261, is clearly the least efficient initiator studied. Little information is available in the literature comparing the efficiency of this initiator with sulphonium and/or iodonium salts for reactivity with monomers and photodecomposition.

However it is not an insignificant fact that this initiator has not found widespread industrial application. Irgacure 261 is considered to be a slow curing initiator and is rarely used without synergists. This is perhaps due to its relative photochemical stability and poor yield of acid as paralleled in this work.

Solid-state photoinitiator residues obtained after UV irradiation of the triphenylsulphonium hexafluoroantimonate salt were triturated in acetone, filtered and sent to an external laboratory for GCMS analysis (see appendix B, Sec.5.4). In addition to other fractions, the triphenylsulphonium hexafluoroantimonate salt produced fractions generating mass ions at M/e 186 (diphenylsulphide), 281 and 299. The mass ion at M/e 281 is consistent with a fluorinated phenyl sulphur-biphenyl, while the mass ion at M/e at 299 is consistent with a bi-fluorinated phenyl sulphur-biphenyl, Figure 2.3-12. The latter 2 species are further evidence of anion decomposition.
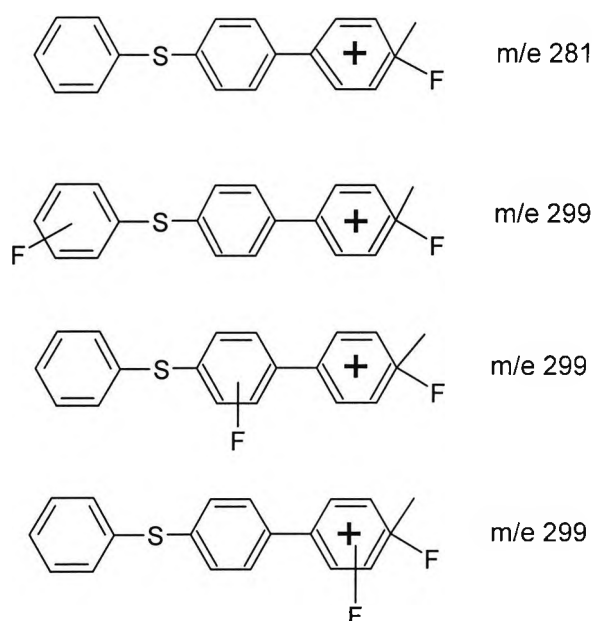
Figure 2.3-12   Mass ions detected following GCMS analysis of photodecomposition residue of UV irradiated triphenylsulphonium hexafluoroantimonate salt

It is interesting that such fluorinated products were not detected in the GCMS analysis of the residues following UV irradiation of the diphenyliodonium hexafluorophosphate and arsenate salts. This points to the increasing instability of the anion on descending the group 5 series. In view of the known (high) polymerising efficiency of salts containing the HFSb anion, this may suggest that the increasing tendency of the anion to decompose on descending the group 5 series to form the Lewis acid, XF_5, is a strong factor in the determining the rate of the polymerisation process, as suggested by Pappas [11]. By extension this data points to the Lewis acid (or indeed HF), rather than the Brønsted acid, as the stabilising counterpart to the activated centre in cationic polymerisation.

2.3.6 Effect Of Free Radical Generating Species On Fluoride Ion Evolution

Photodecomposition experiments were carried out with diphenyliodonium hexafluorophosphate in the presence of Irgacure 651 at 7% and 14% levels on a molar basis. The same quantity of cationic initiator was used in each case.

Irgacure 651, 2,2-dimethoxy-2-phenyl acetophenone, decomposes readily upon UV irradiation to yield free radical species and is widely used as a photoinitiator in the free radical polymerisation of acrylates.

Benzil ketal photoinitiators have photo-fragmentation processes that are well established, Scheme 2.3-9 [81]. For Irgacure 651, the primary photoproducts are known to be the α,α-dimethoxybenzyl radical (1) and the benzoyl radical (2).
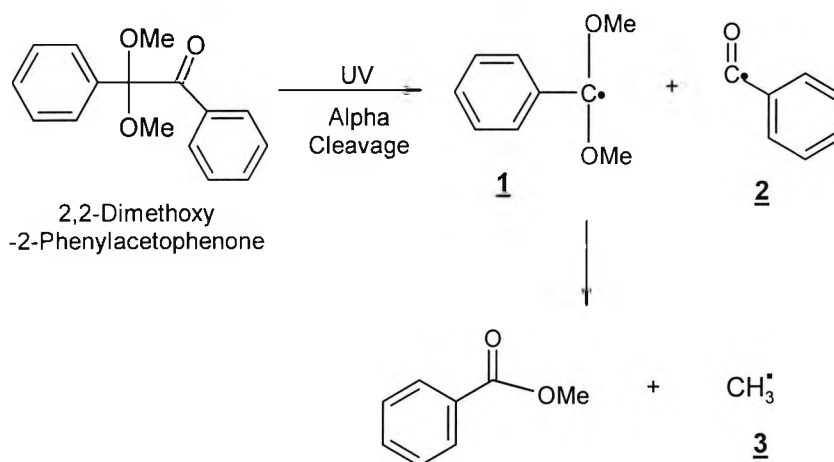
Scheme 2.3-9   photo-fragmentation of benzil ketal initiators

In free radical systems, the unstable benzoyl radical is presumed to be the primary initiating species, having a lifetime of 7.5×10^{-7}s. The more stable benzyl radical, having a lifetime of 170×10^{-7}s, eventually undergoes further fragmentation to yield the benzoate ester and a methyl radical (3). The latter is thought to be an initiating radical that is of only secondary importance to the acrylate curing process.

The purpose of these experiments was to evaluate the effect of the concomitant generation of free radical generating species on the rate of photodecomposition of the iodonium salt. These results are shown in Figure 2.3-13.
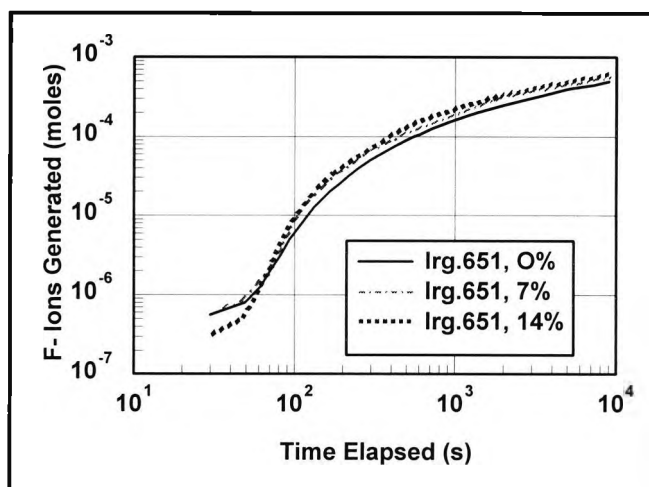
Figure 2.3-13   **Fluoride ion evolution following UV irradiation of solid-state DPIHFP in the presence of Irg.651**

The effect of the presence of the free radical photo-initiator, Irgacure 651, on the photodecomposition of the onium salt, DPIHFP, is quite clear. The maximum rate of photodecomposition increases by about 30-45%. Thus the kinetics of the anion decomposition process are strongly affected. This indicates the involvement of additional processes. The rate and yield data obtained for these experiments are contained in Table 2.3-8.

	0 % Irg.651	7% Irg.651	14% Irg.651
$rate_{max}$ (10^{-7} mols^{-1})	2.6	3.4	3.8
$time_{to\ max\ rate}$ (s)	155	150	155
$yield_{max\ rate}$ (10^{-5} moles)	2.0	2.5	2.9
$Equiv_{max\ rate}$	0.09	0.11	0.12

Table 2.3-8   **Parameters for fluoride ion detection following UV irradiation of solid-state DPIHFP in the presence of Irg.651**

Alpha cleavage free radical photo-initiators and onium salts have been used in combination for quite some time [82,83]. Additional photochemical routes are accessed via such combinations and these are said to explain the increased activity of formulations containing both types of photoinitiator. Interestingly, such processes do not require a source of protons to be identified.

Scheme 2.3-10 represents the work of Ledwith [82] and Sundell [84].

Ledwith et al. (see steps A_1-A_3) proposed that the liberation of the anion is brought about by reduction of the diphenyliodonium cation by a free radical obtained from scission of the free radical photo-initiator. The latter is oxidised to a cation in the process. This redox-derived cation may lead to the formation of an initiation complex in the presence of monomer and bring about cationic polymerisation of divinylethers and cyclic ethers.

Sundell et al. (see steps B_1-B_3) proposed that a similar reduction of the DPI cation may be achieved via the α-ether radical obtained after reaction of the photoinitiator fragments with monomer. An ion pair initiation complex is thus formed.
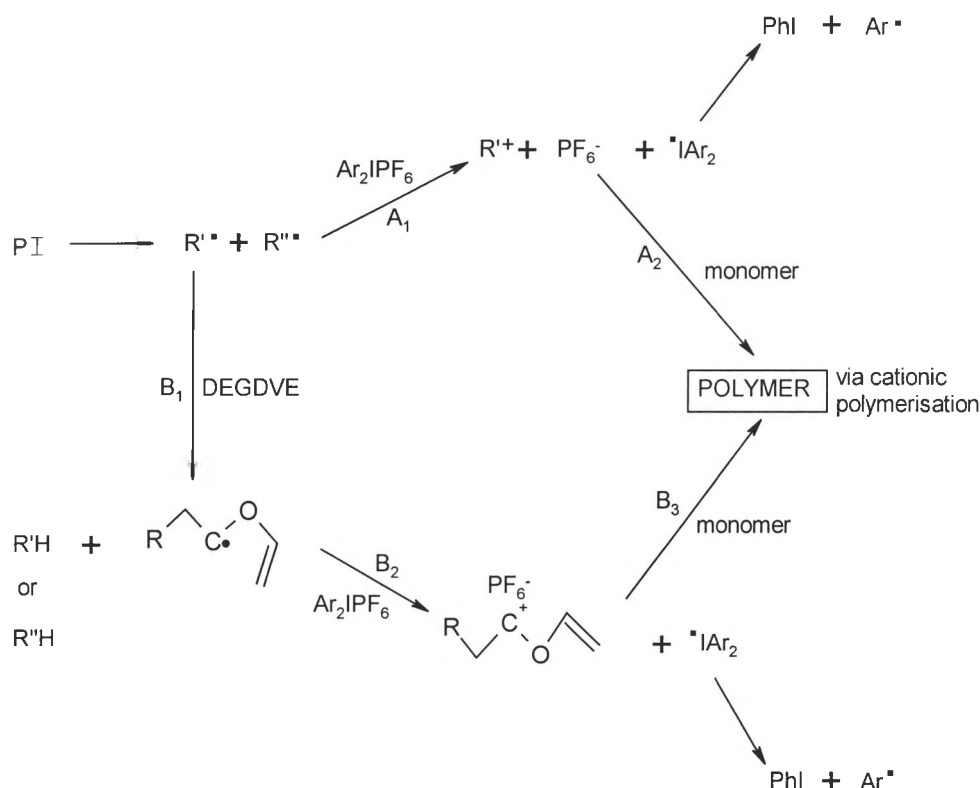
Scheme 2.3-10   **Photo-redox sensitised polymerisation of DVE's: Sundell and Ledwith**

These results indicate, quite significantly, that divinyl ethers can be polymerised

cationically at wavelengths outside the spectral response of the cationic initiator being used, when irradiated in conjunction with the appropriate free radical photo-initiator. In this manner the sensitivity of the system can be extended well into the range of 300-400 nm. The process may, in this manner, proceed without <u>photochemical</u> involvement of the onium salt, and may be mediated by light of wavelengths distant from the absorption maxima of the onium salt.

The feasibility of this process has been shown [81-90] with several ketal photo-initiators, several onium salts and several monomer types. The relative contribution of the redox process will be affected by the absorption maxima of the respective initiator and the wavelength emission spectrum of the UV source. The rate of photodecomposition will be adversely affected if UV screening of the respective initiators occurs due to overlap of their absorption spectra. In such cases the relative concentrations of the 2 initiators will also be a factor.

The rate of reaction will also be affected by the redox potentials of the respective initiators; the energy required to oxidise the radical E_{RAD}^{OX}, must be greater than the energy required for reduction of the onium salt, E_{ON}^{RED}, so that the free energy for the redox process, ΔG^{REDOX}, can be negative and the reaction exothermic, Scheme 2.3-11, [83].

$$\Delta G^{REDOX} = E_{RAD}^{OX} - E_{ON}^{RED} < 0$$

Scheme 2.3-11   Energetic criteria for photo-redox sensitization

The reduction potential of the Ph_2I^+ ion has been determined [90] and found to be -14 $KJmol^{-1}$. The same authors estimated the oxidation potentials of the 3 radicals derived from the photolysis of Irgacure 651 and found them as follows, Figure 2.3-14:

alpha-Ether radical $\leq$ -78 $KJmole^{-1}$

Benzoyl radical   > -78 $KJmole^{-1}$

$CH_3^\bullet$ Methyl radical   0
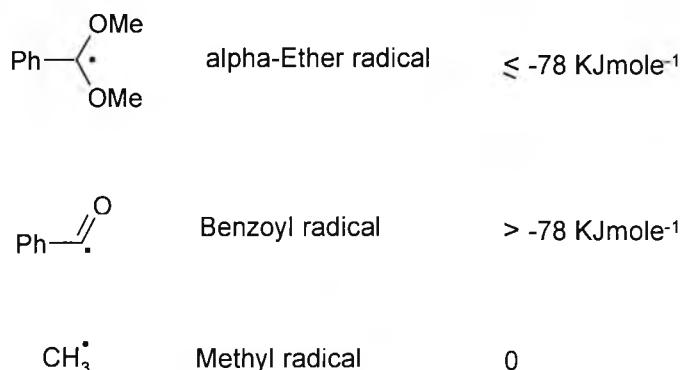
Figure 2.3-14   Estimated oxidation potentials for radicals arising from fragmentation of benzil ketal initiators

This would indicate that in the solid-state experiments (where no monomer is present), the most likely species to reduce the diphenyliodonium cation is the α-ether radical, which is the longer-lived of the 2 main products. The methyl radical cannot be involved.

It is interesting to note that the oxidation potentials for the photo-products of Irgacure 184, (1-benzoylcyclohexan-1-ol), decomposition are reported [84] as $\leq$ 126 KJmol^{-1}, which implies that the latter should be a more efficient photosensitiser than Irgacure 651. Irgacure 184 was not examined in the present study.

With this background, the results of the present study can be understood: Under a polychromatic light source, Irgacure 651 and DPIHFP in combination absorb UV light more efficiently.

Some of the light is absorbed directly by the DPIHFP, which undergoes decomposition and yields PF$_5$, which is subsequently detected as HF in water, following hydrolysis. This is the only process that is taking place when DPIHFP is the only initiator present (i.e. when the Irgacure 651 level is nil).

In the presence of Irgacure 651 at a level of 7% mol/mol, the latter simultaneously absorbs light at different wavelengths, and sensitises the redox-induced photodecomposition of the onium salt. Thus the rate of onium salt decomposition is accelerated (although the final fluoride ion yield remains unchanged).

At a level of 14% mol/mol, the rate of decomposition shows only a modest additional increase. This is possibly due to screening of the DPIHFP salt by the Irgacure 651, due to overlapping absorbance spectra. This will cause a reduction in the primary (cationic) decomposition pathway. The latter problem is only partially offset by the photosensitising effect of the Irgacure 651.

It is interesting to note that for the redox photosensitization to occur in the solid state, the DPIHFP and Irgacure 651 must be co-crystallised which is unusual. While much of the literature in this area concerns the polymerisation of divinylethers by photoredox sensitization, Yagci [86] has also shown that epoxides may be polymerised (thermally) by a photoredox process. There is, thus, no reason why the same cannot be achieved photochemically.

2.3.7   Effect Of Photoinitiator Density Variation

It is of interest, for applications purposes, to determine the effect of photoinitiator surface density/film thickness on the rate and/or extent of production of fluoride ion producing gases.

Solid-state photodecomposition experiments were carried out with equal quantities of the Irgacure 261 initiator, 2.3×10^{-4} moles, at various levels of surface density between $380 gm^{-2}$ and $1760 gm^{-2}$. This variation in initiator surface density, or film thickness, was obtained by evenly depositing the concentrated acetone/initiator solution onto the filter disk substrate to form circles of diameter 2-5cm. The solvent was removed by evaporation. Results are indicated in Figure 2.3-15.
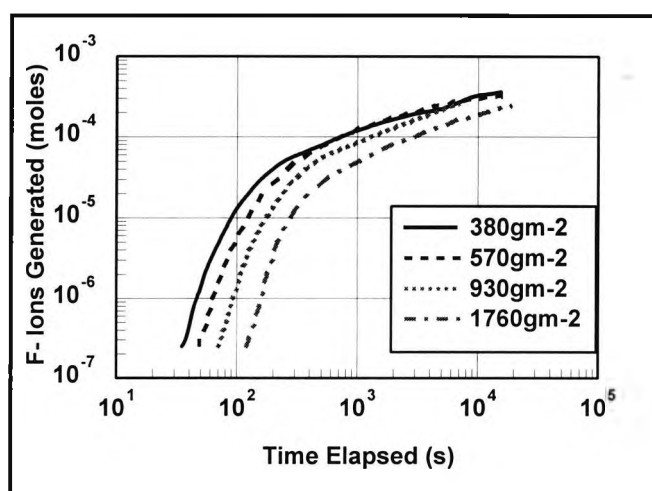
Figure 2.3-15   **Fluoride ion evolution following UV irradiation of solid-state Irg.261 at various surface density values - effect of photoinitiator surface density**

The surface density/film thickness of the solid-state photoinitiator has a very strong impact on the rate of fluoride ion production and the final yield thereof. Increasing the loading from $380 gm^{-2}$ to $930 gm^{-2}$ causes a reduction in the rate of production, while the final yield is unaffected over the duration of the experiment. Increasing the loading further to $1760 gm^{-2}$ has a consistent effect on rate but a reduction in yield is also noted as the rate drops quickly with the evolution of 10^{-5} moles of fluoride, see Figure 2.3-16 and Table 2.3-9.

115
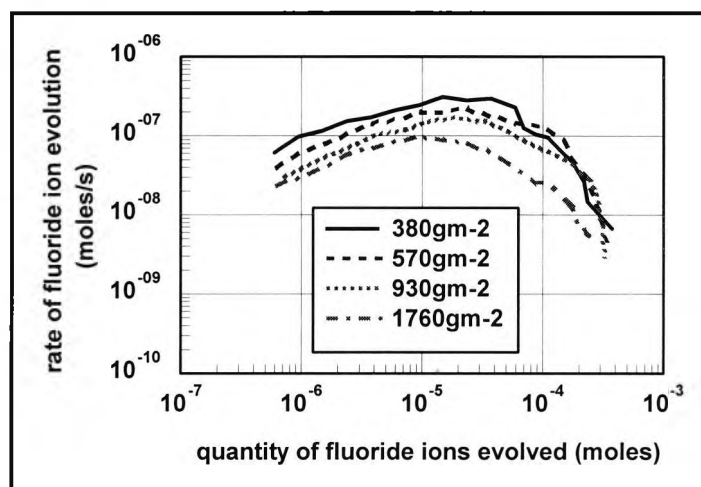
Figure 2.3-16   **Rate of fluoride evolution as a function of quantity evolved fluoride ion evolved, UV irradiation of solid-state Irg.261 at various surface density values - effect of photoinitiator surface density**

It is likely that these effects can be explained by 2 factors:

- Reduced penetration of UV light as surface density increases (screening)

- Reduced escape of gaseous products as surface density increases

These factors combine to favour the use of low photoinitiator densities for the maximisation of fluoride ion yield.

	380 gm^{-2}	570 gm^{-2}	930 gm^{-2}	1760gm^{-2}
rate$_{max}$ (10^{-7} mols^{-1})	3.1	2.4	1.6	1.0
time$_{to\ max\ rate}$ (s)	110	150	220	370
yield$_{max\ rate}$(10^{-5} moles)	1.7	1.8	1.8	1.8
Equiv$_{max\ rate}$	0.07	0.08	0.08	0.08
rate$_{200\ mins}$(10^{-9} mols^{-1})	8.0	1.8	3.7	4.0
yield$_{200\ mins}$(10^{-4} moles)	3.4	3.1	2.9	2.0
Equiv$_{200mins}$	1.4	1.3	1.2	0.9

Table 2.3-9   **Parameters for fluoride ion detection following UV irradiation of solid-state Irg.261 at various surface density values - effect of photoinitiator surface density**

116

2.3.8 Effect Of Photoinitiator Substrate Variation

It is of interest, for applications purposes, to determine the effect of photoinitiator substrate variation on the rate and/or extent of production of fluoride ion producing gases.

Solid-state photodecomposition experiments were carried out on various substrates, with equal quantities of the Irgacure 261 initiator, 1.2×10^{-4} moles, at equal surface density of 570gm^{-2}. The substrates used were filter discs of (a) PTFE, (b) cellulose paper (c) polypropylene and (d) borosilicate glass fibre. Results are indicated in Figure 2.3-17.
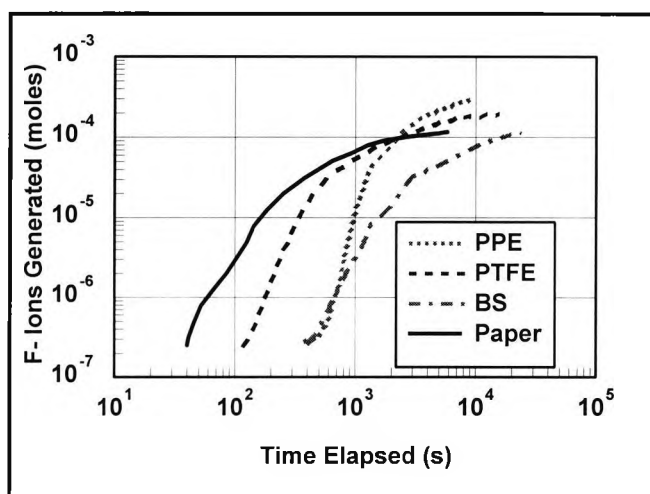
Figure 2.3-17   **Fluoride ion evolution following UV irradiation of solid-state Irg.261 on various substrates - effect of photoinitiator substrate variation on fluoride ion evolution**

There was considerable variation, not only in the chemical composition of the substrate material, but also in the physical morphology i.e. texture, thickness, absorptivity. These experiments show that the choice of substrate has a strong impact on the rate of evolution of the fluoride ion producing gases.

The most rapid evolution occurs with the cellulose substrate, which was the substrate of choice for most of the experiments described previously in this chapter. This result may be explainable in terms of the presence of abstractable protons contributing to the ease of formation of protic decomposition products.

The least rapid evolution occurs with the borosilicate support, which is not a hydrogen source for the decomposition process. Furthermore, this substrate was very thick and absorptive and the results might also be explained by lack of UV light penetration into the substrate. Intermediate results were obtained with the PPE and PTFE substrates which are not rich proton sources but which are thin non-absorbent materials.

3 REMOTE AND DIRECT PHOTO-POLYMERISATION

3.1 Introduction

Polymerisation of epoxides, following U.V. irradiation in the presence of photolytically unstable onium salt initiators, is generally presumed to require and proceed with an intact non-nucleophilic complex counter-ion stabilising the propagating carbo-cation centre. This study (and this chapter in particular) seeks to determine the ability of the gaseous species produced following solid state photolysis of onium salts (described previously) to bring about polymerisation of epoxides. This is compared to the classical or direct process in its ability to achieve the same.

This study required the selection and application of an FTIR sampling method and the consequent imposition of certain formulation constraints. Custom glass, and subsequently PTFE, apparatus were constructed for the polymerisation experiments.

The "remote" process was compared to the direct or "in-situ" process and the effects of some experimental and formulation variables established. Comparison of the "remote" and "in-situ" process profiles may, in view of the gaseous products identified in this study, justify a reconsideration of the accepted "in-situ" polymerisation mechanism and the assumed nature of the propagating species therein.

The remote process has also been conducted in a 2-stage manner i.e. 1st or 'light' stage - U.V irradiation of photoinitiator, 2nd or 'dark' stage - exposure of epoxides to accumulated gases. The efficacy of curing hybrid cationic/free radical systems in selective steps has also been examined.

3.2 Experimental Techniques

3.2.1 Formulation

Several constraints become apparent with regard to the formulation of coatings for this study.

- The test formulation(s) should be capable of wetting the substrate without reticulation over a period of at least 30 minutes, which would turn out (see later) to be the typical duration of remote photo-polymerisation experiments.

- The viscosity of the uncured material should be high enough to prevent noticeable sag if held in any non-horizontal orientation for as long as may be required to obtain an IR spectrum (about 1 minute or less).

- The components of the formulation should be compatible with one another so that the polymerisation may be properly studied in a single homogenous phase. This would also contribute to the quality of IR spectra by eliminating interference from extraneous optical effects.

- The formulation should produce an IR spectrum that enables the bands of interest to be distinguished and quantified in the uncured and in the cured condition.

- The components should not be significantly volatile under experimental conditions to avoid compositional changes that may frustrate quantitative study.

- The components should be sufficiently reactive to be studied in both direct and remote polymerisation processes in a practical time frame (less than 60 minutes). Conversely the materials should not react so quickly that study of them is not practical.

3.2.1.1 Epoxide Systems

Only 3 commercial materials were identified as suitable for the present study:

(a)   VCHDO, Vinyl cyclohexene dioxide

3-Vinyl-1-cyclohexene diepoxide

(Aldrich, #11,015-9, CAS 106-87-6)
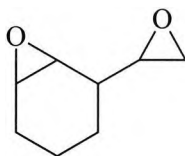
Figure 3.2-1   Vinyl cyclohexene dioxide

(b)   Cycloaliphatic epoxide

3,4-Epoxycyclohexylmethyl-3',4'-epoxycyclohexane carboxylate

(Union Carbide, Cyracure UVR6110, CAS 2386-57-0)
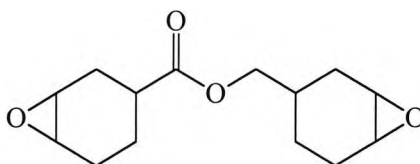
Figure 3.2-2   Cycloaliphatic epoxide

(c) Epoxidised Polybd

Hydroxyl terminated epoxidised polybutadiene

(Sartomer, R451E)
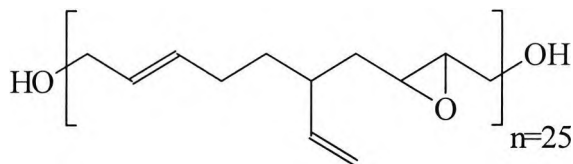
Figure 3.2-3   Epoxidised polybutadiene

Triethylene Glycol Divinyl Ether was obtained from GAF Corporation.

These were combined to meet the criteria mentioned previously as follows:

Formulation	1	2	3	4
Component (% w/w)				
(a) VCHDO	22.2	21.9	21.8	
(b) UVR6110	22.2	21.9	21.8	50.0
(c) Epoxidised Polybd	55.6	54.7	54.4	50.0
DPIHFP		1.5	2.1	
Total	100	100	100	100

Table 3.2-1   **Epoxide formulations used in remote and direct curing experiments**

UVR6110 was subjected to vacuum distillation at room temperature for 3 hours prior to use to remove any water. Materials were blended together by hand and then mixed thoroughly for several hours using a magnetic stirrer at 50°C. Photoinitiators, where introduced, were dissolved initially in (a)VCHDO.

All formulations, 1-4, were clear and transparent.

Formulations containing water, 5-11, were made using distilled water. These were blended rigorously by hand and then mixed thoroughly with a magnetic stirrer at 30°C.

All solutions containing water were found to have a milky appearance indicating the appearance of a bi-phase system i.e. a water-in-'oil' emulsion. Spectra obtained from these formulations were treated with caution. These formulations appeared stable on standing.

Formulation	5	6	7	8
Component (% w/w)				
(a) VCHDO	22.2	21.5	21.1	20.0
(b) Cycloaliphatic epoxide	22.2	21.5	21.1	20.0
(c) Epoxidised Polybd	55.6	53.7	52.7	50.0
Water	2.0	3.3	5.1	10.0
DPIHFP				
Total	100	100	100	100

Table 3.2-2   **Epoxide/water formulations used in remote curing experiments to evaluate the effect of bulk water**

Formulation	9	10	11
Component (% w/w)			
(a) VCHDO	21.4	20.9	20.1
(b)Cycloaliphatic epoxide	21.4	20.9	20.1
(c) Epoxidised Polybd	53.0	52.2	50.4
Water	2.7	4.6	8.0
DPIHFP	1.46	1.43	1.38
Total	100	100	100

Table 3.2-3   **Epoxide/water formulations used in direct curing experiments to evaluate the effect of bulk water**

Formulations 13 & 14 were based on (a)VCHDO only and were low in viscosity and did not form a film of consistent thickness. Spectra obtained from these formulations were treated with caution. Propylene carbonate was incorporated for comparison with formulations containing high levels of water. These formulations and experiments based on them are not reported here as spectra obtained were of poor quality.

Formulation		13	14
Component (% w/w)	Initiator conc (mol kg^{-1})		
(a) VCHDO		83.00	83.00
Water			
Prop. Carbonate		16.18	16.44
DPIHFP	0.015	0.70	
Irgacure 261	0.015		0.56
Total		100	100

Table 3.2-4   **Formulations containing equal molar quantities of different photoinitiators for cure speed comparison**

For purposes of comparison DPIHFP and Irgacure 261 were formulated at an equivalent molar concentration of 0.015 mol kg^{-1}.

3.2.1.2 Hybrid Epoxide/Acrylate Systems

The acrylate resin used for Hybrid curing experiments, HDDA, hexane-1,6-diol diacrylate and N-methyldiethanolamine were obtained from Aldrich Chemical Company. Irgacure 907 (2-methyl-1-[4-(methylthio)phenyl]-2-morpholino propanone-1) was obtained from Ciba Geigy. HDDA was selected because of its compatibility with UVR6110 and because, being difunctional and having similar density to UVR6110, the ratio of epoxide to acrylate functional groups per unit volume is quite similar enabling side by side comparison of cure speed at equi-molar formulation quantities. The formulation examined is given in Table 3.2-5.

Component	Mr	Mass(g)	Moles	%w/w
HDDA	226	0.4036	0.00179	41.2
UVR6110	252	0.4500	0.00179	46.0
Irg.651	228	0.0272	0.000012	2.8
(EtOH)$_2$NMe	119	0.0979	0.00082	10.0
		0.9787		100

Table 3.2-5   **Formulation containg a combinationof acrylate and epoxide resins for hybrid remote/direct curing experiments**

3.2.2 Measurement Of Cure

3.2.2.1 Approach

3.2.2.1.1 Selection Of FTIR

FTIR (Fourier Transform Infrared) was selected as a means of analysing the progress of polymerisation. This instrumental methodology is now well established and thoroughly described in the literature [91]. Polymerisation reactions may be studied by other methods [92] such as photo-calorimetry or Gel Permeation Chromatography. However, the FTIR technique has at least three relevant technical advantages.

(a) Sampling techniques exist (external reflectance) which are completely non-destructive and non-invasive of the sample. Resins subject to polymerisation may be examined at all stages of the process from uncured liquid to hard, glassy polymerised film without the need to separate the material from the substrate or manipulate it in any way.

(b) Measurement can be very fast. Data is collected from all spectral frequencies virtually simultaneously (Felgett advantage) and so a complete infrared spectrum requires only a single scan and, often sufficient for qualitative purposes, may be obtained in less than a second. Multiple scans may be required for quantitative purposes and with 8-16 scans the signal to noise ratio is increased to a level satisfactory for materials in the micrometer range of thickness.

(c) Films subjected to polymerisation may be of known and controlled thickness.

These three points make the FTIR method particularly suitable for the analysis of samples which are undergoing surface directed chemical attack and those which are capable of extended reactivity long after the energy source is removed or switched off. Such is the present case.

3.2.2.1.2 Sampling - General

For many substances transmission measurements are often the preferred method of IR sampling as measurements are uncomplicated. However KBr and NaCl supports are considered unsuitable for studying ionic polymerisations as the substrate is thought to interfere with the reaction. Inert supports such as polyethylene or polypropylene are of limited value as spectral bands from these materials interfere with quantitation of target bands in the sample.

Reflectance methods are also available which may be classified broadly [93] into 2 approaches – Internal Reflection and External Reflection. Both of these approaches have the advantage that the resin is applied to a substrate that is optically reflective, such as metal or crystal, and which interferes little with the IR spectrum or the polymerisation to be studied. Several publications exist [91-94] which discuss and sub-classify these techniques in the following manner:

3.2.2.1.3 Sampling By Internal Reflection IR Spectroscopy

The internal reflectance technique involves the use of an inert and non-absorbing crystal support. IR light is made to reflect, multiple times, internally along the length of the crystal support that is in contact with the sample. When internal reflectance occurs at a point of contact with an IR absorbing material, the latter is in contact with an evanescent wave set up as the interference wave of the incident and reflected waves at the boundary of the crystal. The IR absorption causes the attenuation of the propagating IR beam - ATR, attenuated total reflection.

The internal reflectance technique increases the effective path length of the interrogating beam through the material. Thus spectra of weakly absorbing materials can be obtained more effectively. Reproducible contact is maintained between sample and crystal by a variable pressure device.

A feature of this method is that the spectra are obtained at a certain depth of penetration of the sample. This depth depends on the wavelength of incident light and the refractive indices of the crystal and sample media. Thus the depth of penetration varies across the IR spectrum and varies also, for a given wavelength, if the refractive index of the sample changes upon polymerisation.

These factors combine to make the technique problematic for the study of surface acting and gas mediated processes in functionalised resins where a number of functional groups are to be studied at wave numbers from 800 cm^{-1} to 3500 cm^{-1}, and where strong changes in refractive index are known to occur upon polymerisation from a liquid medium to solid medium.

Furthermore the technique is quite invasive. It is not possible, in semi-cured films which potentially having variation in functional group conversion throughout the film thickness, to estimate the impact of the technique on the condition of the sample prior to the acquisition of the spectrum.

For these reasons the use of ATR was restricted to a number of direct cure experiments.

3.2.2.1.4 Sampling By External Reflection IR Spectroscopy

The external reflection technique involves the application of a sample to a reflective substrate and a mirror arrangement that permits the sample to be interrogated with incident light and collection of the reflected light following transmission, Figure 3.2-4.
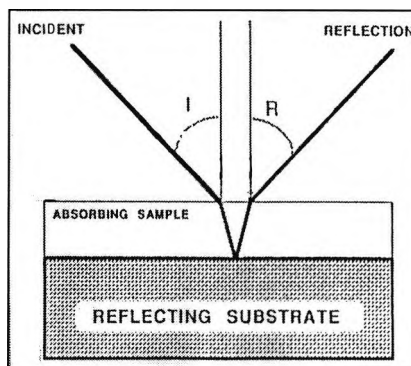
Figure 3.2-4   **Optical path for external reflection measurements**

This technique has the advantage that it is completely non-destructive of the sample. A transmission\absorbance spectrum can be obtained which, in principle, should not require any mathematical transformation or modification. Furthermore, due to reflection at the substrate\resin interface, the path length is effectively more than double the thickness of the film, which enables satisfactory spectra to be obtained with even very thin films (1μm).

3.2.2.1.5 Complications Affecting The Interpretation Of External Reflectance Spectra

However, reflection processes are always complicated. Greenler [95] was amongst the first workers to address the problem of optical artefacts in IR spectra, and since then numerous contributions have been made [95-101] which identify these artefacts and enable proper methodological development. A summary of this work follows in this section. Spectra found in this section as illustration have been obtained experimentally.

The resin-on-substrate sample should be viewed as consisting of 3 interfaces. In the order in which the light encounters these interfaces they are:

- air/resin interface

- resin/aluminium interface

- resin/air interface

At each of these interfaces light may undergo reflection or transmission, Figure 3.2-5.

Reflection and transmission at an interface
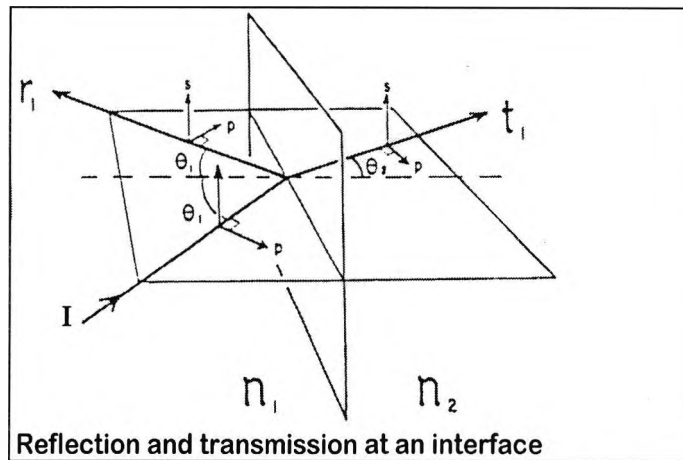
Figure 3.2-5   **Optical paths at an interface between transmitting media having different refractive index values**

At the air/sample interface a proportion of the light is transmitted into the sample film and a proportion reflected. If the surface at the second interface is completely reflective, such as aluminium, light transmitted to that interface from the first interface undergoes complete reflection. At the final interface a proportion of the light transmitted to that interface is reflected internally within the sample film and a proportion is transmitted through the interface to the air. This light, having undergone transmission-reflection-transmission, can be collected subsequently at the IR detector.

If the sample interacts energetically with the light to absorb energy at specific wavelengths, a transmission IR spectrum is the result, and this can be converted directly into an absorbance plot. When an absorbance spectrum, Figure 3.2-6, is obtained only from transmitted light in this way, the spectrum is straightforward and is termed reflectance-absorption (RA).
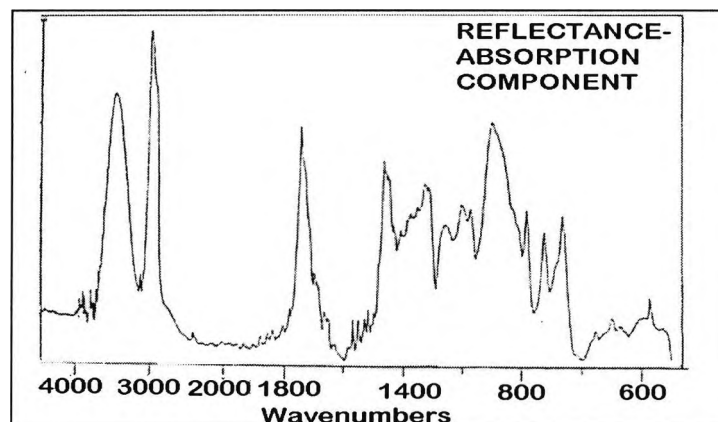
Figure 3.2-6   **Reflectance-Absorbance IR spectrum for an uncured epoxide formulation at acute angle of incidence (specular component minimal)**

Light reflected at the first interface, Figure 3.2-7, is called specular reflection (SR) and if it interacts with the sample and is collected, an IR spectrum can be obtained.
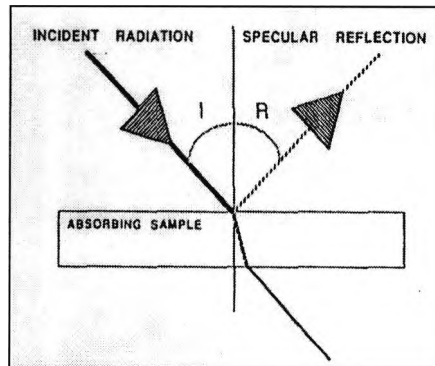
Figure 3.2-7   **Optical path for light reflected at the interface between two transmitting media – specular reflectance**

However, the bands in an SR spectrum are subject to distortion and generally have a first derivative shape. Specular absorption bands are strongly subject to refractive index variation, η_2 , of the sample. If no absorption takes place then η_2 is constant and the dispersion of reflectance is constant and flat. If the sample has an absorption band then η_2 undergoes a characteristic dispersion with wavelength, Figure 3.2-8.
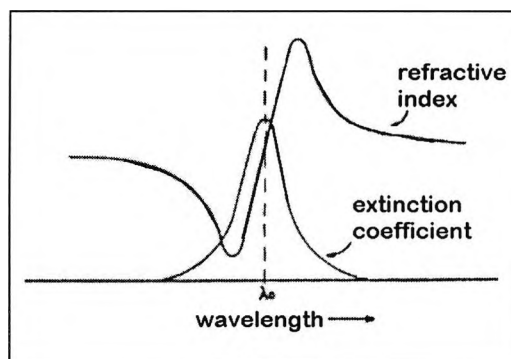
Figure 3.2-8   **Influence of IR absorption on the refractive index of an absorbing material**

Since the amount of reflected light vs. transmitted light at any wavelength is a function of the refractive index of the reflective medium, then a dispersion of the refractive index as indicated in Figure 3.2-9 will produce a reflectance band of similar shape.

130
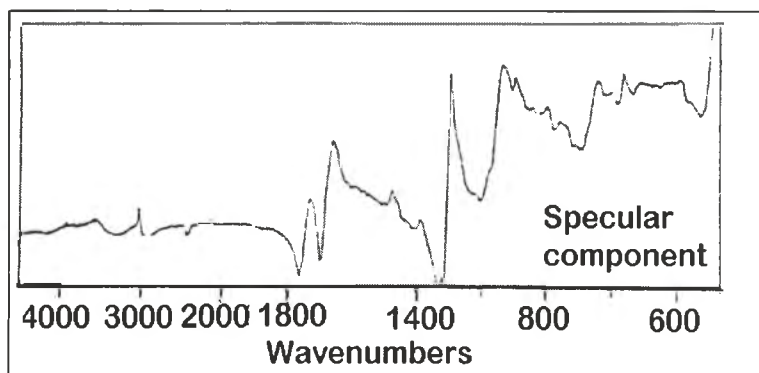
Figure 3.2-9   **Specular Reflectance IR spectrum for a cured epoxide formulation at grazing angle (RA component minimal)**

Essential differences between an SR spectrum and an RA spectrum are that the RA spectrum represents a phenomenon related to thickness or path length and extinction i.e. conforms to the Beer-Lambert Law, where as SR spectra are neither path nor extinction related, i.e. Beer-Lambert Law does not apply. This makes the latter unsuitable for quantitative purposes as absorbance spectra.

In practice, external reflection spectra of most samples are combination spectra and contain a specular component and a reflection-absorption component. This may be termed mixed reflection (MR). The reflectance spectrum is a superimposition of the 2 components, Figure 3.2-10.
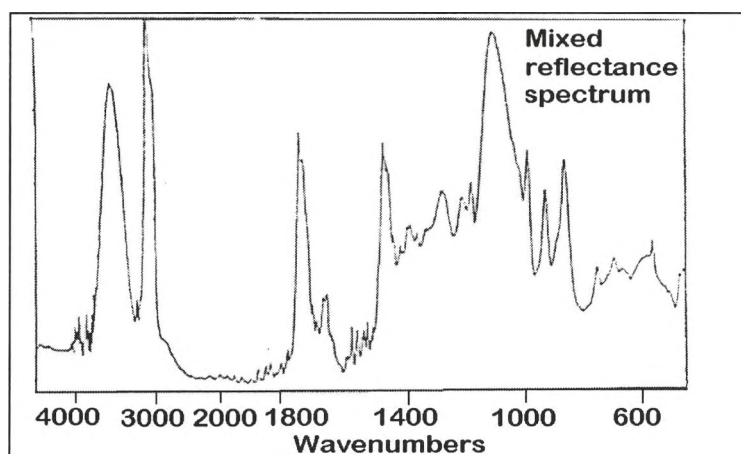
Figure 3.2-10   **Mixed reflectance IR spectrum of uncured epoxide formulation – typical conditions**

The effect of the specular component is to distort the spectrum and frustrate interpretation and quantitation. Where possible the SR effects should be small and development of experimental procedure therefore requires minimisation of this component.

Reflection and transmission at an interface are governed by the Fresnel equations,

Equation 3.2-1, which show a strong dependence on the angle of the incident light and the refractive indices of the media at each side of the interface, η_1 and η_2.

Fresnel's equations at an interface

$$r_{1(s)} = \frac{n_1 \cos \theta_1 - n_2 \cos \theta_2}{n_1 \cos \theta_1 + n_2 \cos \theta_2}$$

$$r_{1(p)} = \frac{n_2 \cos \theta_1 - n_1 \cos \theta_2}{n_2 \cos \theta_1 + n_1 \cos \theta_2}$$

$$t_{1(s)} = \frac{2n_1 \cos \theta_1}{n_1 \cos \theta_1 + n_2 \cos \theta_2}$$

$$t_{1(p)} = \frac{2n_1 \cos \theta_1}{n_2 \cos \theta_1 + n_1 \cos \theta_2}$$

$$R = r^2$$

$$T = t^2 n_2 / n_1$$

Equation 3.2-1 **Fresnel equations describing the path of S and P polarised light at an interface between transmitting materials, as a function of angle of incidence, and refractive index**

Figure 3.2-11 show solutions to the Fresnel equations for reflectance and transmission of s-polarised light where the refractive index varies between 1.0 and 2.0 and where the angle of incidence varies through 90°. The refractive index of air, η_1, is assumed to be unitary and invariable. Liquid epoxide resins generally have a refractive index, η_2, around 1.4 [71]. The solutions for p polarised light are similar.
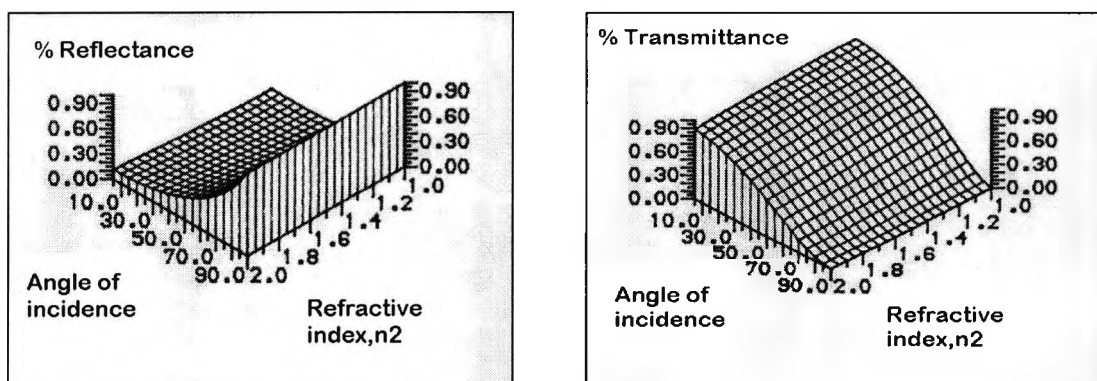
Figure 3.2-11 **Solutions to the Fresnel equations for S polarised light for angles and refractive indices of experimental interest, Reflectance (right) and Transmittance (left)**

These solutions predict an increase in the specular component (% reflectance) as η_2 increases.

As polymerisation (cure) advances there is an increase in the refractive index of the resin [71]. The Fresnel solutions show that polymerisation will be attended by an increase in specular reflectance. Consequently the distortion apparent in the spectra will increase as the reaction proceeds. If the specular component becomes sufficiently large the direct comparison of spectra from cured films with spectra from uncured films will become impossible.

The Fresnel solutions predict that transmission and therefore the reflectance absorption (RA) component will be maximised for s and p polarisations at low incident angles. The specular (SR) component will be maximised at grazing (high) incident angles.

For these reasons it is especially important to obtain reflectance spectra at low incident angles.

Most spectra reported in this work are obtained at 25° which is the lowest angle permitted by the available geometry.

It is clear also that the influence of the SR component can be further reduced by increasing the effective path length for the transmitted light and thereby increasing the RA component. This implies the sampling of films at the highest possible thickness permitted by other constraints (IR detector saturation, reactivity etc.).

3.2.2.1.6 Analysis Of Spectra

Polymerisation of epoxides is generally attended by the appearance/disappearance of at least 3 functional groups and consequently by developments in at least 3 bands in the IR spectrum, Table 3.2-6.

Functional Group	Band Type	Band Centre wavenumber, cm^{-1}	Change
Hydroxyl	O-H stretching	3450	increase
Ether Linkage	C-O stretching	1080	increase
Epoxide	C-H stretching	794	decrease

Table 3.2-6 **Identification and development of principal bands of interest in the polymerisation of epoxides**

In order to follow the polymerisation reaction the appearance and

disappearance of these bands must be quantified. To account for variations in film thickness, variations in the ratio of reflected versus transmitted light due to imperfections in the surface of the sample, an internal reference standard must be chosen from the spectrum. By comparing the intensity of the target band with the intensity of the internal reference band, a ratio can be established which should change only as a result of some development in the target band. Any change in this ratio will permit determination of the percentage change in functional group generation or conversion.

Several general criteria may be defined for selection of internal reference band:

- Minimal variation in intensity or position of band

- Absorbance value greater than 0.4 and less than 1.0 (detector sensitivity)

- Not subject to strong specular distortion

- Band should be of a similar intensity to the studied band

- Band should not be associated with skeletal or other bonds of which the intensity may be sensitive to mechanical, rheological, dielectric or other media effects

By examination of chemical structures and spectra several possibilities were examined as candidates for choice of internal reference standards in the present study, Table 3.2-7:

Functional Group	Band Type	Band Centre wavenumber,cm^{-1}	Advantages	Disadvantages
Carbonyl (cyclo-aliphatic epoxide)	C=0 stretching	1740	• Large. clearly defined • Unaffected by other bands during process	• High extinction, absorbance may exceed 1.0 - saturation • SR effects, band shifts and broadens
-CH$_2$- $_H$>C=C<$_H$ (R451E)	C-H stretching	2900-3100	• Large, clear in the uncured sample • Unaffected by SR	• Strong absorption in aliph. epoxides, absorbance may exceed 1.0 • Affected by growth of broad O-H band
-CH$_2$-	C-H stretching	1440-1450	• Absorbance in same range as epoxide • No involvement with adjacent bands • No band shifts	None

Table 3.2-7   **Identification and comparison of candidate absorption bands for use as internal reference standards for quantitationof other bands**

Based upon these findings the C-H stretch at 1440-1450 was selected as the appropriate internal reference standard.

Figure 3.2-12 indicates the bands of interest in the study of epoxide polymerisation and the band selected as internal reference standard.

135
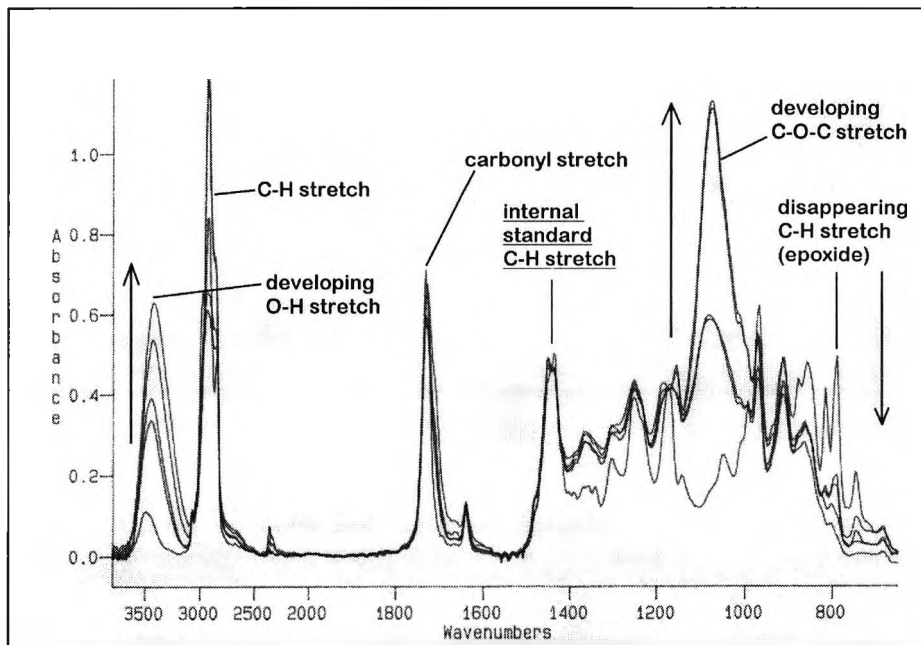
Figure 3.2-12　　　　**example spectra obtained at various stages of epoxide polymerisation, indicating the position and development of all bands of interest**

3.2.2.2 Apparatus

3.2.2.2.1 <u>FTIR Spectrometry</u>

Infra red spectra were obtained with a Digilab FTS60 FTIR spectrometer. Unless otherwise stated the following parameters were applied.

Resolution   8.0 cm^{-1}

Scan speed   5 kHz.

Aperture   2 cm or 1cm or open

Number of scans   16 or 64

Delay   3 secs

Generally, reflectance spectra were acquired through an open sample compartment (without purging) against a recently acquired background spectrum obtained in like manner.

3.2.2.2.2 <u>Sampling</u>

Most spectra reported here were external reflectance (ER) spectra obtained with a variable angle specular reflectance (SR) device from Spectratech. Unless otherwise stated, the incident angle was 25°.

A wet sample was applied by pipette to a polished aluminium substrate of known and reproducible dimensions (approximately 5.0 x 2.5 cm). A film was obtained by manually distributing and smoothing out the sample with the edge of a glass microscope slide. The tared substrate was re-weighed to calculate the mass, volume and thickness of the film (density known). The substrate was fixed in the SR sampling device and a spectrum obtained against a previously acquired background spectrum obtained using an aluminium plate.

A small number of spectra were obtained by attenuated total reflection (ATR) spectra using a device from Spectratech with ZnSe crystal.

The formulation was then drawn down on flexible aluminium foil using a #4 KBar (steel rod tightly wound with wire of specified diameter) and placed in intimate contact with the crystal using a spring-loaded pressure clamp of which the tension had been previously adjusted for optimum spectral quality. A spectrum was obtained using a previously collected background spectrum through the crystal in contact with air only.

3.2.2.3 Treatment of Spectra

Spectra were obtained as absorbance spectra and subjected to multi-linear baseline correction with zero-points established at wavenumbers 3800, 2700, 1800, 1650 and 650.

Band intensity values (absorbance) were obtained by peak height from the baseline corrected spectra.

Intensity values were normalised by reference to the height of the band at 1440-1450cm^{-1}.

i.e. Normalised Absorbance target band = $\dfrac{\text{Actual Absorbance [target band]}}{\text{Actual Absorbance [reference band]}}$

For bands exhibiting a disappearance with polymerisation, e.g. the epoxide C-H stretch at 794 cm^{-1}, the progress may be expressed, for the polymerised (cured) material, as a percentage of functional group consumption/conversion by reference to the normalised absorbance value obtained from a spectrum of the unpolymerised (neat) material.

i.e.

% Epoxide Conversion = $\dfrac{\text{Norm ABS[794 cm}^{-1}]_{neat} - \text{Norm ABS[794 cm}^{-1}]_{cured}}{\text{Norm ABS[794 cm}^{-1}]_{neat}}$ X $\dfrac{100}{1}$

This procedure may not be applied to emerging bands associated with newly generated functional groups as it is not possible to establish a theoretical end point for the reaction from the IR spectrum.

3.2.3   Direct Polymerisation

Resin samples were prepared as described in Sec.3.2.2.2.2.

Samples were irradiated directly beneath the 150W high-pressure mercury lamp for a predetermined period of time.

An IR spectrum is immediately obtained as described in Sec.3.2.2.2.1. and the spectrum is treated as described in Sec.3.2.2.3.

3.2.4 Remote Polymerisation

3.2.4.1 Apparatus

3.2.4.1.1 Glass Cell

Some of the photo-polymerisation experiments described in this section were conducted in a custom glass apparatus.

This device essentially consists of an enclosed chamber, of approximate volume 100 cm^3, with a ground flange sealed to a polypropylene rim with locking nuts and rubber 'o' rings. The window consists of quartz glass of thickness 5mm, sealed in place with commercial silicone cement.

The device is equipped with inlet and outlet lines to allow for purging of the chamber.

The polymerisable epoxide resin is coated onto an aluminium slide which is placed beneath, but not in contact with, the initiator support - the latter being supported with a separation of 5-10 mm on a three-pronged vertical wire support in a back-to-face (rather than a face-to-face) arrangement.

The U.V. source is a 150 W high power mercury lamp enclosed in a silvered jacket, providing for illumination of the sample at a distance of 10cm from the point centre of the source.
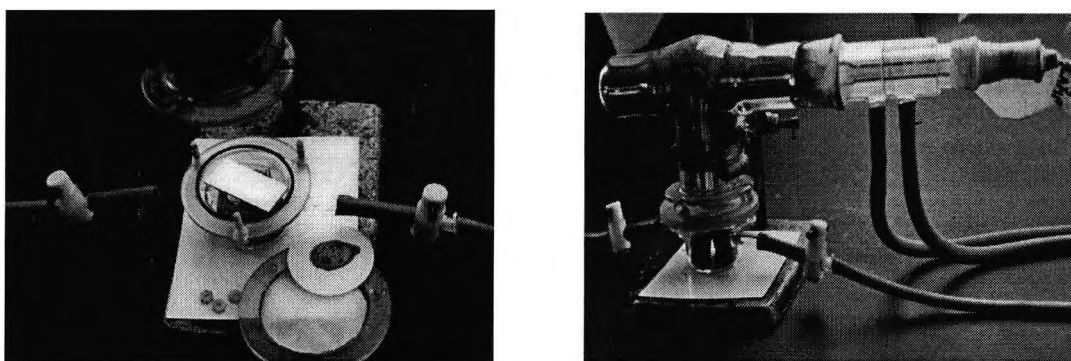
Figure 3.2-13   **Glass apparatus for remote polymerisation experiments, open (left) and closed (right)**

Both the quartz window and the glass walls of the vessel were etched and rendered opaque following U.V. irradiation of the initiator. This led to the construction of an apparatus that would be inert to all photo-products.

3.2.4.1.2 <u>PTFE Cell</u>

Subsequently an apparatus was constructed in PTFE and the remainder of polymerisation experiments were conducted with this device. This apparatus represents a variation of the apparatus described in Sec.2.2.1.2 for the photo-decomposition experiments. This cell was used also in conjunction with the 1500 W medium pressure mercury halide with iron iodide discharge lamp described in Sec.2.2.1.2.
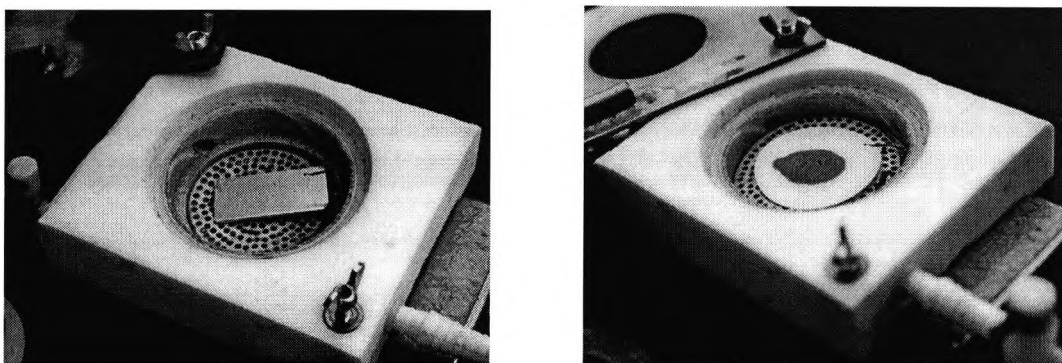
Figure 3.2-14 **PTFE apparatus for remote polymerisation experiments, open, with placing of resin sample (left) then with placing of initiator sample (right)**

An additional shelf is cut into the base permitting the resin sample to be placed on a PTFE support beneath the photoinitiator sample. The latter is placed above (but not in contact with) the resin on a support which essentially consists of a PTFE sheet perforated to about 50% of its area by holes of diameter 2 mm. The separation (gap width) between photoinitiator and support is about 5 mm. This separation can be increased to about 15 mm by introducing spacers between the resin support and the initiator support.
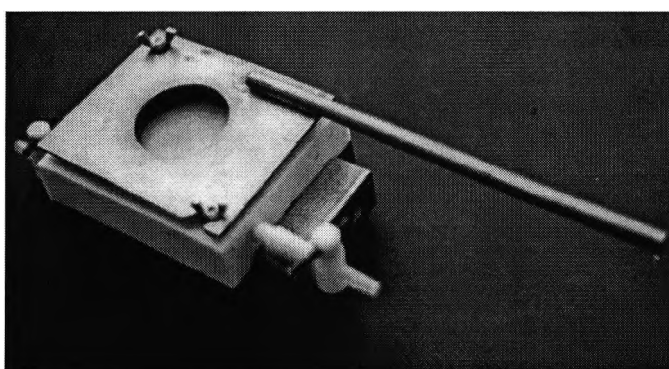
Figure 3.2-15 **PTFE apparatus for remote polymerisation experiments, closed prior to use**

Relative humidity (%RH) within the cell can be measured by means of a thermo-hygrometer and probe (BDH,1991, Cat# 750/1132/10, 750/1132/04).
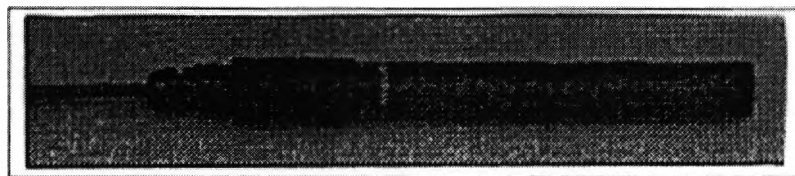
Figure 3.2-16   **Fluoride specific electrode for fluoride ion quantitation**

The probe, of diameter about 20 mm, is inserted into the cell via a bore cut into the cell intersecting the cell directly beneath the resin and communicating with the chamber above by means of a perforated PTFE disc as described previously. The vessel and probe are sealed by means of a tightly fitting 'O' ring.

3.2.4.2 Method

Unless otherwise stated, all experiments were conducted under an atmosphere of dry nitrogen supplied from a cylinder (Matheson Gas Products) and further dried in-line by passage through concentrated sulphuric acid (2 flasks), glass wool and sodium hydroxide pellets.

Photoinitiator supports were prepared as described in Sec.2.2.1.2.

Resin formulations were prepared as described in Sec. 3.2.1.

Resin samples were prepared as described in Sec. 3.2.1.1.

The following method was applied to experiments involving both glass and PTFE apparatus.

The vessel is cleaned with acetone and dried. The resin sample and initiator support are enclosed within the vessel and the vessel sealed to give an air tight-seal. The vessel is flushed with dry nitrogen (about 5 minutes) and the relative humidity measured with gas flowing through. Values were in the range of 0-3 %RH. The probe is withdrawn and this orifice sealed. Closing the stopcocks with a slight internal positive pressure isolates the vessel.

The sealed vessel is placed beneath the appropriate lamp and irradiated for a pre-determined period of time. At the end of the experiment the gaseous contents of the cell

The sealed vessel is placed beneath the appropriate lamp and irradiated for a pre-determined period of time. At the end of the experiment the gaseous contents of the cell are exhausted to an external vent by forcing nitrogen through the line, and the vessel opened.

The resin sample is recovered and an IR spectrum obtained without further delay as described in Sec.3.2.2.2.1 and the spectrum is treated as described in Sec 3.2.2.3.

The relative humidity of the atmosphere within the cell was controlled where necessary by passing the nitrogen directly from the cylinder to a flask of distilled water submerged in a heating bath and then to the cell. To avoid passage of airborne water droplets into the cell, a flask of glass wool was placed between the water bath and the cell. The temperature of the bath was raised to increase the %RH as measured down stream in the purging sample vessel prior to the start of the experiment. Once the measured humidity was stabilised at the required value the vessel was isolated and the probe removed as indicated previously and the experiment commenced. The appropriate water bath temperature was pre-determined in advance of the experiment. No condensation was noted in the photo-polymerisation vessel.

3.2.5 Two-Stage Polymerisation

3.2.5.1 Apparatus

The photodecomposition apparatus and 1500 W lamp can also be used in conjunction with a second cell which is also constructed out of PTFE with dimensions 10.0 cm x 4 cm x 6 cm. The cell is bored to a depth of 6 cm and diameter 2.8cm and fitted with stopcocks at each end. When connected in series the photodecomposition cell may contain the photoinitiator while the second cell will contain the resin sample.
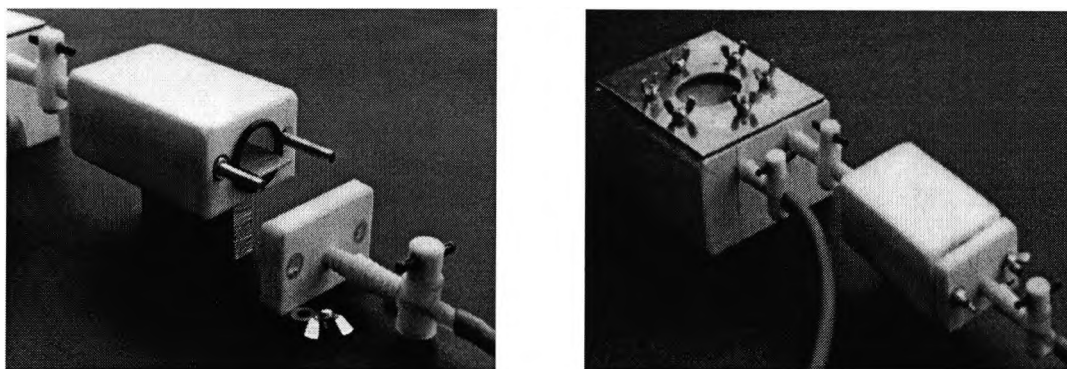
Figure 3.2-17   **PTFE apparatus for 2-stage remote polymerisation experiments, secondary cell open (left) and closed (right)**

3.2.5.2 Method

Unless otherwise stated, all experiments were conducted under an atmosphere of dry nitrogen supplied from a cylinder (Matheson Gas Products) and further dried in-line by passage through concentrated sulphuric acid (2 flasks), glass wool and sodium hydroxide pellets.

Photoinitiator supports were prepared as described in Sec.2.2.1.2.

Resin formulations were prepared as described in Sec. 3.2.1.

Resin samples were prepared as described in Sec. 3.2.1.1.

Both cells are cleaned in advance with acetone and dried. The photoinitiator support is placed in the photodecomposition cell and the resin sample in the second cell. The 2 cells are connected in series and sealed. The vessels are flushed with dry nitrogen and each isolated. The photodecomposition cell is left with a slight positive internal pressure and irradiated for a pre-determined period of time.

144

Towards the end of the irradiation period the second cell is evacuated continuously with a vacuum pump. As the lamp shutter is closed to terminate the irradiation the stopcock connecting the second cell to the vacuum is closed, and the stopcock connecting the 2 cells is opened permitting communication of the 2 cells and passage of decomposition gases from the high pressure cell containing the photoinitiator to the low pressure cell containing the resin, until equal pressure is achieved.

The vacuum is switched off and the resin sample left in contact with the decomposition gases for a pre-determined period of time.

The vessels are then flushed to an exhaust vent with nitrogen and the resin sample recovered. An IR spectrum is obtained without further delay as described in sec.3.2.2.2.1 and the spectrum is treated as described in Sec. 3.2.2.3.

3.3   Results And Discussion

This section reports and discusses the following results:

1. Experiments that confirm the feasibility of measuring cure response in an example epoxide formulation containing photoinitiator - 'Direct curing'.

2. Experiments which explore the feasibility of using the gaseous photoproducts obtained by irradiation of onium salts in the solid state to polymerise cationically curable films - 'Remote Curing'.   The latter film is initiator-free and is adjacent to but not in contact with the nearby solid-state initiator in a closed cell.

3. Explore several parameters affecting the 'Remote' process in comparison also with the 'Direct' process, particularly the effect of water (bulk and humidity) and the effect of film thickness.

4. Experiments that examine the feasibility of using Direct curing of acrylates with the Remote curing of epoxides in a two-step 'hybridized' manner.

Spectra and tabulated data are given as examples for the first Direct Curing experiment and the first Remote curing experiment. These are also included in appendix C (Sec.6) with corresponding headings and captions. All other experiments have the relevant spectra and data located only in the appendix similarly referenced by footnotes.

3.3.1 Development Of Polymerisation In The Direct Process

Polymerisation in the direct process was successfully carried out with an example epoxide formulation (Sec.3.2.1.1, form.2) containing 1.5% DPIHFP photoinitiator, and a 150W Hg lamp (Sec.2.2.1.2) with total output at the initiator surface of approximately 0.12 Wcm^{-2}. The photoinitiator level is consistent with commercial formulations. By contrast, the lamp power is lower by a factor of 10^3. The low light intensity was selected for 2 reasons:

1. To enable the polymerisation to be studied in a stepwise manner by FTIR.

2. To be consistent with the intensity obtained during remote experiments (Sec.2.2.2.2.1). This could not be easily modified.

The spectra and data are provided below (Figure 3.3-1, Table 3.3-1).
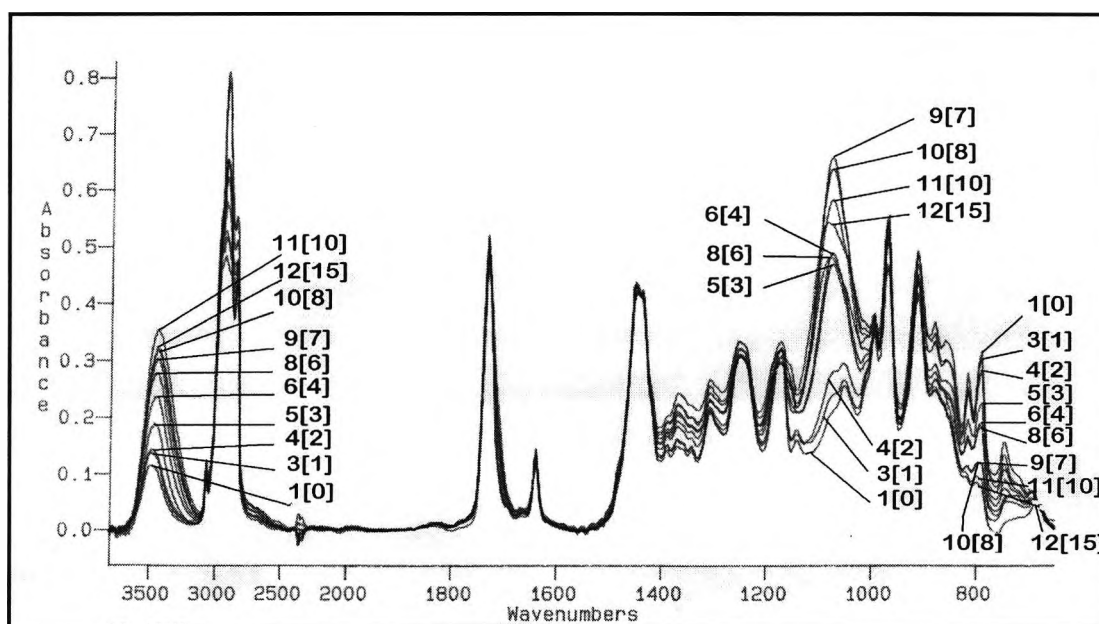
Figure 3.3-1   **Direct curing, IR spectra for direct curing of epoxide**

Expt Number [11]	Sample Thickness (mm)	Elapsed Time (mins)	Band Data								% Conver.
			A 3455 cm^{-1}		B 1444 cm^{-1}		C 1080 cm^{-1}		D 792 cm^{-1}		
			Abs	Abs.N	Abs	Abs.N	Abs	Abs.N	Abs	Abs.N	
4-1		0	0.19	0.27	0.71	1.00	0.35	0.49	0.54	0.76	0.0
4-2	22.6	0.5	0.22	0.31	0.70	1.00	0.36	0.51	0.51	0.73	3.2
4-3	24.2	1	0.26	0.33	0.80	1.00	0.45	0.56	0.58	0.72	4.4
4-4	19.9	2	0.19	0.34	0.56	1.00	0.37	0.66	0.38	0.68	10.6
4-5	20.0	3	0.27	0.45	0.60	1.00	0.67	1.12	0.32	0.54	29.2
4-6	23.0	4	0.35	0.56	0.63	1.00	0.73	1.17	0.29	0.46	39.6
4-7	23.2	5	0.35	0.60	0.57	1.00	0.71	1.24	0.26	0.44	41.3
4-8	23.8	6	0.57	0.66	0.85	1.00	0.98	1.15	0.38	0.44	41.8
4-9	21.2	7	0.33	0.72	0.46	1.00	0.72	1.55	0.13	0.29	62.3
4-10	20.6	8	0.32	0.75	0.43	1.00	0.64	1.49	0.12	0.28	63.2
4-11	22.7	10	0.70	0.84	0.83	1.00	1.07	1.28	0.18	0.21	71.8
4-12	23.9	15	0.49	0.76	0.64	1.00	0.89	1.38	0.12	0.19	75.3

Table 3.3-1   **Direct curing, IR spectral data and experimental data for direct curing of an epoxide**

This data indicates that the polymerisation was successfully followed using the selected methodology. Calculation of the epoxide consumption shows that the reaction proceeds to an epoxide conversion of around 80 % within 10 minutes (Figure 3.3-2).
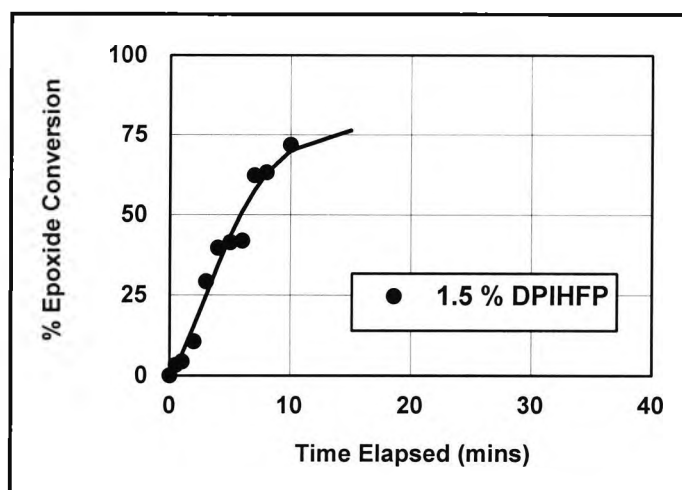
Figure 3.3-2   **Direct Curing, epoxide conversion for direct cure**

This data is consistent with the known mechanism (Scheme 3.3-1) involving the decomposition of initiator (1) to yield the complex Brønsted acid HPF$_6$ (2) and the formation of a fully ionic activated complex (4) with the epoxide monomer (3) and propagation through the classical route. Similar profiles were obtained by Crivello and Co-workers [21].
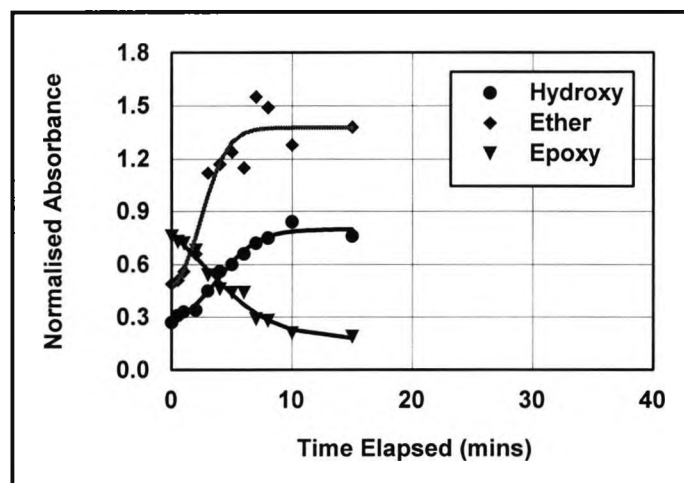
Figure 3.3-3   **Direct curing of an epoxide, IR absorbance bands for relevant functional groups for direct epoxide polymerisation**

It is clear in this case also that the development of functional groups is simultaneous Figure 3.3-3. The appearance of the hydroxyl groups and ethereal linkages is concomitant with one another and the disappearance of the epoxide.
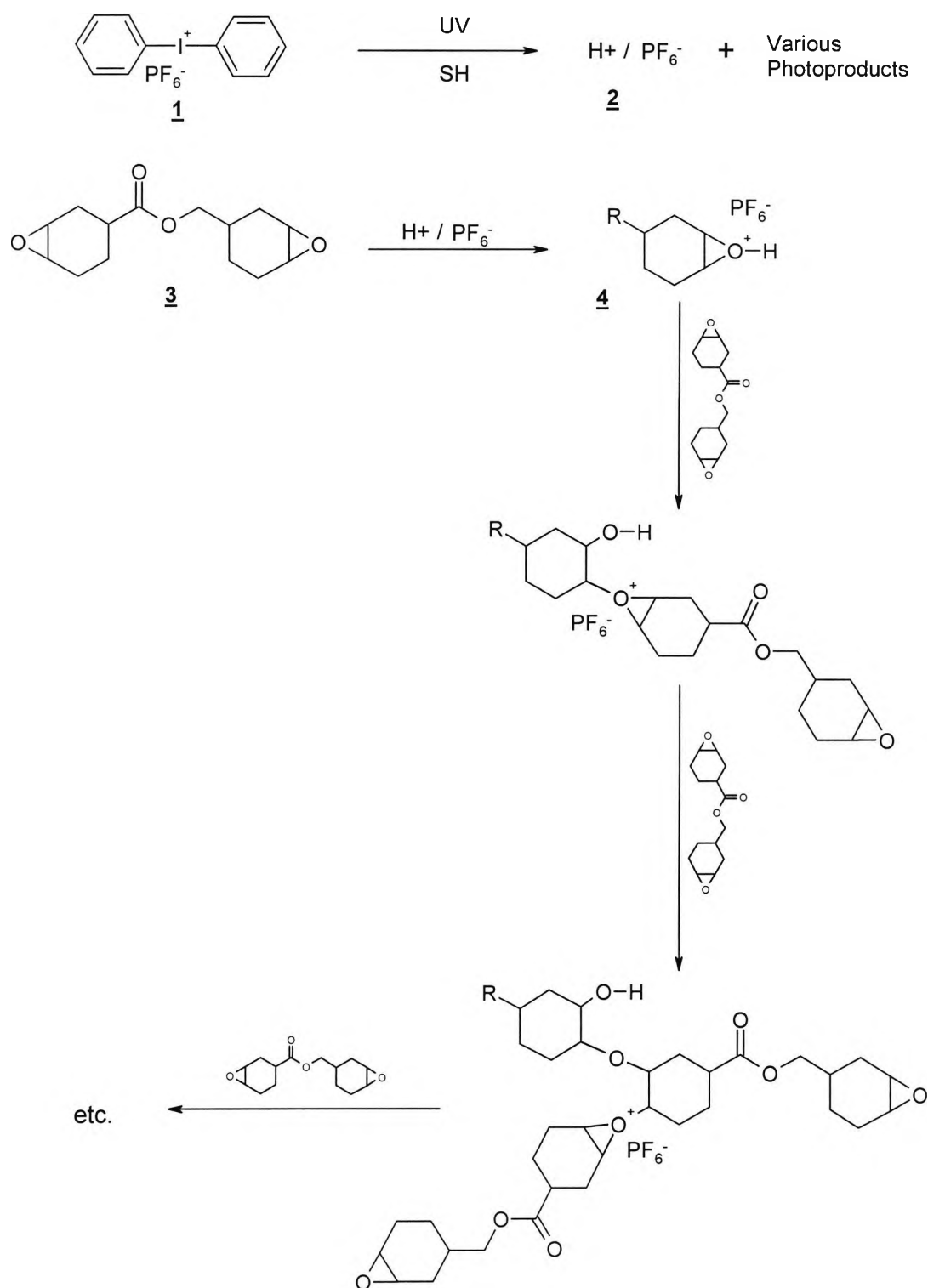
Scheme 3.3-1   **Mechanism for cationic polymerisation of epoxide**

3.3.2 Development Of Polymerisation In The Remote Process

Resin formulation 1 (Sec. 3.2.1.1) was irradiated in the presence of 0.1g of DPIHFP initiator. The film was cured to hardness in less than 30 minutes.

The FTIR spectra are provided below; see Figure 3.3-4. Examination of these spectra clearly indicates the disappearance of the epoxide (792 cm^{-1}) and appearance of hydroxyl groups (3450cm^{-1}) and ethereal linkages (1080 cm^{-1}).
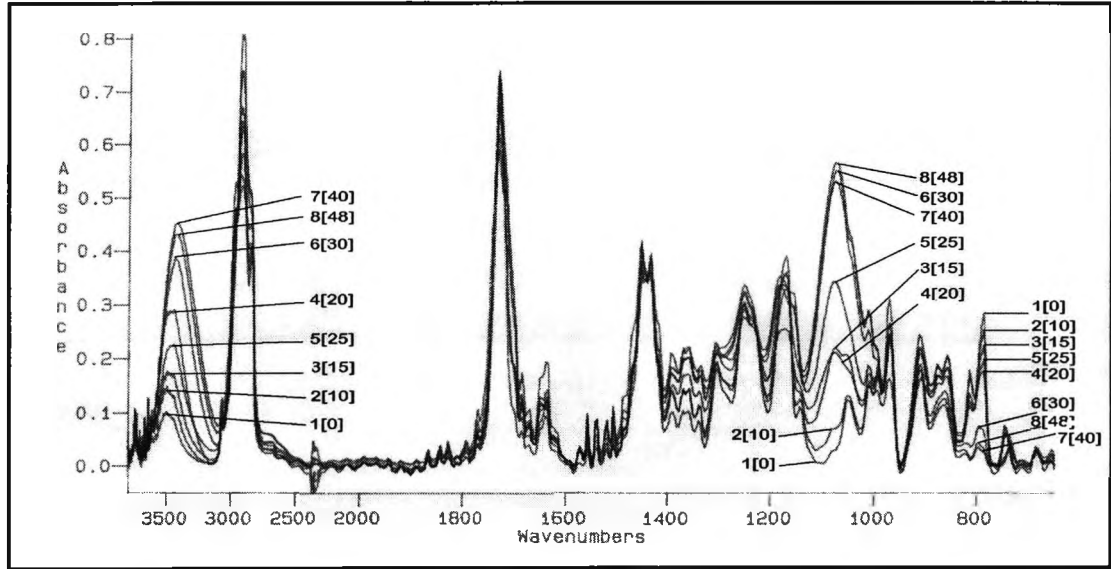
Figure 3.3-4   **Remote curing, IR spectra for remote curing of epoxide**

Expt Number	Sample Thickness (µm)	Elapsed Time (mins)	Band Data								% Conver.
			A 3450 cm^{-1}		B 1440 cm^{-1}		C 1080 cm^{-1}		D 792 cm^{-1}		
			Abs	NAbs	Abs	NAbs	Abs	Nabs	Abs	NAbs	
1	14	0	0.12	0.25	0.48	1.00	0.04	0.08	0.39	0.81	0.0
2	15	10	0.12	0.39	0.29	1.00	0.06	0.22	0.22	0.74	9.1
3	14	15	0.17	0.49	0.34	1.00	0.22	0.64	0.22	0.65	19.4
4	16	20	0.19	0.82	0.23	1.00	0.14	0.61	0.12	0.52	35.7
5	15	25	0.38	0.63	0.61	1.00	0.59	0.98	0.33	0.55	32.0
6	17	30	0.36	1.12	0.32	1.00	0.52	1.62	0.06	0.20	75.6
7	14	40	0.61	1.31	0.46	1.00	0.72	1.55	0.04	0.08	90.4
8	14	48	0.44	1.24	0.36	1.00	0.58	1.63	0.04	0.10	87.9

Table 3.3-2   **Remote curing, IR spectral data and experimental data for remote curing of epoxide**

The absorbance data can be found in Table 3.3-2. The spectra were subjected to

numerical normalisation as described in (3.2.2.3) and the progression of the epoxide, ether and hydroxyl bands compared.

Examination of the data indicates that the resin samples were of consistent thickness (14-17μm) and all actual absorbance values for target bands were less than 1.0, which is satisfactory for linear detection.

The normalised absorbance values for the 3 functional groups can be plotted as a function of time, Figure 3.3-5, to show the development of these groups.
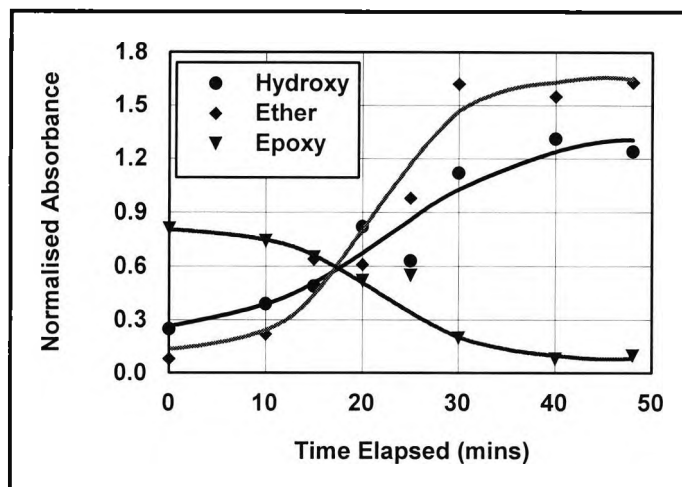
Figure 3.3-5   **Remote curing, IR absorbance band for relevant groups in remote epoxide polymerisation**

It is clear that all 3 bands develop simultaneously and in the complementary manner consistent with the known mechanism of polymerisation [13]. The epoxide band can be plotted as a function of time in the form of percentage conversion, Figure 3.3-6.

The polymerisation follows a sigmoidal type of behaviour characterised by an induction period of around 10 minutes where the conversion rate is slow, followed by a steady rise to about 80% conversion within the next 15-20 minutes followed by a final phase of slow conversion as the epoxide concentration is reduced to a final level which is less than 10% of its original value.
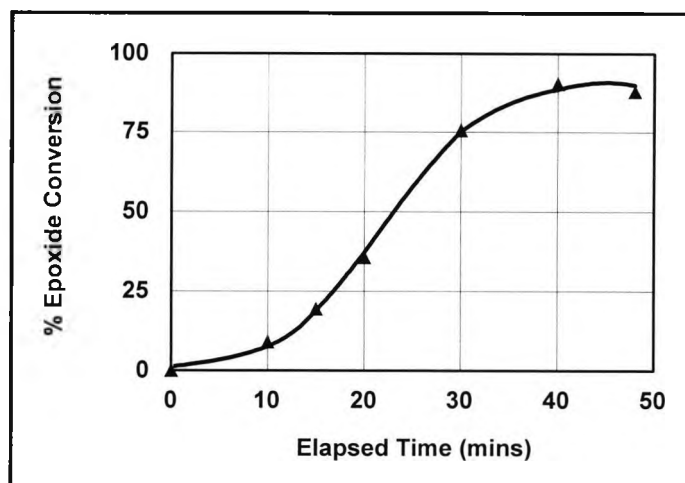
Figure 3.3-6　　　　**Remote curing, epoxide conversion, in glass apparatus**

In the PTFE apparatus, see Figure 3.3-7, the reaction proceeds with a similar degree of conversion but in contrast there is no induction period before the polymerisation process gets underway. Consumption of epoxide groups and appearance of reaction products occurs immediately after irradiation is begun.
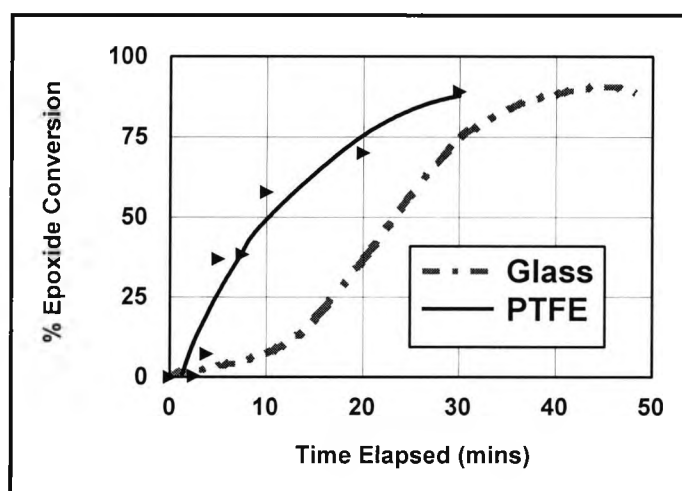
Figure 3.3-7　　　　**Remote curing, comparison of epoxide conversion in glass and PTFE apparatus**

It is likely that the lag observed with the glass apparatus may be explained in terms of the preferential reaction of the gaseous initiating species with the glass vessel. In fact, an etching of the glass cell was observed following the remote experiment. This may cause a lapse of time before the accumulation of initiating species is sufficiently high to permit polymerisation to take place at a significant rate.

It is clear then that polymerisation of the epoxide formulation can be achieved by irradiation of the solid-state photoinitiator, which is in proximity to but not in contact with

the film in a closed container. This is strong evidence that the polymerisation is brought about by the gaseous products identified in the first experimental section (Sec.2.3), namely HF and XF_5. In this case X=P.

This result is supported further by a 2-stage experiment (Sec.3.2.5) in which the initiator is irradiated separately in a closed cell for 20 minutes - the light stage. Following irradiation, the lamp is turned off and the seated cell is permitted to communicate with a second cell containing the epoxide film by opening a tap, which separates them - the dark stage.

Figure 3.3-8 indicates the epoxide conversion when 4 such experiments were carried out with exposure of the film to the gaseous products for various times. The irradiation of the light stage was for an equal length of time in each case.
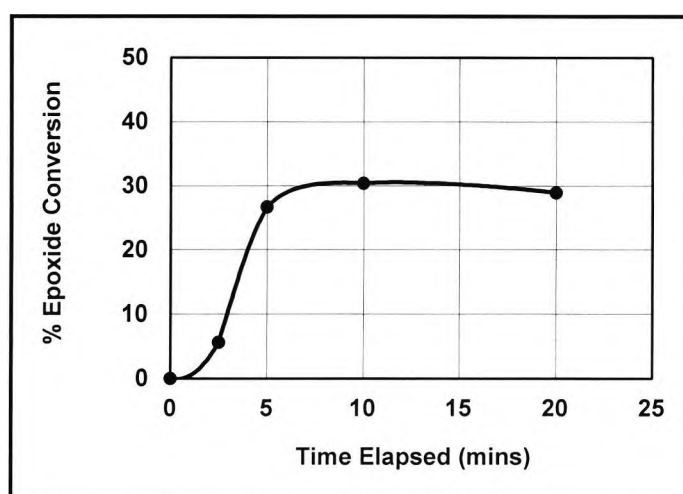
Figure 3.3-8   **Remote curing, epoxide conversion showing 'Dark Stage' polymerisation in 2-step process**

Examination of this data yields 2 important observations:

1. The reaction conversion is low, around 30 %, compared to around 90 % obtained when the same amount of initiator is irradiated for the same length of time - but in the presence of the film (i.e. in the same cell)

    This low conversion probably arises due to the fact that the concentration of the gaseous products per unit volume of atmosphere in the combined cell is, by virtue of the longer combined volume, reduced. The concentration will be 1/3rd of the concentration to which the film is exposed in a similar single-cell experiment. Evidently the concentration of gaseous initiator products is quite critical.

2. The reaction requires minutes to come to completion. It is known that the polymerisation reaction, once underway, does not operate over a time frame of

minutes - a directly cured sample exposed to the same intensity of light reaches completion much faster. This should suggest that the reaction is substantially controlled by the rate of diffusion of gaseous products into the film.

It is interesting to note that the remote process proceeds with the formation of hydroxyl groups. This outcome is not expected for mechanisms involving pure Lewis acids such as have been used [16] to describe polymerisations involving diazonium salts, Scheme 3.3-2.
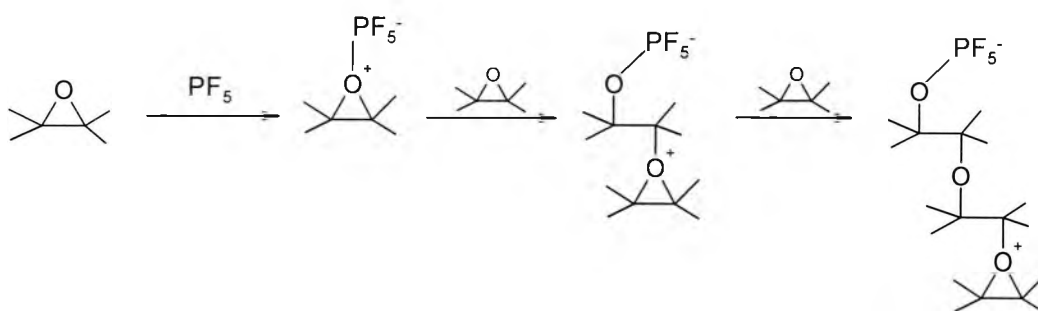
Scheme 3.3-2   **Initiation and propagation steps for epoxide polymerisation with Lewis acid catalyst**

A weakness of this mechanism is that the propagation would involve an unstabilised cation as the propagating oxonium ion becomes increasingly distant from the anionic centre, which is fixed at the α end of the polymer. Work [13-18] on cationic polymerisations via Brønsted acid mechanisms has proved the importance of cation stabilization (by the complex counter ion, X^-) and has shown that the speed of reaction and polymer molecular weight is highly dependent on anion stability.

For the same reason, polymerisation via the Brønsted acid, HF, seems unlikely as the counterion, F^-, is very small and highly nucleophilic, and would result in slower propagation and a tendency towards chain termination with addition of F^- to the polymer (Scheme 3.3-3).
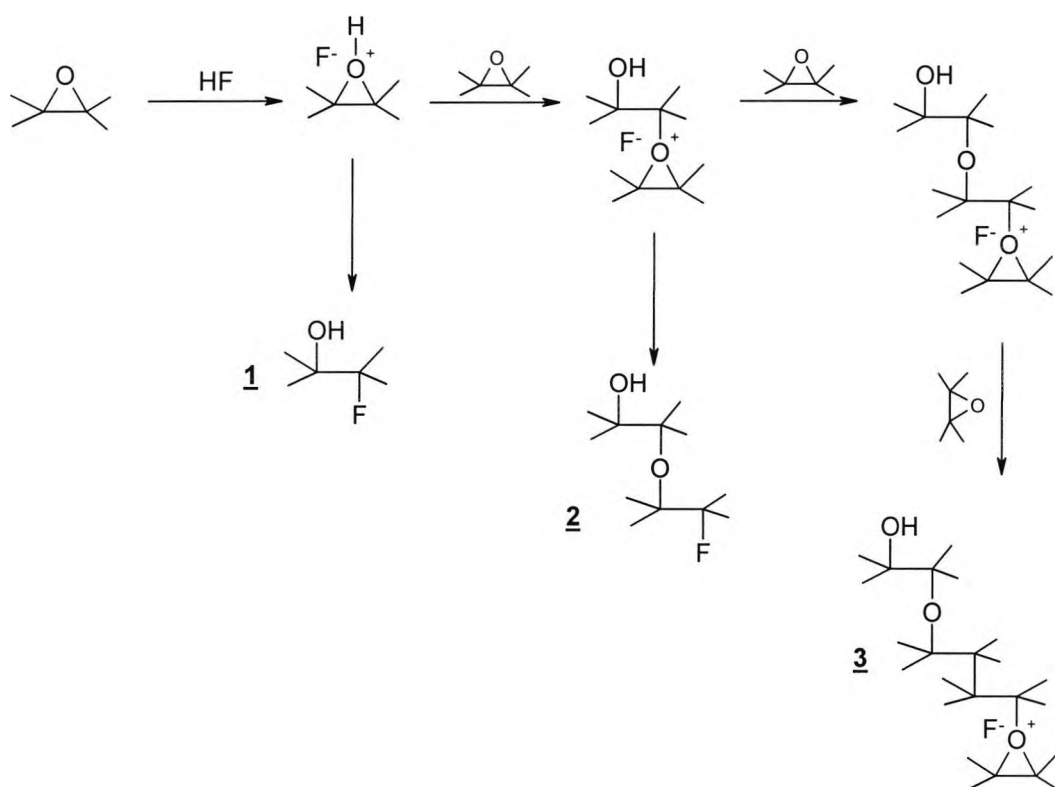
Scheme 3.3-3   **Propagation and termination in epoxide polymerisation with the fluoride anion as counterion**

Although the propagating polymer (1) and the terminated polymer (2) would contain the hydroxyl group found here in the IR spectra, the fluorine termination is not observable in the spectra (Figure 3.3-9).
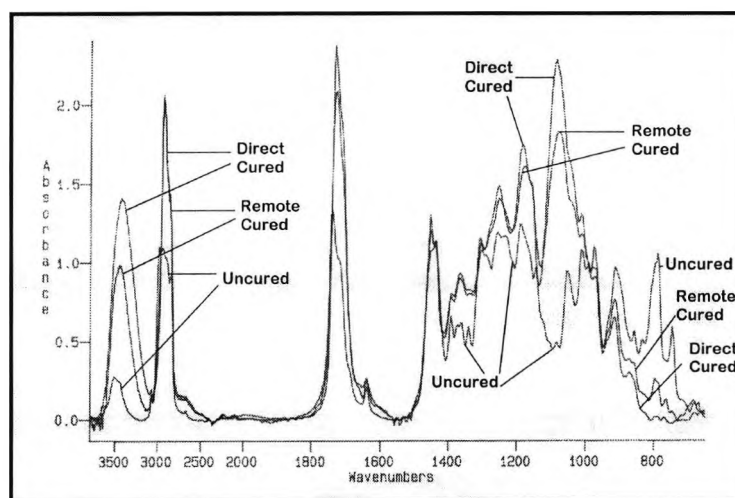
Figure 3.3-9   **Comparison of IR spectra for epoxide cured by remote and direct methods**

In fact the spectra obtained from the direct and remote processes are quite similar. Fluorocarbons arising from termination would show up as strong C-F stretches between

156

1000 cm^{-1} and 1400 cm^{-1} [102] and as a weak C-H stretch at 3050cm^{-1}. No such features are noted.

Other mechanisms [61,62] have been proposed which can be applied to epoxides to account for a stabilised cation from a Lewis acid catalyst, but do not allow for the development of hydroxyl functionalities, Scheme 3.3-4.
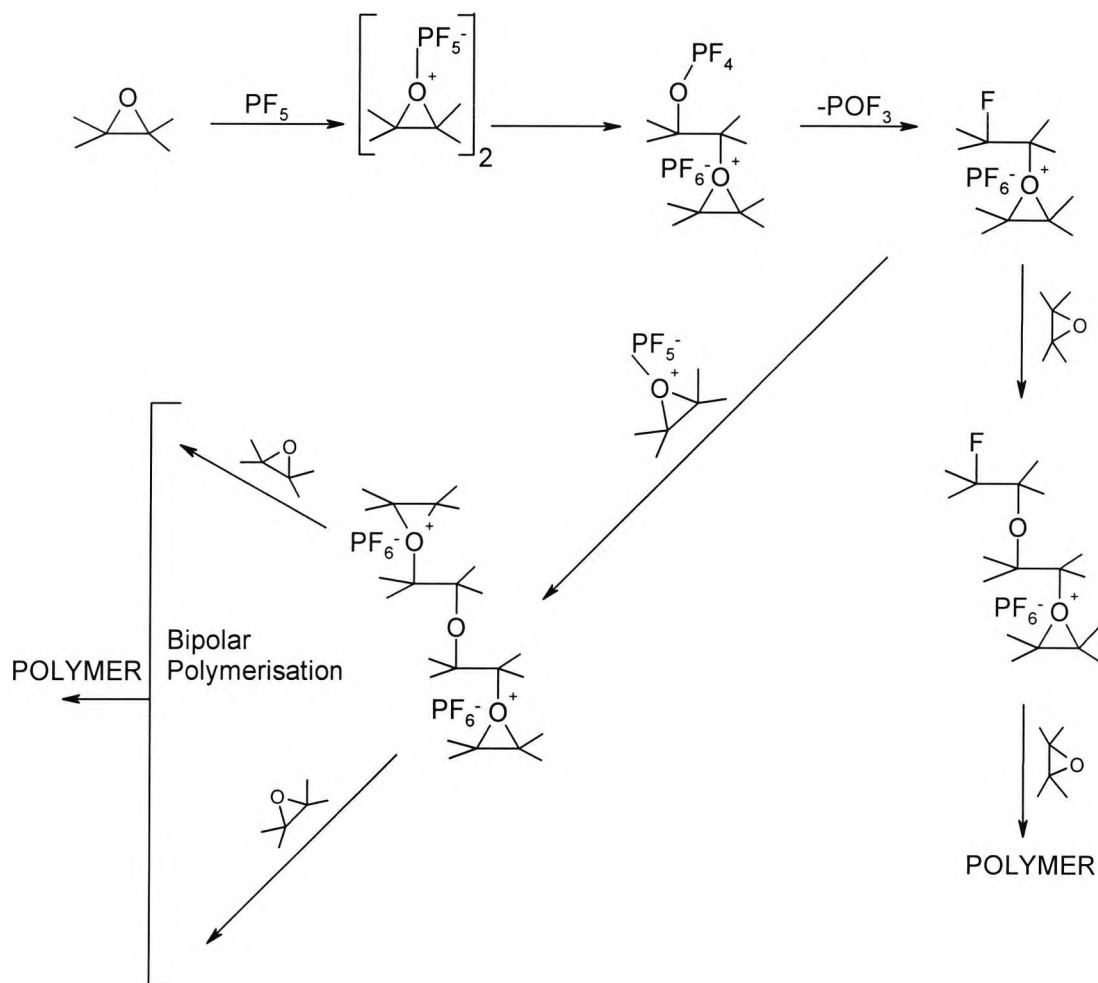
Scheme 3.3-4   **Generation of PF6- counterion -alternative schemes for initiation and propagation in epoxide polymerisation with a Lewis acid**

It seems more likely [7,11] - and consistent with present experimental results - that the Lewis acid undergoes hydrolysis in the presence of trace quantities of water in the epoxide film to yield a Brønsted acid:

$$PF_5 \quad + \quad H_2O \quad ------- \blacktriangleright \quad H^{\oplus} \quad + \quad {}^{\ominus}PF_5OH$$
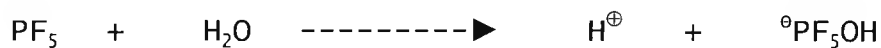
Polymerisation would then proceed in the following manner Scheme 3.3-5:
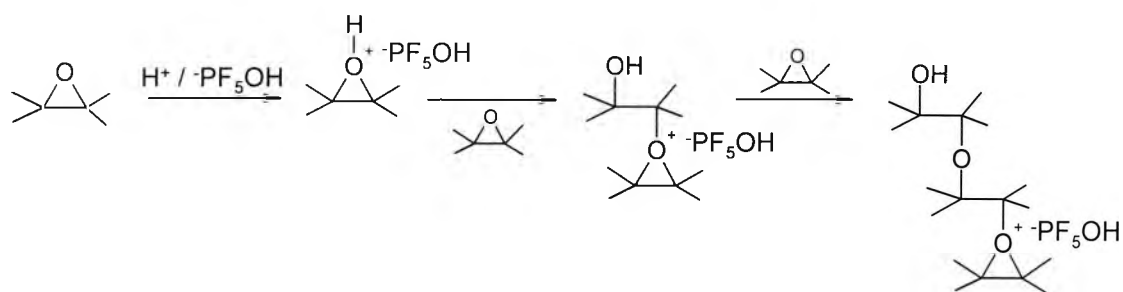
Scheme 3.3-5 **Initiation and propagation in epoxide polymerisation with Lewis acid in the presence of water**

Such a scheme will account for the hydroxyl formation following initialization from the presence of a Lewis acid, as is the present case.

3.3.3 Effect Of Gap Width On Remote Cure

Figure 3.3-10 shows the effect on polymerising efficiency (% epoxide conversion after 10 minutes of exposure) when the separation between initiator layer and resin layer is increased between 5 and 15 mm. Experiments were carried out with resin formulation 4 (Sec.3.2.1.1) in the PTFE cell (Sec.3.2.4.1.2). All other polymerisation experiments carried out in the PTFE cell made use of a gap width of 10 mm.
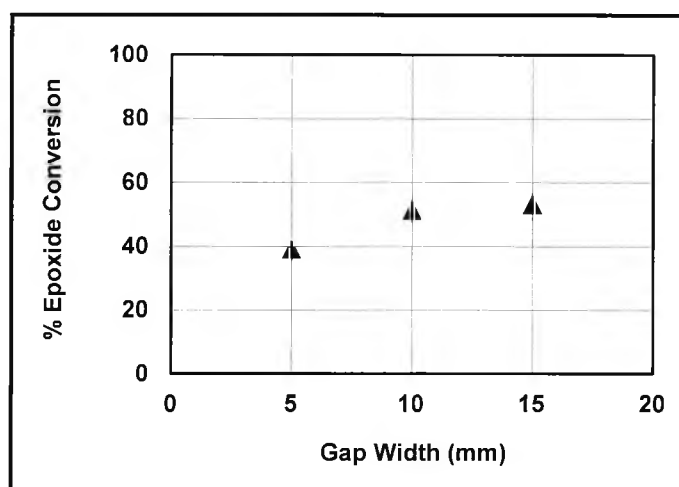
Figure 3.3-10   **Remote cure, effect of gap width on epoxide**

The results show that at gap widths 10 mm and 15 mm, the %conversion is, within experimental error, approximately the same at about 55%. At gap width 5 mm the epoxide conversion is clearly lower at about 38%. The apparent reduction in conversion may be explained in terms of a reduced circulation of polymerising gases when the 2 surfaces are in such close proximity.

3.3.4 Effect Of Initiator Selection On Remote Cure

Experiments were carried out to compare the effect of variation in the choice of initiator, each at the level of 0.2g deposited in the solid-state. Figure 3.3-11 indicates the difference in polymerising efficiency of the DPIHFP initiator and the Irgacure 261 initiator with resin formulation 4 (Sec.3.2.1.1) in the PTFE cell (Sec.3.2.4.1.2).
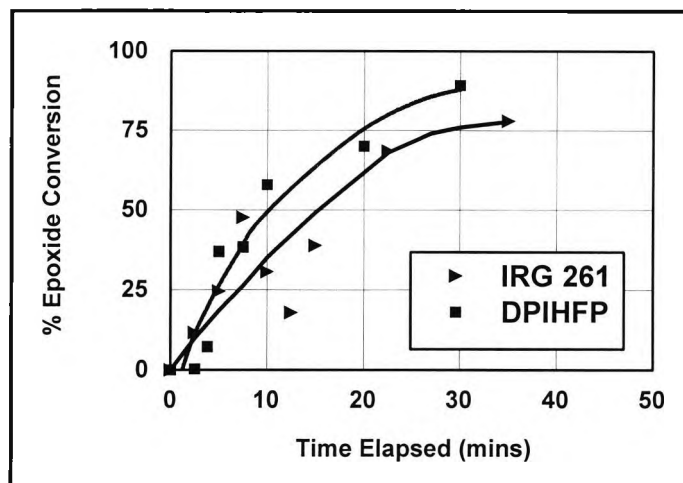
Figure 3.3-11   Remote cure, epoxide conversion in remote cure with DPIHFP and Irg261 initiators

It is clear that Irgacure 261 is less efficient for remote cure than the DPI salt. The results obtained may be compared with the results obtained previously (Sec.2.3.5) for the photodecomposition and fluoride ion yield with the same 2 initiators. See Figure 3.3-12.
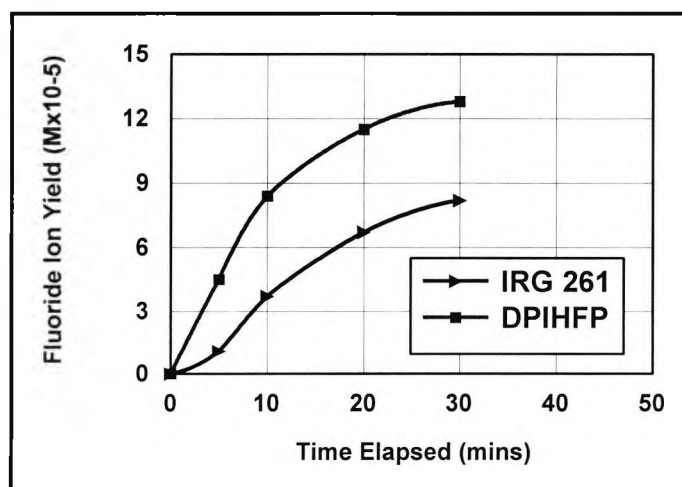
Figure 3.3-12   Fluoride yield from DPIHFP and Irg261 following solid-state photodecomposition

160

The yield of fluoride generating gases is quite different and this has a corresponding impact on the rate of polymerisation. By contrast, a parallel experiment using directly cured formulations (Formulations 2 and 3, 3.2.1.1) containing bulk photo-initiators at equal molar concentrations yields quite different results after equal irradiation time. These indicate that that the DPIHFP and Irgacure 261 are similar in efficiency. Figure 3.3-13 below indicates these results.
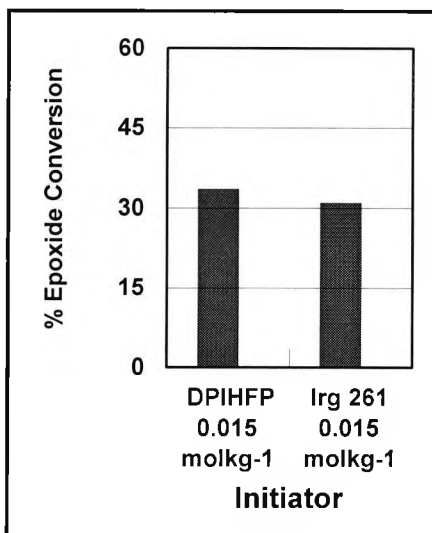
Figure 3.3-13   **Direct cure, epoxide consversion in direct cure of epoxide with DPIHFP and Irg261 initiators**

The relative efficiency of Irgacure 261 and in the remote and direct experiments, versus DPIHFP, is consistent with the accepted mechanism [38], Scheme 3.3-6, for photo-decomposition for this initiator in epoxide formulations.
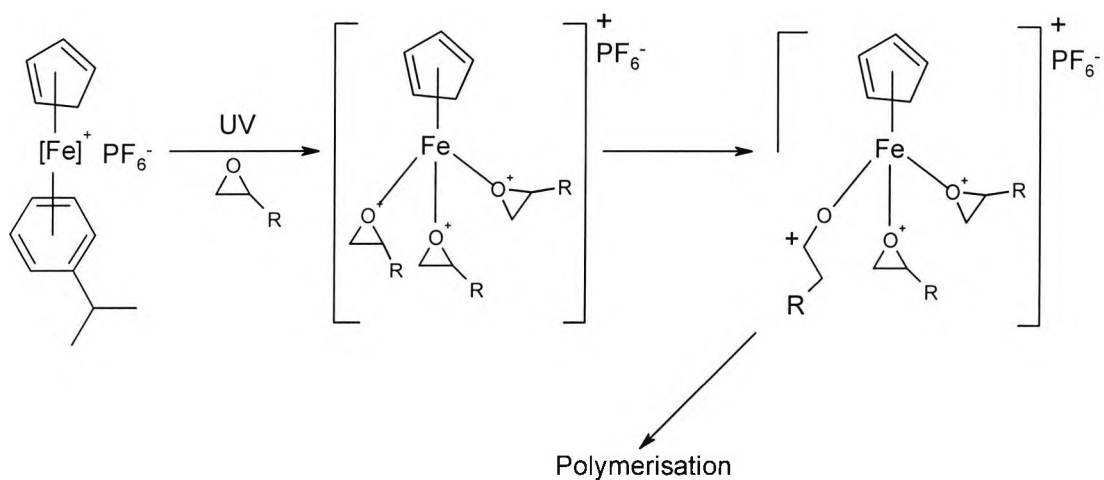
Scheme 3.3-6   **photodecomposition of Irg.261 ligand exchange in presence of epoxide followed by epoxide ring opening**

This mechanism involves participation of the epoxide monomer and the organometallic cation in the form of a complex obtained by ligand exchange of 3 epoxide monomers for the cumene moiety, which is released. It would appear that the present results confirm the importance of the epoxide in the photodecomposition of Irgacure 261 and similar photo-initiators. This is quite different from photo-polymerisations involving onium salts in which the cation is presumed to decompose, releasing the complex acid HX, achieving polymerisation without the participation of the cation.

3.3.5 Effect Of Film Thickness On Remote Cure

The effects of film thickness on remote and directly cured films were studied. Figure 3.3-14 illustrates the profile of epoxide conversion with time for films of thickness 4µm and 15µm. Both series of experiments were carried out in the PTFE vessel (Sec.3.2.4.1.2) using resin formulation 4 (3.2.1.1), which is initiator free under N_2 atmosphere.
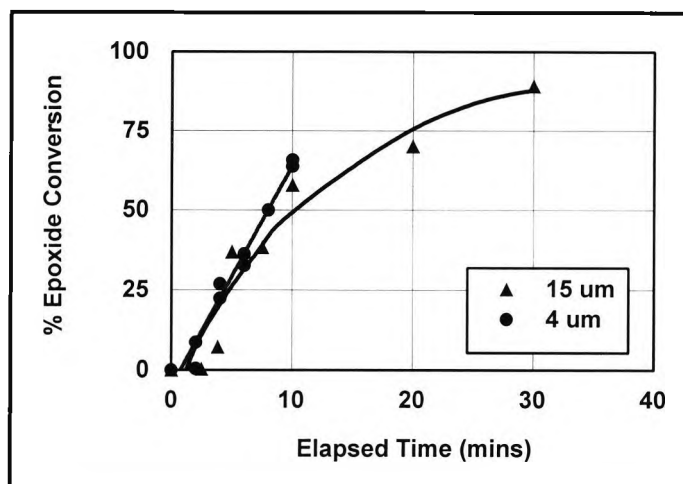
Figure 3.3-14   **Remote Cure, effect of film thickness on epoxide conversion – reaction profiles at 4µm and 15µm thickness**

The initial rates of epoxide consumption are very similar but the thinner film reaches completion faster as the polymerisation rate in the later stages is slower for the thicker film. Further experiments were done to examine this phenomenon over a wider range. Figure 3.3-15 shows the results obtained when the epoxide films were exposed in remote experiments of duration 10 minutes. Film thickness was varied in the range of 4-50 µm.
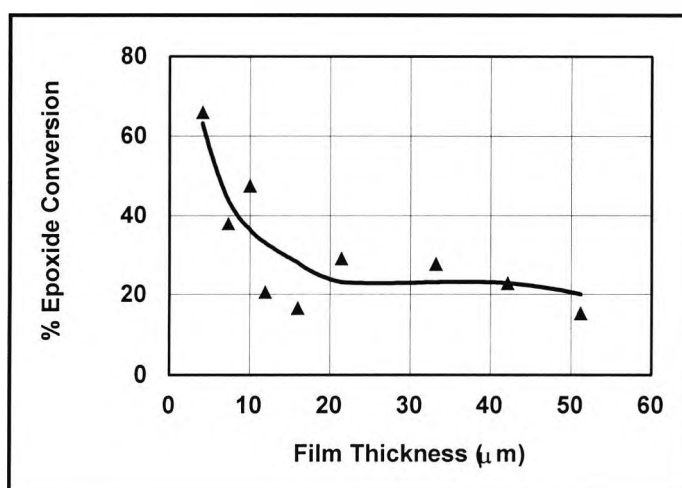
Figure 3.3-15   **Remote cure, variation in epoxide conversion with film thickness**

163

There is considerable scatter in the data, which probably arises from the difficulty in accurately measuring film weight with the required precision and the tendency of the film to spread during the experiment. This is especially true if polymerisation is not rapid and the film thickness and temperature of the cell are high. Nevertheless the overall picture is quite clear – the percentage conversion is highly sensitive to film thickness. The dependence of conversion on film thickness, particularly in the range 0-20 μm, is quite large.

A similar outcome is obtained for the directly cured films containing 2.1% of DPIHFP initiator, which were cured over a 1-minute time frame. See Figure 3.3-16 below
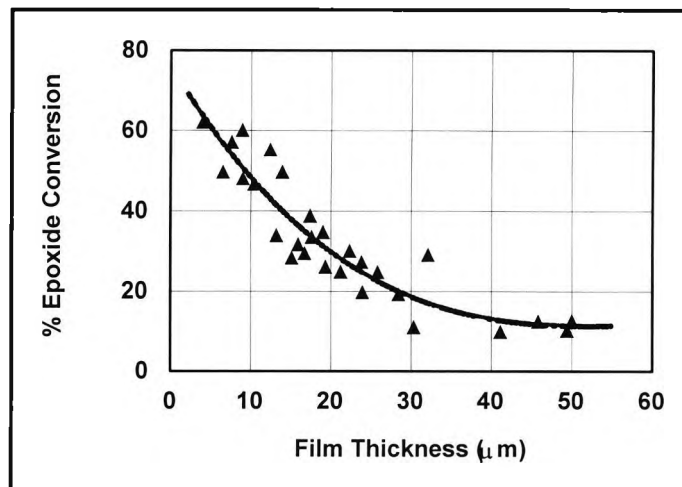
Figure 3.3-16   **Direct cure, variation in epoxide conversion with film thickness**

164

Decker and Moussa [12] also observed a thickness effect in epoxide films, using RTIR. It is interesting to examine the results based on total polymer yield per unit area, as a function of film thickness. The results of Decker can be compared with those of the present work. Figure 3.3-17 combines this information in a single chart below:
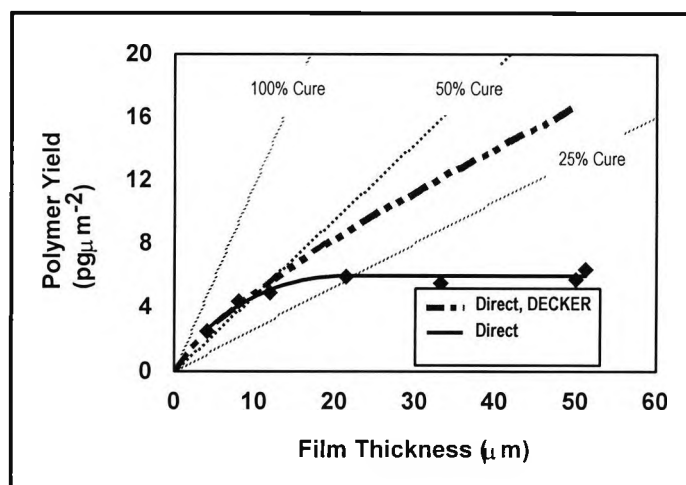
Figure 3.3-17   **Direct cure, effect of epoxide film thickness on polymer yield – comparison of experimental and literature data**

Decker and Moussa asserted that a thickness effect is observed which they attribute (I) to U.V. screening of the photoinitiator molecules in the lower part of the film by those in the upper part of the film, as the thickness increases, and (II) to a depletion of hydroperoxide molecules formed by interaction of diffused atmosphere oxygen. These are said to be favourable to cure.

This effect is reiterated here, as the polymer yield, although almost linear above 10 µm film thickness is not strictly proportional to the film thickness – increasing deviation from the 100% cure line. This would confirm an interference with the polymerisation, which limits polymer yield.

The directly cured samples in the present work deviate even further from the 100% line and above 10 µm film thickness the polymer yield is constant, regardless of thickness. It is relevant to note that Decker and Moussa used KI185$^\alpha$ at a molar concentration (0.025 moleskg^{-1}), which is 50% of the molar concentration of DPIHFP used in the present work (0.050 moleskg^{-1}). Since each KI185 bears 2 counterions, the molar concentration of counterion in each formulation is equal. However, 2 acid groups are released from every photolysed KI185 molecule and so the quantum yield of acid in the Decker formulation will

be approximately double that of the formulation used in the present work. This doubled photochemical efficiency of Decker's formulation explains the more moderate film thickness effect noted in his work. Differences in U.V. screening power are not likely to be a factor: KI185 has 2-3 times the absorbance of DPIHFP, but is used at half the level on a molar basis.

The same approach can be applied to remote cure. Figure 3.3-18 is similarly revealing with regard to the effects of film thickness in remote curing. In this case the resin formulation is photoinitiator-free and there can be no U.V. screening or photoinitiator efficiency effects to consider. Furthermore, the reaction is conducted under nitrogen and so the issue of hydroperoxides does not arise either.
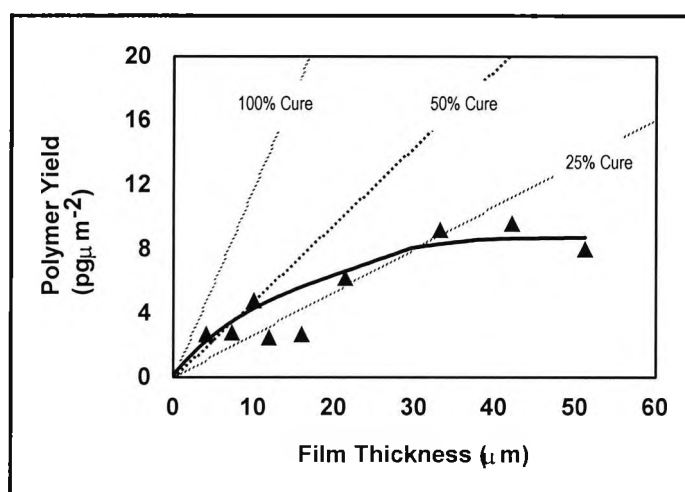
Figure 3.3-18   **Remote cure, effect of epoxide film thickness on polymer yield**

Notwithstanding the scattered data, it is clear that above film thickness $20\mu m$, the polymer yield is constant per unit area of substrate (about $8\text{-}10pg\mu m^{-2}$), regardless of film thickness.

The methodology measures only the average cure (and therefore average polymer yield) throughout the film and does not distinguish degree of polymerisation at different depths within the film. Consequently the issue of diffusion gradients of acidic materials within the film cannot be addressed directly. It is more appropriate to state that regardless of the actual concentration of the acid (PF_5, HPF_6 or HPF_5OH), the polymer yield is constant.

---

[a] ™Degussa (bis[4-(diphenylsulphonium)-phenyl]sulphide-bis-hexafluorophosphate)

166

This suggests that as film weight is increased either or both of the following factors govern the polymer yield:

- The polymer yield is limited by the kinetic chain length of polymerisation initiated by a given <u>quantity</u> of initiator, PF_5, absorbed (anywhere) in the film.

- The polymer yield is limited by the actual <u>quantity</u> of initiator, PF_5, which can diffuse (anywhere) into a film of any thickness, in an experiment of fixed duration.

In either case, the reaction is <u>not</u> limited by the <u>concentration</u> of initiator in the film. The system may be viewed as a reaction depending on a bimolecular initiation step. Assuming the yield of acid is the same for each experiment in the series, the effective (average) concentration of reactant A (PF_5, HPF_6 or HPF_5OH) in the film will decrease with increasing quantity of reactant B (monomer) added to the mixture - by way of increased film thickness. Nevertheless, as stated previously, the polymer yield is constant, affected only by the quantity of initiator in the film rather than the concentration.

This would suggest - indirectly - that diffusion effects are not operating in this case. In other words, **diffusion rate > polymersation rate**.

3.3.6 Effect Of Humidity On Remote Cure

Remote polymerisation experiments were carried out under atmospheres of nitrogen at varying levels of humidity, see section 3.2.4.2. Atmospheres were supplied to the reaction cell at humidity levels of 1%, 23%, 43% and 100% Relative Humidity (%RH), and a single (otherwise identical) 10 minute polymerisation experiment was carried out at each level. All experiments were carried out in the PTFE cell with resin formulation 4, film thickness 20μm, and the DPIHFP initiator, 0.1g.

Qualitative examination of the relevant bands in the spectra of the irradiated samples indicates quite expectedly that irradiation is attended by a decrease in the epoxide and increases in the ether and hydroxyl bands. See Figure 3.3-19.
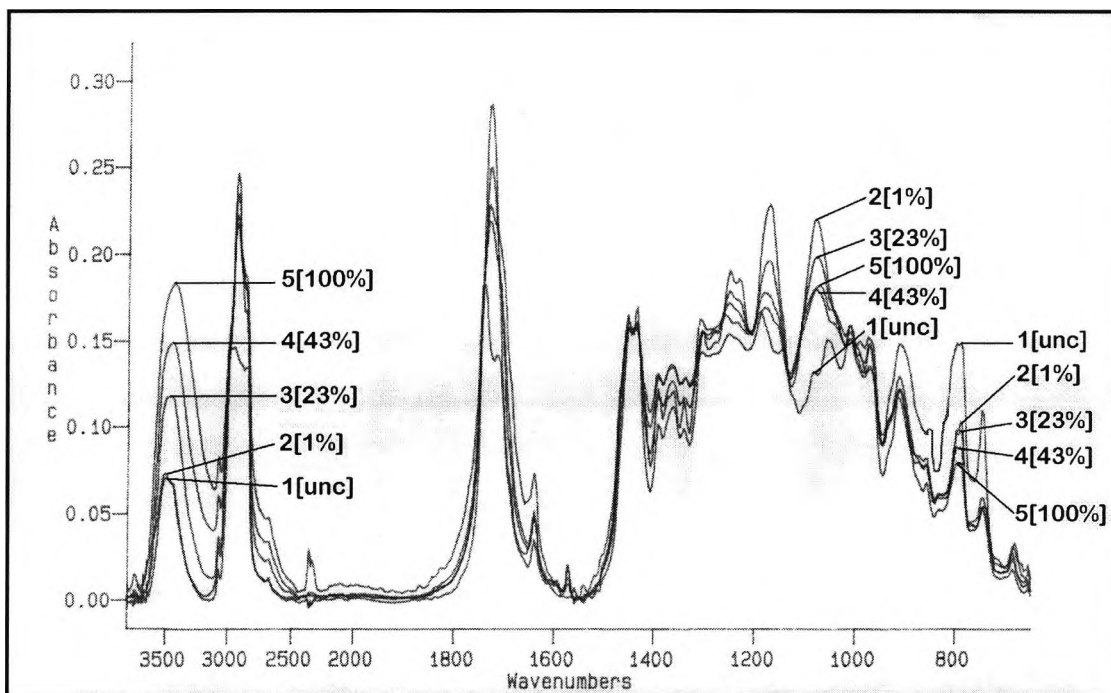
Figure 3.3-19   **Remote cure, polymerisation of epoxide formulation at various levels of humidity**

Figure 3.3-20 shows how the consumption of the epoxide group in the remote process is affected by the presence of water in the atmosphere surrounding film and initiator.
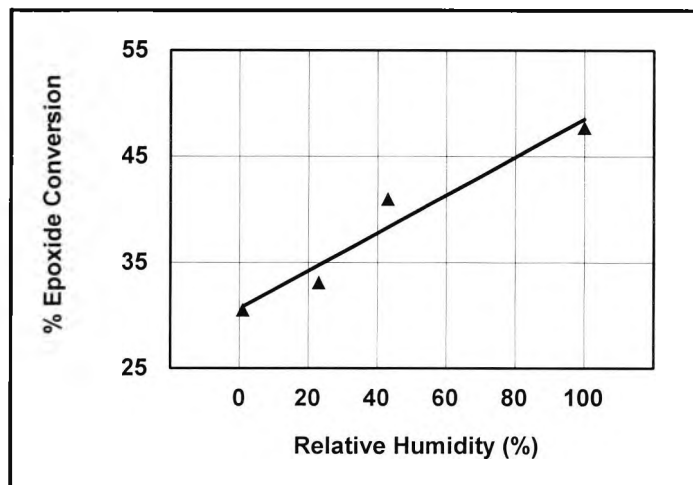
Figure 3.3-20   **Remote cure, epoxide conversion at various levels of humidity**

U.V. exposure at high ambient water levels clearly accelerate epoxide consumption compared to exposure under dry conditions. This appears to be at odds with industry experience; Cationic polymerisation is known to be negatively affected by high ambient humidity [103] and under such conditions inferior film properites are frequently obtained [23,104,105]. However, when the epoxide, ether and hydroxyl bands are examined simultaneously, the discussion becomes clearer and the data remains consistent. See Figure 3.3-21.
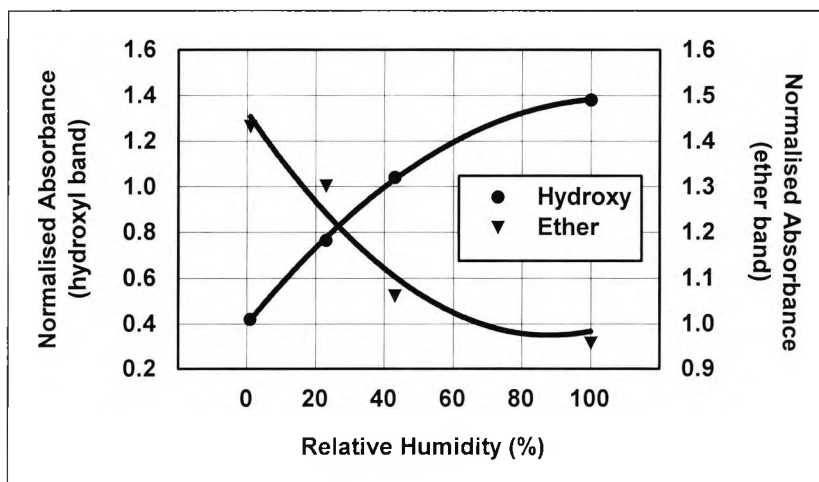
Figure 3.3-21   **Remote cure, development of ether and hydroxyl IR spectral bands as a function of humididty**

Assuming linearity, the development of (i) ether linkages and (ii) hydroxyl groups can be estimated, from the experimental data, at identical reaction coordinates - i.e. 40% epoxide conversion. This clearly demonstrates that as the ambient humidity is raised the outcome of ring opening (epoxide consumption) is more frequently chain termination with hydroxyl development (Scheme 3.3-7-1a/b) than chain extension with ether linkage formation (Scheme 3.3-7-2a/b).
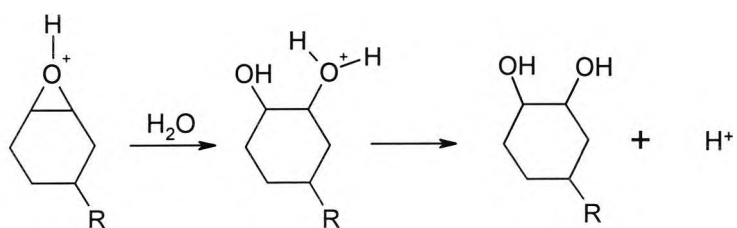
Scheme 1A
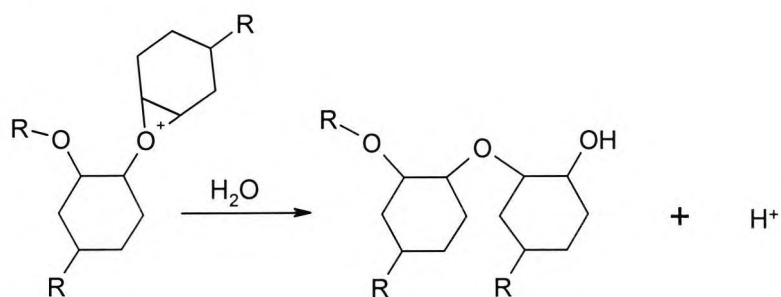
Scheme 1B
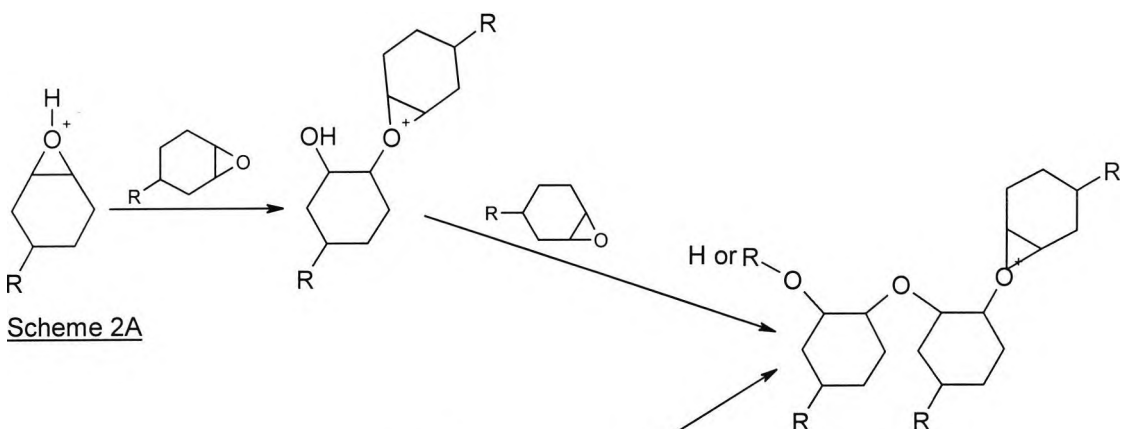
Scheme 2A
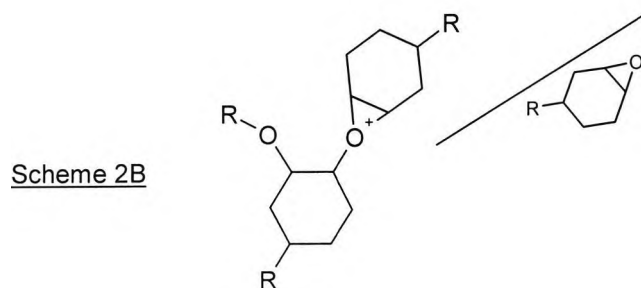
Scheme 2B

Scheme 3.3-7   **1a/1b epoxide monomer ring opening in the presence of water, 2a/2b propagation and polymerisation of epoxide in the absence of water**

The inferior mechanical film properties associated with high humidity line conditions are probably due to the net reduction in kinetic chain length and consequent lower polymer molecular weight resulting from the preponderance of termination processes. Watt [23] has theorized a similar explanation without experimental verification, for directly cured systems.

It is interesting to note that under very dry conditions, 1%RH, the hydroxyl band shows no development upon irradiation. This would indicate that under these conditions the process consists predominantly of chain extension, and chain termination is not significant. Nevertheless, as indicated by Scheme 3.3-7a/2a, ring opening is always followed by the development of at least 1 mole of hydroxyl per polymer chain initiated. The apparent lack of early hydroxyl development relative to the hydroxyl groups present in the uncured sample (hydroxyl terminated epoxidised polybutadiene), would suggest, therefore, a relatively small number of chains initiated. Initial epoxide consumption would then occur via rapid elongation (without significant chain termination) of a small number of chains. This would be consistent with the fairly low levels of initiating species present (HF and PF_5) in the early stages, and the surface directed nature of the process.

Clearly these phenomena require some explanation. Firstly, it is worth pointing out that ambient water can indeed diffuse into the film and significant quantities accumulate. The permeability of photo-polymer films to atmospheric water has been demonstrated by Best and Moylan [106], and is dependent on the partial pressure of water vapour in the atmosphere. Pre-formed acrylic films were shown to accumulate as much as 6% by weight of water when exposed statically in a saturated atmosphere, i.e. 100% RH at 25°C. At 1% RH at 25°C the same film will absorb less than 0.1% by weight of water (see Table 3.3-3). The film thickness affects only the time taken to reach the equilibrium water concentration.

relative humidity at 25°C %	dew point °C	water content of air (gm⁻³)	water vapour pressure at 25°C (Nm⁻²)	amount of water in film % wt./wt.	relative humidity at 60°C %
1.0^{α}	-60.0^{γ}	0.23^{δ}	32^{ι}	0.1^{ι}	0.2^{δ}
23.0^{α}	1.3^{β}	5.30^{δ}	720^{ι}	1.4^{ι}	4.9^{δ}
43.0^{α}	10.8^{β}	9.91^{δ}	1360^{ι}	2.6^{ι}	9.1^{δ}
100.0^{α}	25.0^{β}	23.05^{β}	3170^{ε}	6.0^{ε}	21.2^{δ}
------	60.0^{γ}	108.76^{γ}	------	-------	100.0^{γ}

α experimental values	δ by calc: %RH x water content at saturation temp.
β ref [63], table E41B	ε ref [106], hard acrylate film, d=1.224 gcm⁻³
γ by extrapolation from β	ι by calc: from ε

Table 3.3-3   **Relative humidity at various temperatures and relation of RH to water content of air**

If the same observations apply to uncured epoxide films in a static environment, then 6% w/w represents as much as 50% composition on a molar basis. It is likely that under dynamic conditions (experimental and industrial line conditions) the absorption of water would be much less. Nevertheless, the water content of an epoxide film can be quite substantial when in contact with a humid atmosphere. Furthermore, under present experimental conditions, i.e. 60°C, diffusion/absorption will be quite rapid, especially with an uncured (liquid) film.

It is quite clear then, that substantial amounts of water will accumulate in the film. In fact, diffusion of water into the film can be sufficient to produce a 3nm layer at the coating/substrate interface[107] - enough to produce adhesion loss. This absorption can be enhanced by the presence in the film of ionic species, such as are present in cationically polymerising media.

The way in which this absorbed water interacts with the active species to change the mechanism of polymerisation in the manner described previously remains to be explained.

As far as the author is aware, no *specific* mention is made in the literature concerning the influence of water on the photodecomposition of the onium salt cation, stability of the anion, or the rate of acid release thereof. Nevertheless, water could behave as an H donor in the liberation of acid, and thus exert a positive effect in the polymerisation process. This should apply equally to in-situ photodegradation as to photodegradation in the solid state. It should also be valid regardless of the nature of the final acidic species (Brønsted or Lewis acid), as both types require a proton for release from the complex salt.

However, Crivello[108] followed epoxide polymerisation using DSC in dry films and in the presence of bulk water at a level of 1-2%. Various initiators were studied. With the antimonate anion in the presence of water, evidence was found – in the manner of a second exotherm - for the existence of an unidentified additional process, not observed with the same initiator and a dry film. It is possible that the additional exotherm can be attributed to partial hydrolysis of the antimonate anion, which is known to be the least stable of the group V series.

The most likely point at which water could operate on the mechanism and rate of polymerisation is that concerning the formation, stability and propagation of the active species. The interaction of water with the activated complex can be viewed with reference to the transition complex described earlier (Scheme 3.3-8).
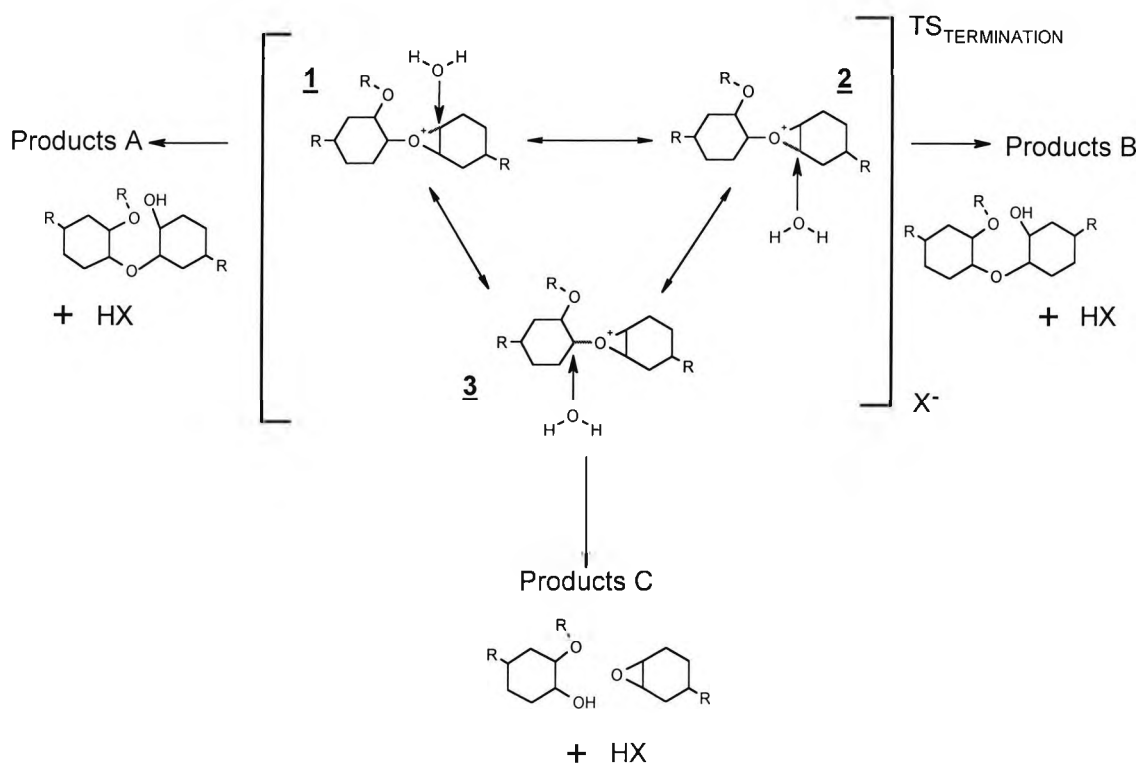
Scheme 3.3-8   **Nature of activated complex in transition state with attack by water**

Water, being much smaller than the epoxide monomer is less sterically hindered in its approach to the activated complex. This thermodynamic consequence of this reduced steric interaction is a reduction of the energy banner associated with reaction of the activated complex with water as compared to reaction with the epoxide. In the presence of both water and monomer, chain termination will always be thermodynamically preferred (Scheme 3.3-9) and this is observed in the present work.

Reaction Coordinate
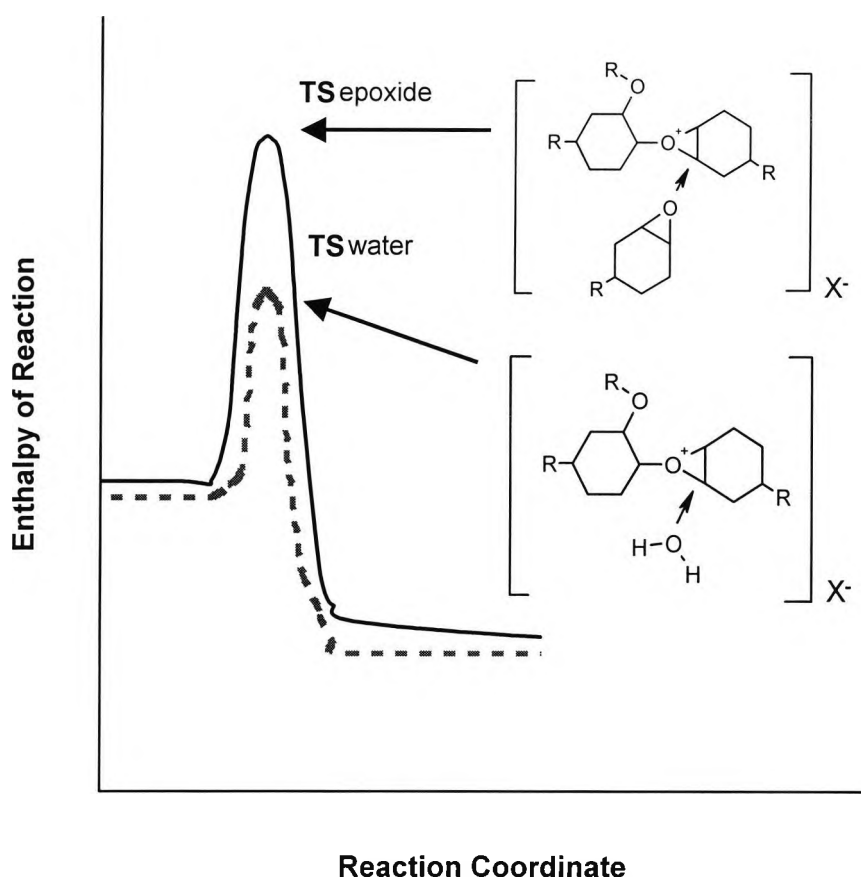
Figure 3.3-22   **thermodynamic diagram for transition states for propagation with attack of the activated complex by monomer and water**

Since the products from both reactions involve release of ring strain the energy level in each case is similar and the reaction is associated with a similar negative ΔH.

In the context of the present work and the observations of Tonge, Hupfield and Hurford [109], the presence of water in the polymerising media could have 2 additional and relevant consequences:

- To provide a means of solvating the complex acid

- To increase the dielectric permeability of the medium.

Increasing the solubility of the complex acid destabilises the activation complexes 1 and 2, see Scheme 3.3-9. In effect, equilibrium exists between the propagating ion pair and the hydroxyl terminated chain/complex acid.
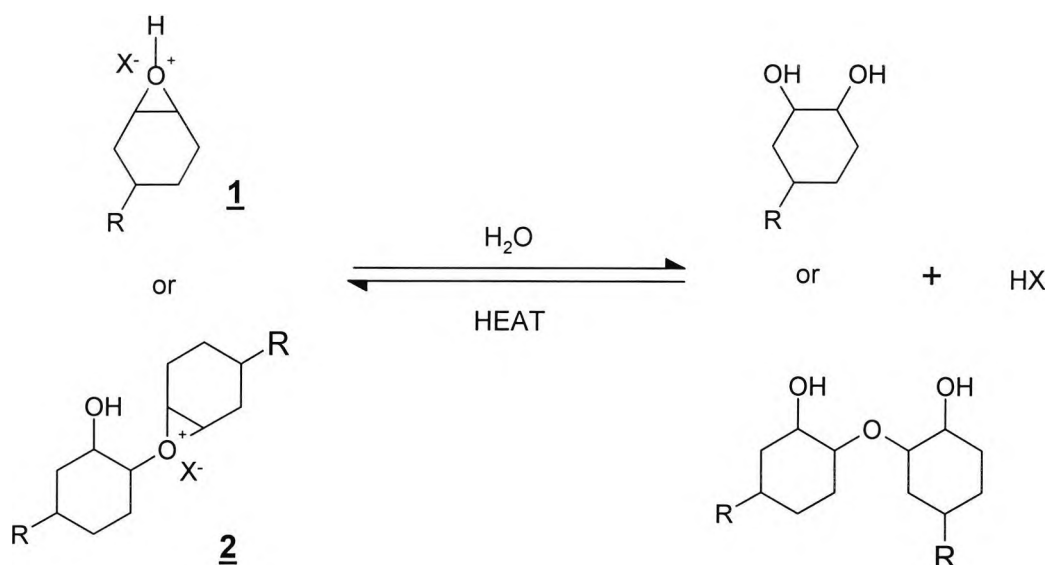
Scheme 3.3-9   Equilibrium between activated complex and deactivated complex with water – solvation of HX

The presence of water in the medium favours the solvation of HX and drives the equilibrium to the right yielding solvated HX and hydroxyl terminated chains. The absence of water keeps the equilibrium to the left preserving the activated complex, permitting propagation and chain extension. In this manner high levels of water are consistent with a preponderance of hydroxyl-terminated chains. The complex acid remains available for the formation of further complexes, with continued epoxide consumption, hydroxyl formation and relatively little ether linkage and chain extension. The molecular weight remains low and the viscosity of the medium does not increase. The low viscosity of the film favours rapid consumption of epoxide, and disappearance of this group in the IR will be more rapid than irradiation under dry conditions.

In the latter case, stability of the activation complex permits chain extension with disappearance of epoxide and formation of ether links with relatively little hydroxyl development. Molecular weight and viscosity rise comparatively fast causing the rate of epoxide consumption to subsequently reduce in the classical manner [80].

An increase in the dielectric permeability of the polymerising medium in the presence of water also has the effect of increasing the rate of epoxide consumption. In a higher dielectric medium the separation of charges in the activated complex is larger. Effectively the counterion, X^-, becomes less nucleophilic and the activated complex more reactive.

The beneficial effect of large ion pair separation and low counter ion nucleophilicity for cationic processes is well known [13-18]. At the same time, this effect is partially mitigated by the increased association of water by H bonding with the activated complex. This gives rise, as described earlier, to increased hydroxyl termination and less polymerisation. This effect can be offset [23,105,106,109,110] by raising the operating temperature. This increases further the ion pair separation and reduces the H bonding association of water.

In the absence of water the dielectric permeability of the medium is lower, and charge separation in the ion pair is smaller, producing a less reactive activation complex and slower epoxide consumption.

Table 3.3-4 provides a summary of the observed effects of humidity on epoxide polymerisation, the inferences drawn with regard to the mechanism and the explanations provided in terms of the effects of water on dielectric properties of the medium, solvation of the ion pair and the manner in which the viscosity of the medium is affected by these changes and further impacts the degree of polymerisation.

	Conditions	
	Dry	**Humid**
Observations	Slow epoxide consumption Ether bridges formed Good film	Fast epoxide consumption hydroxyls formed Poor Film
Inference	Chain extension predominates	Chain termination predominates
Explanation	**Low dielectric** Anion more nucleophilic Slower reaction **HX unsolvated** polymer-anion complex stable $\rightarrow$ propagation **Viscosity increases rapidly** Epoxide consumption slows down	**High dielectric** Anion less nucleophilic Faster reaction **HX solvated** polymer-anion complex unstable $\rightarrow$ termination **Viscosity remains low** Epoxide consumption at steady rate (faster)

Table 3.3-4   **Summary of humidity effects and conclusions**

Implications as to the impact of temperature on the negative effects by high humidity, line conditions

Several workers [23,105,106,109,110] have determined that the negative effects of high humidity on cure (tack-free time) can be either completely or partially overcome by raising the temperature of the line from 35°C to 45-50°C.

Brann [105] points out that paperboard will pick up double the usual weight of water at high RH and observes a modest negative impact on cure. This effect would presumably be reduced at higher temperatures due to desorption of water from the board. However, the observations of Brann do not bear upon the problems of curing on non-absorbent substrates such as metal and PVC.

Watt [23] attributes this to condensation of water on the film at low temperatures and high humidity causing complexation with the initiator and hydrolysis of epoxy groups. Such condensation is said to be eliminated at higher temperatures. However, the explanation of Watt is weakened because it cannot be used to explain the beneficial effects of increased temperature under atmospheres which are already above the dewpoint at the lower temperature i.e. % RH<100%. In such cases, the relative humidity may be very high but condensation cannot occur.

In any case the role of condensed water on the film surface is questionable. Such a system would be bi-phasal and it has not been shown that condensed water could cross a phase boundary with sufficient speed to interfere with polymerisation under practical line conditions. Furthermore, polymerisation of epoxides in the presence of bulk water is known to occur quite effectively.

As described previously the presence of atmospheric water can cause an accumulation of water in the film by diffusion (rather than condensation). Water accumulated in this manner does certainly interfere with polymerisation quite considerably.

The amount of accumulated water in the film depends almost linearly on the partial pressure of water in the atmosphere. However, application of the gas laws provides that a temperature rise of 20 K hardly changes the partial pressure of water at all, when expansion of the air volume is taken into account (open system). In any case, the change in partial pressure with increasing temperature, even it were significant, would be positive. In addition, increasing temperature has a very profound impact on viscosity (liquid) films causing a reduction in viscosity of approximately 1 order of magnitude for every 10 K temperature rise. This is very favourable to inward diffusion of gases.

Together these 2 factors imply that more diffusion, higher levels of accumulated water and more interference with the polymerisation process should be associated with a line temperature increase. Clearly the theory of reduced condensation is inadequate to explain the phenomena and, at the same time, the diffusion effect is groundless as the temperature factor operates, if at all, in a direction opposite to industry and experimental findings.

The beneficial effect of increasing temperature in humid conditions can be more satisfactorily explained by reference to the transition states associated with interaction of water and monomer with the activated complex described earlier (Scheme 3.3-8). At all temperatures, success of the forward reaction (polymerisation) in the presence of water depends on the incoming monomer competing successfully with water and the complex anion, X^-, to interact with any of the electron-deficient sites described by the resonance hybrids 1, 2 and 3.

Water has an advantage since it is smaller and so $TS^{\ddagger}_{T}$ (termination) is lower in energy than $TS^{\ddagger}_{P}$ (polymerisation), and reaction in the presence of water favours termination rather than polymerisation.

As the temperature is raised the dielectric permittivity of the film is increased permitting an increased charge separation between the activated complex and the complex anion. In addition the viscosity of the medium is substantially reduced permitting increased mobility on monomers within the polymerising matrix.

Both of these factors will strongly improve the feasibility of an interaction between monomer and activated complex. The effect on the interaction with the activated complex in the case of water will be less marked as this interaction is less limited by steric factors.

In thermodynamic terms, the energy barrier associated with the transition complex involving the activated complex and monomer, $TS^{\ddagger}_{P}$, is reduced more than the transition complex involving water $TS^{\ddagger}_{T}$. The difference between the energy barriers associated with monomer and water becomes smaller, favouring the polymerisation reaction, (Figure 3.3-23).

This will especially be true in the earlier stages of the reaction owing to a preponderance of monomer molecules over water molecules in the matrix under dynamic conditions.
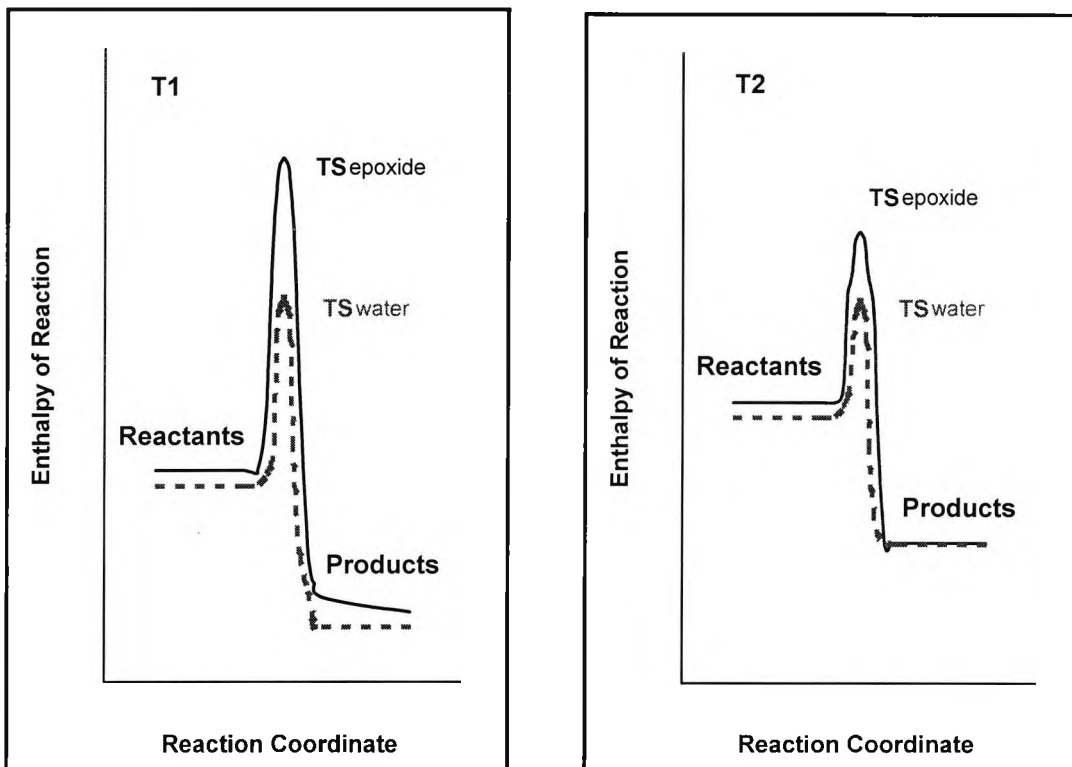
Figure 3.3-23   **Impact of temperature on energy level of the transition complex between monomer /monomer and monomer/water, left at a lower temperature, T_1, and right at a higher temperature, T_2**

It is worth pointing out also, quite apart from the above thermodynamic considerations, that the interaction of water consumes the water molecule with regeneration of the complex acid (Scheme 3.3-9), and once the water is consumed the polymerisation reaction is able to proceed unhindered by termination processes associated with water. Clearly the reduction in viscosity associated with an increase in film temperature will favour propagation at more advanced stages of the reaction with this additional consumption of monomer offsetting that which is "poisoned" earlier in the reaction by interaction with water.

3.3.7 Effect Of Bulk Water On Remote Cure And On Direct Cure

Remote curing and direct curing experiments were carried out with formulations containing bulk water, to assess the impact of water on cure response and enable a comparison of the two processes. Water composition was in the range 0-10% w/w.

Remote curing experiments were carried out using formulations 5,6,7,& 8 (Sec.3.2.1.1) using the 150W lamp in an air atmosphere. The lamp was positioned in close proximity to the curing cell to maximise cure response. Direct curing experiments were carried out using formulations 9,10,11 & 12 (Sec.3.2.1.1) and cured using the 150W lamp in an open atmosphere of air. The position of the lamp was adjusted to give a (slower) cure response, measurable in minutes rather than seconds.

In both cases the method for including the water is described previously (Sec.3.2.1.1). All formulations were hazy/milky in appearance indicating a bi-phase system or emulsion. The relevant IR spectra are located elsewhere (Sec.6.8,6.9). Examination of the epoxide bands indicates quite different behaviours for the two processes in the presence of water (Figure 3.3-24).
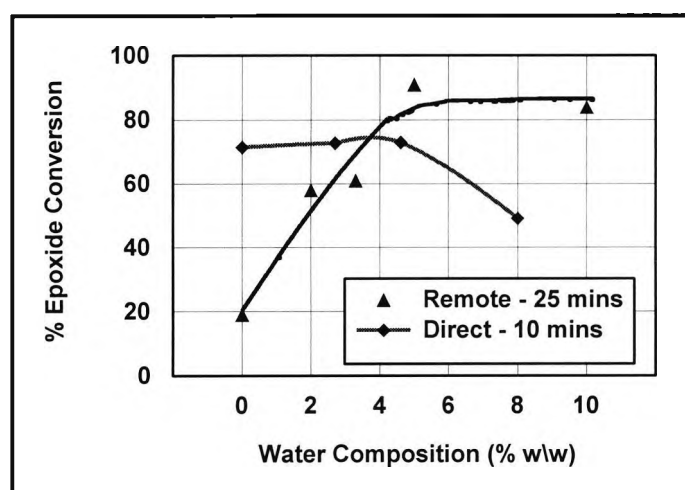
Figure 3.3-24   **Effect of bulk water on epoxide conversion
in direct and remote curing**

Clearly the directly cured film is unaffected by the presence of water in the bulk up to a level somewhere between 5 and 8 % w/w.

Watt has obtained similar results and explained this [80] by the fact, clearly apparent when the films are examined visually, that the water and epoxide are immiscible. Since the water is excluded from the epoxide phase it is not available to interfere with polymerisation. Water has a very high tendency towards association due to hydrogen

bonding and this is underlined by the very high surface tension value (72 Nm^{-2}), which is known for this material. Consequently when introduced in the bulk phase, rather than by diffusion, as is the case for water absorbed in humid environments, this material will form an emulsion and polymerisation proceeds in the epoxide phase quite independent of the presence of water in the second phase.

In the present case it is worth pointing out that the photoinitiator was dissolved in the organic phase prior to the addition of water. Consequently photodecomposition of the photoinitiator proceeds in the organic phase and initiates polymerisation in the usual manner. At some level higher than 5%, the rate of polymerisation is impeded although the mechanism of reaction is likely to be unaltered. This is perhaps due to the increasing volume occupied by water micelles limiting the availability of monomer and the space available within the matrix for propagation to occur.

Note: The hydroxyl band cannot be studied quantitatively because it is affected by the presence of water in the film.

Similarly the remote reaction is not affected mechanistically by the presence of bulk water as the ether band shows similar absorbance calculated at an equivalent level of epoxide consumption (Figure 3.3-25). Clearly bulk water does not participate in the polymerisation taking place within the epoxide phase (and probably with the same explanation as for the direct case). However it is quite apparent (Figure 3.3-24) that the rate of polymerisation is substantially increased when water is included in the bulk.
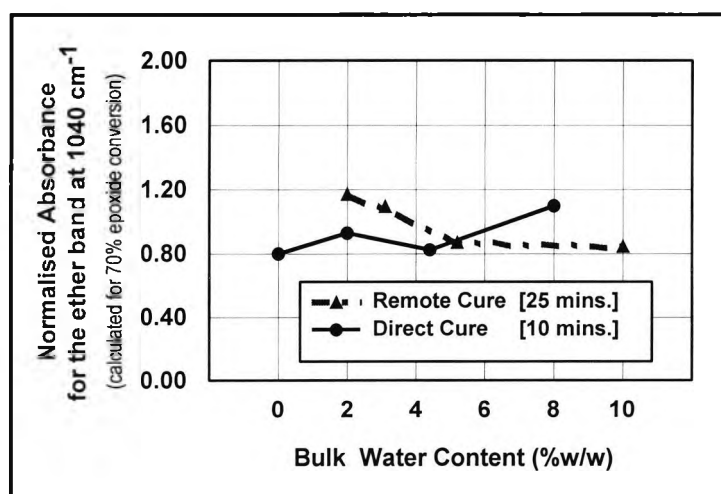
Figure 3.3-25   **Normalised IR absorption band for the ether linkeage in remote and direct curing in the presence of bulk water**

Since, as stated above, the bulk water does not interfere with the polymerisation reaction, it seems likely that bulk water is affecting in some manner the absorption of the acidic

183

species into the film. This is produced in the gaseous phase and diffuses into the film with which it is in close proximity.
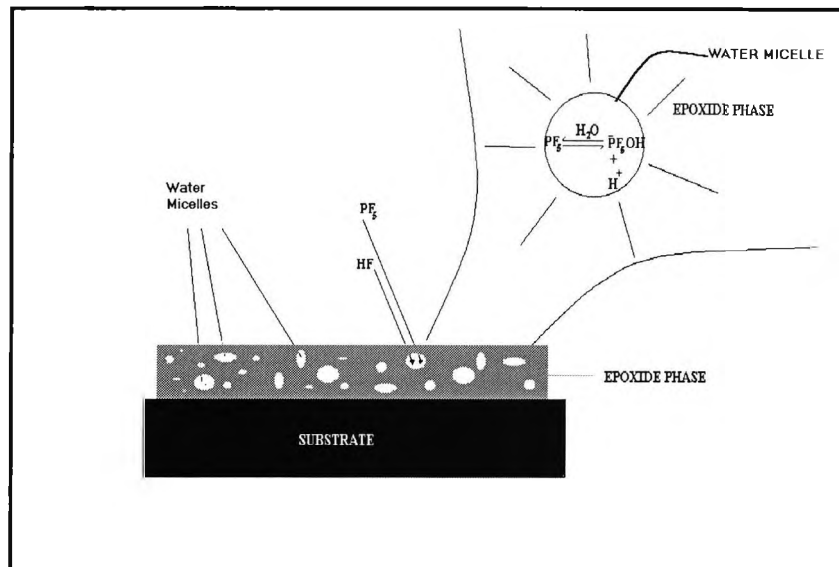
Figure 3.3-26   **Absorption of gases and interaction with monomer/water in remote polymerisation**

See Figure 3.3-26, In a film of thickness 10-20 μm, a substantial proportion of water micelles will be in contact with the air/epoxide interface where they will readily absorb gaseous acidic species such as PF_5 and HF. Once within the micelle these species will undergo hydrolysis to yield the hydroxylated Brønsted acid. This latter species is capable of initiating cationic polymerisation with the epoxide monomers surrounding the micelle. The presence of these micelles at the surface then, represents a rapid means of moving acidic species into the film from the atmosphere with the consequence of accelerated polymerisation.

3.3.8 Effect Of Initiator Quantity On Remote Cure
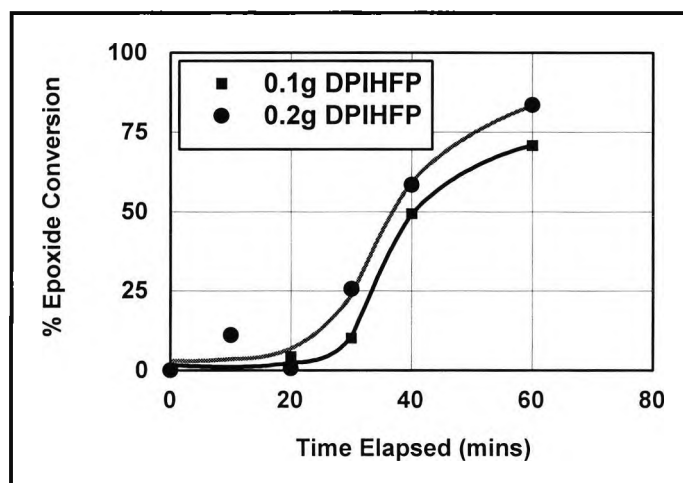
Figure 3.3-27   **Remote curing, effect of doubling initiator quantity on epoxide conversion**

Figure 3.3-27 indicates the consequence of doubling the photoinitiator quantity. Experiments were conducted with the DPIHFP initiator on a paper support using resin formulation 4 in the glass cell.

Doubling of the initiator quantity leads to an increase in all reaction indices, namely duration of lag phase, % epoxide conversion at any time stage, and completion time. However, these increases are evidently not proportional to the doubling of the initiator quantity.

Examination of the data indicates that at any time the value of epoxide conversion is about 10% higher with 0.2g of DPIHFP than with 0.1g. Furthermore, with 0.1g of DPIHFP the lag phase is passed after the elapse of about 27 minutes whereas with 0.2g of DPIHFP, this stage is reached in about 22 minutes.

This finding is consistent with the outcome of decomposition experiments which were done to assess the effect of variation of initiator quantity on rate of photodecomposition and HF generation. Although the present case involves the DPI anion and the aforementioned results were obtained with the less effective ferrocinium anion in Irg.261, this data is informative.

	Moles HF produced				Time to produce quantity of HF	
time	0.1g	0.2g		Quantity	0.1g	0.2g
10mins	7.9e-5	10e-5		0.00010m	14min	10min
43mins	15.8e-5	17.8e-5		0.00018m	60min	43min

Table 3.3-5   **Solid-state photo-decomposition, effect of initiator quantity on quantity of fluoride ions produced, Irgacure 261**

At any time the doubling of the initiator quantity is associated with about a 20% increase in fluoride generated (or initiator decomposed). To produce 0.0001m of HF requires 14min with 0.1g DPIHFP. By doubling the quantity this figure is reduced to 10min. This is also the experience with polymerisation. By doubling the initiator concentration the lag time is reduced from 27 to 22 minutes. This would suggest that the onset of polymerisation is contingent on the formation of a minimum quantity (concentration) of active species. This is achieved somewhat faster in the presence of a higher initial amount of initiator. Results in Sec.2.3.7 also confirm that if the increase in initiator quantity is achieved only by doubling the surface density of initiator on the substrate then the efficiency of gas generation actually drops per mole of initiator laid down. This explains why the net effect encountered with polymerisation is not the doubling, which might be expected, as the initiator is laid down by both an increase in area of substrate covered and an increase in surface density across the said area.

3.3.9 Hybrid Cationic/Free Radical Polymerisation

In 1979, Ketley and Tsao [111] noted that acrylate monomers could be cured in conjunction with epoxide monomers making use of the free radical onium salt photo-decomposition products. It was noted that 'hybridized' films had improved adhesion to metals and could be cured in thicker sections than had previously been possible with epoxide monomers alone, and more rapidly at such thicknesses than had previously been possible with acrylate monomers alone. It was suggested that the surface is initially sealed by epoxide polymerisation, permitting acrylate polymerisation to proceed in the bulk – unhindered by N_2 inhibition. DSC exotherms were larger, and shorter induction periods were noted. The addition of free radical photoinitiators was found to speed up the polymerisation further.

In 1986, Watt [110] made similar observations and in 1989, Manus [112] noted improved hardness and solvent resistance in hybrid films. Vara et al. [113,114] also found that the method could be applied to DVE's with similar advantages.

It was of interest to establish the feasibility of the hybrid cure approach in conjunction with remote cure.

A formulation (Sec.3.2.1.2) containing equal quantities of di-functional epoxide (UVR6110) and di-functional acrylate (HDDA) was devised in conjunction with 3% of the free radical initiator, Irgacure 907, and 10% (EtOH)$_2$NMe. Films of thickness 15μm were exposed alternately to direct irradiation, 5 mins. and to remote irradiation, 5 mins.

Figure 3.3-28, Figure 3.3-29 and Figure 3.3.9-3 show the IR spectra for the uncured resin, the resin partially cured after stage 1 (direct irradiation, free radical polymerisation of the acrylate monomers) and after stage 2 (indirect/remote irradiation, cationic polymerisation of the epoxide monomers).
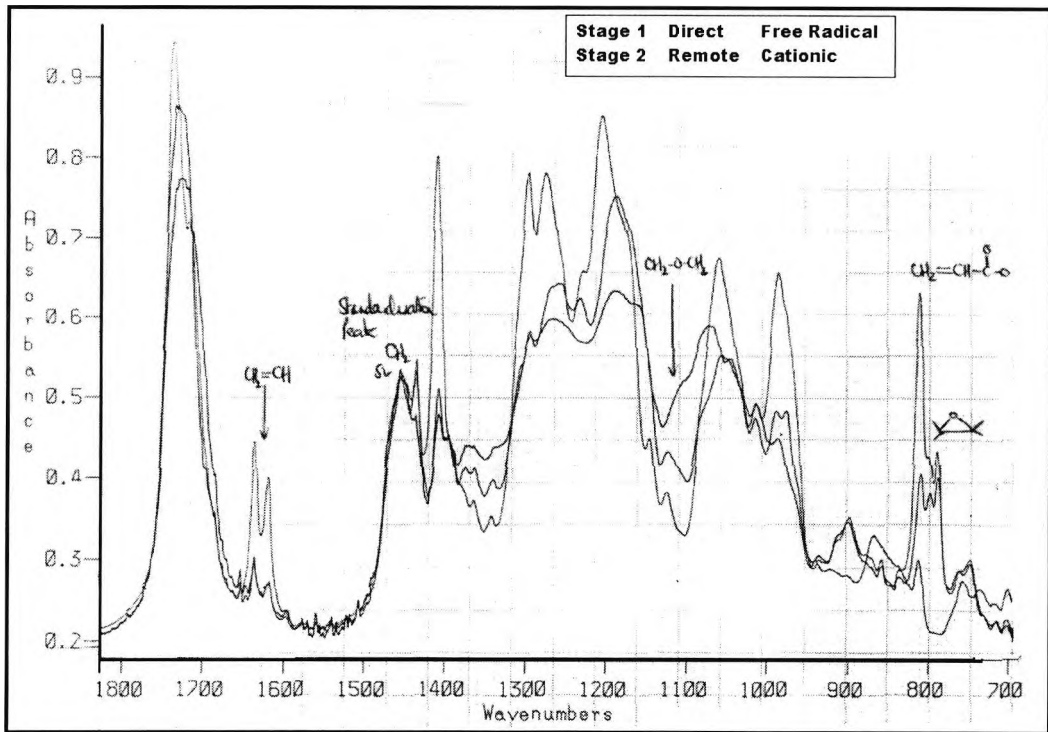
Figure 3.3-28   IR spectra (800-1800cm⁻¹) indicating Hybrid cure with remote cationic polymerisation of epoxide monomers in the 1ˢᵗ step and direct free radical cure of acrylate monomers in the 2ⁿᵈ step
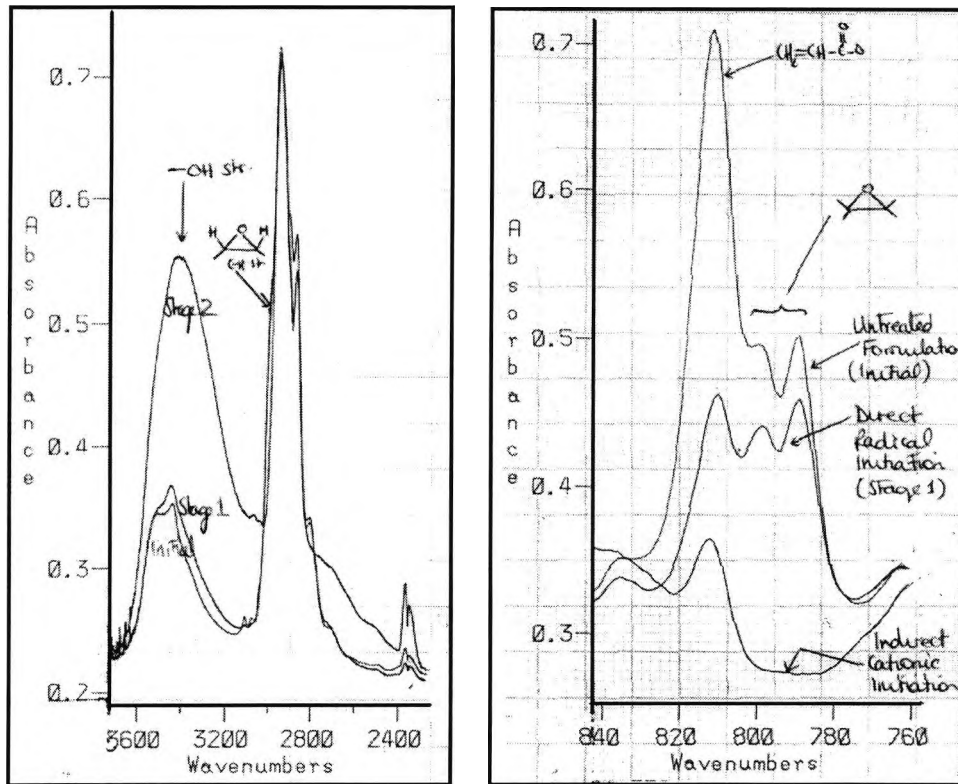
Figure 3.3-29 (left - 2400-3600cm⁻¹) and Figure 3.3-30 (right - 760-840cm⁻¹) IR spectra indicating Hybrid cure with remote cationic polymerisation of epoxide monomers in the 1ˢᵗ step and direct free radical cure of acrylate monomers in the 2ⁿᵈ step.

Examination of these spectra indicates the almost complete disappearance of the vinyl C-

188

H stretch of the acrylate at 812cm^{-1} while the epoxide C-H stretch at 794cm^{-1} remains intact.

The second stage of irradiation, remote, consumes the epoxide group completely. It should be noted that this represents a rapid rate of consumption for the epoxide when compared with previous experiments on remote polymerisation in this section.

The process was also completed in reverse, i.e. remote polymerisation of the epoxide occurring in the 1st stage, and direct polymerisation of the acrylate occurring in the 2nd stage. IR spectra for these experiments are contained in Figure 3.3-31, Figure 3.3-32 and Figure 3.3.9-6. These results are almost identical.
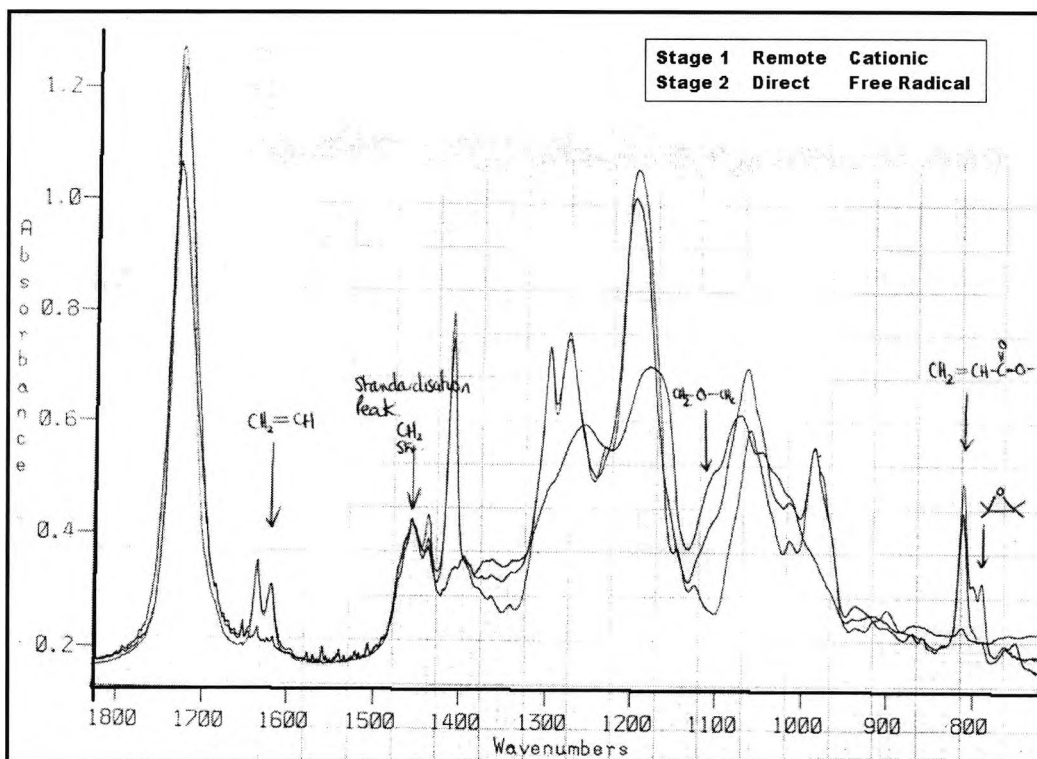
Figure 3.3-31 IR spectra (800-1800cm⁻¹) indicating hybrid cure with direct free radical cure of acrylate monomers in the 1st step and remote cationic polymerisation of epoxide monomers in the 2nd step
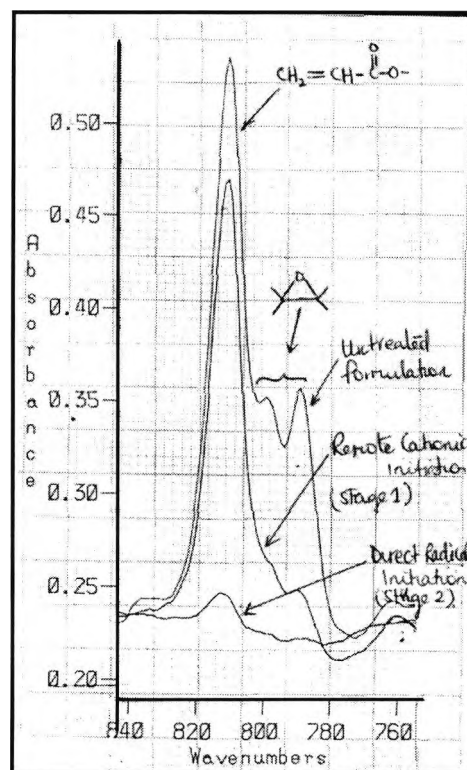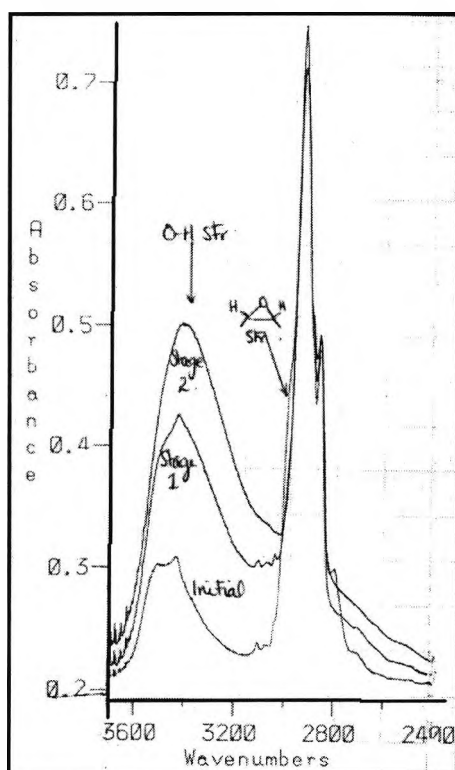
Figure 3.3-32 (left - 2400-3600cm⁻¹) and Figure 3.3-33 (right - 760-840cm⁻¹) IR spectra indicating Hybrid cure with direct free radical cure of acrylate monomers in the 1st step and remote cationic polymerisation of epoxide monomers in the 2nd step.

190

3.3.10 Remote Polymerisation Of Divinyl Ethers (DVE's)

Divinyl ethers (DVE's) are a class of monomer which has been found to be polymeriseable by cationic routes [17,18,21,25,83-85,89,90] and which has been used in conjunction with epoxides [113,114].

It was of interest to examine DVE's as substrates for remote cationic polymerisation by the gaseous photo-products arising from UV irradiation of solid state onium salts.

Solid state DPIHFP, 0.2g, was exposed to UV light in the presence of the DVE of triethylene glycol for 10 mins. The latter was rapidly converted to a hard, solid film. Cure was observed also by IR measurements, see Figure 3.3-34.

**Figure 3.3-34   IR Spectra, Remote cure of Diethylene
Glycol Divinyl Ether**

Comparison of IR spectra for the cured and uncured sample indicated disappearance of the following bands present in the uncured sample:

- strong band at 1650cm^{-1} assignable to the C=C stretching absorption of the vinyl group

- bands at 850cm^{-1} and 1000cm^{-1} assignable to the C-H out-of-plane deformations of the vinyl group

- band at 1350cm^{-1} which may be assigned to the C-O stretching absorption involving an unsaturated carbon (vinyl carbon)

The latter band is replaced, in the spectrum of the cured resin, by a band at 1250cm^{-1} that may be assignable to a C-O stretching absorption involving a saturated carbon (addition to vinyl bond, polymer).

These observations are consistent with a polymerisation involving addition to the vinyl double bond as an activation step, and S_N1 substitution of the carbocation in the propagation step, Scheme 3.3-10.
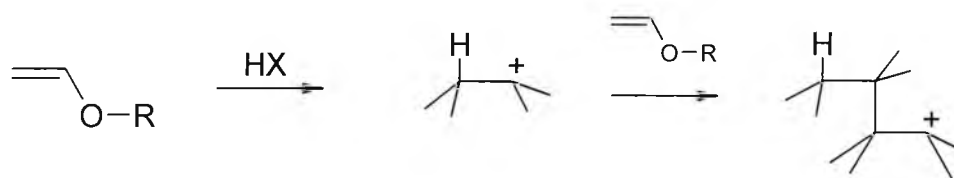
Scheme 3.3-10   Cationic polymerisation of a DVE

Such a mechanism is widely accepted for in-situ polymerisation (7,25). However, this mechanism supposes activation with the complex acid, HX, generated from decomposition of the onium salt as described previously. The counterion, X$^-$, is therefore of the type PF$_6^-$, AsF$_6^-$ etc. In the present case, i.e. polymerisation via gaseous intermediates, no such counterion can be available and an alternative mechanism must be supplied. As far as the author is aware, cationic polymerisation of DVE's via Lewis acid species has not yet been proposed, and a purely Lewis acid mechanism is difficult to justify in combination with propagation via the formal carbocation intermediates, which are not disputed.

Nevertheless, if the initial polymerising species is, in fact, the gaseous Lewis acid, PF$_5$, the polymerisation can be easily accounted for by interaction of the latter with residual and adventitious water to form the Brønsted acid, H$^+$/HOPF$_5$, that is derived from aquation of the Lewis acid, PF$_5$, See Scheme 3.3-11. This theory also explains the presence, in the spectrum of the cured sample, of a large hydroxyl band at 3500cm^{-1}. As far as the author is aware, this band is otherwise unaccounted for.
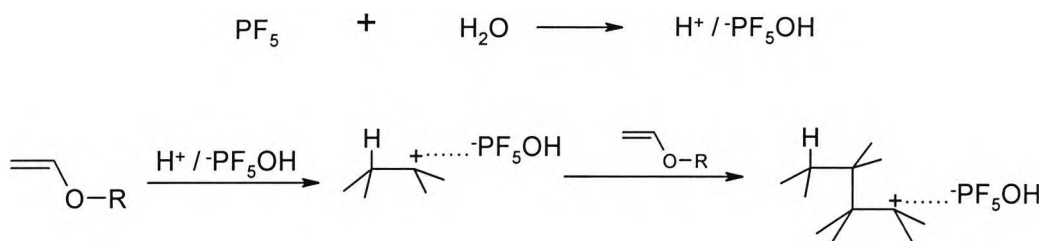
Scheme 3.3-11   Proposed polymerisation of DVE by aquated Lewis acid

In view of the expected tendency of hydrogen halides to undergo addition to vinyl bonds with halohydrin formation, the role of HF as a polymerising species in this case is questionable. This experiment further supports the identification of the pentahalide as the initial polymerising intermediate produced from UV irradiation of onium salts in the solid state.

4 APPENDIX A – TREATMENT OF DATA OBTAINED USING FLUORIDE SPECIFIC ELECTRODE (FSE)

4.1 Functions, Models, Equations and Derivatives – Analytical Approach

Unsuccessful efforts were made to fit the data to empirical kinetic models in an attempt to identify the order and rate constants of the photodecomposition reaction.

At any stage the decomposition yield becomes the complex product of several processes which are experimentally related:

- rate of photo-decomposition & no. of initiator molecules participating

- rate of HF evolution (chemical and/or diffusion constants)

- rate of XF_5 evolution (chemical and/or diffusion constants)

- rate (if any) of spontaneous hydrolysis of XF_5 in-situ

- rate (if any) of reactions involving attack of PF_5/HF with cation decomposition fragments and/or unreacted photoinitiator molecules.

- speed of transfer of gaseous products from decomposition vessel to water flask

- rate of hydrolysis of pentahalides in water (stepwise and/or partial hydrolysis of pentahalides yielding undetermined multiple equivalents with a distinct rate constant for each step)

These points serve to indicate that the experiments are not well designed for conventional kinetic analysis in the following important respects:

- The reaction pathway cannot be unambiguously identified.

- The 'concentration' or quantity of reactants cannot be established for the various stages of reaction.

- The appearance of product cannot be linked directly and stoichiometrically to the 'disappearance' of reactant.

- The temperature of the reaction cannot be controlled.

Even using the appearance of product (fluoride ion) as an index of reaction progress - which in any case requires unsafe assumptions concerning stoichiometry - the data could not be fitted to first, second and third order models, or to models for reactions involving multiple and sequential steps.

It is not surprising therefore that the results from these experiments do not provide any easy access to functions such as rate equations etc.

In the absence of kinetic devices to describe and analyse the process, the data was fitted to mathematical curve fitting functions so that derivatives as a function of time could be estimated with more accuracy. In this manner a rate value for the decomposition can be determined at important stages in the process.

Attempts at fitting the data over the its entire range to common linear and non-linear functions were unsatisfactory - irrespective of natural or logarithmic numerical treatment.

Nevertheless, it has been possible to divide the data into 2 regions which can be fitted satisfactorily to separate equations (see appendix) which overlap at the centre. The data for the first 50 minutes of the reaction can be fitted to function (A) while the data between 50 and 1200 minutes requires the polynomial function (B).

(A) $Ln[F^-]=a_0-a_1/[time]$.

(B) $Ln[F^-]=b_0+b_1Ln[time]+b_2(Ln[time])^2$

Efforts were made to fit the data to a large number of models in an attempt to identify some relationship with established chemical and/or physical processes. No such correlation was achievable.

Furthermore attempts at fitting the data by least squares methods to common linear and non-linear empirical functions were not satisfactory over the entire data range - irrespective of the numeric treatment applied - natural or logarithmic. The fact that the data spans 6 orders of magnitude in 'x' and 4 orders of magnitude in 'Y' with only 25 data points extracted visi-manually from the raw output chart certainly contributes to this difficulty.

Nevertheless, by careful inspection it has been possible to divide the data into 2 regions which can be fitted satisfactorily to empirical equations which overlap at the centre and have some utility for determining rates within the strict limits via the derivatives.
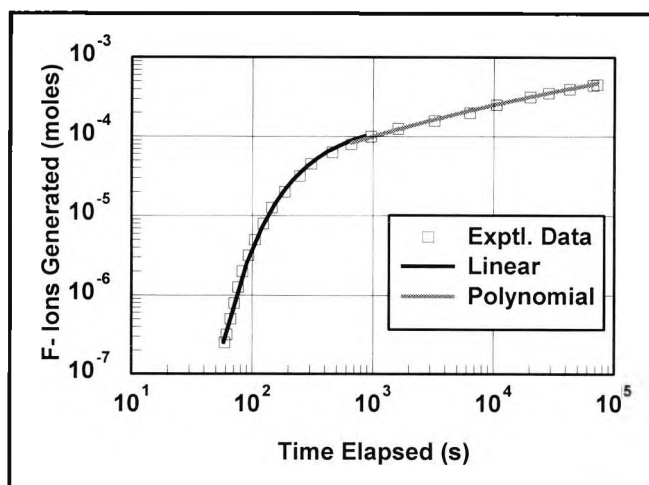
Figure 4.1-1   **Fluoride ion detection following UV induced solid state decomposition of onium salt initiators – curve fitting of experimental data separated into overlapping linear and polynomial regions**

The data for the first 18 points (from 0.98 mins to 54 mins) can be fitted to the following linear function:

$$Lny = a_0 + a_1/x$$

where $a_0 = -8.77$

$a_1 = -372.63$

$r^2 = 0.9983$

The derivative of this function in natural form is:

$$y' = e^{a0} * e^{a1/x} * -a1/x^2$$

In the later stages the log-log data is linear and can be fitted to a 2nd order polynomial regression so that the last 11 points (from 11 mins to 1200 mins) are described by the following function:

$$Lny = b_0 + b_1 lnx + b_2(lnX)^2$$

where $b_0 = -13.11$

$b_1 = 0.688$

$b_2 = -0.018$

$r^2 = 0.9984$

The derivative of this function in natural form is:

$$y' = [e^{b0} * x^{(b1-1)+(b2lnx)}] * [b_1 + 2b_2 lnx]$$

197

The derivatives of the linear and polynomial functions can be plotted as a function of time within the assigned limits to reveal the development of 'reaction' rate as the experiment develops.

4.2 Effect Of Anion Variation On Fluoride Ion Yield

The following table has been split over 2 pages: Table 4.2-1 Fluoride ion evolution following UV induced solid-state decomposition of onium salts bearing hexafluoro-group 5 anions – regression analysis of data with linear and polynomial functions, presentation of equations, equation coefficients and data obtained there from

	DPIHFP	DPIHPAs	DPIHFSb
range	0.98 - 54.00 min	0.66 - 70.00 min	1.83 - 59 min
regression	$\ln y = a_0 + a_1/x$	$\ln y = a_0 + a_1/x$	$\ln y = a_0 + a_1/x$
coefficients a_0	-8.77	-8.55	-9.23
a_1	-372.63	-250.99	-661.53
r^2	0.9983	0.9922	0.9981
y'	$e^{a_0} * e^{a_1/x} * -a_1/x^2$	$e^{a_0} * e^{a_1/x} * -a_1/x^2$	$e^{a_0} * e^{a_1/x} * -a_1/x^2$
y'_{max}	$e^{a_0} * e^{-2} * -4/a_1$	$e^{a_0} * e^{-2} * -4/a_1$	$e^{a_0} * e^{-2} * -4/a_1$
$x_{y'max}$	$-a_1/2$	$-a_1/2$	$-a_1/2$
$rate_{max}$	$= 2.26 \times 10^{-7}$ moless^{-1}	$= 4.17 \times 10^{-7}$ moless^{-1}	$= 8.00 \times 10^{-8}$ moless^{-1}
$time_{to\ max\ rate}$	= 185 s	125 s	330 s

range	11 - 1200 min	8 - 1200 min	7 - 1200 min
regression	$\ln y = b_0 + b_1 \ln x + b_2 (\ln x)^2$	$\ln y = b_0 + b_1 \ln x + b_2 (\ln x)^2$	$\ln y = b_0 + b_1 \ln x + b_2 (\ln x)^2$ $+ b_3 (\ln x)^3$
coefficients b_0	-13.11	-12.09	-36.35
b_1	0.688	0.579	8.20
b_2	-0.018	0.018	-0.83
b_3			0.029
r^2	0.9984	0.9974	0.9996
y'	$[e^{b0}*x^{(b1-1)+(b2\ln x)}]$ $*[b_1 + 2b_2 \ln x]$	$[e^{b0}*x^{(b1-1)+(b2\ln x)}]$ $*[b_1 + 2b_2 \ln x]$	$[e^{b0}*x^{(b1-1)+(b2\ln x)+(b3\ln x^2)}]$ $*[b_1 + 2b_2 \ln x + 3b_3 (\ln x)^3]$
yield$_{100\ mins}$	2.0×10^{-4} moles	2.1×10^{-4} moles	1.2×10^{-4} moles
time double	13.2 hours		31.7 hours
rate$_{100\ mins}$	5.3×10^{-7} moless^{-1}	5.1×10^{-7} moless^{-1}	3.2×10^{-7} moless^{-1}
yield$_{1000\ mins}$	4.4×10^{-4} moles	3.5×10^{-4} moles	1.8×10^{-4} moles
rate$_{1000\ mins}$	2.2×10^{-9} moless^{-1}	1.1×10^{-9} moless^{-1}	2.7×10^{-9} moless^{-1}
Equiv$_{1000mins}$	1.88	1.50	0.77

Table 4.2-1   **Fluoride ion evolution following UV induced solid-state decomposition of onium salts bearing hexafluoro-group 5 anions – regression analysis of data with linear and polynomial functions, presentation of equations, equation coefficients and data obtained there from**

4.3 Effect Of Cation Variation On Fluoride Ion Yield

		DPIHFP	TPSHFP	Irg.261
regression		linear: $\ln y = a_0 + a_1/x$		
range (mins)		1.0 - 43	0.6 - 46	2.0 - 54
coefficients	a_0	-8.7566	-8.7648	-8.9903
	a_1	-373.48	-215.64	-730.29
r^2		0.9983	0.9951	0.9951

		DPIHFP	TPSHFP	Irg.261
regression		polynomial: $\ln y = b_0 + b_1 \ln x + b_2 (\ln x)^2$		
range (mins)		11 - 1200	21 - 1500	17 - 1200
coefficients	b_0	-13.11	-11.25	-18.38
	b_1	0.688	0.398	1.720
	b_2	-0.018	0.011	-0.071
r^2		0.9984	0.9913	0.9996

Table 4.3-1 **Fluoride ion evolution following UV induced solid-state decomposition of various initiators salts bearing hexafluorophosphate anions – regression analysis of data with linear and polynomial functions, presentation of equations, equation coefficients**

4.4 Effect Of The Presence Of Free Radical Initiator (Irgacure 651) On Fluoride Ion Yield

	0 % Irg.651	7% Irg.651	14% Irg.651
regression	linear: $\ln y = a_0 + a_1/x$		
range (mins)	1 - 10	1 - 10	1 - 10
coefficients a_0	-8.8368	-8.5793	-8.4097
a_1	-305.61	-303.99	-315.33
r^2	0.9921	0.9953	0.9970

regression	polynomial: $\ln y = b_0 + b_1 \ln x + b_2 (\ln x)^2$		
range (mins)	6 - 1000	6 - 1100	6 - 217
coefficients b_0	-15.95	-15.87	-16.70
b_1	1.374	1.426	1.767
b_2	-0.048	0.054	-0.082
r^2	0.9975	0.9967	0.9990

Table 4.4-1   **Fluoride ion evolution following UV induced solid-state decomposition of DPIHFP in presence of Irgacure 651 – regression analysis of data with linear and polynomial functions, presentation of equations, equation coefficients**

4.5   Effect Of Surface Density Variation On Fluoride Ion Yield

	380 gm-2	570 gm-2	930gm-2	1760gm-2
regression	linear: $\ln y = a_0 + a_1/x$			
range (mins)	1 - 16	1 - 16	1 - 16	1-16
coefficients a_0	-8.9719	-8.9090	-8.9408	-8.9324
a_1	-224	-304	-441	-742
r^2	0.9984	0.9981	0.9981	0.9928

regression	polynomial: $\ln y = b_0 + b_1 \ln x + b_2 (\ln x)^2$			
range (mins)	12 - 260	8 - 300	9-310	9-260
coefficients b_0	-12.89	-16.87	-17.78	-18.73
b_1	0.659	1.700	1.775	1.804
b_2	-0.015	0.0815	-0.0797	-0.0761
r^2	0.9946	0.9994	0.9979	0.9996

Table 4.5-1   **Fluoride ion evolution following UV induced solid-state decomposition of Irgacure 261 with variation in surface density of initiator – regression analysis of data with linear and polynomial functions, presentation of equations, equation coefficients**

5 APPENDIX B – GCMS DATA FOR SOLID-STATE PHOTO-DECOMPOSITION PRODUCTS

5.1 Diphenyliodonium Hexafluorphosphate
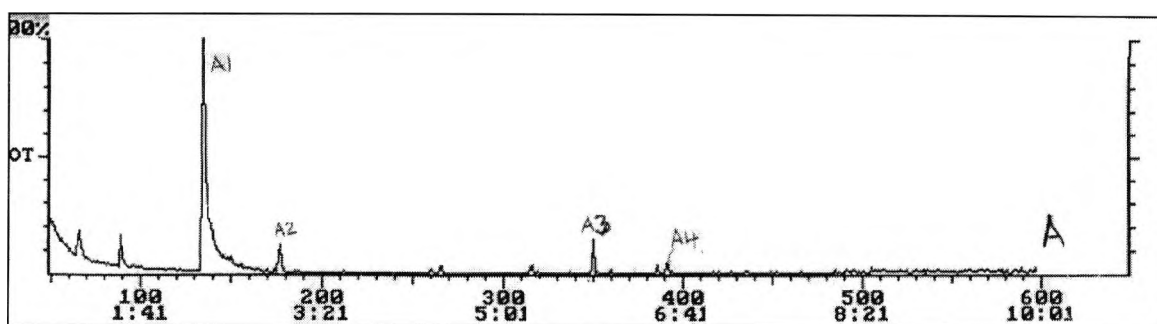
Figure 5.1-1 GC trace for separation of photoproducts obtained after UV irradiation of solid state DPIHFP, photoproducts dissolved in acetone
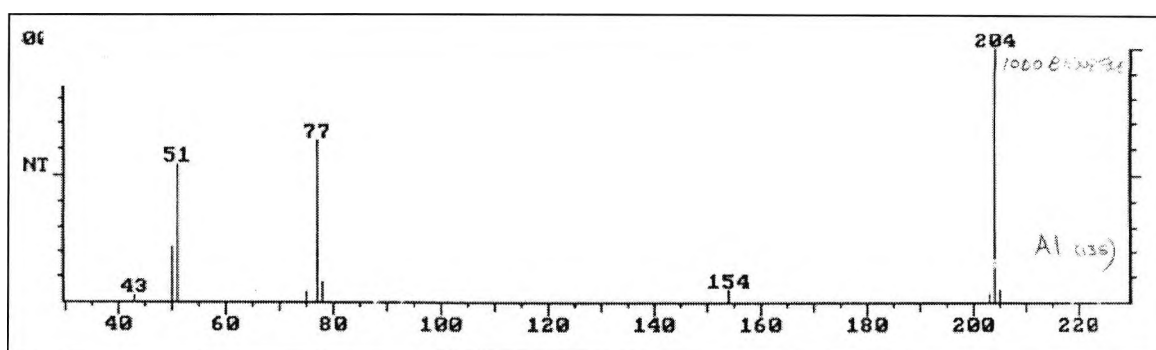
Figure 5.1-2 MS for GC fraction A1 at reference time 135, product obtained from UV irradiation of solid state DPIHFP
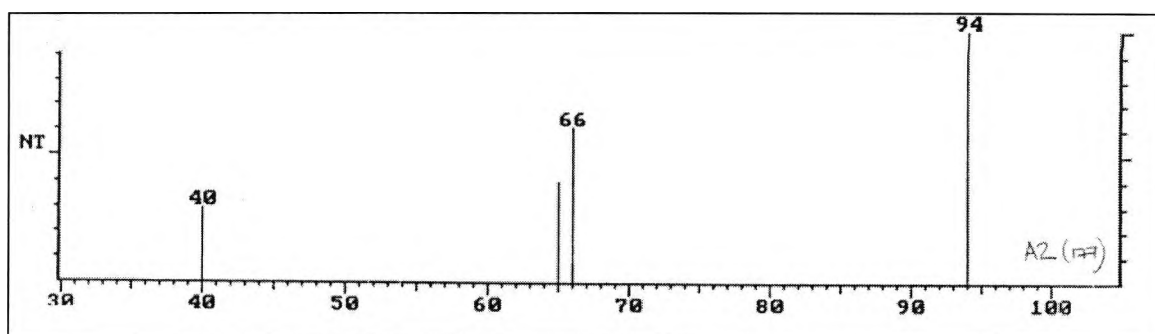
Figure 5.1-3 MS for GC fraction A2 at reference time 177, product obtained from UV irradiation of solid state DPIHFP

205
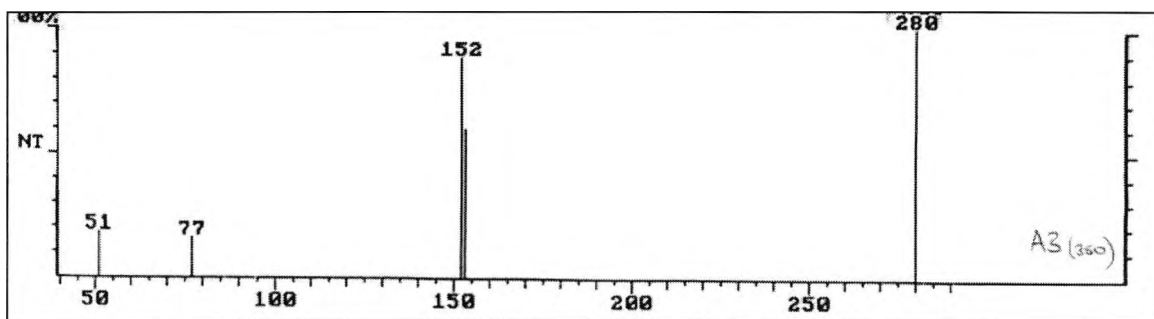
Figure 5.1-4 MS for GC fraction A3 at reference time 350, product obtained from UV irradiation of solid state DPIHFP
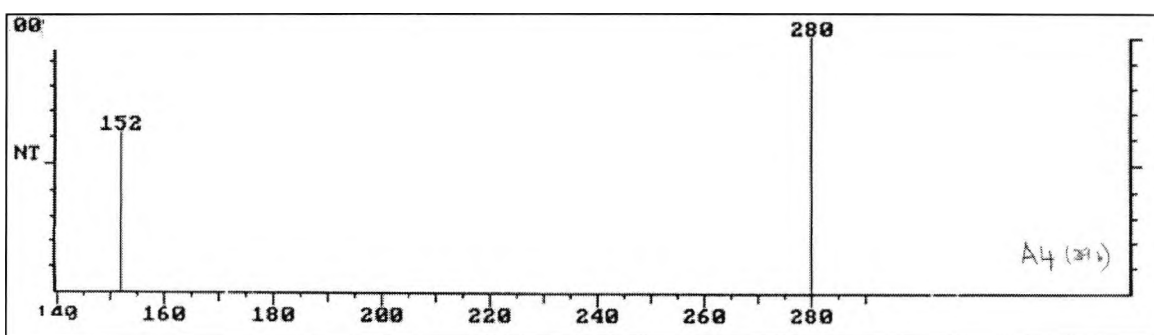
Figure 5.1-5 MS for GC fraction A4 at reference time 391, product obtained from UV irradiation of solid state DPIHFP

5.2   Diphenyliodonium Hexafluoroarsenate
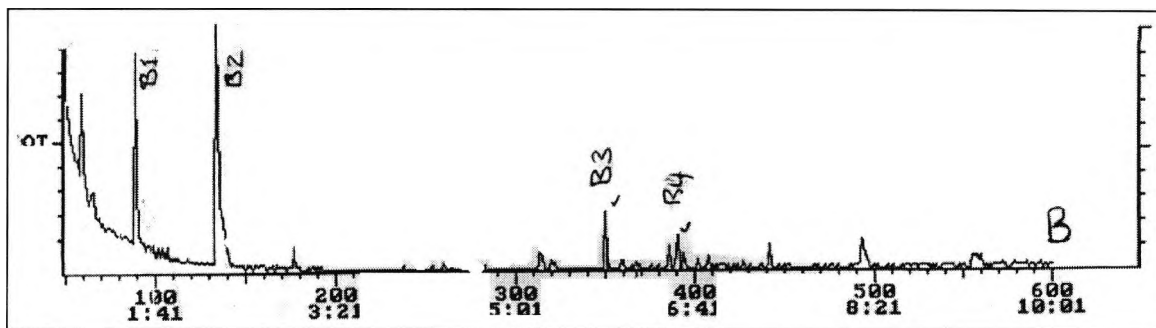
Figure 5.2-1 GC trace for separation of photoproducts obtained after UV irradiation of solid state DPIHFAs, photoproducts dissolved in acetone
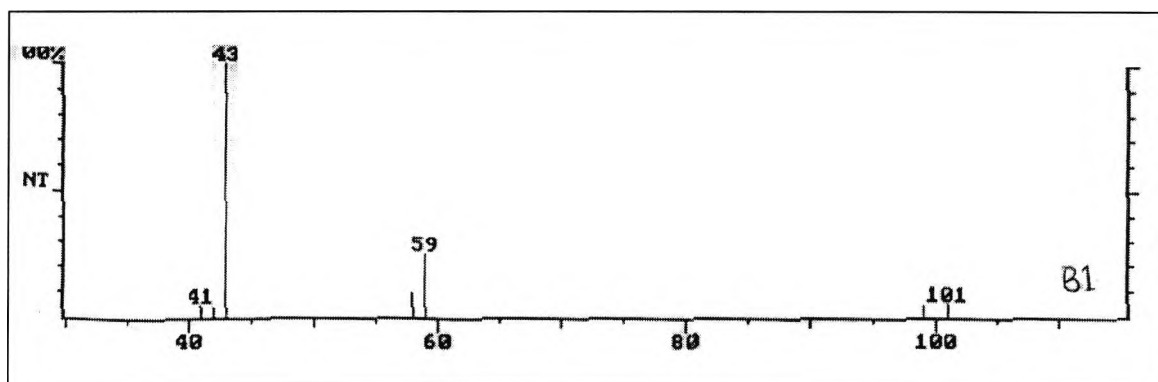
Figure 5.2-2 MS for GC fraction B1 at reference time 89, product obtained from UV irradiation of solid state DPIHFAs
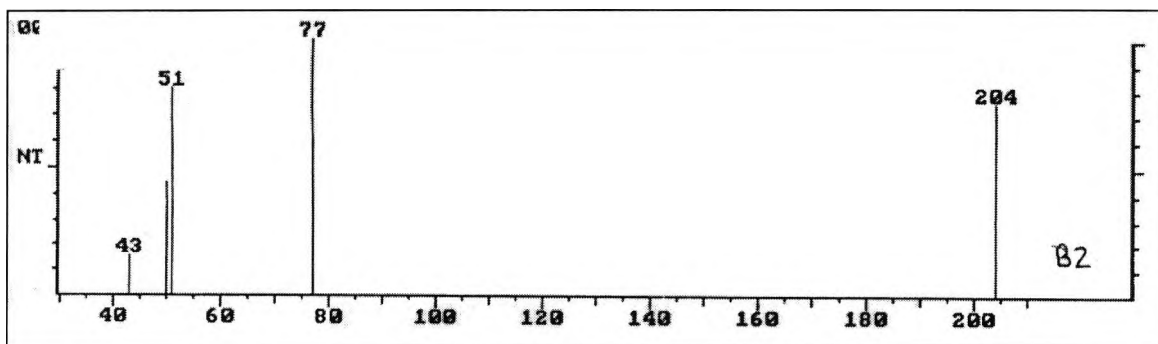
Figure 5.2-3 MS for GC fraction B2 at reference time 135, product obtained from UV irradiation of solid state DPIHFAs
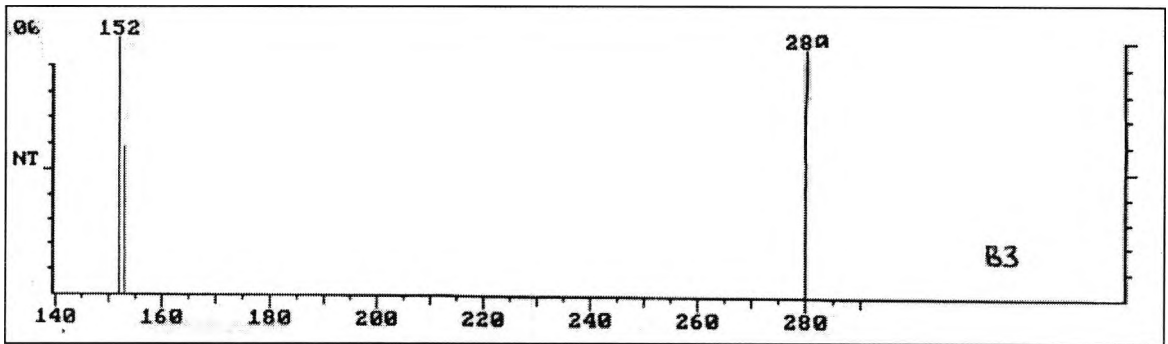
Figure 5.2-4 MS for GC fraction B3 at reference time 350, product obtained from UV irradiation of solid state DPIHFAs
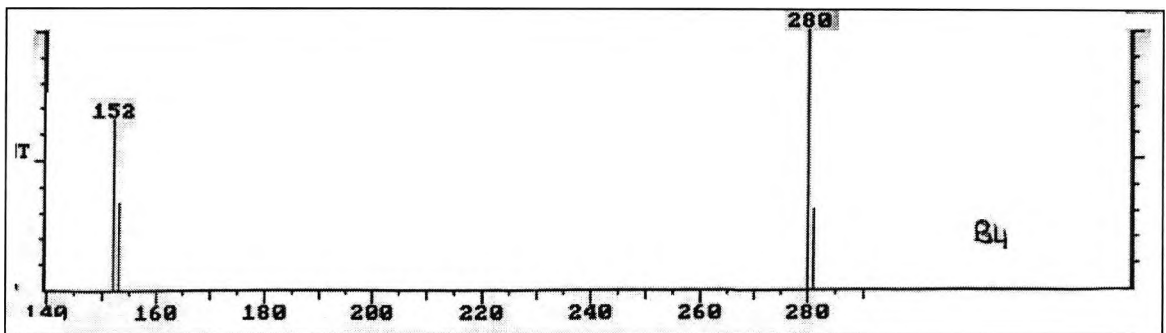
Figure 5.2-5 MS for GC fraction B4 at reference time 391, product obtained from UV irradiation of solid state DPIHFAs

5.3 Triphenylsulphonium Hexafluoroantimonate (Prop Carb)
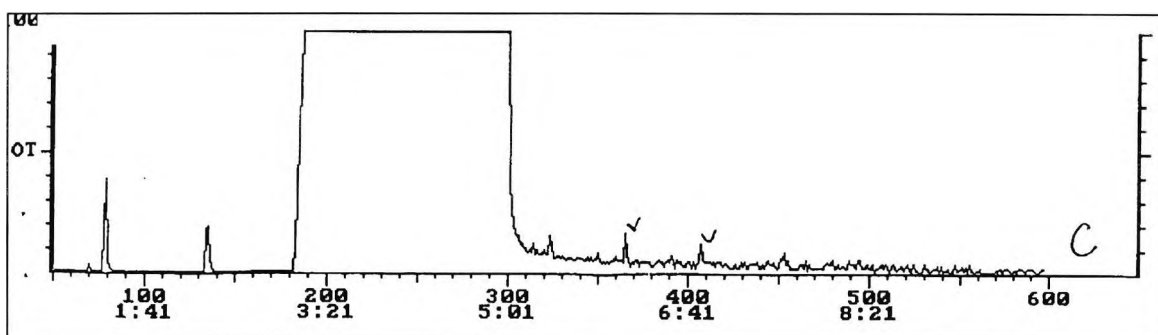
Figure 5.3-1 GC trace for separation of photoproducts obtained after UV irradiation of solid state TPSHFSb, photoproducts dissolved in propylene carbonate
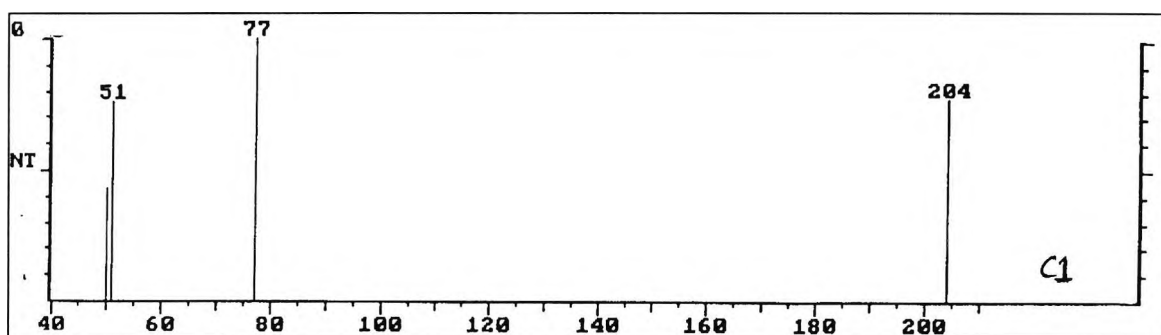
Figure 5.3-2 MS for GC fraction C1 at reference time 135, product obtained from UV irradiation of solid state TPSHFSb
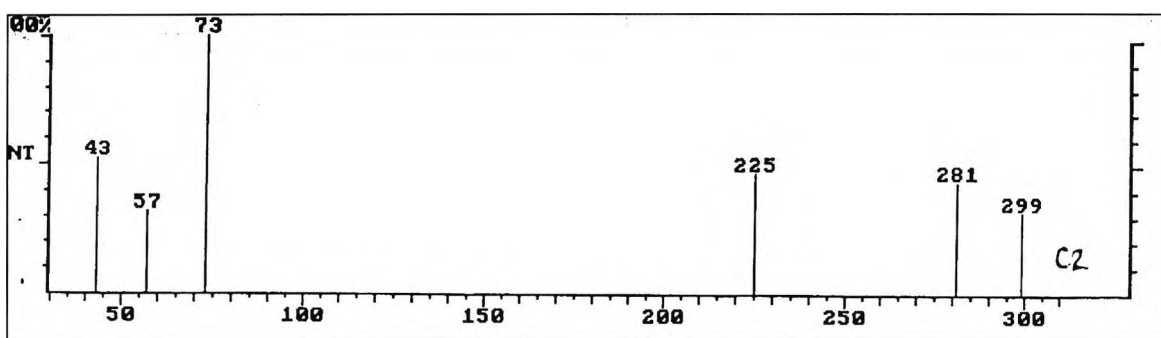
Figure 5.3-3 MS for GC fraction C2 at reference time 365, product obtained from UV irradiation of solid state TPSHFSb
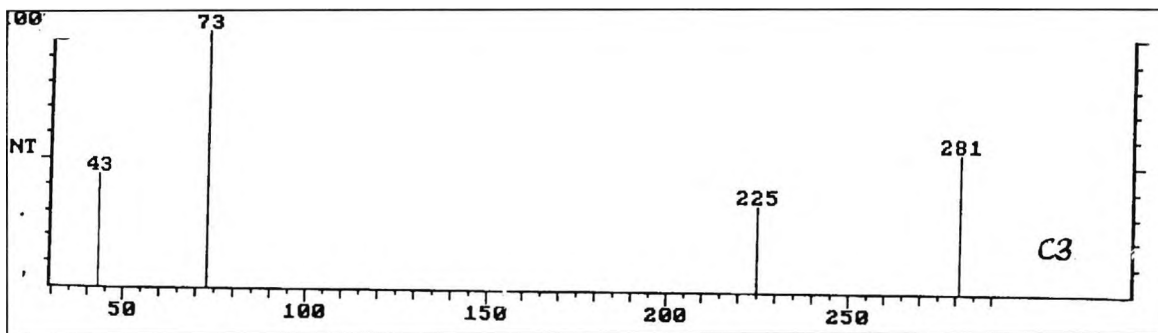
Figure 5.3-4 MS for GC fraction C3 at reference time 407, product obtained from UV irradiation of solid state TPSHFSb

5.4 Triphenylsulphonium Hexafluoroantimonate (Acetone)
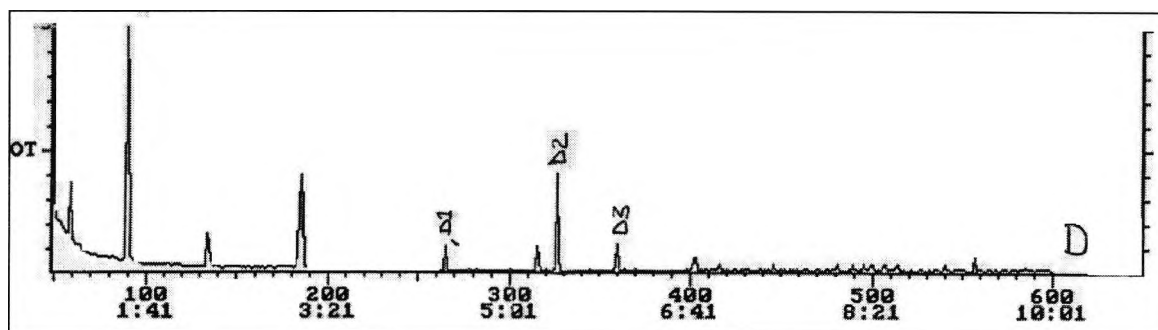
Figure 5.4-1 GC trace for separation of photoproducts obtained after UV irradiation of solid state TPSHFSb, photoproducts dissolved in acetone
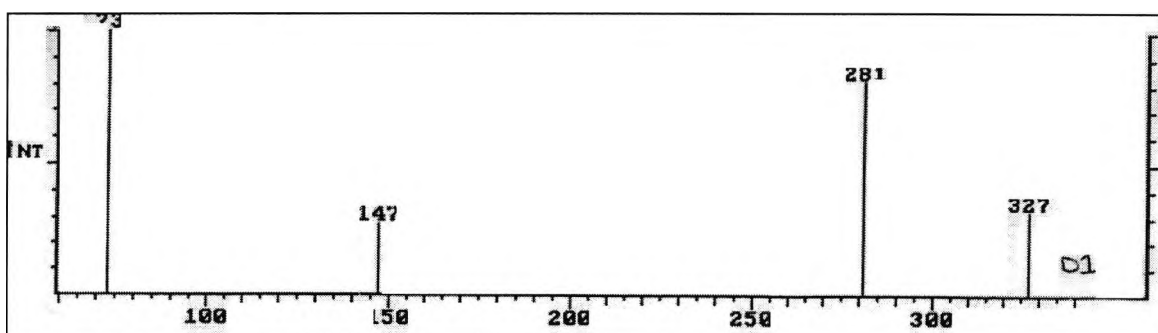
Figure 5.4-2 MS for GC fraction D1 at reference time 265, product obtained from UV irradiation of solid state TPSHFSb
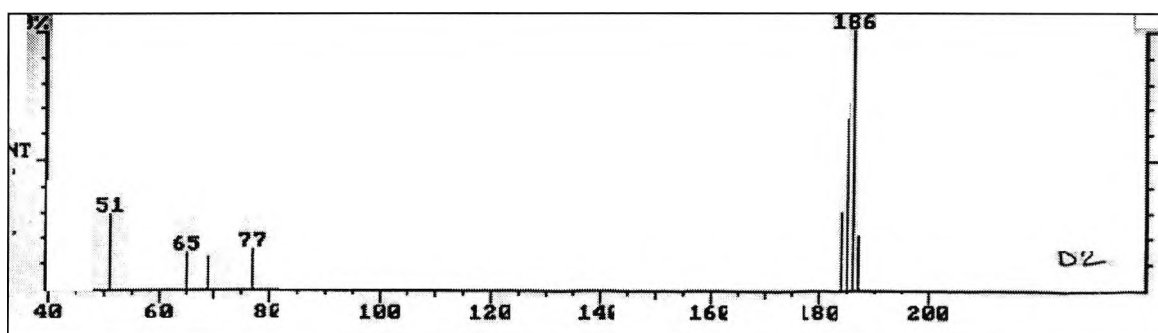
Figure 5.4-3 MS for GC fraction D2 at reference time 326, product obtained from UV irradiation of solid state TPSHFSb
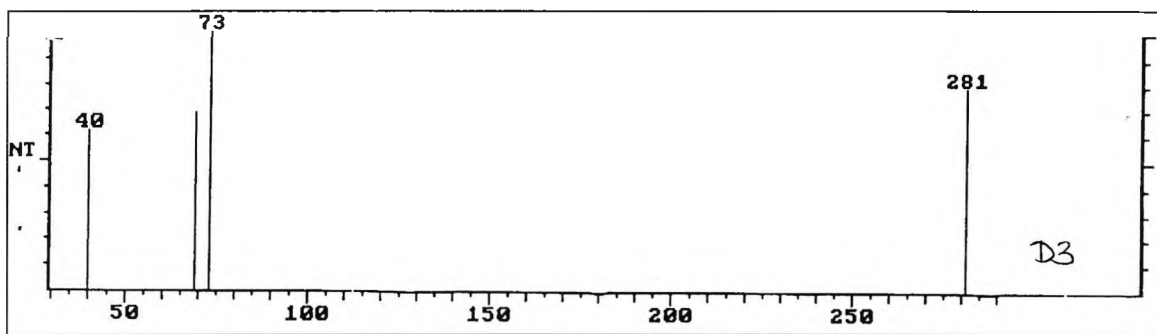
Figure 5.4-4 MS for GC fraction D3 at reference time 403, product obtained from UV irradiation of solid state TPSHFSb

6 APPENDIX C – RAW FTIR DATA AND TREATED DATA – REMOTE CATIONIC POLYMERISATION

6.1   Development of polymerisation in the direct process
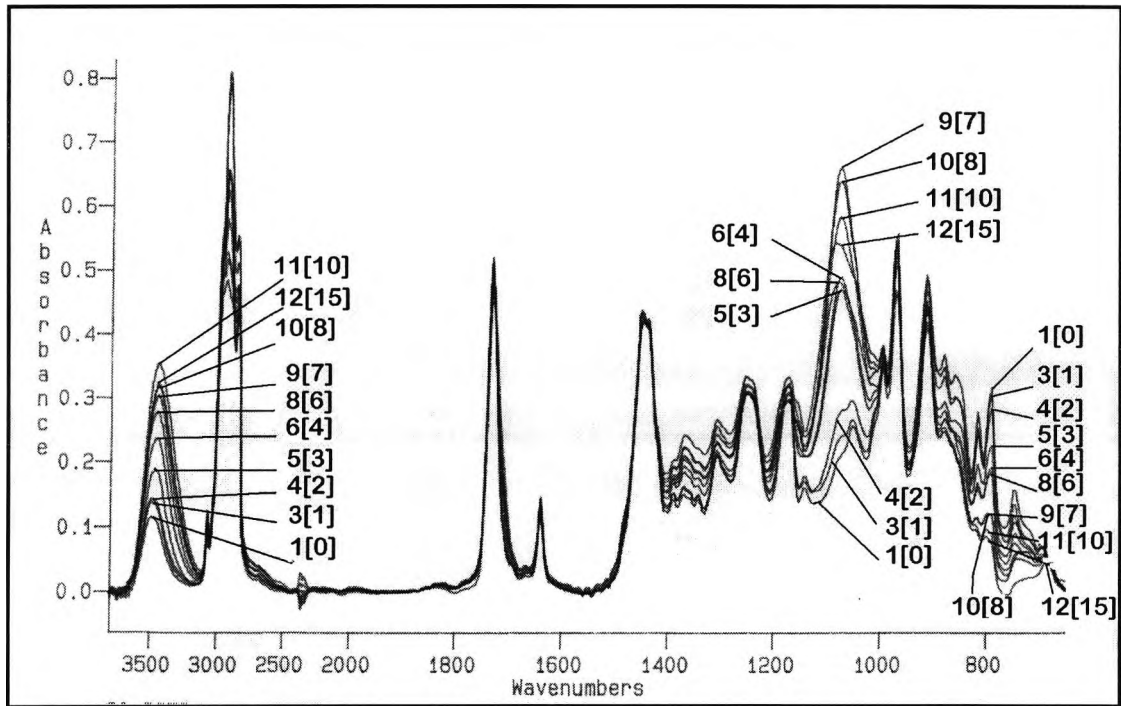
Figure 6.1-1   **Direct curing, IR spectra for direct curing of epoxide, 1.5%DPIHFP, resin formulation 2**

Expt Number [11]	Sample Thickness (um)	Elapsed Time (mins)	A 3455 cm^{-1} Abs	A 3455 cm^{-1} Abs.N	B 1444 cm^{-1} Abs	B 1444 cm^{-1} Abs.N	C 1080 cm^{-1} Abs	C 1080 cm^{-1} Abs.N	D 792 cm^{-1} Abs	D 792 cm^{-1} Abs.N	% Conver.
1		0	0.19	0.27	0.71	1.00	0.35	0.49	0.54	0.76	0.0
2	22.6	0.5	0.22	0.31	0.70	1.00	0.36	0.51	0.51	0.73	3.2
3	24.2	1	0.26	0.33	0.80	1.00	0.45	0.56	0.58	0.72	4.4
4	19.9	2	0.19	0.34	0.56	1.00	0.37	0.66	0.38	0.68	10.6
5	20.0	3	0.27	0.45	0.60	1.00	0.67	1.12	0.32	0.54	29.2
6	23.0	4	0.35	0.56	0.63	1.00	0.73	1.17	0.29	0.46	39.6
7	23.2	5	0.35	0.60	0.57	1.00	0.71	1.24	0.26	0.44	41.3
8	23.8	6	0.57	0.66	0.85	1.00	0.98	1.15	0.38	0.44	41.8
9	21.2	7	0.33	0.72	0.46	1.00	0.72	1.55	0.13	0.29	62.3
10	20.6	8	0.32	0.75	0.43	1.00	0.64	1.49	0.12	0.28	63.2
11	22.7	10	0.70	0.84	0.83	1.00	1.07	1.28	0.18	0.21	71.8
12	23.9	15	0.49	0.76	0.64	1.00	0.89	1.38	0.12	0.19	75.3

Table 6.1-1   **Direct curing, IR spectral data and experimental data for direct curing of an epoxide, 1.5% DPIHFP, resin formulation 2**

6.2 Development of polymerisation in the remote process

Figure 6.2-1   **Remote curing in glass apparatus, IR spectra for remote curing of epoxide, 0.1g DPIHFP, resin formulation 1**

Expt Number [2]	Sample Thickness (μm)	Elapsed Time (mins)	Band Data								% Conver.
			A 3455 cm^{-1}		B 1444 cm^{-1}		C 1080 cm^{-1}		D 792 cm^{-1}		
			Abs	Abs.N	Abs	Abs.N	Abs	Abs.N	Abs	Abs.N	
1	13.8	0	0.12	0.25	0.48	1.00	0.04	0.08	0.39	0.81	0.0
2	15.0	10	0.12	0.39	0.29	1.00	0.06	0.22	0.22	0.74	9.1
3	13.8	15	0.17	0.49	0.34	1.00	0.22	0.64	0.22	0.65	19.4
4	16.2	20	0.19	0.82	0.23	1.00	0.14	0.61	0.12	0.52	35.7
5	14.6	25	0.38	0.63	0.61	1.00	0.59	0.98	0.33	0.55	32.0
6	16.5	30	0.36	1.12	0.32	1.00	0.52	1.62	0.06	0.20	75.6
7	13.8	40	0.61	1.31	0.46	1.00	0.72	1.55	0.04	0.08	90.4
8	13.6	48	0.44	1.24	0.36	1.00	0.58	1.63	0.04	0.10	87.9

Table 6.2-1   **Remote curing in glass apparatus, IR spectral data and experimental data for remote curing of an epoxide, 0.1g DPIHFP, resin formulation 1**

215

Figure 6.2-2　　　**Remote curing in PTFE apparatus, IR spectra for remote curing of epoxide, 0.2g DPIHFP, resin formulation 4**

Expt	Sample	Elapsed	Band Data								%
Number	Thickness	Time	A		B		C		D		Conver.
	(μm)	(mins)	3455 cm^{-1}		1444 cm^{-1}		1080 cm^{-1}		792 cm^{-1}		
[18]			Abs	Abs.N	Abs	Abs.N	Abs	Abs.N	Abs	Abs.N	
1		0.0	0.26	0.24	1.09	1.00	0.54	0.49	1.06	0.97	0.0
2	17.5	2.5	0.05	0.25	0.19	1.00	0.13	0.66	0.18	0.96	0.3
3	14.2	3.8	0.09	0.47	0.20	1.00	0.15	0.76	0.18	0.90	7.2
4	16.8	5.0	0.25	0.46	0.55	1.00	0.86	1.54	0.34	0.61	36.9
5	17.4	7.5	0.14	0.43	0.33	1.00	0.53	1.61	0.20	0.60	38.3
6	16.6	10.0	0.09	0.60	0.15	1.00	0.22	1.47	0.06	0.41	57.9
7	15.1	20.0	0.14	0.71	0.19	1.00	0.29	1.55	0.05	0.29	70.1
8	15.6	30.0	0.47	0.83	0.57	1.00	1.14	2.00	0.06	0.10	89.2

Table 6.2-2　　　**Remote curing in PTFE apparatus, IR spectral data and experimental data for remote curing of an epoxide, 0.2g DPIHFP, resin formulation 4**

Figure 6.2-3 2-step remote curing in PTFE apparatus, IR spectra for 2-step remote curing of epoxide, 0.2g DPIHFP, resin formulation 4

Expt Number	Sample Thickness (μm)	Elapsed Time (mins)	Band Data								% Conver.
			A 3455 cm⁻¹		B 1444 cm⁻¹		C 1080 cm⁻¹		D 792 cm⁻¹		
[20]			Abs	Abs.N	Abs	Abs.N	Abs	Abs.N	Abs	Abs.N	
1		0	0.26	0.24	1.09	1.00	0.54	0.49	1.06	0.99	0.0
2	15.5	2.5	0.17	0.35	0.47	1.00	0.44	0.93	0.44	0.93	5.6
3	16.0	5	0.07	0.65	0.11	1.00	0.14	1.26	0.08	0.73	26.7
4	16.0	10	0.16	0.87	0.19	1.00	0.21	1.15	0.13	0.69	30.4
5	15.0	20	0.13	0.77	0.17	1.00	0.22	1.29	0.12	0.70	28.9

Table 6.2-3 2-step remote curing in PTFE apparatus, IR spectral data and experimental data for remote curing of an epoxide, 0.2g DPIHFP, resin formulation 4

6.3 Effect of gap width on remote cure
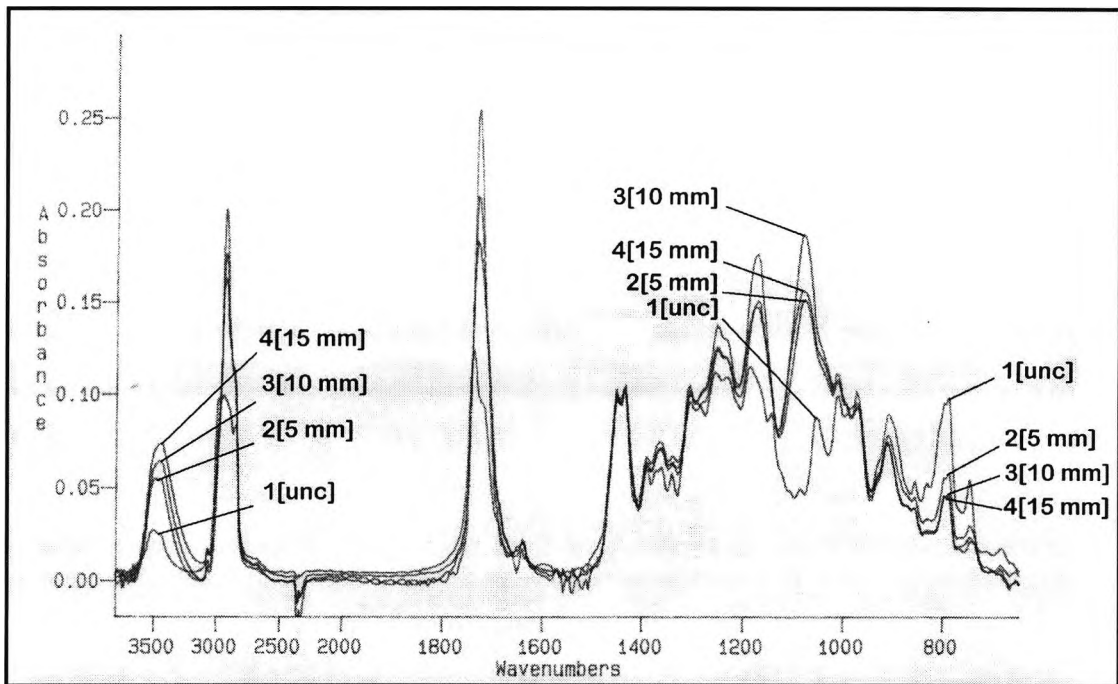
Figure 6.3-1   **Remote curing in PTFE apparatus, IR spectra for remote curing of epoxide with variation (5-15mm) of initiator-resin gap width, 0.2g DPIHFP, resin formulation 4**

Expt Number [17]	Sample Thickness (μm)	Elapsed Time (mins)	Band Data								% Conver.
			A 3455 cm⁻¹		B 1444 cm⁻¹		C 1080 cm⁻¹		D 792 cm⁻¹		
			Abs	Abs.N	Abs	Abs.N	Abs	Abs.N	Abs	Abs.N	
1		0.0	0.22	0.22	1.01	1.00	0.46	0.46	1.00	0.99	0.0
2	7.7	10.0	0.05	0.58	0.09	1.00	0.15	1.60	0.06	0.60	39.2
3	8.1	10.0	0.08	0.67	0.13	1.00	0.25	1.93	0.06	0.48	51.5
4	7.7	10.0	0.13	0.76	0.17	1.00	0.29	1.66	0.08	0.46	53.4

Table 6.3-1   **Remote curing in PTFE apparatus, IR spectral data and experimental data for remote curing of an epoxide with variation (5-15mm) of initiator-resin gap width, 0.2g DPIHFP, resin formulation 4**

6.4 Effect of initiator selection on remote cure
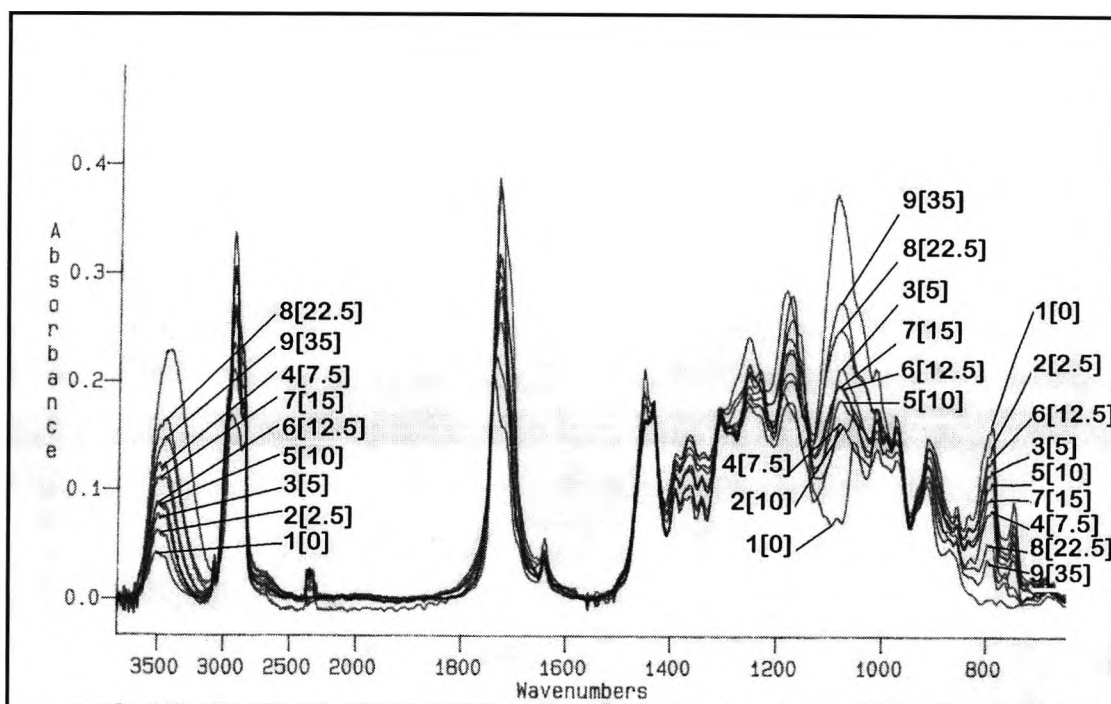
Figure 6.4-1   **Remote curing in PTFE apparatus, IR spectra for remote curing of epoxide, 0.2g Irgacure 261, resin formulation 4**

Expt Number [13]	Sample Thickness (μm)	Elapsed Time (mins)	Band Data								% Conver.
			A 3455 cm⁻¹		B 1444 cm⁻¹		C 1080 cm⁻¹		D 792 cm⁻¹		
			Abs	Abs.N	Abs	Abs.N	Abs	Abs.N	Abs	Abs.N	
1		0.0	0.27	0.24	1.10	1.00	0.48	0.44	1.04	0.95	0.0
2	16.7	2.5	0.06	0.37	0.17	1.00	0.16	0.97	0.14	0.84	11.6
3	16.8	5.0	0.06	0.47	0.14	1.00	0.18	1.28	0.10	0.72	24.6
4	18.0	7.5	0.11	0.74	0.15	1.00	0.14	0.96	0.07	0.50	47.6
5	16.6	10.0	0.07	0.54	0.14	1.00	0.15	1.09	0.09	0.66	30.7
6	19.1	12.5	0.25	0.52	0.47	1.00	0.56	1.20	0.37	0.78	17.9
7	19.8	15.0	0.15	0.65	0.22	1.00	0.27	1.20	0.13	0.58	38.8
8	17.2	22.5	0.21	0.96	0.22	1.00	0.32	1.45	0.07	0.30	68.6
9	17.1	35.0	0.14	0.88	0.16	1.00	0.27	1.65	0.03	0.21	78.1

Table 6.4-1   **Remote curing in PTFE apparatus, IR spectral data and experimental data for remote curing of an epoxide, 0.2g Irgacure 261, resin formulation 4**

219

Expt Number [4]		Elapsed Time (mins)	Band Data								% Conver.
			A 3455 cm^{-1}		B 1444 cm^{-1}		C 1080 cm^{-1}		D 792 cm^{-1}		
			Abs	Abs.N	Abs	Abs.N	Abs	Abs.N	Abs	Abs.N	
	Form 13 DPIHFP	0	0.05	0.08	0.59	1.00	0.32	0.55	0.76	1.29	0.0
		10	0.09	0.27	0.33	1.00	0.53	1.59	0.29	0.86	33.6
	Form 14 Irg 261	0	0.06	0.11	0.52	0.63	0.56	1.08	1.03	1.97	0.0
		10	0.14	0.23	0.60	1.00	1.06	1.77	0.81	1.36	31.0

Table 6.4-2 **Direct curing, IR spectral data and experimental data for direct curing of an epoxide, having 0.015 molkg^{-1} DPIHFP (resin formulation 13) and 0.015 molkg^{-1} Irgacure 261 (resin formulation 14)**

6.5 Effect of film thickness on remote cure

Figure 6.5-1   Remote curing in PTFE apparatus, IR spectra for remote curing of epoxide, 0.2g DPIHFP, resin formulation 4, film thickness = 16 µm +/ 2 µm

Expt Number [18]	Sample Thickness (µm)	Elapsed Time (mins)	Band Data								% Conver.
			A 3455 cm^{-1}		B 1444 cm^{-1}		C 1080 cm^{-1}		D 792 cm^{-1}		
			Abs	Abs.N	Abs	Abs.N	Abs	Abs.N	Abs	Abs.N	
1		0.0	0.26	0.24	1.09	1.00	0.54	0.49	1.06	0.97	0.0
2	17.5	2.5	0.05	0.25	0.19	1.00	0.13	0.66	0.18	0.96	0.3
3	14.2	3.8	0.09	0.47	0.20	1.00	0.15	0.76	0.18	0.90	7.2
4	16.8	5.0	0.25	0.46	0.55	1.00	0.86	1.54	0.34	0.61	36.9
5	17.4	7.5	0.14	0.43	0.33	1.00	0.53	1.61	0.20	0.60	38.3
6	16.6	10.0	0.09	0.60	0.15	1.00	0.22	1.47	0.06	0.41	57.9
7	15.1	20.0	0.14	0.71	0.19	1.00	0.29	1.55	0.05	0.29	70.1
8	15.6	30.0	0.47	0.83	0.57	1.00	1.14	2.00	0.06	0.10	89.2

Table 6.5-1   Remote curing in PTFE apparatus, IR spectral data and experimental data for remote curing of an epoxide, 0.2g DPIHFP, resin formulation 4, film thickness = 16 µm +/ 2 µm

Figure 6.5-2   **Remote curing in PTFE apparatus, IR spectra for remote curing of epoxide, 0.2g DPIHFP, resin formulation 4, film thickness = 4 μm +/ 1 μm**

Expt Number	Sample Thickness (μm)	Elapsed Time (mins)	Band Data								% Conver.
			A 3455 cm^{-1}		B 1444 cm^{-1}		C 1080 cm^{-1}		D 792 cm^{-1}		
[19]			Abs	Abs.N	Abs	Abs.N	Abs	Abs.N	Abs	Abs.N	
1		0.0	0.21	0.21	1.01	1.00	0.47	0.46	1.00	0.99	0.0
2	4.6	2.0	0.04	0.34	0.12	1.00	0.09	0.81	0.12	0.98	0.4
3	3.8	4.0	0.04	0.45	0.10	1.00	0.13	1.32	0.07	0.72	26.9
4	4.2	6.0	0.05	0.53	0.10	1.00	0.17	1.69	0.07	0.66	32.6
5	4.0	8.0	0.06	0.64	0.10	1.00	0.17	1.74	0.05	0.49	49.9
6	4.1	10.0	0.13	0.54	0.24	1.00	0.59	2.40	0.08	0.34	65.8

Table 6.5-2   **Remote curing in PTFE apparatus, IR spectral data and experimental data for remote curing of an epoxide, 0.2g DPIHFP, resin formulation 4, film thickness = 4 μm +/ 1 μm**

222
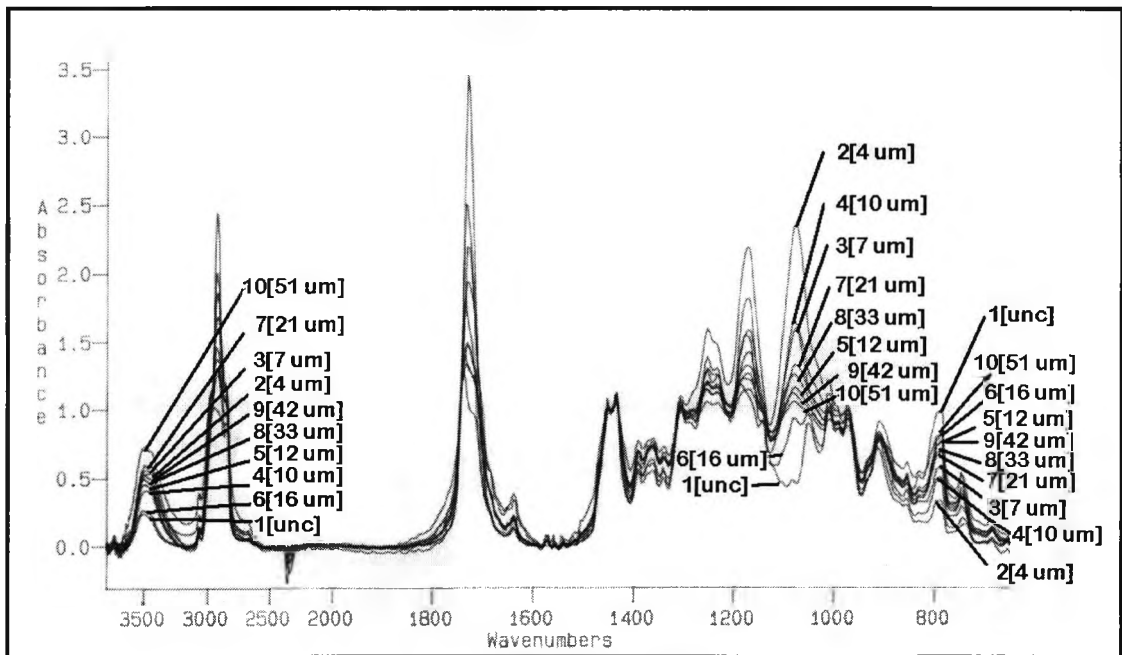
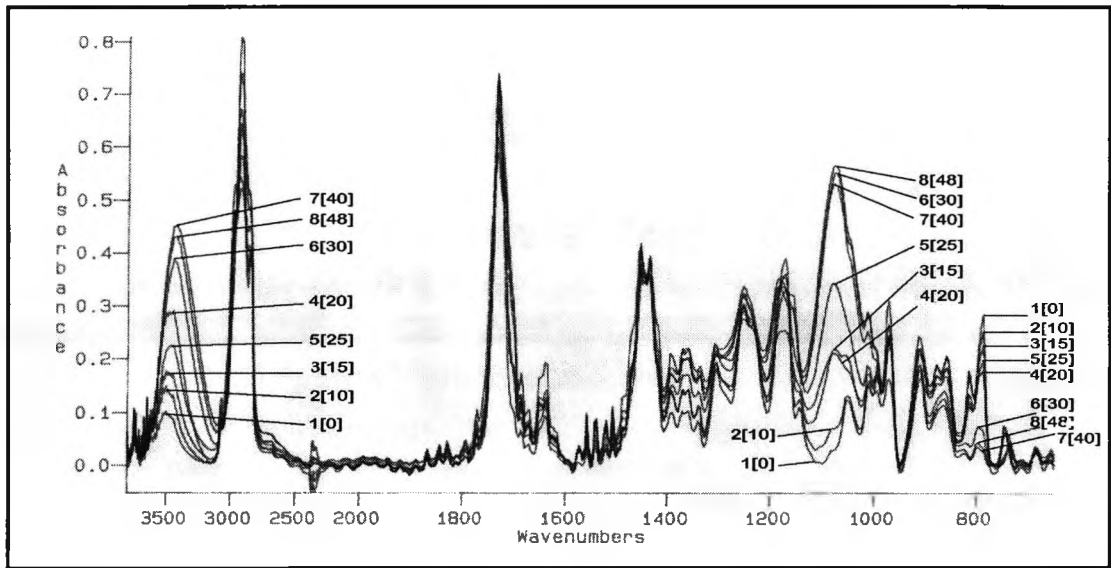**Figure 6.5-3**   Remote curing in PTFE apparatus, IR
spectra for remote curing of epoxide, 0.2g
DPIHFP, resin formulation 4, film thickness
= 4-51 μm and 10 mins. of UV exposure

Expt Number [15]	Sample Thickness (μm)	Elapsed Time (mins)	Band Data								% Conver.
			A 3455 cm^{-1}		B 1444 cm^{-1}		C 1080 cm^{-1}		D 792 cm^{-1}		
			Abs	Abs.N	Abs	Abs.N	Abs	Abs.N	Abs	Abs.N	
1		10	0.22	0.22	1.02	1.00	0.47	0.46	1.00	0.98	0.0
2	4.1	10	0.13	0.54	0.25	1.00	0.59	2.39	0.08	0.33	66.1
3	7.3	10	0.05	0.58	0.09	1.00	0.15	1.60	0.06	0.61	37.9
4	10.0	10	0.21	0.42	0.50	1.00	0.83	1.67	0.26	0.51	47.6
5	11.9	10	0.14	0.45	0.31	1.00	0.36	1.17	0.24	0.78	20.6
6	16.0	10	0.17	0.25	0.68	1.00	0.63	0.93	0.56	0.82	16.6
7	21.4	10	0.07	0.59	0.11	1.00	0.15	1.33	0.08	0.70	28.9
8	33.2	10	0.25	0.47	0.52	1.00	0.65	1.25	0.37	0.71	27.6
9	42.1	10	0.40	0.50	0.81	1.00	0.89	1.09	0.61	0.76	22.8
10	51.2	10	0.36	0.72	0.51	1.00	0.54	1.07	0.42	0.83	15.3

Table 6.5-3   Remote curing in PTFE apparatus, IR
spectral data and experimental data for
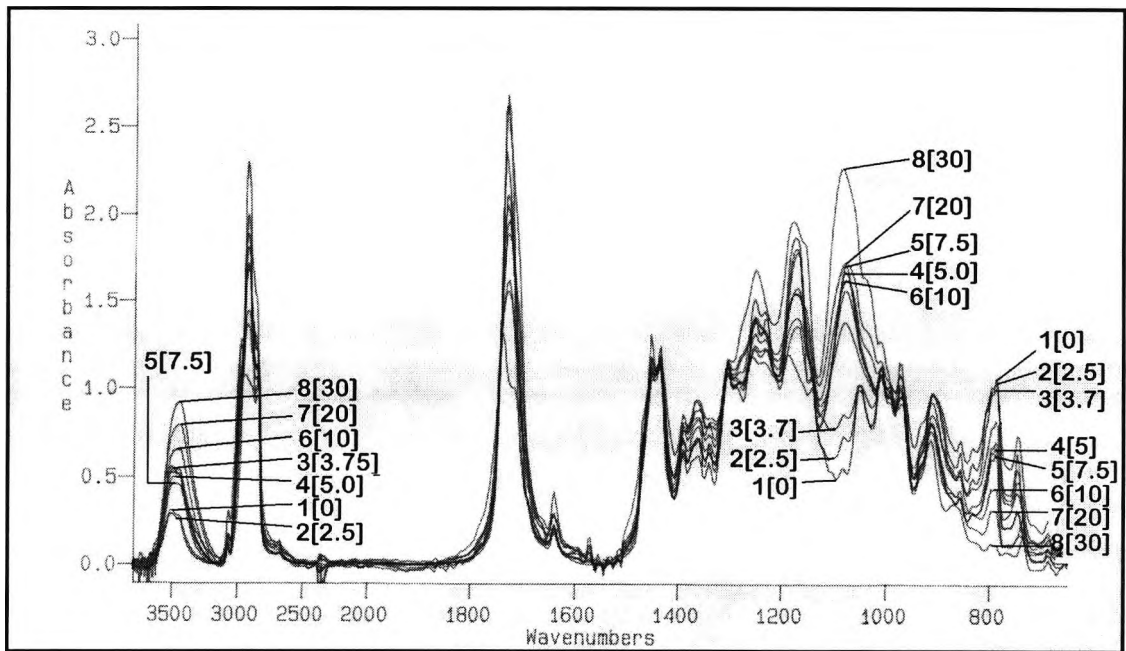remote curing of an epoxide, 0.2g DPIHFP,
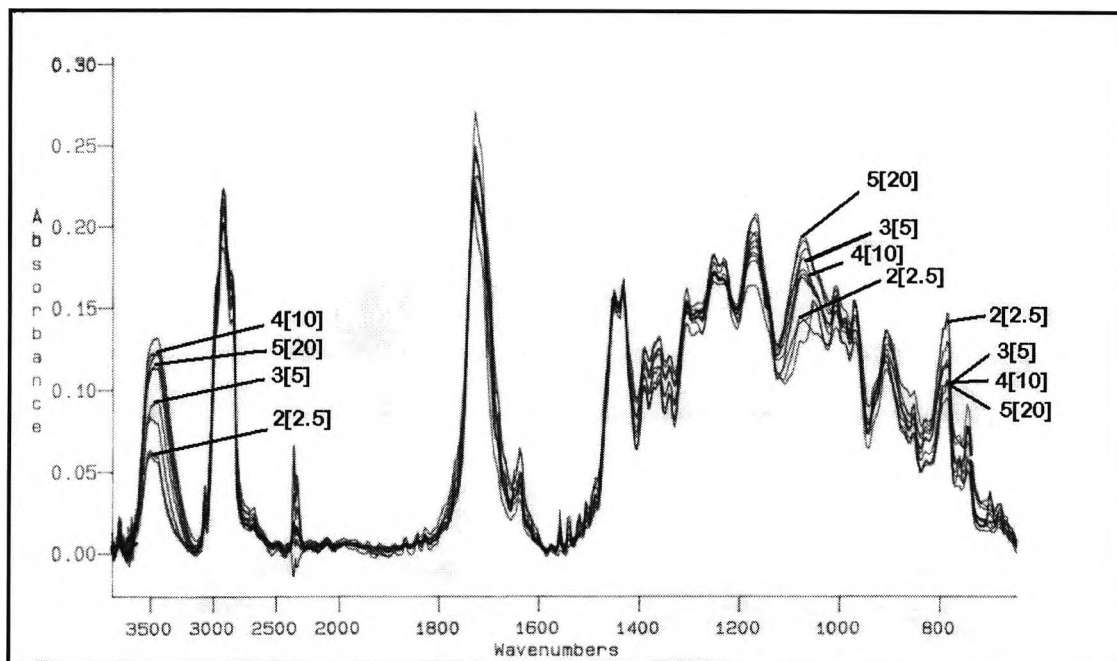resin formulation 4, film thickness = 4-51
μm and 10 mins. of UV exposure

223

6.6 Effect of film thickness on direct cure
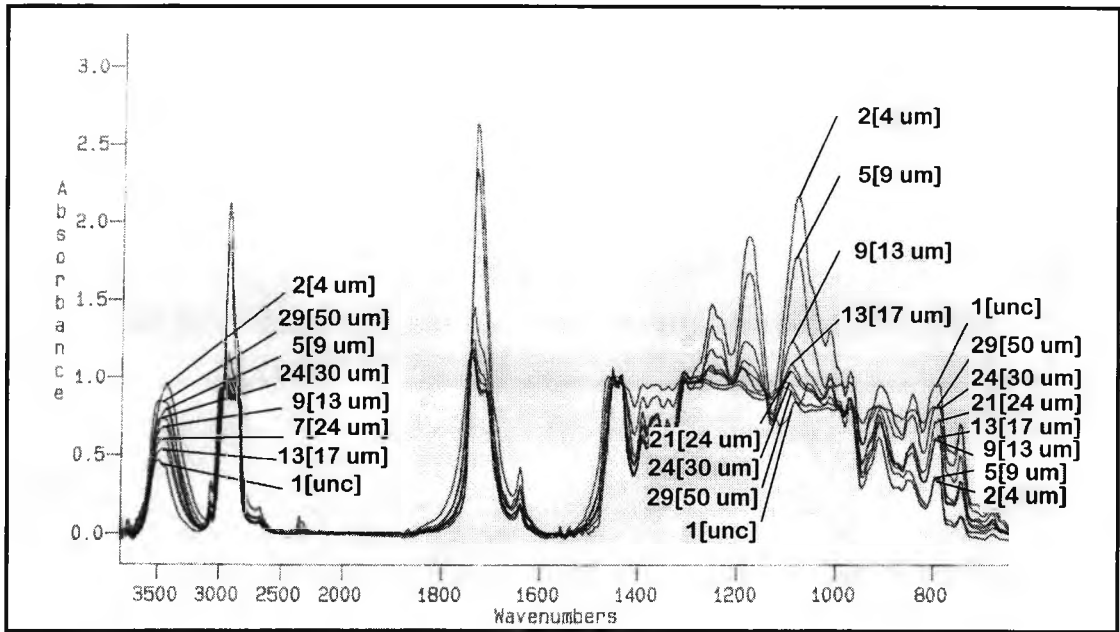
Figure 6.6-1   **direct curing, IR spectra for direct curing of epoxide, 2.1% w/w DPIHFP, resin formulation 3, film thickness = 4-50 μm and 1 min. of UV exposure**

Expt Number [16]	Sample Thickness (μm)	Elapsed Time (mins)	Band Data								% Conver.
			A 3455 cm^{-1}		B 1444 cm^{-1}		C 1080 cm^{-1}		D 792 cm^{-1}		
			Abs	Abs.N	Abs	Abs.N	Abs	Abs.N	Abs	Abs.N	
1		0	0.44	0.42	1.05	1.00	0.76	0.73	0.99	0.95	0.0
2	4.0	1	0.20	0.98	0.20	1.00	0.47	2.29	0.07	0.36	62.2
3	6.5	1	0.28	0.70	0.40	1.00	0.53	1.35	0.19	0.48	49.7
4	7.6	1	0.27	0.83	0.33	1.00	0.56	1.68	0.13	0.41	57.2
5	8.9	1	0.28	0.82	0.35	1.00	0.64	1.86	0.13	0.38	60.2
6	9.0	1	0.30	0.67	0.45	1.00	0.63	1.39	0.22	0.49	48.1
7	10.4	1	0.40	0.65	0.62	1.00	0.93	1.51	0.31	0.50	46.8
8	12.4	1	0.30	0.72	0.42	1.00	0.70	1.66	0.18	0.42	55.3
9	13.2	1	0.53	0.69	0.77	1.00	0.97	1.26	0.48	0.62	34.0
10	13.9	1	0.45	0.66	0.69	1.00	0.98	1.41	0.33	0.48	49.7
11	15.1	1	0.50	0.70	0.72	1.00	0.77	1.08	0.49	0.68	28.4
12	15.9	1	0.58	0.63	0.92	1.00	1.06	1.15	0.60	0.65	31.7
13	16.7	1	0.53	0.57	0.93	1.00	1.07	1.15	0.62	0.67	29.5
14	17.4	1	0.50	0.65	0.78	1.00	1.01	1.30	0.45	0.58	38.8
15	17.6	1	0.49	0.57	0.87	1.00	1.00	1.15	0.55	0.63	33.6
16	19.0	1	0.45	0.60	0.75	1.00	0.98	1.31	0.46	0.62	34.8
17	19.3	1	0.61	0.61	0.99	1.00	1.04	1.05	0.69	0.70	26.1
18	21.2	1	0.60	0.61	0.98	1.00	1.05	1.07	0.70	0.71	24.9
19	22.3	1	0.77	0.72	1.06	1.00	1.05	0.99	0.71	0.66	30.1
20	23.8	1	0.55	0.58	0.94	1.00	1.03	1.10	0.65	0.69	27.3
21	23.9	1	0.59	0.62	0.95	1.00	1.02	1.08	0.72	0.76	19.8
22	25.8	1	0.58	0.60	0.97	1.00	1.05	1.09	0.69	0.71	24.8
23	28.4	1	0.70	0.69	1.02	1.00	1.00	0.98	0.78	0.76	19.3
24	30.3	1	0.76	0.75	1.02	1.00	1.00	0.99	0.85	0.84	11.1
25	32.1	1	0.59	0.66	0.90	1.00	0.96	1.06	0.61	0.67	29.1
26	41.1	1	0.78	0.78	1.00	1.00	0.98	0.98	0.85	0.85	10.0
27	45.8	1	0.72	0.72	1.00	1.00	0.94	0.95	0.83	0.83	12.5
28	49.4	1	0.78	0.82	0.95	1.00	0.88	0.93	0.81	0.85	10.3
29	50.0	1	0.83	0.85	0.98	1.00	0.93	0.95	0.81	0.83	12.7

Table 6.6-1   **Direct, IR spectral data and experimental data for direct curing of an epoxide, 2.1% w/w DPIHFP, resin formulation 3, film thickness = 4-50 μm and 1 min. of UV exposure**

6.7 Effect of humidity on remote cure
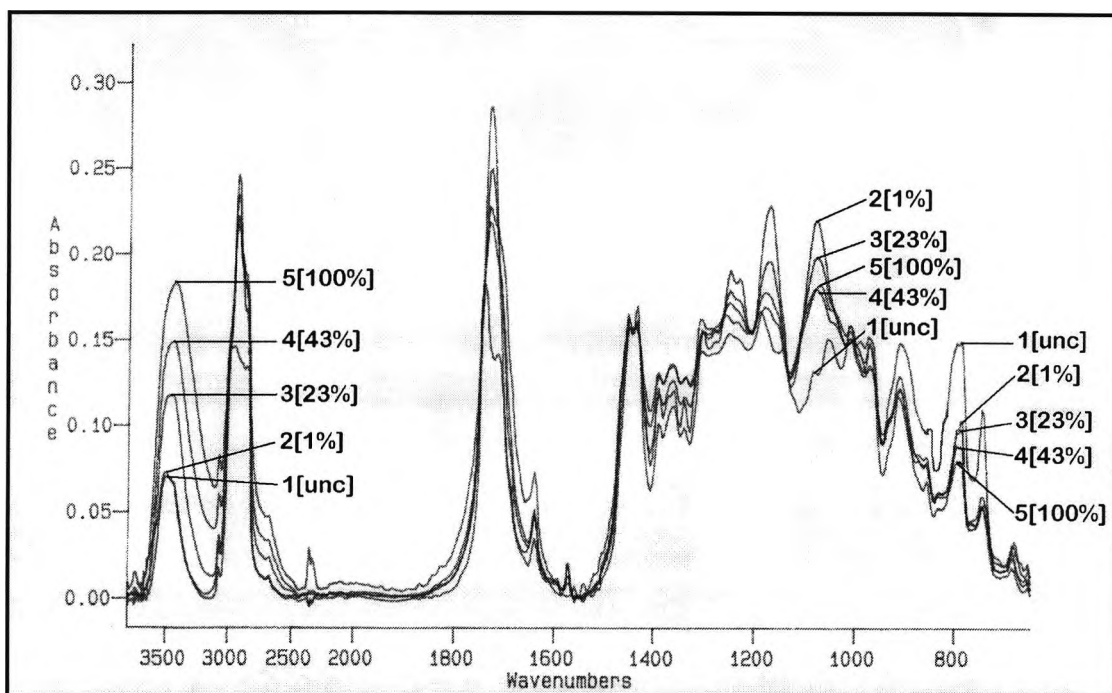
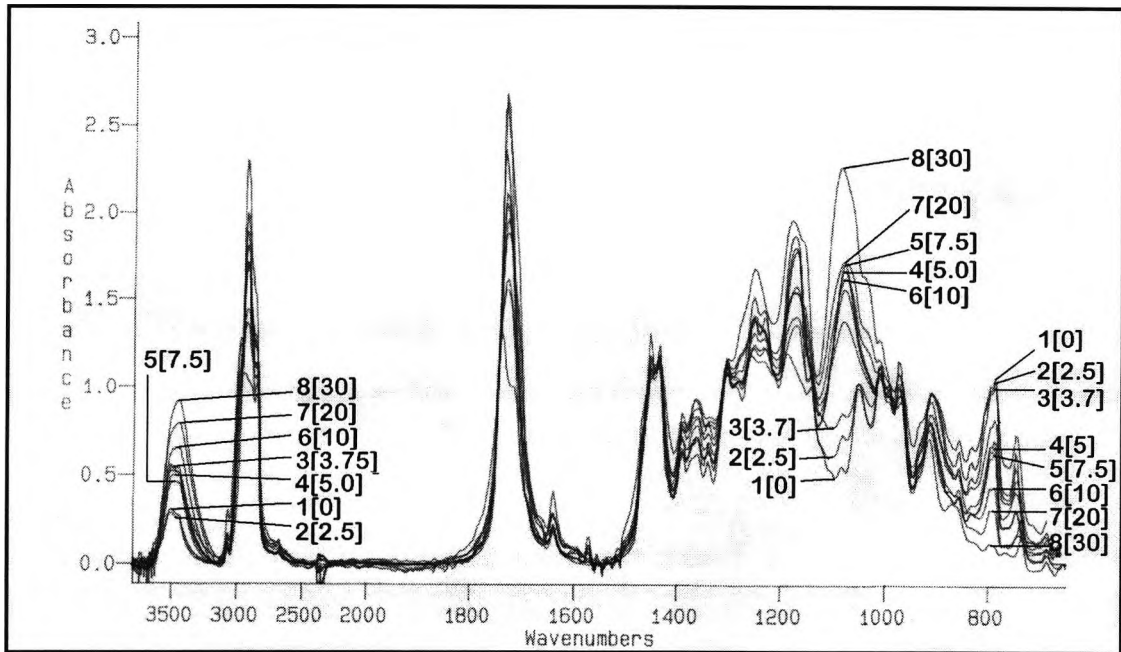**Figure 6.7-1**   Remote curing in PTFE apparatus, IR
spectra for remote curing of epoxide, 0.1g
DPIHFP, resin formulation 4, 1 0 mins. of UV
exposure and variation of humidity between
0 and 100%

Expt Number [14]	Sample Thickness (μm)	Humidity RH %	Elapsed Time (mins)	Band Data								% Conver.
				A 3455 cm⁻¹		B 1444 cm⁻¹		C 1080 cm⁻¹		D 792 cm⁻¹		
				Abs	Abs.N	Abs	Abs.N	Abs	Abs.N	Abs	Abs.N	
1			0	0.45	0.42	1.05	1.00	0.81	0.77	1.00	0.95	0.0
2	20	1.0	10	0.07	0.44	0.16	1.00	0.22	1.42	0.10	0.66	30.5
3	23	23.0	10	0.14	0.76	0.18	1.00	0.23	1.29	0.11	0.64	33.1
4	19	43.0	10	0.26	0.95	0.27	1.00	0.31	1.15	0.15	0.56	41.0
5	20	100.0	10	0.23	1.17	0.20	1.00	0.23	1.17	0.10	0.50	47.7

Table 6.7-1   Remote curing in PTFE apparatus, IR
spectral data and experimental data for
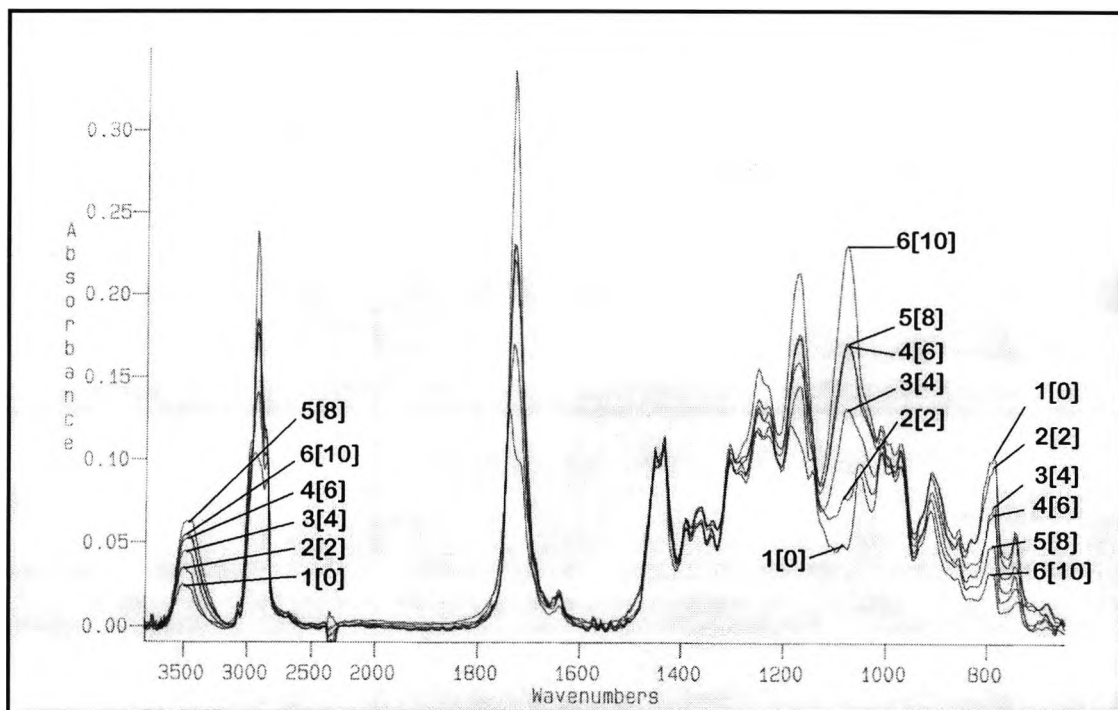remote curing of epoxide, 0.1g DPIHFP,
resin formulation 4, 1 0 mins. of UV
exposure and variation of humidity between
0 and 100%

6.8 Effect of bulk water on remote cure

Figure 6.8-1   **Remote curing in glass apparatus, IR spectra for remote curing of epoxide, 0.1g DPIHFP, resin formulation 1, 0-25 mins. of UV exposure and no added water**

Figure 6.8-2   **Remote curing in glass apparatus, IR spectra for remote curing of epoxide, 0.1g DPIHFP, resin formulation 5, 0-25 mins. of UV exposure and 2% w/w added bulk water**

227

Figure 6.8-3   **Remote curing in glass apparatus, IR spectra for remote curing of epoxide, 0.1g DPIHFP, resin formulation 6, 0-25 mins. of UV exposure and 3.3% w/w added bulk water**

Figure 6.8-4   **Remote curing in glass apparatus, IR spectra for remote curing of epoxide, 0.1g DPIHFP, resin formulation 7, 0-25 mins. of UV exposure and 5% w/w added bulk water**

Figure 6.8-5   **Remote curing in glass apparatus, IR spectra for remote curing of epoxide, 0.1g DPIHFP, resin formulation 8, 0-25 mins. of UV exposure and 10% w/w added bulk water**

229

Expt Number [1]	Sample Thickness (μm)	Water %	Elapsed Time (mins)	A 3455 cm⁻¹ Abs	A 3455 cm⁻¹ Abs.N	B 1444 cm⁻¹ Abs	B 1444 cm⁻¹ Abs.N	C 1080 cm⁻¹ Abs	C 1080 cm⁻¹ Abs.N	D 792 cm⁻¹ Abs	D 792 cm⁻¹ Abs.N	% Conver.
1	19.5	0.0	0	0.19	0.29	0.65	1.00	0.33	0.50	0.67	1.03	0.0
2	20.4	0.0	15	0.13	0.28	0.47	1.00	0.27	0.57	0.44	0.96	7.5
3	19.5	0.0	25	0.30	0.51	0.60	1.00	0.63	1.05	0.50	0.84	19.0
4	12.2	2.0	0	0.09	0.27	0.32	1.00	0.16	0.50	0.33	1.02	0.0
5	12.2	2.0	15	0.12	0.39	0.30	1.00	0.25	0.84	0.24	0.82	18.9
6	10.7	2.0	25	0.14	0.87	0.16	1.00	0.23	1.45	0.07	0.42	58.3
7	16.4	3.3	0	0.12	0.25	0.48	1.00	0.22	0.45	0.52	1.06	0.0
8	19.1	3.3	15	0.17	0.58	0.30	1.00	0.41	1.39	0.19	0.64	40.2
9	16.4	3.3	25	0.33	0.74	0.44	1.00	0.60	1.37	0.18	0.42	60.9
10	15.5	5.1	0	0.09	0.25	0.37	1.00	0.16	0.43	0.37	1.00	0.0
11	15.5	5.1	15	0.21	0.55	0.38	1.00	0.46	1.24	0.25	0.66	34.3
12	22.0	5.1	25	0.35	0.86	0.41	1.00	0.61	1.49	0.10	0.24	76.4
13	17.7	10.0	0	0.19	0.38	0.50	1.00	0.29	0.57	0.51	1.02	0.0
14	19.5	10.0	15	0.34	0.53	0.64	1.00	0.58	0.91	0.55	0.85	16.6
15	11.7	10.0	25	0.34	1.05	0.33	1.00	0.50	1.53	0.05	0.17	83.6

Table 6.8-1   **Remote curing in glass apparatus, IR spectral data and experimental data for remote curing of epoxide, 0.1g DPIHFP, resin formulation 1&5-8, 0-25 mins. of UV exposure and variation of added bulk water between 0-10% w/w**

230

6.9   Effect of bulk water on direct cure
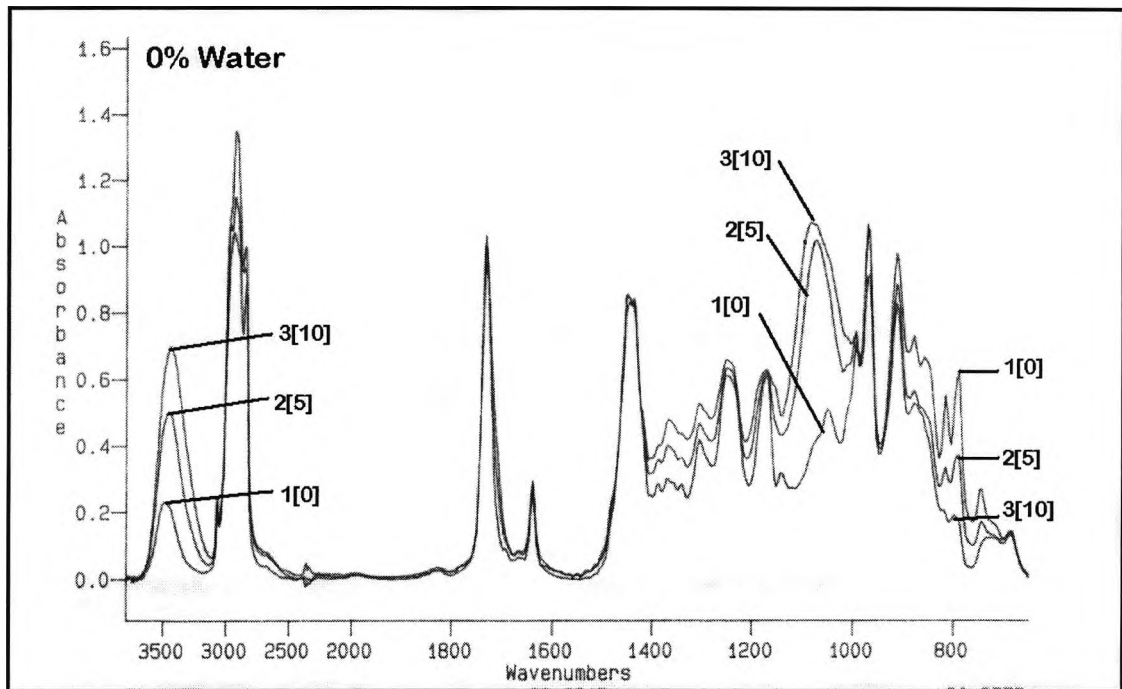
Figure 6.9-1   **Direct curing, IR spectra for direct curing of epoxide, 1.5% w/w DPIHFP, resin formulation 2, 0-10 mins. of UV exposure and no added bulk water**
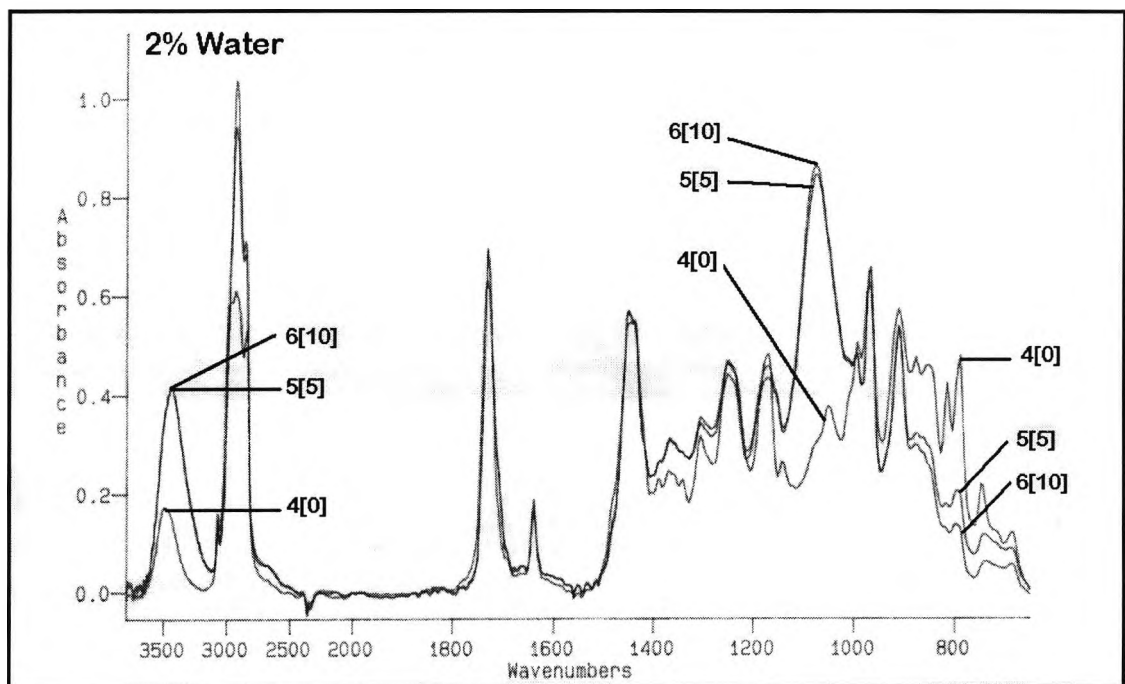
Figure 6.9-2   **Direct curing, IR spectra for direct curing of epoxide, 1.5% w/w DPIHFP, resin formulation 9, 0-10 mins. of UV exposure and 2% w/w added bulk water**

231
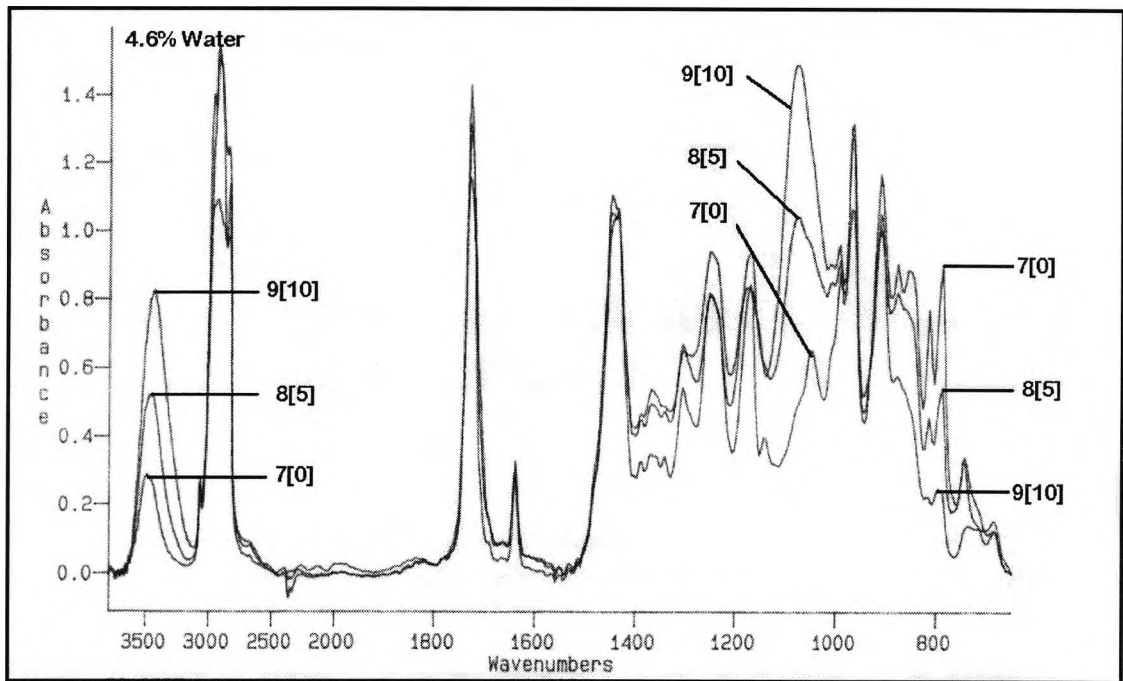
Figure 6.9-3   **Direct curing, IR spectra for direct curing of epoxide, 1.5% w/w DPIHFP, resin formulation 10, 0-10 mins. of UV exposure and 4.6% w/w added bulk water**
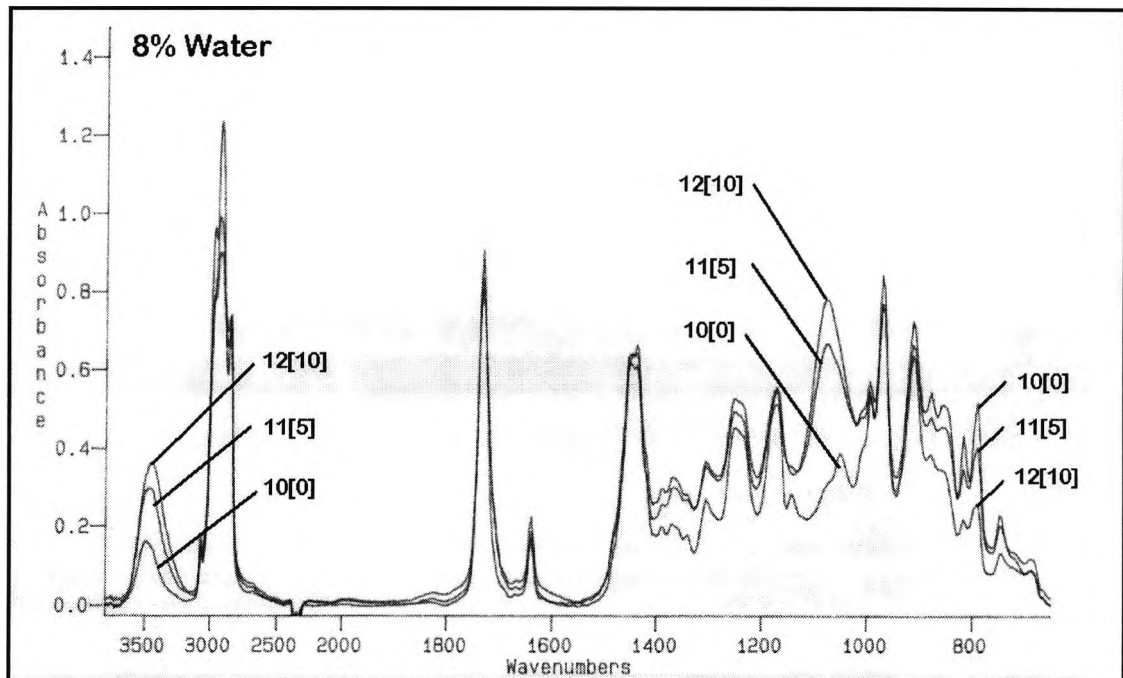
Figure 6.9-4   **Direct curing, IR spectra for direct curing of epoxide, 1.5% w/w DPIHFP, resin formulation 11, 0-10 mins. of UV exposure and 8% w/w added bulk water**

Expt Number [12]	Sample Thickness (μm)	Water %	Elapsed Time (mins)	Band Data A 3455 cm^{-1} Abs	Abs.N	B 1444 cm^{-1} Abs	Abs.N	C 1080 cm^{-1} Abs	Abs.N	D 792 cm^{-1} Abs	Abs.N	% Conver.
11-1		0.0	0	0.19	0.27	0.71	1.00	0.35	0.49	0.54	0.75	0.0
11-2	23.2	0.0	5	0.34	0.59	0.58	1.00	0.71	1.21	0.26	0.44	42.2
11-3	22.7	0.0	10	0.68	0.81	0.83	1.00	1.07	1.28	0.18	0.21	71.5
11-4		2.0	0	0.27	0.33	0.83	1.00	0.46	0.56	0.72	0.87	0.0
11-5	18.0	2.0	5	0.28	0.75	0.37	1.00	0.57	1.51	0.14	0.37	57.3
11-6	16.8	2.0	10	0.42	0.76	0.55	1.00	0.86	1.56	0.13	0.24	72.8
11-7		4.6	0	0.18	0.27	0.69	1.00	0.32	0.47	0.59	0.86	0.0
11-8	19.7	4.6	5	0.52	0.50	1.04	1.00	1.04	1.00	0.54	0.52	39.6
11-9	18.9	4.6	10	0.54	0.75	0.72	1.00	0.99	1.38	0.17	0.23	73.0
11-10		8.0	0	0.10	0.25	0.42	1.00	0.20	0.49	0.34	0.82	0.0
11-11	19.8	8.0	5	0.26	0.46	0.57	1.00	0.60	1.05	0.36	0.63	23.4
11-12	23.8	8.0	10	0.36	0.59	0.61	1.00	0.78	1.28	0.25	0.42	49.1

Table 6.9-1   **Direct curing, IR spectral data and experimental data for direct curing of epoxide, 1.5% w/w DPIHFP, resin formulation 2&9-11, 0-10 mins. of UV exposure and variation of added bulk water between 0-8% w/w**
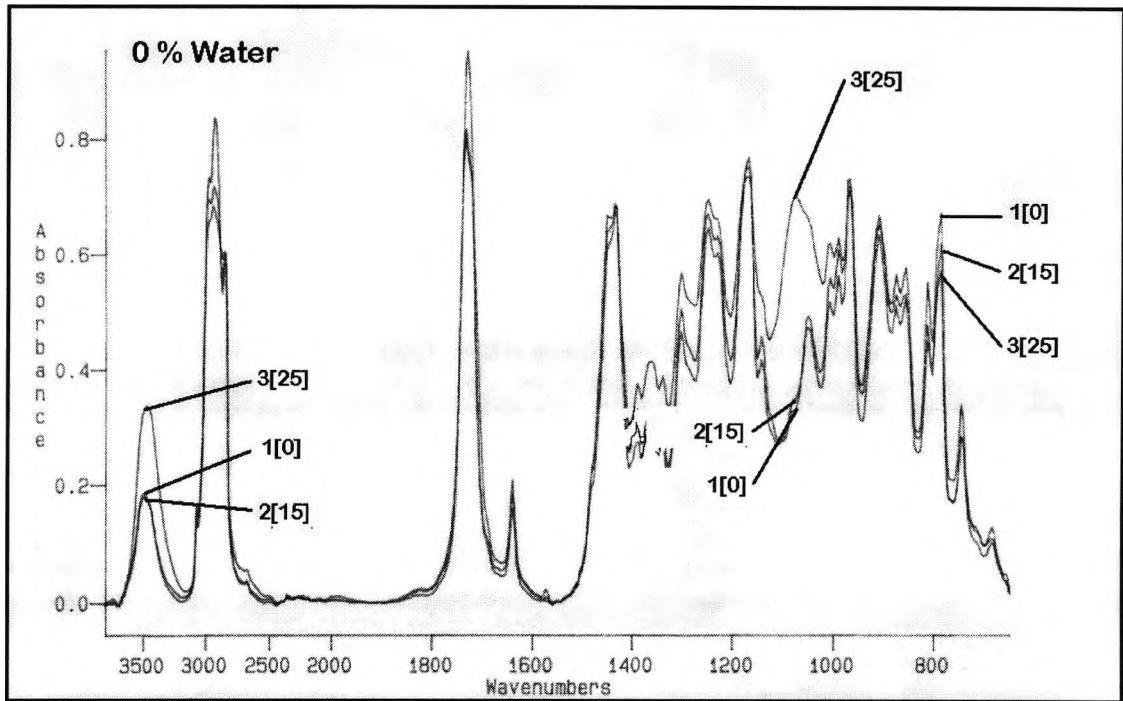
6.10 Effect of initiator quantity on remote cure
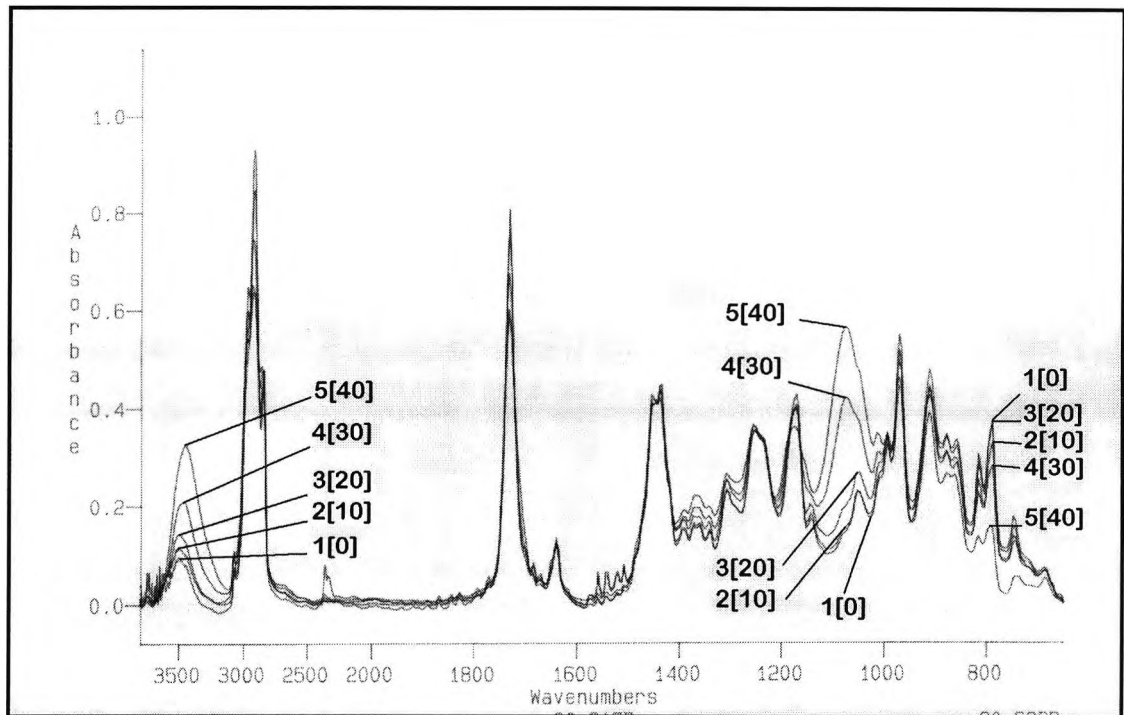
Figure 6.10-1   **Remote curing in glass apparatus, IR spectra for remote curing of epoxide, 0.2g DPIHFP, resin formulation 1**
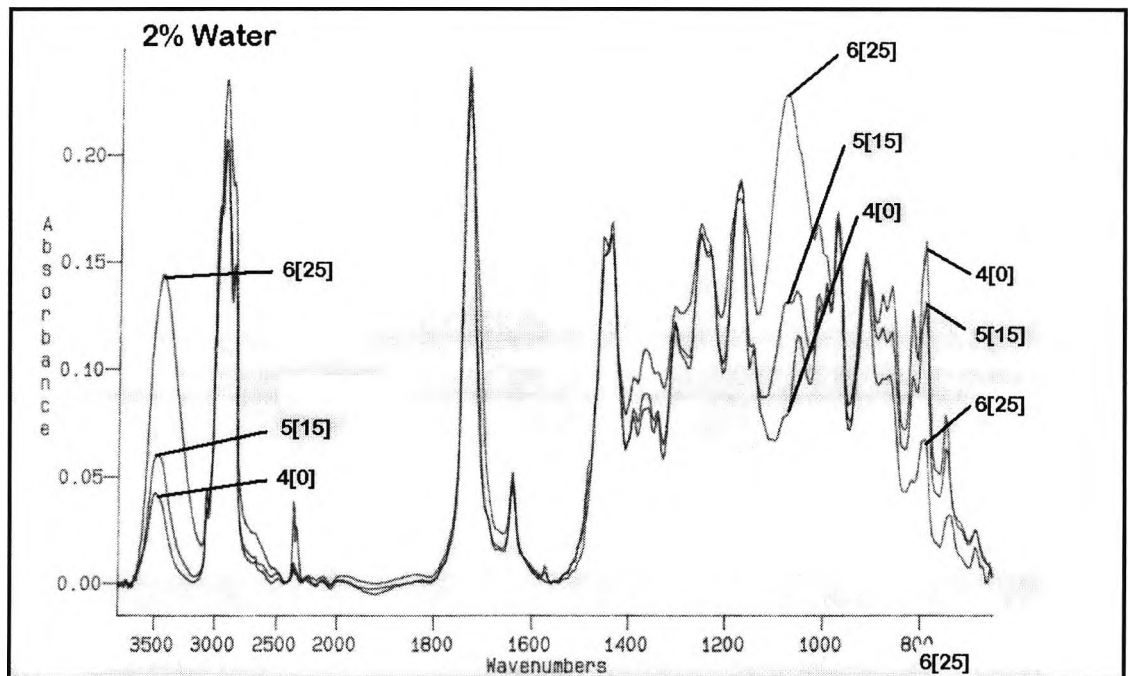

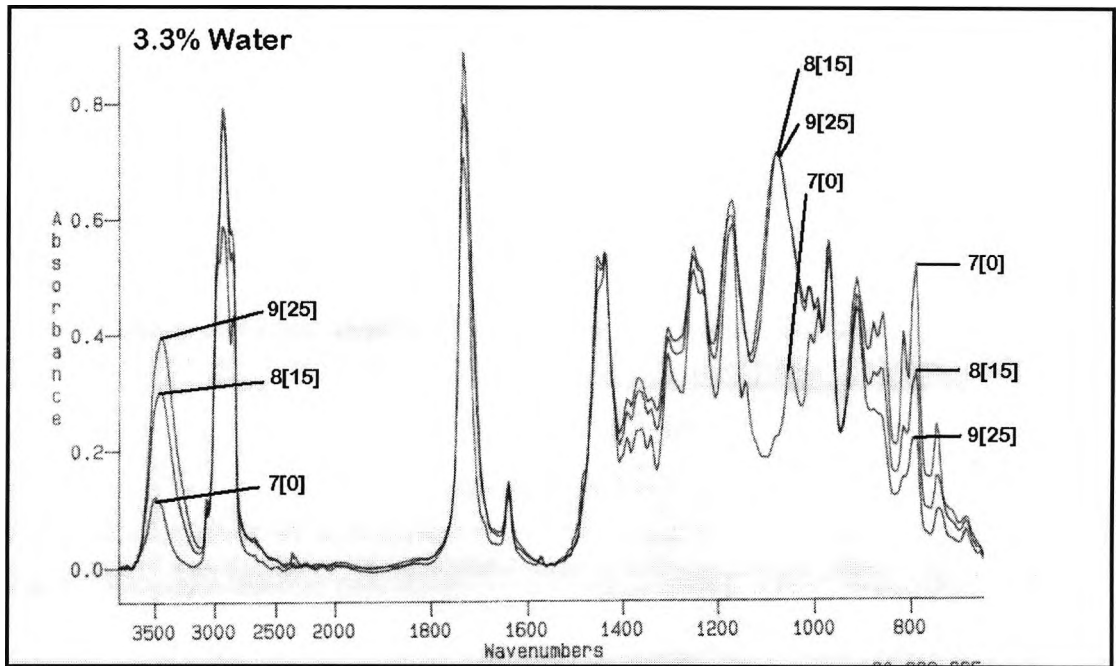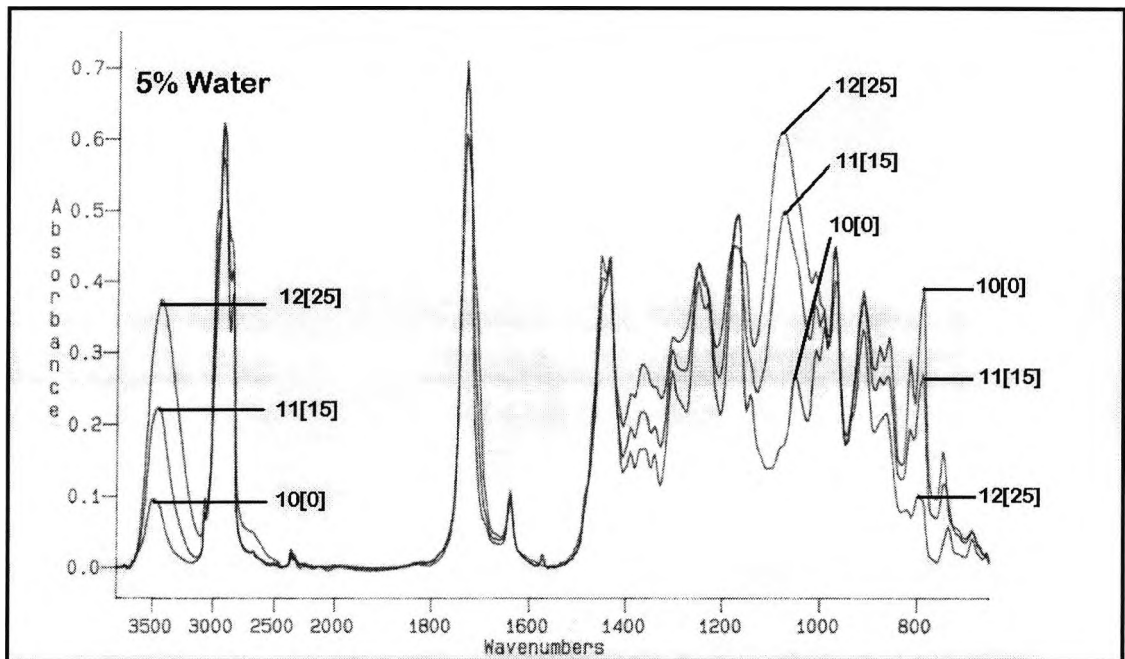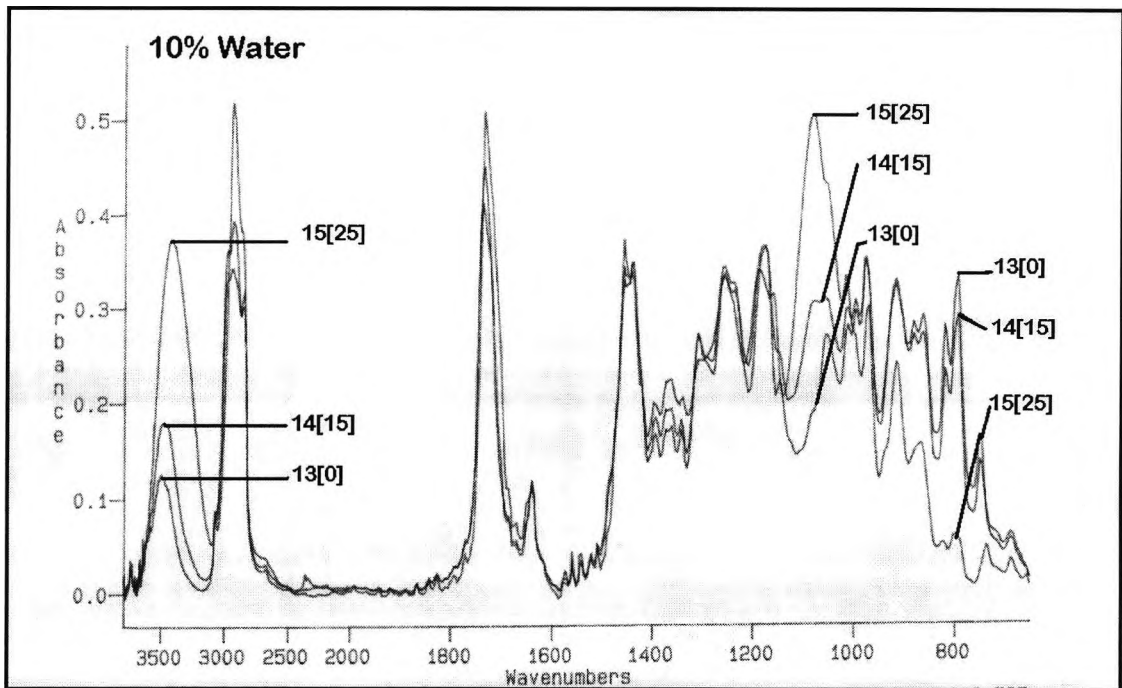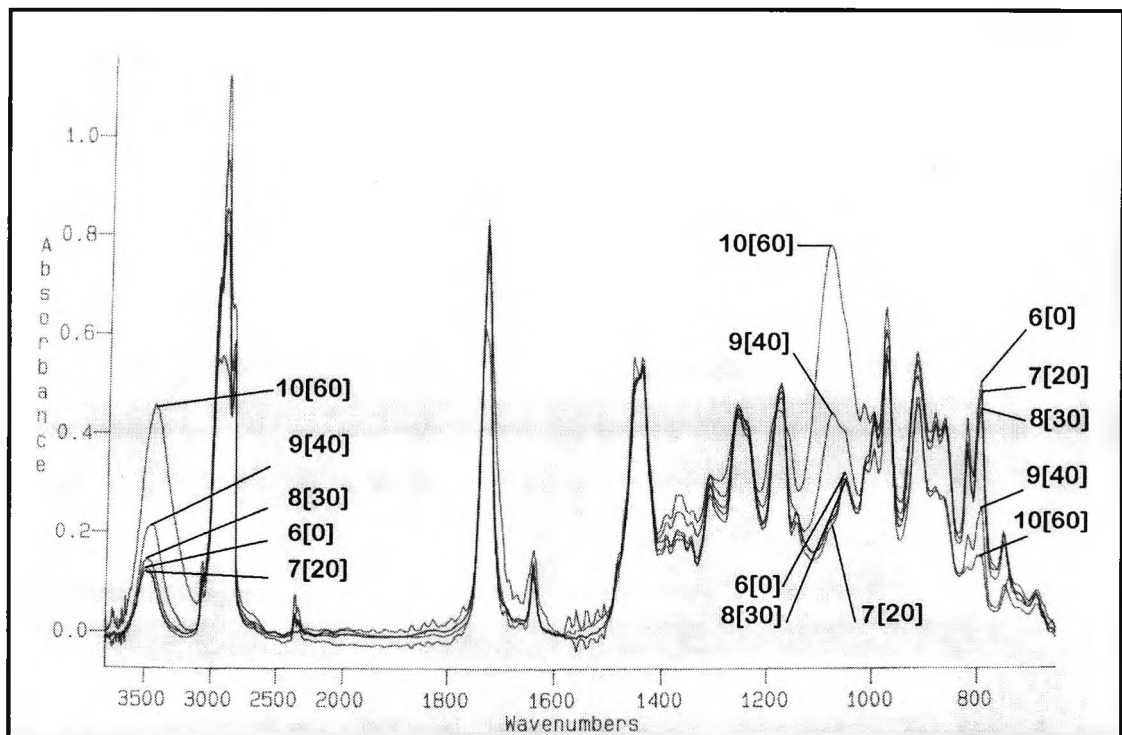**Figure 6.10-2**   **Remote curing in glass apparatus, IR spectra for remote curing of epoxide, 0.1g DPIHFP, resin formulation 1**

Expt Number [9]	Sample Thickness (μm)	Elapsed Time (mins)	A 3455 cm^{-1} Abs	Abs.N	B 1444 cm^{-1} Abs	Abs.N	C 1080 cm^{-1} Abs	Abs.N	D 792 cm^{-1} Abs	Abs.N	% Conver.
0.2g DPIHFP											
1	13.5	0	0.05	0.21	0.24	1.00	0.09	0.37	0.22	0.89	0.0
2	14.1	10	0.07	0.25	0.28	1.00	0.11	0.38	0.22	0.79	11.1
3	15.7	20	0.13	0.33	0.41	1.00	0.20	0.49	0.37	0.89	0.6
4	13.4	30	0.24	0.49	0.50	1.00	0.50	1.01	0.33	0.66	25.6
5	17.6	40	0.44	0.78	0.57	1.00	0.78	1.38	0.21	0.37	58.5
5a	14.6	60			0.55	1.00			0.08	0.15	83.7
0.1g DPIHFP											
6		0	0.24	0.25	0.97	1.00	0.44	0.45	0.96	0.98	0.0
7	24.3	20	0.13	0.23	0.56	1.00	0.23	0.42	0.52	0.94	4.3
8	13.9	30	0.15	0.30	0.52	1.00	0.24	0.46	0.46	0.88	10.2
9	18.3	40	0.11	0.42	0.25	1.00	0.21	0.85	0.12	0.50	49.4
10		60	0.44	0.85	0.52	1.00	0.78	1.51	0.15	0.29	70.8

Table 6.10-1 **Remote curing in glass apparatus, IR spectral data and experimental data for remote curing of epoxide with 0.1g and 0.2g DPIHFP, resin formulation 1**

7 SUMMARY AND CONCLUSION

Prior to this study, which began in 1989, the only published work concerning the photolysis of diphenyliodonium and triphenylsulphonium salts in the solid state, was that of Wilkinson [63]. All earlier investigations addressing the photodecomposition of diphenyliodonium and triphenylsulphonium salts were carried out in dilute organic media. These investigations had provided a series of findings, which were supplemented and coordinated by Hacker and co-workers between 1987-1991 to produce a comprehensive and coherent theory [34,35,37,56,57].

Nevertheless, all the early work, and indeed the Hacker theory, has presumed the anion to remain intact and the acid, HXF_6, to be the ultimate polymerising species.

During the period 1989-1991 Hacker had also undertaken investigations on photodecomposition in viscous media and in the solid state [55,58]. This type of study was increasingly being viewed as more informative, with regard to industrial coating processes, than the previous work which was scientifically elegant but yielding results which were questionably representative.

Hacker's approach enabled the clarification of elusive aspects of cation decomposition, indicating the importance of the cage recombination processes for acid generation. This was an important achievement, as the source of the proton from diphenyliodonium/triphenylsulphonium decomposition had not been satisfactorily identified.

Meanwhile, Wilkinson was focusing on the fate of the anion. Indirect evidence was obtained from solid-state photodecomposition studies for the decomposition of the anion to XF_5 and HF. This finding was of considerable academic interest, as little data had existed in this area.

However, Wilkinson was also able to show that the gases evolved from solid state photodecomposition of diphenyliodonium and triphenylsulphonium salts were capable of polymerising an epoxide film in proximity to, but not in contact with, the initiator being irradiated. This observation led Wilkinson to propose that the ultimate initiator of polymerisation may, in fact, be HF.

Regardless of the exact nature of the polymerising species, the discovery of gas-mediated polymerisation has implications which, in addition to being of academic interest, also have industrial significance. The possibility thereafter exists for the cationic polymerisation of an epoxide, by photochemical means, producing a product free of organic photodecomposition contaminants. Furthermore, since the polymerisation is completely light independent, the process should be unaffected by the presence of all pigments and/or photo labile (perhaps fluorescent) dyes. The latter can be problematic applications in UV curing.

These possibilities gave rise to the present study. The objectives of this work have been to verify and characterise the decomposition of the anion, investigating more thoroughly the solid-state photodecomposition. If the Wilkinson data is to have any industrial relevance, the polymerisation must be studied in a quantitative manner, and compared to polymerisation with 'in-situ' initiators. This was also an objective.

The solid-state photodecomposition of the diphenyliodonium hexafluorophosphate salt was carried out in PTFE apparatus and gaseous products were subjected to FTIR spectroscopy. Direct evidence was obtained for the presence of HF as one of the photodecomposition products, in the form of IR bands matching those quoted in the literature. The spectrum was scrutinized very closely for evidence of phosphorus pentafluoride but the existence of this species could not be confirmed. When exhausted into water, fluoride ions were rapidly detected using a fluoride specific electrode and the latter was used to follow the decomposition process in real time, i.e. fluoride appearance as a function of irradiation time. Both the phosphate and arsenate salts produced around 2 moles of fluoride ions for every mole of photoinitiator irradiated. The antimonate salt, by contrast, produced less than 1 mole of fluoride for every mole of photoinitiator irradiated.

The development of these fluoride ions is attributed firstly to the dissolution of HF, which is liberated following reorganization of the salt at the point of irradiation. The proton is proposed to originate via rearrangement and in-cage recombination of cation fragments as proposed separately by Pappas [11,27,46,50,51] and Hacker [34,35,37,56,57] . The iodobiphenyl product was detected in the residual solid-state initiator residue following irradiation, by mass spectrometry. Additional equivalents of fluoride are released secondarily from the hydrolysis of the group V pentahalide yielding multiple equivalents with successive hydrolysis steps. As expected, the antimonate salt yields only fluoride from the dissolution of HF as the antimony pentahalide is a polymeric liquid under experimental conditions and so will not be a gaseous product available for dissolution and hydrolysis. The possibility that the additional quantities of fluoride ion from the phosphate and arsenate salts are arising, in each case, from a second molecule of HF generated by

in-situ reorganisation of the pentahalide in the initiator bulk, may be discounted. This would require multiple protons to be generated per photoinitiator molecule from each in-cage recombination reaction. Since this is not a sustainable proposition, the in-situ initiator decomposition and reorganisation is restricted to the immediate generation of HF and pentahalide. The lack of pentahalide in the IR spectrum may be explained by the weak bands expected for this material and the strong tendency to hydrolysis. IR detection of the pentahalide is therefore quite unlikely under the experimental conditions of this study.

In the context of polymerisation, secondary generation of fluoride by pentahalide hydrolysis may be regarded as an experimental artefact. The primary interest should remain with the aspects of the data that are revealing with regard to the initial anion rearrangement to give HF and pentahalide.

Interestingly, the maximum rate of fluoride ion generation occurs within 3 minutes of the beginning of irradiation and the arsenate generates fluoride ions at almost twice the rate of the phosphate salt. Both penta fluorides are known to undergo very rapid hydrolysis in water and it is not possible to determine unambiguously whether the difference in rates of fluoride ion generation arises from a difference in rates of decomposition of the anions, or rather from differences in rates of hydrolysis of the respective pentahalides.

The 2 processes may be assumed to be concomitant. Since the rate of evolution as a function of moles of fluoride ions generated follows a similar profile for <u>all 3 salts</u>, it can be proposed that the rates are indicative of the order of anion stability being as follows:

Anion Stability: $\quad$ PF_6^- $\quad$ > $\quad$ AsF_6^- $\quad$ (> $\quad$ SbF_6^-)
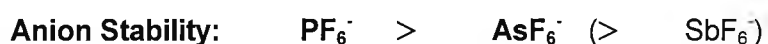
$$\text{no pentahalide - HF only}$$

This order is consistent with the order of polymerising efficiency known for the series of salts in classical polymerisation experiments. It seems likely, therefore, that the order of polymerising efficiency is in fact due as much to the instability of the anion as to the relative nucleophilicity of the latter, and that the initiating species is either the pentahalide or HF.

No experiments were carried out to determine which of these candidates is responsible. The fact that polymerisation with the pentahalide Lewis acid is widely known while polymerisation with HF and other acids bearing nucleophilic counterions has always been found to be limited, supports the candidature of the pentahalide. Wilkinson's '3 phase'

polymerisation experiments with the antimonate salt, indicate only marginal epoxide consumption where the sole acid is HF.

It is therefore proposed that under most practical circumstances the anion decomposes to yield the pentahalide, which in the presence of adventitious water in the film forms the hydroxypentahalide Brønsted acid. This is the ultimate initiator of polymerisation. Polymerisation may at the same time proceed with an intact counterion as the two processes need not be exclusive.

Experiments to determine the effect of cation selection also indicated a very strong effect. The diphenyliodonium, triphenylsulphonium and iron arene salts were compared. Overall fluoride ion yields are higher with the diphenyliodonium salts, which is consistent with the work of Crivello [13-15]. This effect is likely to be attributable to differences in light absorbing properties arising from variation in crystalline structure. Certainly the triphenylsulphonium and diphenyliodonium salts have very similar UV absorption spectra in solution. However, initial rates are higher with triphenylsulphonium salts. This may be explained by the work of Pappas [46] who showed that the solvent used for the triphenylsulphonium salt, methanol, is a nucleophile, which accelerates the decomposition of the salt. The iron arene complex, Irgacure 261, is notably inferior to the onium salts in rate and yield. This is consistent with industry findings.

The solid-state decomposition of the anion may be photo-redox sensitised as experiments have shown that the rate of onium salt decomposition is increased by almost 50% when irradiation is carried out with 14% of Irgacure 651 co-crystallised. The increased rate of cation decomposition has the obvious effect on anion decomposition and fluoride ion generation.

The rate of anion decomposition is also profoundly affected by the surface density of the solid-state photoinitiator. At a surface density of $380 gm^{-2}$ the maximum rate is 3.1×10^{-7} $mols^{-1}$. This value is halved when the surface density is doubled. Since the anion is of course the same in each case, this must arise from the rate of salt decomposition, and the rate of escape of HF and PF_5 into the gas phase. This information has certain value to industry, as photoinitiators are expensive and this finding pushes potential processing costs in the direction of economy.

A second factor tending towards process economy in an industrial situation is the selection of initiator substrate. The effect of substrate selection on anion decomposition rate was investigated, and the most rapid evolution was obtained from cellulose-type paper. This material probably provides an additional source of protons, accelerating the decomposition of the salt.

Decomposition experiments were also carried out in the presence of epoxide and vinyl ether monomers. Both were found to polymerise readily. The progress of the reaction was followed by FTIR, quantifying both the disappearance of the epoxide group and the development of ether linkages which are the consequence of chain extension.

A direct comparison of reaction rates between the remote or indirect polymerisation and the classical or direct polymerisation is not straightforward as it is not possible to quantify the concentration of photo-generated polymerising species in the same manner in each case.

Direct polymerisation with 1.5%w/w of DPIHFP came to completion (75% epoxide conversion) after about 10 minutes of continuous UV exposure. By contrast, 20 minutes of UV exposure was required in a remote experiment using 0.1g of the same initiator in the solid state ($800gm^{-2}$) to polymerise a film of thickness $15\mu m$. Doubling the photoinitiator quantity in the latter case was found to reduce the necessary exposure time by $1/3^{rd}$. However, the direct exposure method remains appreciably faster at the same light intensity. Based on earlier experiments measuring fluoride ion generation, it now seems obvious that the most effective approach towards a reduction of cure time would be to simultaneously increase the amount of solid state photoinitiator exposed to light while also reducing the surface density thereof; e.g. 0.2g at $400gm^{-2}$, rather than 0.1g at $800gm^{-2}$.

The rate of remote polymerisation was found to be reduced in glass apparatus, probably due to the unwanted consumption of HF and PF_5 on the walls of the vessel. Etching of the glass was noted. In the PTFE vessel, the polymerisation rate was unaffected by variation in initiator/monomer film gap width (in the range 5-15mm). The impact of this variable is probably diminished, under laboratory conditions, by the small, limiting volume of the vessel in which the experiments were carried out.

Polymerisation experiments were also carried out comprising separate light and dark stages. In the 'light stage' the solid-state photoinitiator is irradiated in the absence of the epoxide monomer. In a second 'dark stage' the epoxide is exposed, in the combined volume of the 2 cells, to the gases generated in the light stage. Polymerisation was shown to be incomplete (30% epoxide conversion) and was shown to require 5-10 minutes to occur.

All the experiments thus far described indicate that the degree of polymerisation obtainable is crucially dependent on the concentration of active gaseous species. The entire process is dependent on the rates of several processes:

- rate of onium salt decomposition

- rate of anion rearrangement

- rate of diffusion of active species into monomer/polymer film

- rate of epoxide polymerisation in the presence of active species

The importance in remote curing of diffusion rate and concentration of active species in the monomer/polymer matrix is underlined by the effect of film thickness on the degree of polymerisation. The remote process is strongly affected by film thickness. A maximum thickness constraint of 10-15μm must be imposed on any attempt to use the remote process for practical purposes.

There is no spectral evidence to show that the mechanism of polymerisation in remote cure is different from that in direct cure. Fluorinated hydrocarbons were not detected in either case, and both processes proceed with the development of hydroxyl functionalities. This information seems to point, once again, to polymerisation via a common mechanism involving the same Brønsted active species - probably the hydroxylated Lewis acid, $OHXF_5^-/H^+$.

From a mechanistic point of view, the finding that the iron arene complex, Irgacure 261, is able to bring about remote polymerisation (admittedly more slowly than the onium salts) is interesting. The commonly recited polymerisation mechanism for these salts requires the participation of epoxide in the decomposition of the initiator. Clearly no such epoxide is available in the present work, and polymerisation is achieved indirectly. This may suggest that even in direct or classical polymerisation, coordination of the epoxide into the ligand shell of the iron may not, in fact, be an essential part of the process. Certainly there are many questions as yet unanswered with regard to the mode of activity of these salts.

In general, the remote process is just as adversely affected by the presence of atmospheric water (humidity) as classical or direct polymerisation. This phenomenon is widely appreciated, but not understood, in the industry. It is proposed that water diffuses into the film in a non-associated manner and competes successfully with the larger, sterically hindered monomer to attack the activated complex with chain termination being the result. Deactivation will be favoured over chain extension as the viscosity and/or

relative humidity increases. Increasing the temperature of the film causes viscosity reduction and reduces the steric or mobility disadvantage of the incoming monomer. This increases the probability of chain extension. The ease of attack by water is relatively little affected by changes in viscosity.

By contrast, experiments have shown that direct polymerisation is relatively little affected by the presence of bulk water. It is proposed that bulk water, having a strong tendency towards association, will form a micro-emulsion. Water thus trapped in a discrete and separate phase interacts only minimally with the polymerising epoxide film and up to 5% w/w in the film, polymerisation is unaffected. Examination of all relevant bands in the IR spectra confirms that chain extension does indeed follow ring opening in such cases.

The remote polymerisation process is even more tolerant of bulk water and may even be assisted by it. Polymerisation was found to be accelerated by bulk water at up to 5% w/w and further tolerated at up to 10% w/w. It is proposed that diffusion of readily hydrolysable gaseous species such as XF_5 and HF occurs more rapidly from the atmosphere into water micelles than into the organic phase of the film. Within the micelles, the previously described hydrolysis step occurs:

$$XF_5 \quad + \quad H_2O \quad \rightarrow \quad H^+ \quad + \quad XF_5OH^-$$

The micelles serve as reservoirs of active species, which initiate epoxide polymerisation at the phase boundary where the epoxide functionality is at abundance.

This finding is advantageous for practical applications of remote cure as the rate of polymerisation can thus be accelerated by addition of cost-free formulating material (water).

Formulating flexibility can also be extended by the addition of free-radically polymeriseable monomers such as TMPTA and HDDA. In line with other published work, these monomers can be polymerised in conjunction with epoxide monomers to yield formulations which resist both oxygen inhibition (cationic) and nitrogen inhibition (free radical), and which yield hard, glossy, scuff resistant finishes.

When used in remote experiments, polymerisation may be achieved in 2 stages: remote (cationic) and direct (free radical). It is a matter of preference as to which of these stages is completed first. This offers many formulating and processing possibilities in practical usage.

8 RECOMMENDATIONS FOR FURTHER WORK

Two important elements of this thesis have not been proven satisfactorily. These are:

- That HF is capable of polymerising epoxides and DVE's (although its presence has been proven among the gaseous photo-products which have been used to polymerise epoxides and DVE's).

- That group 5 pentafluorides are present in the gaseous photo-products (although they are known to be capable of bringing about polymerisation of epoxides and DVE's).

The experimental work therefore lacks a number of experiments that may be informative with regard to the nature of the gases produced on UV induced solid-state photo-decomposition of onium salts and with regard to the nature of polymerising species in (remote) cationic polymerisation.

1. Remote Polymerisation with DPIHFSb

Although the DPIHFSb salt was subjected to solid-state photo-decomposition and fluoride ion analysis – and the quantity of fluoride ions produced was much lower than the other group 5 analogues – no experiment was done to determine the efficiency of remote polymerisation with this salt.

Remote polymerisation experiments with antimonate salts would be most interesting as antimony pentafluoride is probably a polymeric liquid under experimental conditions. The reduced fluoride ion yield with this salt has already been explained by the lack of pentahalide available for hydrolysis, with the implication that HF is the primary component of the gaseous products obtained from solid-state irradiation of the antimonate salt.

Remote polymerisation experiments with the antimonate salt would therefore confirm whether or not HF is capable of epoxide polymerisation. Such a conclusion, if supported by FTIR spectroscopy, should be

243

confirmed, in the case of epoxides, by evidence of ring opening drawn from disappearance of the epoxide C-H stretch at 794cm^{-1}. Additionally and of equal importance, there must also be evidence of chain extension in the form of a C-O-C stretch at 1040cm^{-1}, corresponding to the ether linkages which necessarily develop as polymerisation proceeds. Analogous results would be required for DVE's. This evidence was also lacking from the work of Wilkinson [63], and so the viability of HF as a polymerising agent remains unproven.

2. Verification of the presence of group 5 polyfluorides in the photo-product gases.

In the absence of FTIR evidence, the presence of polyfluorides could be confirmed indirectly by elemental analyses (e.g. Atomic Absorption) of the aqueous solutions known to contain fluoride ions after exhaust of photo-product gases following UV irradiation of the solid-state initiator(s). The presence of phosphorus, arsenic or antimony would be consistent with the generation of polyfluoride gases. A negative result in such experiments would indicate that all the fluoride ions detected originate from the photolysis reaction and multiple equivalents of fluoride are not, as described earlier, to be regarded as experimental artefacts of fluoride ion measurement.

3. Evaluation of factor(s) which may affect the rates of hydrolysis of polyfluorides (if present) in aqueous solution after exhaust of photo-product gases obtained by UV irradiation of the solid-state initiator(s).

It would be of interest to conduct solid-state photo-decomposition/fluoride ion analysis experiments (for all group 5 series onium salts) in conjunction with variation of the temperature of the water into which the gaseous photo-products are exhausted and dissolved. If variation in water temperature was shown to have a strong effect on the rate of fluoride ion evolution, this would confirm the importance of the sequential pentafluoride hydrolysis steps in terms of the contribution of the pentafluoride to the overall fluoride ion yield. The relative rates of the aforementioned hydrolysis steps will almost certainly be affected by temperature variation. A negative result in such experiments would indicate that all the fluoride ions detected originate from the photolysis reaction and multiple equivalents of fluoride are not, as described earlier, to be regarded as experimental artefacts of fluoride ion measurement.

equivalents of fluoride are not, as described earlier, to be regarded as experimental artefacts of fluoride ion measurement.

Similar indications could be gained at a fixed water temperature by either switching off the UV lamp or discontinuing the flow of exhaust gases into the water, at an early stage in the process. If the fluoride ion yield continues to rise after such a step, then this would indicate that hydrolysis of pentafluorides is contributing to the fluoride ion yield.

Other aspects of the work could also be developed further:

The remote polymerisation of DVE's and hybrid cure processes yielded interesting results that could be combined in various ways to enhance cure rate. Remote cure of DVE/epoxide combinations is possible and they can be combined with acrylates in hybrid cure systems.

The incorporation of pigments and dyes into remote curing should be considered particularly those pigments and dyes that are problematic for conventional UV curing such as TiO_2 and Carbon Black. The method would also be suitable for fluorescent and phosphorescent dyes, which tend to be photo-labile and therefore unsuited to conventional UV curing.

9 REFERENCES

1   (1978) Encycl.Polym.Sci.Tech, 3rd Edn., Kirk-Othmer,**6**,222-226

2   G.North, (1991) Conf.Proc.Radtech'91 (Europe),9

3   H.H.Bankowsky, E.Beck, W.Reich, P.Enenkel and M.Lokai, (1997) Conf.Proc.Radtech '97 (Europe),9

4   K.Lawson, (1995) Conf.Proc.Radtech'95 (Europe),321-331

5   K.Lawson, (1998) Conf.Proc.Radtech'98 (North America),1

6   G.Odian, (1981) Principles of Polymerisation, 2nd Ed.,McGraw-Hill Publ.Corp.,517

7   J.P.Kennedy and E.Marechal, (1981) J.Polym.Sci.,Macromol.Rev.,**16**,193-198

8   (1986) Encycl.Polym.Sci.Eng.,**6**,283-284

9   (1986) Encycl.Polym.Sci.Eng.,**6**,340-343

10 S.P.Pappas, (1985) Progr.Org.Coat.,**13**,35-64

11 S.P.Pappas, (1985)J.Imag.Tech.,**4,11**,146-157

12 C.Decker and K.Moussa, (1990)J.Polym.Sci.Part A.Polym.Chem.,**28**,3429-3443

13 J.V.Crivello and J.H.W.Lam, (1977) Macromolecules,**6,10**,1307-1315

14   J.V.Crivello and J.H.W.Lam, (1976) J.Polym.Sci.,Symp.No.56,383-395

15   J.V.Crivello and J.H.W.Lam, (1979) J.Polym.Sci.,Polym.Chem.Ed.,**17**,977-999

16   T.S.Bal, A.Cox, T.J.Kemp and P.Pinot de Moira, (1980) Polymer,**21**,423-428

17   J.V.Crivello, J.L.Lee and D.A.Conlon, (1983) J.Rad.Curing,10,**6**,6-13

18   P.E.Sundell, S.Jonsson and A.Hult, (1991) J.Polym.Sci.,Polym.Chem.Ed., **29**,1535-1543

19A   A.D.Ketley and J.H.Tsao, (1979) J.Rad.Curing,2,**6**,22-26

19B   I.Shahak, Sh.Manor and E.D.Bergmann, (1968) J.Chem.Soc.C,2129-2131

20   J.V.Crivello and J.H.W.Lam, (1978) ACS Ser.114 (Epoxy Resin Chemistry),1-16

21   J.V.Crivello, J.L.Lee and D.A.Conlon, (1988) Makromol.Chem., Macromol.Symp.13/14,145-160

22   J.V.Crivello and J.H.W.Lam, (1978) ACS Div.Org.Plast.Chem.,**39**,31-35

23   W.R.Watt, (1978) ACS symp.ser.114.,Epoxy Resin Chem.,publ.1979,17

24   C.A.May and Y.Tanaka, (1973) Epoxy Resins, Chem.&Tech.,Decker NY,135-237

25   M.Sawamoto, (1991) Modern Cationic Vinyl Polymerization, in Progr.Polym.Sci.,1,**16**,111-172

26   P.H.Plesch, M.Polanyi and H.A.Skinner, (1947) J.Chem.Soc.,257

27   S.P.Pappas and L.R.Gatechair, (1981) Proc.Water-Borne Higher-Solids Coat.Symp.,8th,85-99

28   J.F.Rabek, (1982) Experimental Methods In Photochemistry And Photophysics, Part 2, Wiley-Interscience,727-745

29   (1988)UV and EB Curing Formulation For Printing Inks, Coatings And Paints, R.Holman and P.Oldring, Eds., 2nd Edn., SITA Tech.,U.K.,64-69

30   D.C.Neckers and W.Jager, (1998) Chemistry And Technology of UV And EB Formulations for Coatings, Inks And Paints, Wiley-SITA Tech.Ltd., Vol. 7,

31   J.J.Licam and P.C.Crepeau, (1965) U.S.Patent 3,205,157

32   S.I.Schlesinger, (1974) Polym.Eng.Sci.,**14**,**7**,513

33   R.O.C.Norman, (1978) Princ.Org.Synth., 2nd Edn., Chapman and Hall,

34   J.L.Dektar and N.P.Hacker, (1990) J.Org.Chem.,**55**,639-647

35   N.P.Hacker, D.V.Leff and J.L.Dektar, (1991) J.Org.Chem.,**56**,2280-2282

36   J.W.Knapczyk, J.J.Lubinkowski and W.E.McEwen, (1972) Tett.Lett.,**35**,3739-3742

37   J.L.Dektar and N.P.Hacker, (1987) J.Chem.Soc.,Chem.Commun.,1591-1592

38   K.Meier and H.Zweiffel,(1986) J.Radiat.Curing,**4**,**13**,26-32

39   J.V.Crivello, (1991) J.Coat.Tech.,**793**,**63**,35-37

40   Fletcher and Hinchelwood, (1936) J.Chem.Soc.,**58**,157

41   H.Irving and R.W.Reid, (1960) J.Chem.Soc.,2078

42   D.F.Banks,(1966) Chem.Revs.,**66**,243-266

43   S.P.Pappas and J.H.Jilek, (1979) J.Soc.Photog.Sci.Eng.,**3**,**23**,140-143

44   H.Ito and C.G.Willson, (1984) ACS Ser.242,11-23

45   Y.Yagci and W.Schnabel, (1988) Makromol.Chem., Macromol.Symp.13/14,161-174

46   S.P.Pappas, B.C.Pappas, L.R.Gatechair and J.F.Jilek, (1984) Polym.Photochem., **5**,1-22

47   R.S.Davidson and J.W.Goodin, (1982) Eur.Polym.J.,**18**,589-595

48   J.W.Knapczyk and W.E.McEwen, (1970) J.Org.Chem.,**8**,**35**,2539-2543

49   A.Ledwith, S.Al-Kass, D.C.Sherrington and P.Bonner, (1981)Polymer,**22**,143-145

50   S.P.Pappas, B.C.Pappas, L.R.Gatechair and W.Schnabel, (1984) J.Polym.Sci., Polym.Chem.Ed.,**22**,69-76

51   M.Tilley, B.Pappas, S.P.Pappas, Y.Yagci, W.Schnabel and J.K.Thomas, (1989) J.Imag.Sci.,**2**,**33**,62-64

52   H.Irving, G.P.A.Turner and R.W.Reid, (1960) J.Chem.Soc.,2082

53   J.H.Jilek, (1979) Ph.D. Thesis, NDSU, Fargo ND,

54   J.L.Dektar and N.P.Hacker, (1988) J.Org.Chem.,**53**,1833-1835

52   H.Irving, G.P.A.Turner and R.W.Reid, (1960) J.Chem.Soc.,2082

53   J.H.Jilek, (1979) Ph.D. Thesis, NDSU, Fargo ND,

54   J.L.Dektar and N.P.Hacker, (1988) J.Org.Chem.,**53**,1833-1835

55   N.P.Hacker, J.L.Dektar, D.V.Leff, S.A.MacDonald and K.M.Welsh, (1991) J.Photopolym.Sci.Tech.,**3**,**4**,445-453

56   J.L.Dektar and N.P.Hacker, (1991) J.Org.Chem.,**56**,1838-1844

57   N.P.Hacker and J.L.Dektar, (1989) ACS Div.Polym.Sci.Eng.,**61**,76-85

58   N.P.Hacker, D.V.Leff and J.L.Dektar, (1990) Mol.Cryst.Liq.Cryst.,**183**,505-511

59   B.D.Hanrahan, P.Manus and R.F.Eaton, (1998) American Ink Maker,59-73

60   R.C.Petterson, A.de.Maggis, A.L.Herbert, T.J.Haley, J.P.Mykytka and I.M.Sarkas, (1971) J.Org.Chem.,**5**,**36**,631

61   R.Hoene and K.H.W. Reuchart, (1976) Makromol.Chem.,**177**,3545

62   F.Andanuzzi, A.Prescia and G.Ceccarelli, (1975) Makromol.Chem.,

63   S.A.Wilkinson, (1989) Ph.D. Thesis, City University,

64   P.E.Sundell, (1990) Personal Communication to R.S.Davidson, 1990-09-24,

65   A.Chapiro, (1962) Radiation Chemistry of Polymeric Systems, Vol. 15, Interscience,526

69   C.J.Pouchert, (1981) Aldrich Library of IR Spectra, 3rd Edn., # 561A, Aldrich Chem. Co.

70   C.J.Pouchert, (1981)Aldrich Library of IR Spectra, 3rd Edn., # I-763-2, Aldrich Chem. Co.

71   (1980) Hdbk.Chem.Phys.,61st edn.,

72   (1977) Perry's Chem.Eng.Hdbk.,7th Edn.,McGraw-Hill,

73   C.J.Pouchert, (1981) Aldrich Library of IR Spectra, 3rd Edn., # F600-1, Aldrich Chem. Co.

74   J.Overend and S.Reichman, Spectrochim.Acta, Part A, (1970), 2, **26**, 377-89

75   J.P.Pemsler and W.G.Planet, (1956) J.Chem.Phys.,920-21

76   W.A.Mazeika and H.M.Neumann (1966) Inorg.Chem.,**5**,309-311

77   L.R.Gatechair, (1981) Ph.D. Thesis, NDSU, Fargo ND,

78   S.P.Pappas, B.C.Pappas, M.Tilley, Y.Yagci, W.Schnabel (1988) Proc.IUPAC Photochem.Conf., Bologna,

79   D.C.Pepper and P.J.Reilly, (1962) J.Polym.Sci.,**58**,639-647

80   W.R.Watt, (1985) UV Curing: Sci. & Tech., Vol II, S.P.Pappas, Ed., Tech.Marketing.Corp.,Norwalk, CT,247-282

81   H.J.Hageman, (1989)Photopolym.Photoimaging Sci.Technol., Elsevier,1-53

82   A.Ledwith, (1978) Polymer,**19**,1217-1219

83   A.Hult, P.E.Sundell and S.Jonsson, (1989) Proc.Div.Polym.mater.Sci.eng.,**61**,86-90

84   P.E.Sundell,   S.Jonsson   and   A.Hult,   (1991)   J.Polym.Sci.:
        Polym.Chem.Edn.,**29**,1525-1533

85   P.E.Sundell, S.Jonsson and A.Hult, (1990) A.C.S.Polym.Reprints,**31**,373-374

86   S.Denizligil, Y.Yagci and C.McArdle, (1995) Polymer,16,**36**,3093-3098

87   A.M.Abdul-Rasul, A.Ledwith and Y.Yagci,(1978) Polymer,**19**,1219-1222

88   (1991)Chemistry And Technology Of UV/EB Coatings, Inks And Paints,
        K.K.Dietliker, P.K.T.Oldrind, Eds., SITA Tech.Ltd., Vol.3,400-402

89   A.B.Hult and P.E.Sundell, (1989) Polym.Mater.Sci.Eng.,**60**,453-457

90   C.E.Hoyle   and   J.F.Kinstle,   Eds.,(1989)   Rad.Curing.Polym.Mat.,   A.C.S.
        Symp.Ser.417,1990,**32**,459-473

91   H.Ishida, (1987) Fourier Transform Infrared Characterization Of Polymers,
        Polym.Sci.Tech.,Plenum Press, **36**

92   J.P.Fouassier and J.F.Rabek, Eds., (1993) Radiation Curing in polymer science
        and Tech.,Vol1,Chapter7,329-452

93   J.A.Reffner and W.T.Wihlbourg, (1990) Amer.Lab., **4**, 26-34

94   H.Ishida, (1987)Rubber Chem, and Tech.,**60**,497-554

95   R.G.Greenler, (1966)J.Chem.Phys., **44**, 1, 310-315

96   D.L.Allara, (1979)Appl.Spec., **33**, 358-361

97   R.T.Graf, J.L.Koenig and H.Ishida, (1985)Appl.Spec., **39**, 405-408

98   R.N.Jones, D.Escolar, J.P.Hawranek, P.Neelakantan and R.P.Young, (1973) J.Molec.Struc., **19**, 21-42

99   R.G.Greenler, (1969)J.Chem.Phys., **50**, 1963-1968

100   G.K.Ribbegard and R.N.Jones, (1980) Appl.Spec.,**34**, 6, 638-645

101   R.G.Greenler, R.R.Rahn and J.P.Schwartz, (1971) J.Catalysis, **23**, 42-48

102   D.H.Williams and I.Fleming, (1980) Spectroscopic methods in organic chemistry, 3rd Edn., McGraw-Hill

103   A.Carroy, 1996 Technical Bulletin, Union Carbide, Geneva,1-9

104   B.D.Hanrahan, (1988) Proc 15th Water-borne & higher solids coatings symp.,420

105   B.L.Brann, (1989) Conf.Proc.Radtech'98 (Europe),565-579

106   M.Evans Best and C.R.Moylan, (1992) J.Appl.Polym.Sci.,**45**,17-23

107   T.Nguyen, D.Bentz and E.Byrd, (1995) J.Coatings Tech.,844,**67**,37-46

108   J.V.Crivello, (1981)Proc.7th.Internat.Conf.Org.Coatings Sci.Tech., Athens,Part1,35-53

109   P.C.Hupfield, S.R.Hurford and J.S.Tonge, (1998) Conf.Proc.Radtech'98 (North America),468-473

110   W.R.Watt, (1986) Radiation Curing,4,**13**,7-24

111   A.D.Ketley and J.H.Tsao, (1979) J.Rad.Curing,**1**,22-28

112   PJ.M.Manus, (1989) Conf.Proc.Radtech'89 (Europe),535-553

113   F.J.Vara and J.A.Dougherty, (1989) Conf.Proc.Radtech'89 (Europe),523-533

114   G.J.Wilkins,   W.J.Burlant,   J.S.Plotkin   and   F.J.Vara,   (1991) J.Oil.Col.Chem.Assoc.,480-482